THE UNIVERSITY
of EDINBURGH

Investigating the role of eukaryotic translation elongation factor eEF1A2 in autism, epilepsy and intellectual disability.

Fiona McLachlan

A thesis submitted for the degree of Doctor of Philosophy

The University of Edinburgh 2019

Declaration

I declare that this thesis has been written by me and that all the work presented within is my own unless clearly stated. All sources of information and other individuals' contributions have been appropriately acknowledged. This work has not been submitted for any other degree or professional qualification.

Fiona McLachlan

Dedication

To Wispa, who lay on my keyboard every time she thought this thesis was getting more attention than her.

Acknowledgements

To Cathy, for the unbelievable patience and faith. Thank you so much. I am very grateful for all the support and leadership you gave.

To the Abbott Lab, a fantastic group to work and laugh with. Thank you for making work such an enjoyable place to be. Thanks for the support, both academically and emotionally.

To Shane, Katerina and Panos, thank you for the food, shoulders to cry on and Nixon trivia. Thank you for the pep-talks during the hard times, the late-night tissue culture sessions and the constant laughter.

To 'Winemergency' and 'Pub Club', thank you for the beers, the hangovers and the fantastic friendships. A great team and I am proud of all of us.

To Anna, Eimear, Tom and Billy. Thank you for the kindness, support and belief in me which you supplied throughout this, even when I really doubted myself.

To my Mum, Dad, Calum and Rachel, who have put up with me and my bad mood whilst I wrote this. I could not be more grateful for you all. I love you.

List of contents

Abstract

Eukaryotic translation elongation factor eEF1A2 is responsible for delivering aminoacylated tRNAs to the ribosome during protein synthesis. Heterozygous de novo missense mutations in *EEF1A2* have been identified in individuals with epilepsy, autism and intellectual disability. The primary aim of this thesis was to assess whether these mutations operated through a loss of function, gain of function or dominant negative mechanism. To investigate this, I analysed eEF1A2 protein interactions, how these interactions varied between mutations and the functional consequences of changes in the interactome.

I used affinity purification mass spectrometry to identify the interactome of eEF1A2 and compared the changes resulting from mutations in eEF1A2. Co-immunoprecipitation experiments determined that mutations could be grouped by changes in their interaction with the cognate guanine exchange factor eEF1B. One group showed complete or partial loss of binding to all four subunits of the eEF1B complex, whilst another cluster showed no change in binding compared to wild-type eEF1A2. No specific patterns of clinical features or phenotypic severity could be attributed to these groupings. My results suggested that protein synthesis would be impaired by this disrupted interaction. *In vivo* and *in vitro* protein synthesis experiments failed to detect any differences that could be attributed to the presence or absence of the D252H mutation. As no apparent differences in protein synthesis could be detected between muscle tissue from *Eef1a2*$^{-/-}$ and *Eef1a2*$^{+/+}$ mice or between eEF1A2$^{-/-}$ and wild-type cells, it is likely that in both cases the protein synthesis assay employed was not performing adequately.

Comparative analysis of *Eef1a2*$^{D252H/D252H}$ and *Eef1a2*$^{-/-}$ mouse phenotypes determined that there is a gain of function or dominant negative element to the eEF1A2^{D252H} mutation, highlighting that this mutation does not operate simply through a loss of function mechanism. Interactome was unable to successfully identify what this might be.

In conclusion eEF1A2 mutations may operate via both a loss and gain of function mechanism. Depending on the precise mutation, eEF1A2 may be compromised in

its ability to operate in protein synthesis, but at least some mutations may also result in a degree of toxicity.

List of figures

List of tables

List of abbreviations

Abbreviation	Definition
$A\beta_{42}$	amyloid beta 42
aCSF	artificial cerebrospinal fluid
AP-MS	affinity purification mass spectrometry
BCA	Bradford colorimetric assay
BDNF	brain derived neurotrophic factor
BSA	bovine serum albumin
CamKII	calmodulin-dependent protein kinase II
cAMP	cyclic adenosine monophosphate
cDNA	complementary deoxyribonucleic acid
CHX	cycloheximide
c-JNK	c-Jun N-terminal kinases
CNS	central nervous system
Co-IP	Co-Immunoprecipitation
CREB1	CAMP responsive element binding protein
CRISPR	clustered regularly interspaced short palindromic repeats
CST	cell signalling technology
CSF	cerebrospinal fluid
DDD	deciphering developmental disorders
ddH_2O	double distilled water
DHPG	(S)-3,5-dihydroxyphenylglycine
DIV	days *in vitro*
DMSO	dimethyl sulfoxide
DNA	deoxyribonucleic acid
ECL	enhanced chemiluminescence
eEF1	eukaryotic elongation factor 1
eEF1A	eukaryotic elongation factor 1 alpha
eEF1A1	eukaryotic translation elongation factor 1 alpha 1
eEF1A2	eukaryotic translation elongation factor 1 alpha 2
eEF1B	eukaryotic elongation factor 1 beta
eEF2	eukaryotic elongation factor 2
eIF2α	eukaryotic translation initiation factor 2 alpha
eIF2β	eukaryotic translation initiation factor 2 beta
eIF4β	eukaryotic translation initiation factor 4 beta
eIF4γ	eukaryotic translation initiation factor 4 gamma
ExAc	exome aggregation consortium
FACS	fluorescent associated cell sorting
FCS	foetal calf serum
FMRP	fragile x mental retardation protein

FRET	fluorescence resonance energy transfer
FTD	fronto-temporal dementia
FXS	fragile x syndrome
GDP	guanosine diphosphate
GEF	guanine exchange factor
GFAP	glial fibrillary associated protein
GFP	green fluorescence protein
GO	gene ontology
gRNA	guide ribonucleic acid
GTP	guanosine triphosphate
HCL	hydrogen chloride
HFS	high frequency stimulation
HRP	horse radish peroxidase
IP	immunoprecipitation
iPSCs	induced pluripotent stem cells
LFQ	label free quantifications
LTD	long term depression
LTP	long term potentiation
LUHMES	lund human mesencephalic
mACHR	muscarinic acetylcholine receptor
MDM2	mouse double minute 2 homolog
mGluR	metabotropic glutamate receptor
MLR	most-likely-ratio
MRI	magnetic resonance imaging
mRNA	messenger ribonucleic acid
mTOR	mammalian target of rapamycin
NaOH	sodium hydroxide
NMDA	N-methyl-D-aspartate
PBS	phosphor-buffered saline
PCR	polymerase chain reaction
PDVF	Polyvinylidene difluoride
PET	positron emission tomography
PFA	paraformaldehyde
PKA	protein kinase A
PLO	poly-l-ornithine
qPCR	quantitative polymerase chain reaction
RBPs	ribonucleoparticles
RIPA	radioimmunoprecipitation assay
RNPs	ribonucleoparticles
RT-PCR	reverse-transcriptase polymerase chain reaction
SDM	site-directed mutagenesis

SGs	stress granules
siRNA	small interfering ribonucleic acid
SUnRISE	SUnSET-based ribosome speed of elongation
SunSET	SUrface SEnsing of Translation
TAS	total area sums
TBS	tris buffered saline
TGS	tris-glycine-SDS
TOP	terminal oligopyrimidine
TRAP-Seq	translating ribosome affinity purification-mRNAseq
tRNA	transfer ribonucleic acid
UTR	untranslated region
WT	wild-type

Chapter 1: Introduction

1.1Translation

1.1.1 Translation elongation

Protein synthesis is divided into 3 steps; initiation, elongation and termination. Met-tRNA is recruited to the 80S subunit of the ribosome for initiation of the polypeptide chain, mediated via a complex of initiation factors. Once peptide formation is established, further complementary aminoacylated tRNAs are recruited to the ribosome by elongation factors. Finally stop codon recognition terminates polypeptide elongation and induces the release of the polypeptide from the ribosome, facilitated by release factors (1).

In eukaryotes, the eEF1 complex responsible for elongation can be subdivided into two components. eEF1A, a GTPase protein, delivers aminoacylated tRNAs to the ribosome in a GTP dependent manner. eEF1B – a complex of proteins - acts as the cognate guanine exchange factor for eEF1A.

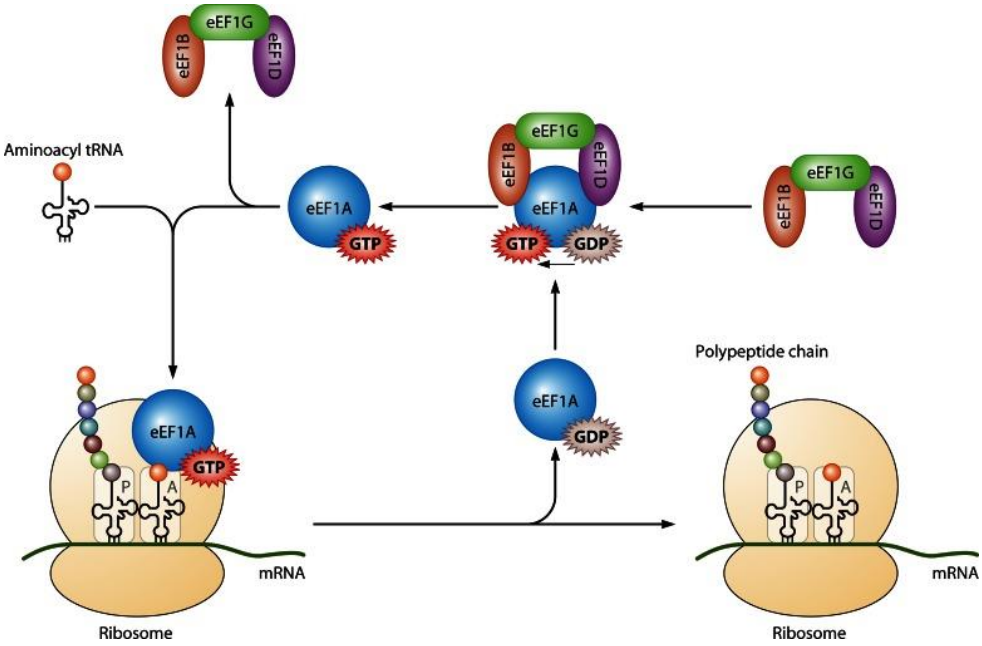

Figure 1.1: Schematic diagram of translation elongation. *eEF1A-GTP directs aminoacylated tRNAs to the A site of the ribosome resulting in GTP hydrolysis. eEF1A-GDP disassociates from the ribosome and is bound to the eEF1B complex for GDP recycling. The eEF1B complex is displayed as its 3 constituent subunits*

eEF1Bα, eEF1Bδ and eEF1Bγ. GDP recycling allows eEF1A to repeat the process, lengthening polypeptide chains. Figure: Li et al, 2013 (2).

1.2 eEF1A

1.2.1 Two eEF1A isoforms with differential expression patterns.

Throughout eukaryotic species several isoforms of eEF1A are present. Drosophila and *Xenopus* have been reported to have 2 and 3 copies of eEF1A gene respectively (3,4). The presence of multiple isoforms appears not to be consistent within non-mammalian vertebrae. Zebrafish have been reported to express only one isoform (5,6). This has, however, been contested within our lab, with several isoforms reported in all tissues studied (personal communication with Nwamaka Idigo)

In mammals the presence of a second isoform was first detailed in rat. Named as statin-1 (from here on called eEF1A2), the isoform demonstrated a 92% identical (and 98% similar) amino acid sequence homology with eEF1-α (from here on called eEF1A1) (7). In humans, *EEF1A1* and *EEF1A2* genes are located on chromosomes 6 and 20 respectively (8), and their proteins display distinct and reciprocal expression patterns. eEF1A1 is expressed ubiquitously throughout development, before being switched off in terminally differentiated myocytes, cardiomyocytes and neurons in mammals including rodents and humans (7,9,10). There is evidence that this switch is conserved in vertebrates. Drosophila express one isoform ubiquitously as a housekeeping gene (F1), and a second (F2) isoform during the pupal stage (3). In *Xenopus* a switch between two eEF1α isoforms is regulated post-translationally in muscle. In pigs, eEF1A2 expression was found in adult muscle, tongue, brain and heart. eEF1A1 is expressed prenatally and in most adult tissue – with downregulation in heart, liver and brain (11).

Techniques such as immunofluorescence and immunohistochemistry allowed for analysis of eEF1A1 and eEF1A2 expression within specific cell populations in tissues. Initial immunostaining experiments by Pan and colleagues compared WT and *Eef1a2*$^{-/-}$ mice (discussed further in Section 1.5.1). Although they found eEF1A1 expression in all developing neurons, upon terminal differentiation, most

staining in neurons was attributed to eEF1A2. eEF1A1 staining was limited to glial cells (12). Further examination of eEF1A2 expression in nervous system cell types was performed by Newbery and colleagues (13). Immunohistochemistry staining of eEF1A1 and eEF1A2 in mouse spinal cord and brain sections demonstrated reciprocal expression. eEF1A2 was expressed in terminally differentiated motor neurons and Purkinje cells, whilst eEF1A1 is expressed in glial cells. This was in agreement with Pan et al (12), however extends upon the results by confirming the complete reciprocal expression of these isoforms in different neuronal cell types.

The timing of the switch in mice became well documented by studies of *Eef1a2*$^{-/-}$ mice (discussed in Section 1.5.1). However, less is known about the switch in humans. The use of databases such as Braincloud and Brainspan allows us to view transcriptome profiles collated from multiple RNAseq experiments (14,15). Figure 1.2 demonstrates a reciprocal expression pattern in neurons, showing eEF1A1 mRNA down-regulated postnatally, with up-regulation of eEF1A2 occurring at a similar timepoint. The expression change of isoforms is complete by ~2 years after birth.

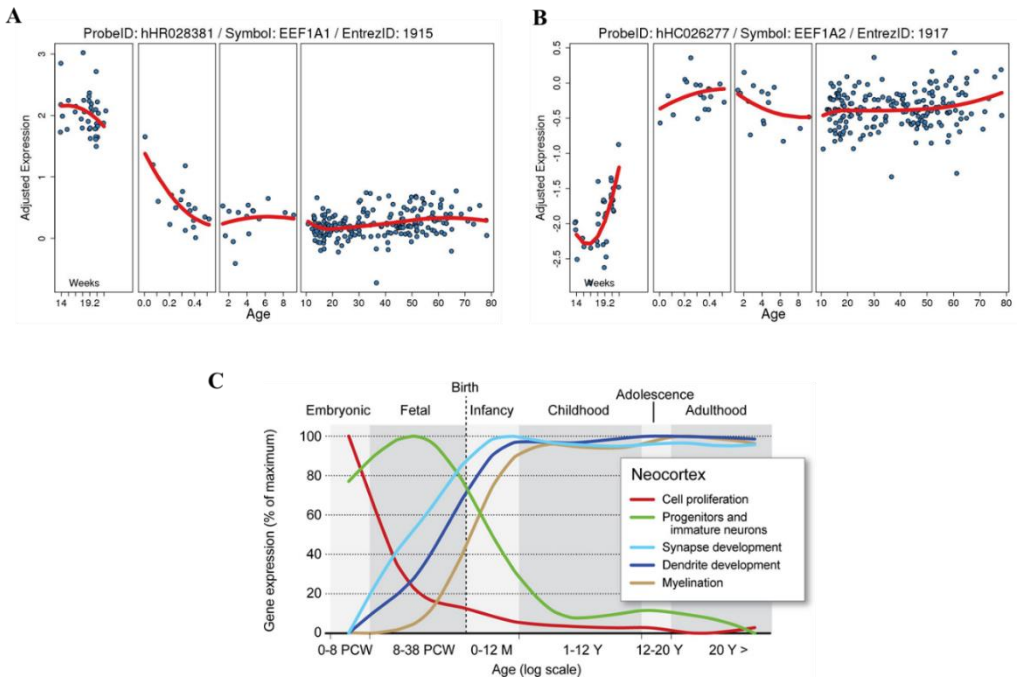

Figure 1.2: RNAseq data demonstrating the mRNA expression of eEF1A1 (A) and eEF1A2 (B) in human throughout development. *Graphs from the BrainCloud depository.* ***C*** *demonstrates the patterns of gene expression during development. Adapted from Tebbenkamp et al (15).*

1.2.2 Structural differences between eEF1A1 and eEF1A2

Despite their high sequence homology, there are distinct structural differences between the variants which might explain the conserved presence of two isoforms. eEF1A is composed of 3 domains. The first domain forms two α helices and two anti-parallel β strands. A linker connects domain I to domain II, which is a β barrel structure composed of two β-sheets. Domain III is a second, larger, β-barrel made of seven β-sheets, connected to domain II with a second linker (16). Soares et al provided structural analysis of the changed amino acid residues and found they were distributed between all 3 domains. 3D modelling determined that eEF1A has a "conserved" face, containing the residues which participate in eEF1B binding, and a "variable" face (see Figure 1.3B). This variable face has two clusters of amino acids which differ between the two isoforms. There is minimal amino acid variation both within and near the eEF1B binding sites, suggesting there is likely no functional difference to eEF1B binding capacity.

Changes however, are seen in both GTP and possible actin binding sites (17). Post translational modifications appear to cluster in a similar manner to the changed residues, further supporting that these clusters mediate the different functions of the isoforms (18). This structural analysis was supportive of experimental data. eEF1A1 and eEF1A2 show slightly increased affinities for GTP and GDP respectively, although similar overall translational kinetics are reported (19). In terms of actin binding, mutational analysis of yeast eEF1A showed that at least one of the residues changed in eEF1A2 is important in actin bundling (20). Additionally, recent evidence found different actin organisation properties of eEF1A1 and eEF1A2 (discussed further in Section 1.2.4.3) (21). Outwith protein synthesis and actin bundling, it is possible post-translational changes afford the opportunity for varied interacting partners. Panasyuk et al highlighted that eEF1A2 displayed increased tyrosine phosphorylation allowing it to interact with specific domains of signalling molecules such as RasGap, which eEF1A1 could not (22). Although changes in structure between the two isoforms result in slightly varied affinities with GTP, it is also reported that this does not impact upon global translational kinetics (19). Most structural changes between the two isoforms appear to modulate differing binding partners related to non-canonical functions.

A

```
eEF1A1      MGKEKTHINIVVIGHVDSGKSTTTGHLIYKCGGIDKRTIEKFEKEAAEMGKGSFKYAWVL    60
eEF1A2      MGKEKTHINIVVIGHVDSGKSTTTGHLIYKCGGIDKRTIEKFEKEAAEMGKGSFKYAWVL    60
            ************************************************************

eEF1A1      DKLKAERERGITIDISLWKFETSKYYVTIIDAPGHRDFIKNMITGTSQADCAVLIVAAGV    120
eEF1A2      DKLKAERERGITIDISLWKFETTKYYITIIDAPGHRDFIKNMITGTSQADCAVLIVAAGV    120
            **********************:***:**********************************

eEF1A1      GEFEAGISKNGQTREHALLAYTLGVKQLIVGVNKMDSTEPPYSQKRYEEIVKEVSTYIKK    180
eEF1A2      GEFEAGISKNGQTREHALLAYTLGVKQLIVGVNKMDSTEPAYSEKRYDEIVKEVSAYIKK    180
            ****************************************** **:***:*******:****

eEF1A1      IGYNPDTVAFVPISGWNGDNMLEPSANMPWFKGWKVTRKDGNASGTTLLEALDCILPPTR    240
eEF1A2      IGYNPATVPFVPISGWHGDNMLEPSPNMPWFKGWKVERKEGNASGVSLLEALDTILPPTR    240
            ***** ** ********:********* ********** **:*****.:****** ******

eEF1A1      PTDKPLRLPLQDVYKIGGIGTVPVGRVETGVLKPGMVVTFAPVNVTTEVKSVEMHHEALS    300
eEF1A2      PTDKPLRLPLQDVYKIGGIGTVPVGRVETGILRPGMVVTFAPVNITTEVKSVEMHHEALS    300
            ********************************:*:***********:****************

eEF1A1      EALPGDNVGFNVKNVSVKDVRRGNVAGDSKNDPPMEAAGFTAQVIILNHPGQISAGYAPV    360
eEF1A2      EALPGDNVGFNVKNVSVKDIRRGNVCGDSKSDPPQEAAQFTSQVIILNHPGQISAGYSPV    360
            ********************:*****.****.*** *** **:****************:**

eEF1A1      LDCHTAHIACKFAELKEKIDRRSGKKLEDGPKFLKSGDAAIVDMVPGKPMCVESFSDYPP    420
eEF1A2      IDCHTAHIACKFAELKEKIDRRSGKKLEDNPKSLKSGDAAIVEMVPGKPMCVESFSQYPP    420
            :*****************************.** *********:**************:***

eEF1A1      LGRFAVRDMRQTVAVGVIKAVDKKAAGAGKVTKSAQKAQKAK-     462
eEF1A2      LGRFAVRDMRQTVAVGVIKNVEKKSGGAGKVTKSAQKAQKAGK     463
            ******************* *:**:.***************
```

B

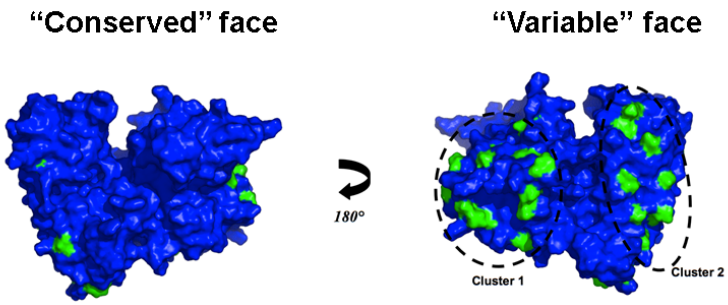

*Figure 1.3: **A** alignment of the amino-acid sequences of eEF1A1 and eEF1A2 using Clustal Omega, with varied residues in red. **B** Structural representation of eEF1A1 and the amino acids which differ in eEF1A2 (green). Adapted from Soares et al, 2009 (17).*

1.2.3 eEF1A2 structure in mammals

The mammalian structure of eEF1A2 was determined by X-Ray diffraction after the protein had been purified from rabbit skeletal muscle. Like the yeast structure, it consists of three domains and binds GTP and eEF1B. The structure was pulled down as a dimer, suggesting this conformation is pertinent to some function(s) (23).

It was first proposed that eEF1A acts in its actin bundling function in dimer conformation. eEF1A in tetrahymena bound to actin in a 1:1 manner. For actin bundling to occur, eEF1A would have to cross-link two actin filaments. The authors hypothesised that as eEF1A only contains one actin binding site, anti-parallel eEF1A dimer formation would enable the binding of two actin filaments in close enough proximity for actin bundling to occur (24). eEF1A dimer formation was experimentally proven in 2006 by Bunai and colleagues. They confirmed that eEF1A dimer formation was required for actin bundling. Bundling activity was dependent upon eEF1A dissociation from calmodulin. Calmodulin did not influence the association of eEF1A with actin, but did impair actin bundling activity (25). Interestingly, this work looked at actin bundling during cytokinesis. If eEF1A is essential for actin bundling in the cell division process, it is possible this function could be attributed to eEF1A1 rather than eEF1A2, and by extension the monomer to dimer ratio. More recent work in the mammalian forms confirms the existence of dimers. Trypsinolysis of eEF1A1 removed 69 amino acids from its N-terminal (a portion of domain I). Work with this truncated protein demonstrated that only domain III binds to actin, but for bundling to occur, the missing portion of domain I was required too. The removal of this segment inhibited dimerisation, suggesting that eEF1A1 requires a dimeric structure for actin bundling (26). Comparison of dimerisation of the two mammalian isoforms found eEF1A1 was more likely to self-associate due to its increased hydrophobicity. This evidence fits nicely with the experimental evidence that eEF1A1 has more of a role in actin bundling that eEF1A2 (as discussed in Section 1.2.4) (27)

1.2.4 Functional differences of eEF1A1 and eEF1A2

1.2.4.1 Overview of functional differences between eEF1A1 and eEF1A2

The two eEF1A isoforms must operate in different manners to an extent, so as to justify such a conserved switch. Evidence currently suggests there is no difference in the translational kinetics (19), even with slight difference in the GTP affinity of the two isoforms. The conserved presence of two isoforms is,

therefore, likely owing to their differing non-canonical properties (28). As the second most highly expressed protein in the cell, it is unsurprising that eEF1A has been implicated in several functions (29). However, the extent to which these are shared between the isoforms is debated. Table 1.1 summarises the reported non-canonical functions of both eEF1A isoforms.

Table 1.1: Reported non-canonical functions of eEF1A and the role each isoform takes.

Function	Isoform		Comments	Reference
	eEF1A1	eEF1A2		
Heat shock	X		eEF1A1 but not eEF1A2 has been shown to be instrumental in the heat shock response.	(30)
Actin bundling	X	?	Expression of eEF1A1 and eEF1A2 shows different actin bundling properties.	(17,21)
Transcription dependent nuclear export	X	?	eEF1A is involved in the nuclear export of translational apparatus.	(31–33)
Proteolysis of malformed peptides	X	X	Both isoforms have been implicated in the targeting of malformed peptides for degradation. c-JNK was highlighted as specifically phosphorylating eEF1A2, increasing its role in nascent peptide degradation.	(34–36)

Aggresome formation	?	?	Inhibition of eEF1A prevents aggresome formation	(37)
ZPR1 interaction and spindle formation	X	?	eEF1α interacts with ZPR1 in quiescent and proliferating cells. Required for cell proliferation.	(38)
Apoptosis	X	X	Isoforms display opposing roles in apoptosis. eEF1A1 and eEF1A2 act in a pro- and anti-apoptotic manner respectively.	(39–41)
Receptor scaffolding at the synapse	X	X	Both eEF1A1 and eEF1A2 have been shown to inhibit M4 mACHRs recycling.	(42)
Synaptic translation	X	X	eEF1A mediates local protein synthesis in dendrites in late-phase LTP and LTD.	(43–47)
RNA transport to synapse	X	X	Transport of mRNA in RNA transporting granules to the synapse.	(48,49)

1.2.4.2 eEF1A at the synapse

eEF1A has been implicated in local protein synthesis at the synapse. First the role of eEF1A is discussed, before evidence for the role of each isoform is examined. Long term facilitation, a mainstay of synaptic function, can be subdivided into long-term potentiation (LTP), and long-term depression (LTD).

Long term potentiation can be further subdivided into early (immediate response to frequency stimulation) and late (a more permanent change to synapse structure as a result of persistent stimulation). Although early-phase LTP can be managed by post-translational modification (50), both late-phase LTP and LTD require local protein synthesis to facilitate synaptic changes (51). eEF1A function was first identified as integral to late-LTP by studies in aplysia. Aplysia eEF1A (Ap-eEF1A) was identified as a late response gene which became up-regulated after serotonergic stimulation. eEF1A was not transported as protein to the synapse in response to serotonin, but instead as mRNA for local translation. The authors identified the increased Ap-eEF1A was dependent upon cAMP and the CREB1 pathway – a well-established signalling pathway in synaptic plasticity (52). The targeting of Ap-eEF1A to specific stimulated synapses may be key to controlling specific synaptic maintenance. Early and late-response genes are transcribed and therefore expressed cell wide, but the targeting of Ap-eEF1A to specific synapses might help control synaptic maintenance at the translational level. Ap-eEF1A favoured translation of mRNAs with terminal oligo-pyrimidine (TOP) sequences in their 5' untranslated region (UTR). Proteins associated with synaptic plasticity are enriched for the presence of these 5'UTR TOP sequences in their mRNAs, including structural (actin) and functional proteins (CamKII and calmodulin). Ap-eEF1A was only required for synaptic maintenance (late-LTP) and not induction (early-LTP) as the latter does not involve protein synthesis. This result implicated eEF1A in potentiation of synapses required for memory storage (43).

Mammalian eEF1A has been shown to work in a similar manner. *N*-Methyl-D-aspartic acid (NMDA) receptor activation using high frequency stimulation (HFS) resulted in the phosphorylation of mammalian target of rapamycin (mTOR) and its downstream signaller p70S6K. This phosphorylation resulted in increased eEF1A. This affect was not seen in lower frequency stimulation, associated with early-LTP formation. Meaning eEF1A is implicated in the protein synthesis required for late-LTP. The authors concluded that the increased eEF1A was a result of *de novo* protein synthesis and not a redistribution of residual eEF1A, as the application of a protein synthesis inhibitor before HFS prevented

this from happening. Furthermore, stimulation of isolated dendrites provided the same increase in eEF1A for 1-2 hours post HFS, suggesting that eEF1A mRNA is translated directly at the synapse and is not reliant of changes in expression at the soma (44). Further, Inamura and colleagues discovered that brain-derived neurotrophic factor (BDNF) stimulated not only initiation factors, but elongation factors eEF1A and eEF2. BDNF stimulates the mTOR pathway, phosphorylating eEF1A (stimulating activity) and eEF2 (inhibiting activity), the combination of which resulted in significantly increased ribosomal transit time (an inverse measure of protein synthesis). Inhibiting mTOR suppressed this result, determining that BDNF signalling was again mediated through the mTOR pathway via stimulation of downstream signalling target p70S6K (45).

Increases in eEF1A expression upon LTD induction have also been seen. Huang and colleagues used (S)-3,5-Dihydroxyphenylglycine (DHPG) to treat rat hippocampal slices. This drug stimulated metabotropic glutamate receptors (mGluRs) and resulted in increased eEF1A expression in dendrites as a result of *de novo* protein synthesis (46). This increase has been attributed to stimulation of the mTOR pathway in further studies (47). Huang and colleagues used HFS to induce LTP, which did not result in *de novo* protein synthesis of eEF1A, merely the redistribution of eEF1A into the dendrite. Despite increased eEF1A expression in both the LTP and LTD condition, no notable increase in protein synthesis could be detected. The authors conceded the method used may not be sensitive enough to detect changes in individual dendrites. However, the authors did note an increase in F-actin in response to DHPG treatment, a response which could be blocked (46). It is well established eEF1A interacts with actin (as discussed previously) and it is highly likely that it functions at the synapse outwith its canonical function of protein synthesis.

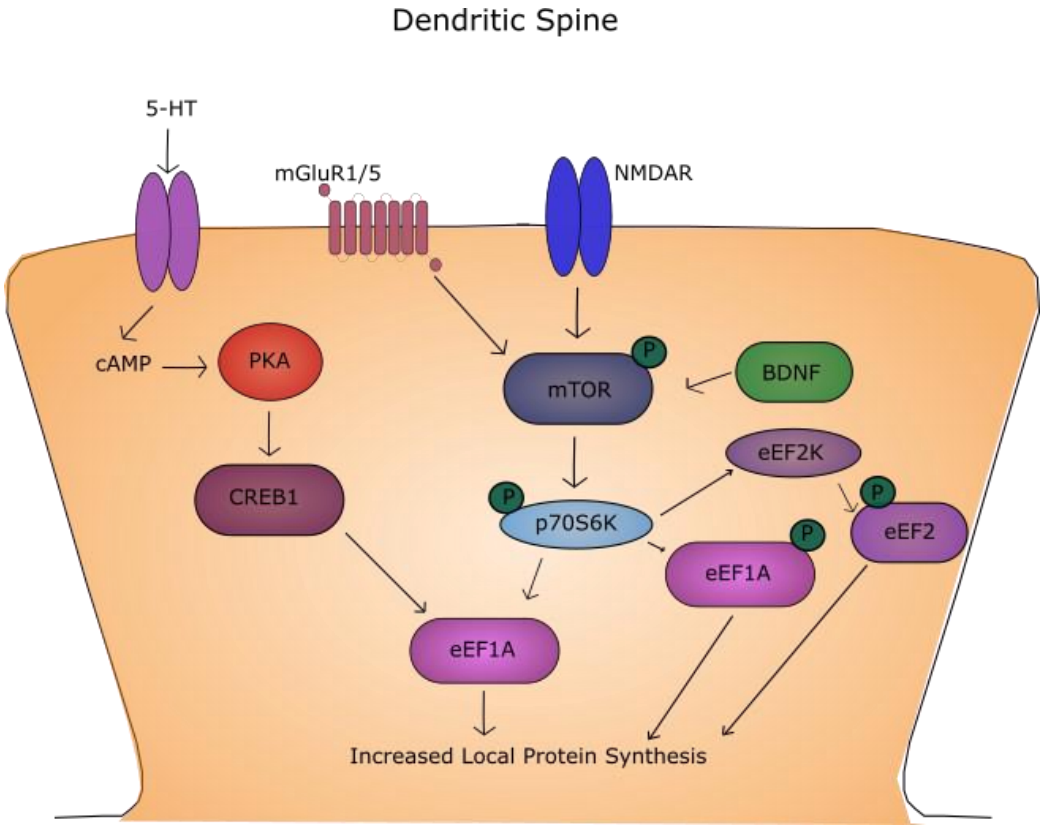

Figure 1.4: Mechanisms of eEF1A activation in late phase LTP and LTD for local protein synthesis. *Increased eEF1A and phosphorylated-eEF1A have both been reported in dendritic synapses as a response to high frequency stimulation inducing-LTP and metabotropic stimulated LTD. eEF1A has been reported to be upregulated owing to several signalling pathways (43–47).*

eEF1A playing a role other than protein synthesis at the synapse is a well-established idea supported by several arguments. 1) eEF1A is expressed in greater quantities than the subunits of its corresponding guanine exchange factor eEF1B (53). 2) eEF1A expression has been seen in early-LTP despite no known protein synthesis being reported at this time. This evidence proposes the idea that in early-LTP phase eEF1A participates in other functions.

Both isoforms have been reported to inhibit M4 muscarinic receptor recycling from endosomes (54). eEF1A is has been identified as part of ribonucleoprotein granules (RNPs) which are involved in the transport of RNA granules to the synapse (48,49). The alpha subunit of the M3M4 loop of glycine receptors was

seen to interact with eEF1A. This subunit has also been shown to interact to structural clustering protein gephyrin. Stimulation of glycine receptors implicated eEF1A in gephyrin-mediated glycine receptor clustering. Further, the authors discovered that when stimulating glycine or NMDA receptors in older cultured neurons, eEF1A was redistributed from synapses to the cytoskeleton (55). This evidence is supportive of a larger theory that eEF1A may play a significant role in actin bundling and restructuring at synapses, which is discussed in the next section.

The specific role each isoform plays in neuronal activity is harder to determine. It is often difficult to identify which isoform is present, firstly because often commercial antibodies cannot distinguish the two isoforms when immunostaining, and secondly because glial cells express eEF1A1 making whole tissue lysate analysis via western blot impossible. In most of the previously mentioned studies, no reference to the isoform involved is made, so elucidating the role of each isoform in neurons is challenging.

As eEF1A2 is the dominant neuronal isoform, it might be assumed that most of the eEF1A functions in differentiated neurons is mediated by this isoform. It is the case that eEF1A2 is the only isoform in terminally differentiated motor neurons (13). The up-regulation of eEF1A2 mRNA in human mRNAseq appears to coincide with synaptogenesis (Figure 1.2**B** & **C** (15)), also previously demonstrated for rat eEF1A2 (56). This suggests eEF1A2 is the dominant isoform for formation and maintenance of synapses. However, experimental evidence suggests eEF1A1 may play a role in developing neurons. eEF1A1 and eEF1A2 have both been found in post-synaptic densities (57,58). eEF1A1 mRNA is present in dendrites and was increased by neuronal depolarisation. This mRNA increase was accompanied with a greater increase in eEF1A protein, but the isoform is not specified (59). GFP-tagged eEF1A1 was targeted to dendritic spines by domain III. As domain III is most associated with actin bundling, the authors suggested that domain specific targeting might imply a function in spines (60) eEF1A1 also appears to be a target for Cilostazol influencing neurite

outgrowth (61). The evidence suggests eEF1A1 protein certainly plays a role in neurons, at least some point during neuronal development. There is some argument that even in subtypes of mature neurons eEF1A1 may not be completely switched off. Both McClatchy et al and Khalyfa et al found some eEF1A1 staining in terminally differentiated neurons (42,62). Therefore, although the timing and conservation of the genetic switch suggests eEF1A2 is likely the dominant neuronal isoform, the role which eEF1A1 plays in neuronal development/maintenance has yet to be fully established.

Interestingly as Bluem et al cultured their primary neurons a shift in eEF1A from synapses to actin filaments at 21-28DIV could be seen. Although it is impossible to tell if this is reflective of a change in isoform expression, it is intriguing that as neurons matured, a redistribution of eEF1A could be seen. It is possible this redistribution is for alternative function (55). More work to determine the role of each isoform will be possible as techniques which do not rely on antibodies continue to be developed.

1.2.4.3 eEF1A and actin interactions

One well-established function of eEF1A is actin bundling (63). Actin bundling is conserved between prokaryotic and eukaryotic variants of the protein (64,65). eEF1A bundles F-actin in Tetrahymena in the absence of calcium/calmodulin (24). The bundling of actin by eEF1A may be crucial in cell division, maintenance and synaptogenesis.

The roles of eEF1A in both protein synthesis and actin bundling might not be mutually exclusive. eEF1A has been shown to tether mRNA to actin filaments for local translation. There is a large body of evidence that the cytoskeleton may regulate the spatial control of translation by interacting with translational machinery (29). Translational impairments have been shown to be directly correlated with disruption to F-actin filaments (66). Mutagenic studies of eEF1A in yeast displayed dysregulation of growth and the cytoskeleton. This was partnered with a reduction in translation rate, however translation was inhibited at the initiation stage in the first instance, suggesting actin works to affect feedback

on translation at the initiation stage (67) with elongation as a secondary target (68).

When comparing the activities of eEF1A1 and eEF1A2, it is possible that actin bundling is the major difference between the two isoforms. Recent experimental evidence supports this hypothesis. Functional analysis of the difference in eEF1A2 and eEF1A1 actin bundling has been recently reported. Novosylna et al examined both the Ca^{2+}-calmodulin and actin binding properties of eEF1A1 and eEF1A2. They report that eEF1A2, unlike eEF1A1, did not bind to Ca^{2+}-calmodulin. In the case of eEF1A1, this interaction resulted in the inhibition of actin bundling. The authors further explored the consequence of this difference between isoforms by comparing the formation of F-actin bundles of each isoform. eEF1A1 and eEF1A2 created differently structured actin bundles, highlighting that this was an important difference between the two isoforms (21).

Abbott et al suggested that eEF1A2 up-regulation might occur in terminally differentiated cells because a more stable cytoarchitecture is required. Less (or altered) actin bundling would be required to maintain this specific cytoarchitecture (28).

1.3 eEF1B

1.3.1 eEF1B complex

eEF1B is a complex comprised of two guanine exchange factors (eEF1Bα and eEF1Bδ) and a structural anchoring protein (eEF1Bγ). Associated with the complex in mammals is valyl tRNA synthetase. Cognate (partner) guanine exchange factor eEF1B recycles eEF1A-GDP, allowing it to deliver amino-acylated tRNAs to the ribosome. In *Artemia* it has been proposed that EF1βγ (the eEF1B equivalent) increases the rate of GDP recycling in EF1α by a factor of 1000, making it the rate limiting step of protein synthesis (69). Although it is suspected to be less of a requirement in the mammalian protein (23), the presence of eEF1B and its binding to eEF1A is conserved. Initially it was proposed that only eEF1A1 bound to eEF1B (70). However, Cao et al discovered eEF1A2 also bound to all subunits (71). Cao et al showed siRNA mediated deletion of the

eEF1B subunits individually demonstrated no observable impact on cell cycle or survival in the short term (71). However, these knock-down experiments only examined the suppression of one subunit at a time. Given the conserved interaction of eEF1A and eEF1B, it seems likely to provide a function.

Mutations in subunits of the eEF1B complex have been reported in mouse models. Mouse model with *Eef1b2* exon deletion has been reported in the KOMP mouse phenotyping database (http://www.mousephenotype.org/data/genes/MGI:1929520#section-associations). Mice are reported to have defects in bone growth and abnormal behaviour. Kaitsuka and colleagues also recently reported a knock out mouse model of the long neurological isoform of eEF1Bδ (eEF1BδL) (see 1.3.3 for further details). This mouse model also resulted in neurological deficits (72). It is important to note that both mouse models are compatible with life. Therefore, losing elements of the eEF1B complex may not be as critical to normal function for cell types as with neurons.

1.3.2 eEF1Bα

Gene *EEF1B2* encodes the dominant form of the protein eEF1Bα, one of the two guanine exchange factor proteins in the eEF1B complex. The C-terminal of the protein has been shown to possess the catalytic activity (69), whilst the N-terminus binds to anchoring protein eEF1Bγ. Indeed the N-terminal section may actually impede the GDP exchange activity of eEF1Bα, at least in its interaction with eEF1A2 (73). There are reports of an intronless gene, *EEF1B3*, transcribed only in brain and muscle in humans (56,74).

1.3.3 eEF1Bδ

The other guanine exchange factor eEF1Bδ (encoded by *EEF1D*) is similar to eEF1Bα. The two share a high level of similarity in their C-terminals, where the GDP exchange activity is controlled (75). Although the N-terminal of eEF1Bδ still binds to eEF1Bγ (76), the sequence varies from that of eEF1Bα (77). This divergence in sequence enables the N-terminal of eEF1Bδ to bind to Valyl tRNA

synthetase (discussed in 1.3.4) (78). Alternative splicing of the *EEF1D* gene provides 3-4 translated proteins. Three proteins around 38kDa appear to be expressed ubiquitously. A fourth isoform has been reported in brain and testes. This isoform is considerably larger, encoding the complete sequence of the previous 3 isoforms, with an extended 367 amino acid N-terminus which includes a nuclear localisation signal (71,79,80). This isoform, termed eEF1BδL is expressed in both the cytoplasm and the nucleus. During stress the isoform functions as a transcription factor for heat shock elements. Upon heat shock, the canonical isoforms are down-regulated to stop translation, and eEF1BδL is upregulated for heat shock element transcription (79). It is not yet clear whether eEF1BδL participates in the eEF1B complex in the same way as the shorter isoforms to contribute to translation. Kaitsuka and colleagues created an eEF1BδL knock-out mouse model and saw an increased performance in protein synthesis, which they argued suggested eEF1BδL inhibited protein synthesis. Further investigation into this would be interesting and is discussed in 3.5.2.

1.3.4 eEF1Bγ

Structural anchoring protein eEF1Bγ (*EEF1G* gene) has no guanine exchange activity itself, instead providing two binding sites for eEF1Bα and eEF1Bδ (81).The N-terminal of eEF1Bγ has been associated with tubulin, keratin and the endoplasmic reticulum, in keeping with its role in the as an anchoring protein (82–84).

1.3.5 Valyl tRNA synthetase

Although not a component of the eEF1B subunit, Valyl tRNA synthetase (ValRs) has been associated with the eEF1B complex in mammals and higher eukaryotes (85). ValRs is responsible for synthesising the aminoacylation of valine-tRNAs. It has been proposed that its association with eEF1B is due to the amino-acid channelling hypothesis, a principle by which the components of translation are ‘streamlined’ to the ribosome to reduce non-specific interactions in cytoplasm and optimise protein synthesis (86).

1.4. Translation and neurological disorders

1.4.1 Neurons display a high requirement for protein synthesis

The brain has a high metabolic requirement owing to its dynamic and active environment. Neurons also require a greater spatial and temporal control of protein synthesis than other cells. Neurons must modulate specific synapses in response to stimulation and require a timely translational response. With these cells reaching up to a metre from synapse to soma in humans, the transport of proteins from the cell body would not be sustainable for immediate response to synaptic stimuli. The answer to the above issues is local protein synthesis. It is not surprising that even slight disturbances in protein synthesis could disproportionately affect neurons over other cell types and result in neurological disorders.

1.4.2 Translation initiation and neurological disorders

Initiation, the first stage of translation, is the phase most implicated in neurological disorders. Notable targets include eIF2α, eIF4G and eIF4B. Phosphorylation of eIF2α inhibits protein synthesis (87). eIF2α, its cognate guanine exchange factor eIF2β, and associated kinases have all been associated with neurodegenerative diseases including Alzheimer's disease and vanishing white matter syndrome (88–90).

In terms of neurodevelopmental disorders, one of the most well-known to affect translation initiation is fragile X syndrome (FXS). FXS is the leading inherited cause of intellectual disability (91). A trinucleotide amplification of over 200 CGG repeats in the 5'UTR of the *FMR1* gene results in a functional null copy of protein fragile X mental retardation protein (FMRP) (92). FMRP normally binds to initiation factor complex eIF4F, repressing translation in favour of actin bundling. When FMRP is lacking, an increase in 15-20% of protein synthesis is seen in hippocampal neurons (93). This redistribution of initiation factor activity results in irregular synapse function and morphology (94).

Elongation factor eEF1A has also been associated with FMRP. Sung and colleagues determined that Xenopus FMRP directly interacted with EF-1A (the Xenopus equivalent of eEF1A) and negatively regulated the expression (95). Tsai and colleagues also found that in the absence of FMRP, eEF1A bound to E3 ubiquitin-ligase protein MDM2. Under normal conditions MDM2 is responsible for post-synaptic density 95 (PSD-95) ubiquitination. Ubiquitinated PSD-95 is then transported to the proteasome and synapse elimination occurs. However, when eEF1A interacts with MDM2, PSD-95 is no longer ubiquitinated and the synapse is maintained (96). Synaptic pruning is key to healthy neuronal development, and too many synapses are associated with neurodevelopmental disorders such as Autism and possibly FXS (97,98). It has also been suggested FMRP might bind directly to the RPL5 subunit of the 80S ribosome, potentially inhibiting interaction of eEF1A during translation elongation (99). Therefore, even in disorders primarily affecting translation initiation, eEF1A may be an interacting component.

1.4.3 Translation elongation and neurological disorders

There is growing evidence that elongation factors are playing a role in both neurodevelopmental and neurodegenerative disorders. As with initiation, balanced translation elongation is key to optimal neuron performance. Mutations in gene *EEF2* have been reported in individuals with spinocerebellar ataxia (100). eEF1A expression dysregulation has also been reported in Alzheimer's and Parkinson's diseases. $A\beta_{42}$ treatment of hippocampal slices reduced eEF1A expression. Further, $A\beta_{42}$-mediated LTP reduction was rescued with eEF1A treatment (101). eEF1A was implicated to have a role in aggresome formation following ubiquitin proteasome system upregulation. There are strong links between aggresome and aggregated protein inclusions, such as Lewy Bodies, in Parkinson's disease (37). Given the age of onset, it is assumed the isoform implicated in these conditions would be eEF1A2. The role of eEF1A2 in neurodegeneration is discussed in more detail in Section 1.5.1.

Recent evidence has identified mutations in genes coding for translation elongation factors in individuals with neurodevelopmental disorders. eEF1A2 is the most reported, with over 50 individuals, as discussed in detail in 1.5.2.

Genomic sequencing of individuals with neurodevelopmental disorders, including intellectual disability and microcephaly, has identified homozygous mutations in subunits of the eEF1B complex. Table 1.2 summarises the mutations discovered and condition of the affected individual(s).

Table 1.2: Mutations in subunits of the eEF1B complex resulting in neurodevelopmental disorders

Gene	Mutation	Clinical Features	Reference
EEF1B2	chr2:206734676-206738530del3855	Moderate intellectual disability	(102)
EEF1D	Glu24Serfs*26	Severe intellectual disability, microcephaly	(103)
EEF1D	p.Trp316*	Global developmental delay, intellectual disability and epilepsy	(104)
VARS	L885F	Severe intellectual disability, seizures, microcephaly and cortical atrophy	(105)
VARS	R1058Q	Severe intellectual disability, seizures, microcephaly and cortical atrophy	(105)

Elongation factors had not, until recently, been identified as causative genetic variants in neurodevelopmental conditions. Several components of the eEF1B complex have been implicated.

Mapping of mutation Glu24Sers*26 on *EEF1D* gene demonstrates that this truncation appears to affect only the longer isoform eEF1BδL, which is expressed in brain and testes. eEF1BδL contains an identical C-terminal to the ubiquitously expressed shorter isoforms, where all the guanine exchange factor activity is, but

contains an additional N-terminal nuclear localisation sequence. This additional sequence allows eEF1BδL to function as a transcription factor for heat shock proteins. It is not clear whether this alternative function is in addition, or instead of, the role in eEF1A GDP exchange. The mutation causes a truncation which would ablate both functions. Dysregulation of both protein synthesis and heat shock mediated recovery have been associated with neurological disorders previously. Further evidence associating eEF1BδL in neurodevelopmental disorders has recently been published. Mutation p.Trp316* was reported in three siblings with severe neurodevelopmental disorder and epilepsy. The authors report that this mutation also lay within the neuronal specific eEF1BδL alternative splice product.

A deletion on chromosome 2, which included most of *EEF1B2*, resulted in a similar intellectual disability phenotype (102). *EEF1B2* is not a neuronal specific isoform; therefore, it is surprising that the clinical features are so specifically neuronal. *VARS* mutations also resulted in a similar neuronal specific phenotype, despite ubiquitous expression. The *VARS* and *EEF1B2* evidence supports the hypothesis that neurons are more sensitive to protein synthesis disturbances than other cell types.

VARS mutations join a growing number of mutations to amino-acyl tRNA synthetase genes which result in neurodevelopmental and neurodegenerative disorders. One of the most commonly reported conditions is the neuropathic disorder Charcot-Marie-Tooth disease, which has been reported in individuals with mutations in *AARS*, *GARS*, *HARS*, *KARS*, *MARS* and *YARS* (106). Table 1.3 summarises some of the other research into ARS mutations reviewed and summarised in (87).

Table 1.3: Aminoacyl synthetase genes with mutations reported to cause neurological disorders.

Gene	Condition	Reference
AARS	Microcephaly, epilepsy and spasticity	(107)
	Epileptic encephalopathy with peripheral neuropathy	(108)
DARS	Leukoencephalopathy, hypomyelination in brain stem and spinal cord, and spasticity	(109)
HARS	Usher syndrome	(110)
KARS	Charcot-Marie-Tooth disease	(111)
RARS	Hypomyelination with plasticity	(112)
YARS	Developmental delay, liver dysfunction, lung cysts, abnormal subcortical white matter and general failure to thrive	(113)
QARS	Early onset encephalopathy	(114)
	Progressive microcephaly and epilepsy	(115)

Although ARS mutations are reported to affect other tissues, the CNS appears to be the most implicated system, despite ubiquitous expression of ARS genes. There are several possibilities for this phenomenon. 1) As discussed before, neurons have a higher metabolic requirement than other cells and are therefore more sensitive to disruption. 2) An ARS mutation might affect the expression profile in a cell-type specific manner, possibly in a codon-dependent manner (106). 3) The expression profile of certain tRNAs have been shown to be up-regulated in central nervous system (CNS) tissues over other cell types. Mutations in the corresponding ARS gene would therefore disproportionately affect synthetase activity in these cells (106,116). 4) Tissue specific alternative splicing of tRNA synthetases for non-catalytic functions has been reported (117). If mutations are in alterative spliced products which are only present in neurons this could explain why cases present as with specifically neurological deficits. Any or a combination of these factors could explain the CNS specific pattern of clinical symptoms in ARS gene mutations.

1.5 eEF1A2 and neurological disorders

1.5.1 eEF1A2 and neurodegeneration

eEF1A2 was first associated with neurodegeneration when a spontaneous 15kb deletion on chromosome 2 occurred in mice in the Jackson laboratories. This deletion included the promoter for the *Eef1a2* gene and resulted in no expression of eEF1A2 mRNA. Subsequent interbreeding resulted in a homozygous genetic null mouse, *Eef1a2*$^{-/-}$. At P21 in *Eef1a2*$^{-/-}$ mice, when eEF1A1 is down-regulated to undetectable levels, muscular and neurodegenerative symptoms (including gait problems, ataxia and weight loss) begin to appear, with death occurring by P28 (56). Newbery et al proved that the loss of *Eef1a2* was solely responsible for the phenotype. Expression of the *Eef1a2* gene in *Eef1a2*$^{-/-}$ mice rescued the phenotype (13). Expression of eEF1A2 in muscle only did not rescue this phenotype, demonstrating that the pathology is mediated primarily by neurodegeneration (118).

Molecular examination of *Eef1a2*$^{-/-}$ spinal cord revealed extensive damage to motor neurons and neuromuscular junctions. Whilst changes to motor skills are only visible from roughly p21 onwards, damage could be seen at the molecular level from day 17. An increase in glial fibrillary associated protein (GFAP), a marker of neuronal damage, was noticeable in spinal cord sections. Further, a decrease in innervation of motor endplates in skeletal muscle was observed. After this, muscular denervation occurred, progressing more caudally along the spinal cord with age (119). These molecular changes mimic changes seen in amyotrophic lateral sclerosis patients.

Unlike their homozygous littermates, heterozygous mice display no observable phenotype or molecular pathology when compared to WT mice. Even aged heterozygotes (one year to 21 months), displayed no discernible difference in molecular pathology or motor performance (120). This suggests the missense mutations in humans do not operate through haploinsufficiency in the main. However, aged heterozygous mice on the same genetic background as the *Eef1a2*$^{-/-}$ mice do display deficits in learning and memory compared to their WT

counterparts (121). Whilst there are no reported null mutations in patients, evidence from mice highlights the key role of eEF1A2 in maintenance and protection of neurons.

1.5.2 eEF1A2 and neurodevelopmental disorders

Recent exome sequencing has identified heterozygous *de novo* missense mutations in *EEF1A2*. Individuals with these mutations all present with intellectual disability often concomitantly with autism and epilepsy. Table 1.4 details the reported cases of eEF1A2 mutations, with variant pathogenicity predictions. Unless otherwise stated, all mutations are heterozygous *de novo* missense mutations. Reports of seizures and developmental delay are often reported from infancy. Often children are born with statistically small head circumference, suggesting prenatal developmental growth may be impaired.

All mutations are at residues which are conserved, both in eEF1A1 and yeast. The *EEF1A2* gene is in the top 5% of constrained genes according to the Exome Aggregation Consortium (ExAc) database, suggesting it does not tolerate polymorphisms as they would affect mutations. Modelling analysis shows mutations cluster upon the 'conserved face' near functional sites including eEF1B and GTP binding sites (see Figure 1.5).

Whilst most reported mutations are heterozygous and *de novo*, there has been one published case of inheritance of a mutation. The reported two children who died in infancy were both homozygous for the mutation P333L. Neither parent has officially been diagnosed with a neurodevelopmental disorder, although the father has three other children with a different partner, all which have been diagnosed with developmental disorders. This report suggests that in a heterozygous form, the mutation is mild. The inherited homozygosity, however, led to extreme epileptic seizures and death caused by dilated cardiomyopathy. The death of these children associates with a time roughly where RNAseq data (Figure 1.2 (15)) suggests eEF1A1 expression would have likely subsided, although this has not been formally tested (122).

Clinical presentation varies between patients (summarised in table 1.4). Some individuals have a clinically mild presentation. The heterozygous parents in the P333L case do not present as severely affected (122). One of the patients with the E124K mutation attended mainstream primary school (123). Other individuals

have severe epilepsy, and developmental delay severe enough to impede head support. It is unclear, however, how much of this range is due to varying levels of mosaicism between individuals (although it is speculated to be low), or if mutations impact upon protein function to varying degrees. The first line of evidence would be to compare severity between individuals with the same mutation. As the numbers of cases in some mutations increase, this is becoming possible (G70S and E122K), but for the majority, mutations are still individual cases. Even in the cases with the same reported mutation, variation in reports from clinicians and available information is likely to cause issue with clear conclusions.

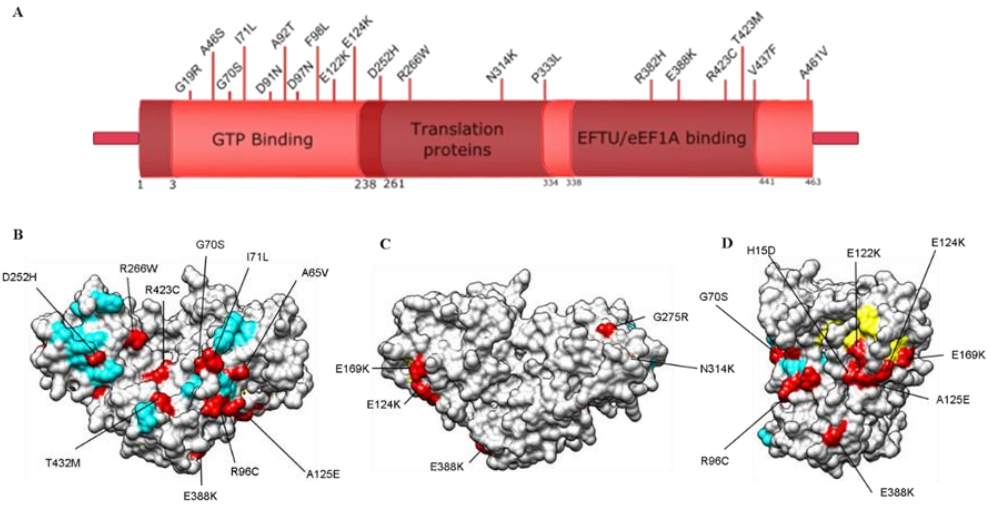

Figure 1.5: Depictions of mutation distribution in eEF1A2 protein. A*, a schematic diagram of the distribution of published mutations and their location relative to protein domains of eEF1A, as defined by Pfam.* ***B-D****, 3D modelling of the eEF1A2 protein – the crystal structure of which was determined by X-ray diffraction (23). Cyan residues show binding sites of eEF1B as defined in the yeast model. Yellow sites show GTP-binding area, and red demonstrates mutations (published and unpublished). The protein is displayed showing the "conserved face" (**B**), the "variable face" (**C**) and the GTP binding area (**D**). Information on protein structure was obtained from Protein Data Bank and modelled using Chimera program.*

Table 1.4: Summary of clinical presentations of eEF1A2 missense mutations. *Mutations are reported with known symptoms, a summary of other features and a collection of prediction software. * indicates it is identified as a causative variant. – indicates data was not available.*

Mutation		Number of cases	Epilepsy	Intellectual disability/Developmental delay	Autism	Head size/ cerebral imaging	Other notes	Variant predictions				Reference
cDNA	Protein							S	P2	MT	LRT	
c.55G>A	G19R	1	Yes	-	-	-	-	*	*	*	*	(124)
c.71C>T	T24M	1	Yes	No	No	-	Verbal	*	*	*		(125)
c.208G>A	G70S	6	Yes	Yes	No	Head circumference in the 91st percentile at 9 months	Hypotonia and dysphagia	*	*	*	*	(123)
			Yes	Yes	Yes	Normal head circumference at 22 years.	Walk independently from age 6					(126)
			Yes	Yes	No	Microcephaly PET scan: hypometabolism left temporal and parietal lobes						(127)
c.211A>C	I71L	1	Yes	Yes	-	Head circumference > 25 centile at age 5	Did not walk until 5 years old.	*	*	*	*	(123)
c.271G>A	D91N	2	Yes	Yes	No	8.75 years was 51.5 cm (<50th centile)	Non-verbal and cannot walk independently	*	*	*	*	(123)
			Yes	Yes	-	-	Mosaic					DDD

c.274G>A	A92T	1	Yes	Yes	Yes	Generalised cerebral atrophy	Rett syndrome-like clinical presentation	*	*	*	*	(128)
c.289G>A	D97N	1	No	Yes	Yes	-	-	*	*	*	*	DDD
c.292T>C	F98L	1	Yes	Yes	No	50 cm at 6 years, >2nd percentile	Cannot sustain head. Non-verbal.	*		*	*	(123)
c.364G>A	E122K	6	Yes	Yes	No	head circumference below the 2nd centile	Non-verbal but uses sign language. Prominent facial features.	*	*	*	*	(123)
			Yes	Yes	Yes	-	Overlapping toe					DDD
			Yes	Yes	No	-	Distinct facial characteristics, short stature, delayed puberty					DDD
			Yes	Yes	Yes	Mild atrophy of the cerebrum, especially cortex	Walking independently aged 8.					(129)
			Yes	Yes	No	MRI normal at 10 months	Characteristic facial features,					(130)
			Yes	Yes	No	1 year 9 months revealed cerebral atrophy	Characteristic facial features					(130)
c.370G>A	E124K	2	Yes	Mild/moderate		51 cm at 5.2 years (25th centile)	Verbal and attended mainstream school.	*		*		(123)
			No	Yes	No	Multifocal cerebral white matter abnormalities	-					DDD

c.505G>A	E169K	2	Yes	Yes	No	-	Maternally inherited	*	*	*	*	DDD
			Yes	Yes	No	-	Maternally inherited					DDD
c.754G>A	D252H	2	Yes	Yes	Yes	48.2 cm head circumference at age 8.	Distinct facial characteristics	*	*	*	*	(129)
			Yes	Yes	-	-						DDD
c.796C>T	R266W	4	Yes	Yes	No	Diffuse cerebellar and cerebral atrophy. Microcephaly	Distinct facial characteristics	*	*	*	*	DDD
			No	Yes	No	Postnatal microcephaly	Distinct facial characteristics, overlapping toe, tapered finger.					DDD
c.942C>G	N314K	1	-	Yes	-	-	-	*	*	*		(131)
c.1164C>T	P333L	2	Yes (homozygous)	Yes (homozygous)	No (homozygous)	MRI normal	Homozygous inherited. Cardiac myopathy, resulting in death by 3 years.	*	*	*		(122)
c.1145G>A	R382H	1	Yes	Yes	Yes	-	-	*		*	*	(132)
c.1267C>T	R423C	2	Yes	Yes	No	Mild hypoplasia of corpus callosum and mild global volume loss (which is progressive with time)	Non-verbal and cannot walk.	*		*		(123)
			Yes	-	-	-	-					(133)

c.1295C>T	T432M	1	No	Yes	No	-	Ventricular septal defect	*	*	*		DDD

1.6: Project Aims

The aim of this project was to help in understanding the mechanism by which eEF1A2 mutations act and their role in epilepsy, autism and intellectual disability. More specifically, I aimed to assess whether mutations operated through a dominant negative, gain or loss of function mechanism, and what molecular functions were impacted.

It was imperative to determine the type of mechanism missense mutations cause. Mutation consequence is key to an effective treatment strategy. Mutations which cause a gain or loss of function to the same protein can have differential results for the same drug treatment (134). Secondly, gain of function mutations are more likely to be treatable with drug treatments (135), whilst functional null proteins may be more reliant on gene therapy for a solution. It is also not as simple as just treating using gene therapy of eEF1A2 to compensate for mutant proteins; if proteins work in a dominant negative manner, the application of drugs to up-regulate endogenous eEF1A2 may exacerbate the phenotype.

Using a variety of *in vivo* and *in vitro* techniques to assess eEF1A2 missense mutations, I investigated this aim. Initially, to gain an overall impression of the consequences of mutations, I assessed how protein interactions were altered in mutant forms of eEF1A2. Any gain of loss of binding may reveal a dominant negative, gain or loss of function. I aimed to explore the interaction disruptions, validate disruptions and investigate the functional consequences, with a view to understanding how eEF1A2 mutations impact upon protein function.

Chapter 2: Materials and Methods

2.1 Materials

2.1.1 Cell culture

Table 2.1: Cell lines used in thesis.

Cell Line	Species	Cell type	eEF1A isoform expression
HEK293T	Human	Embryonic Kidney	eEF1A1
SH-SY5Y	Human	Neuroblastoma	eEF1A1 + eEF1A2
LUHMES	Human	Foetal mesencephalon	eEF1A1 + eEF1A2

2.1.2 Primers and DNA oligomers

2.1.2.1 CRISPR/Cas9 in LUHMES cells

Table 2.2: All primer sequences for attempt at introducing the G70S mutation into EEF1A2 gene in LUHMES cells using CRISPR/cas9 *(designed by myself and Faith Davies).*

G70S CRISPR guides	
Guide A top	5’- CACCGCTTCAGCTTGTCCAGCACCC -3’
Guide A bottom	5’- AAACGGGTGCTGGACAAGCTGAAGC -3’
Guide B top	5’- CACCGCTGAAGGCGGAGCGTGAGCG -3’
Guide B bottom	5’- AAACCGCTCACGCTCCGCCTTCAGC -3’
gRNA sequencing primer	
Forward	5’-GAGGCCTATTTCCCATGATTCC-3’
G70S PCR primers	
Forward Primer	5’-TGGTTGAGGAAGGGATCTGG-3’
Reverse Primer	5’- TGTGTCCACGTCCCCATC-3’
G70S Sequencing primers	
Forward Primer	5’-GTTTATCCCATCTGGCGGCT-3’
Reverse Primer	5’-ACTCTGACACTGGCTGGAT-3’

Table 2.3: All primer sequences for attempt at introducing the G70S mutation into EEF1A2 gene in LUHMES cells using CRISPR/cas9 (designed by Faith Davies).

D252H CRISPR guides	
Guide A top	5'-CACCGGCTTGTCCGTGGGGCGCGTG-3'
Guide A bottom	5'-AAACCACGCGCCCCACGGACAAGCC-3'
Guide B top	5'-CACCGCAGGACGTGTACAAGATTGG-3'
Guide B bottom	5'- AAACCCAATCTTGTACACGTCCTGC-3'
gRNA sequencing primer	
Forward	5'-GAGGCCTATTTCCCATGATTCC-3'
D252H PCR primers	
Forward Primer	5'-TTCCTCATCTCAAAGGGCACG-3'
Reverse Primer	5'-CAAGTTTAGCCTGAACAGCAGTA-3'
D252H sequencing primers	
Forward Primer	5'-CCCACAGAAGTGTGTGGTAAG-3'
Reverse Primer	5'-TTGGAGACAGCCAGTCTTG-3'

Table 2.4: Repair template constructs for homology directed repair of CRIPSR/cas9 mutations in LUHMES cells *(designed by Faith Davies).*

Genotype	Repair Template 5' – 3'
G70S	GTCCCGCCCTCAGCCGTGACCCTCACCCGCTCCAGATGGG GAAGGGATCCTTCAAGTATGCCTGGGTGCTGGACAAGCT GAAGGCGGAGCGTGAGCGC**G**GCATCACCATCGACATCTC CCTCTGGAAGTTCGAGACCACCAAGTACTACATCACCATC ATCGATGCCCCCGGCCACCACCGCGACTTCATCAAGAAC ATGATC
D252H	AAGGAAGGAACAAGCGGCGTGTCCCTGCTGGAAGCC CTGGACACAATCCTGCCCCCCACCCGCCCCACCGAC AAGCCCCTTCGTCTACTGCAG**G**ATGTATACAAGATT GGTGTGAGTGAGAATTCAGTGCGGAGCTCACTGCTT CCTGCAGGTTGAGCGTGCCCCAAACCTTGACCAGGA CATCAA

2.1.2.2 Site Directed Mutagenesis primers

Table 2.5: Site directed mutagenesis primers for introduction of missense mutations into eEF1A2-V5 construct.

D91N	
SDM Forward Primer	5'-GGCCGGGGCATTGATGATGGTGATGTAGT-3'
SDM Reverse Primer	5'-ACTACATCACCATCATCAATGCCCCCGGCC-3'
E124K	
SDM Forward Primer	5'-GAGATGCCCGCCTTGAACTCGCCCAGCG-3'
SDM Reverse Primer	5'-CGTGGGCGAGTTCAAGGCGGGCATCTC-3'
Sequencing Primer	
D91N	5'-CACACAACATCGTGGTCATCGGCCACG-3'
E124K	5'-CACCATCATCGATGCCCCCG-3'

2.1.2.3 Genotyping

2.1.2.3.1 *Eef1a2*/D252H genotyping primers

Table 2.6: Primers for genotyping Eef1a2/D252H mouse line.

Primer	Sequence
Forward	5'-AGGCTACCCCTTAGGCAGGT-3'
Reverse	5'-TGAACAAATGGTAGGTGGGAGG-3'

2.1.2.3.2 *Eef1a2*/del22ex3 genotyping primers

Table 2.7: Primers for genotyping Eef1a2/del22ex3 mouse line.

Primer	Sequence
Forward	5'-TGAGTTGTGCCTCTACCCTT-3'
Reverse	5'-TACAGGCACATCCCAGGTGT-3'

2.1.2.3.3 *Eef1a2*/wst genotyping primers

Table 2.8: Primers for genotyping Eef1a2/wst mouse line.

Primer	Sequence
WT allele Forward	5'-TAGTGGCTCCTTGGAACAG-3'
WT allele Reverse	5'-CTACTCTCCCTGAATGCCTT-3'
Wasted allele Forward	5'-ATAAGCTCCCCAATGGTAGAGAA-3'
Wasted allele Reverse	5'-CGCGCCATTCTTGTATTGTT-3'

2.1.2.4 RT-PCR and qPCR of eEF1A2 mRNA

Table 2.9: Primers for eEF1A2 mRNA quantification.

Primer	Sequence
eEF1A2 exon 7-8 Forward	5'-CCCACATCAACATCGTGGTC-3'
eEF1A2 exon 7-8 Reverse	5'-CTCCACGTTCTTGATGACGC-3'
eEF1A2 exon 3 Forward	5'-ACATGATCACGGGTACATCCC-3'
eEF1A2 exon 3 Reverse	5'- CATTTGTTCACGCCCCACGA-3'
TOP1 forward	5'-GTCAGCGTTCTACCAGGCAA-3'
TOP1 Reverse	5'-TGACGACTCTAACAGGTGCG-3'
RPL34 Forward	5'-CCTTTGAGCTGGTGTAGGGG-3'
RPL34 Reverse	5'-AGGTCTTACAGCACGAACCC-3'

2.1.3 Buffers and solutions

2.1.3.1 RIPA buffer

Table 2.10: RIPA buffer composition. *1 Complete Protease inhibitor tablet (Roche) added to every 10ml of RIPA buffer directly before use.*

Reagent	Concentration
Sodium Chloride	150mM
NP-40	1% (v/v)
Sodium Deoxycholate	0.5% (w/v)
SDS	0.1% (v/v)
Tris-HCl (pH8.0)	50mM

2.1.3.2 Trypsin working reagent

Table 2.11: Solution for trypsin digestion of proteins after affinity purification and prior to mass spectrometry

Reagent	Concentration
Trypsin Protease (Pierce, MS grade)	42.9mM
1M DTT	1mM
UREA	2M
1.5M Tris pH8	50mM
MS grade ddH_2O	-

2.1.3.3 Laemmeli buffer

2.1.3.3.1 2X Laemmeli buffer

Table 2.12: Recipe for 2X Laemmeli Buffer used in preparation of protein extracts for western blotting.

Reagent	Concentration
SDS	10% (w/v)
Glycerol	20%
1M Tris-HCl (pH6.8)	120mM
Bromophenol Blue	0.02% (w/v)
H_2O	-

2.1.3.4 Stripping buffer

Table 2.13: Recipe for stripping buffer used in re-probing of western blot membranes*. After composition in H_2O, pH is adjusted to 2.2 before immediate use.*

Reagent	Concentration
1M Tris-HCl (pH6.8)	62.5mM
20% SDS	10% (v/v)
β-mercaptoethanol	0.7% (v/v)
H_2O	-

2.1.3.5 Artificial cerebrospinal fluid (aCSF) for AHA-click it chemistry experiments

Table 2.14: Recipe for HEPES buffered aCSF as described in (136)*. HEPES used as buffering agent. pH checked after making to ensure a pH of 7.8.*

Reagent	Concentration
Glucose	10mM
Sodium Chloride	136mM
Potassium Chloride	2.5mM
Magnesium Chloride	1.3mM
HEPES	10mM
Calcium Chloride	2mM
ddH_2O	-

2.1.3.6 6x DNA loading dye

Table 2.15: Composition of 6X DNA loading dye.

Reagent	Concentration
Bromophenol Blue	0.25%
Xylene cyanol FF	0.25%
Glycerol	30%
ddH_2O	-

2.1.4 Antibodies

2.1.4.1 Co-immunoprecipitation

Table 2.16: Antibodies used in co-immunoprecipitation

Antibody	Company/Product Number	Species	Concentration
GFP	Abcam	Goat	1:1000
eEF1A2	ProteinTech	Rabbit	1:250

2.1.4.2 Western blotting

2.1.4.2.1 Primary antibodies

Table 2.17: Primary antibodies used in western blotting. *The species, size, appropriate secondary method and dilution for respective sample type is reported.*

Antibody	Company/Product Number	Species	kDa	Sample type	Secondary	Dilution
GFP	Abcam	Goat	-	Co-IP cells	HRP	1:1000
eEF1A2	ProteinTech Group	Rabbit	52	Co-IP probe Tissues	Light Chain	1:100
				Western blot – cells/tissue	HRP/ LICOR	1:1000
eEF1Bα	ProteinTech Group	Rabbit	32	Probing Co-IP samples-cells	Light Chain/HRP	1:250
				Probing Co-IP samples-tissue	Light Chain	1:100
eEF1Bδ	ProteinTech Group	Rabbit	38	Probing Co-IP samples-cells	Light Chain/HRP	1:1000
				Probing Co-IP samples-tissue	Light Chain	1:500
eEF1Bγ	Abcam	Rabbit	50	Probing Co-IP samples-cells	Light Chain/HRP	1:1000
				Probing Co-IP samples-tissue	Light Chain	1:500
ValRS	St Johns Laboratory	Rabbit	140	Probing Co-IP	Light Chain/HRP	1:250

				samples -cells		
RPL28	Abnova	Rabbit	16	Probing Co-IP samples -cells	Light Chain/HRP	1:500
RPLPO	Proteintech Group	Rabbit	30	Probing Co-IP samples -cells	Light Chain/HRP	1:500
RPS14	Avivasysbio	Rabbit	17	Probing Co-IP samples -cells	Light Chain/HRP	1:500
eEF1A1	Purified in Lab by Helen Newbery	Goat	52	Probing Co-IP samples -cells	HRP	1:500
V5	Invitrogen	Mouse	-	Probing Co-IP samples -cells	Light Chain	1:1000
				Cells extracts	HRP/LICOR	1:5000
Puromycin	Millipore (12D10)	Mouse	10-150	Cell extracts	HRP/LICOR	1:1000
				Tissue extracts	IgG2a-HRP	1:1000

2.1.4.2.2 Secondary antibodies

Table 2.18: Western blot secondary antibodies used throughout project.

Name	Company	Target Species	Species raised	Conjugate	Dilution
IR Dye 680RD Anti-rabbit	LI-COR	Rabbit	Goat	Fluorescent	1:5000
IRDye 800CW Anti-mouse	LI-COR	Mouse	Donkey	Fluorescent	1:5000

IRDye 800CW Anti-goat	LI-COR	Goat	Donkey	Fluorescent	1:5000
Polyclonal anti-goat	DAKO	Goat	Rabbit	HRP	1:1000
Polyclonal anti-rabbit	CST	Rabbit	Goat	HRP	1:1000
Polyclonal anti-mouse	DAKO	Mouse	Goat	HRP	1:1000
IgG2a anti-mouse	Jackson ImmunoResearch Laboratories Inc	Mouse	Rabbit	HRP	1:1000
Anti-rabbit light chain	Abcam	Rabbit	Mouse	HRP	1:1000
Anti-mouse light chain	DAKO	Mouse	Donkey	HRP	1:1000

2.1.4.3 Immunocytochemistry

2.1.4.3.1 Primary antibodies

Table 2.19: Primary antibodies used in immunocytochemistry.

Antibody	Company	Species	Concentration
EEF1A2	ProteinTech Group	Rabbit	1:500
V5	Invitrogen	Mouse	1:2000
Puromycin	Millipore (12D10)	Mouse	1:1000

2.1.4.3.2 Secondary antibodies

Table 2.20: Immunocytochemistry secondary antibodies.

Antibody	Company	Target	Fluorescent excitation /emission	Concentration
Donkey Anti Goat 488	AlexaFlour	Goat	490/525	1:500
Goat Anti-Rabbit 488	AlexaFlour	Rabbit	490/525	1:500

Donkey Anti-Rabbit 594	AlexaFlour	Rabbit	561/594	1:500
Goat Anti-mouse 654	AlexaFlour	Mouse	633/647	1:500

2.2 Methods

2.2.1 Cell culture

Cell lines used for experiments have been summarised in table 2.1. All lines were incubated at 37^{o}C and 5% CO_2. Passaging was achieved by applying TryplE express (Life Technologies) to cells and incubating at 37^{o}C for 1 minute. PBS was then added to wash cells. The cell suspension was spun at 1200 rpm for 5 minutes to cause pellet formation. Cells were then seeded at the appropriate density for experiment.

For freezing, cells were pelleted as above, and pellets resuspended in freezing media. Freezing media was prepared using respective media for each cell with 20% Foetal Calf Serum (FCS) and 10% DMSO in cryotubes. Tubes were stored in a freezing container with isopropanol for 1 hour at -20^{o}C and then -80^{o}C until transfer into liquid nitrogen storage.

2.2.1.1 HEK293T and SH-SY5Y cells

HEK293T and SH-SY5Y cells were maintained in DMEM (Gibco) + 10% FCS. Cells were passaged when confluent and passage number maintained under 20. Cells were seeded at appropriate densities for transfection in plates/wells of appropriate size for the experiment.

2.2.1.2 LUHMES

2.2.1.2.1 Proliferative state

LUHMES cells were grown in proliferative state, allowing stocks to be generated and maintained as well as perform experiments. To allow cell adhesion, plates and flasks for LUHMES culture were coated using ddH_2O with 50µg/ml poly-L-ornithine (PLO) (Sigma Aldrich) and 1 µg/ml fibronectin (GE healthcare). Coating solution was added, and flasks incubated between 3 and 18 hours at 37^{o}C. Flasks were then washed with sterile filtered ddH_2O and dried using an aspirator. Proliferative media (described below) was added to flasks and re-incubated for 1-2 hours.

Proliferative media was composed of Advanced DMEM/F12 (Gibco) with additions below. Advanced DMEM/F12 (Gibco) is warmed to 37ºC before additives were supplemented. Media was sterile filtered using a 0.22µm syringe (Millipore).

Reagent	Company	Concentration
N2 supplement	Life technologies	1% (v/v)
FGF	Biolegend	40ng/ml(w/v)
L-Glutamax	Thermo Fisher	1% (v/v) (200mM stock)

Cells were seeded in prepared flasks/plates and left to proliferate. Passage number was maintained under p15.

2.2.1.2.2 Differentiated state

Using the tetracycline induction system, LUHMES cells could be differentiated to dopaminergic neurons according to the protocol described by Scholz and colleagues (137). T75 or T25 flasks were coated as described in 2.2.1.2.1. Proliferation media was applied to flasks and heated at 37ºC for 1 hour. Cells were then seeded in flasks and incubated for 24 hours. Media was then exchanged for differentiation media (below). Differentiation media was prepared in Advanced DMEM/F12 (Gibco) and sterile filtered as above. Cells were left for 48 hours in differentiation media.

Reagent	Company	Concentration
N2 supplement	Life technologies	1% (v/v)
FGF	Biolegend	40ng/ml(w/v)
L-Glutamax	Thermo Fisher	1% (v/v) (200mM stock)
GDNF	R & D	20ng/ml
cAMP	Sigma	1mM
Tetracycline	Sigma	1µg/ml

In instances where cells were to be grown on coverslips, slips were prepared by acid coating for 48 hours in 1M HCL. Acid was removed and slips washed in running water for 25 minutes. Slips were stored in 70% ethanol solution and washed in ddH_2O just prior to use.

To prepare for re-seeding of differentiated cells, plates/coverslips/wells were prepared as previously with an additional Geltrex (ThermoFisher) incubation. After 3 hours of PLO/Fibronectin coating, plates/coverslips/wells were washed with sterile filtered ddH_2O and dried. Geltrex (Thermo Fisher) was added to sterile filtered Advanced DMEM/F12 (Gibco) at a concentration of 1:500. The solution was immediately added to plates/slips/wells and incubated at 37^oC for between 3 and 16 hours. The plates/slips/wells were then removed from the incubator and allowed to adjust to room temperature. Plates/slips/wells were washed with sterile filtered advanced DMEM/F12 (Gibco) and had differentiation media added. After a further 1-hour incubation at 37^oC, plates/slips/wells were ready for re-seeding. Cells were trypsinised and spun at 500 rpm for 9 minutes. Cells were counted using Cellometer Vision (Nexcelom) and re-seeded at a density of $1.3x10^5$ cells/cm^2 or $7.5x10^4$cells/cm^2 for coverslips. After this, cells were left to differentiate in incubator for 12 days, with half of the differentiation media replaced with fresh differentiation media every 48 hours.

2.2.2 gRNA cloning

2.2.2.1 gRNA design and cloning

Two rounds of CRISPR were designed and performed by Faith Davies and myself; The first round targeted exon 3 to produce the G70S mutation, whilst the latter targeted exon 5 to generate the D252H mutation. In both instances, nickase CRISPR/Cas9 engineering was used to increase the chance of homology directed repair (138). In both experiments one gRNA of each pair was cloned into pSpCas9n(BB)-2A-Puro (px462) and the other into pSpCas9n(BB)-2A-GFP (px461). Oligonucleotides were designed using the Zhang lab CRISPR design programme (https://zlab.bio/guide-design-resources) and are reported in tables 2.2 and 2.3. Oligonucleotides were phosphorylated and annealed, to create a

double a double stranded fragment for ligation in plasmids. Phosphorylation mixture was made as below:

Reagent	Company	Volume (µl)
sgRNA top (100µM)	Sigma Aldrich	1
sgRNA bottom (100µM)	Sigma Aldrich	1
T4 ligation buffer, 10x	NEB	1
T4 polynucleotide kinase	NEB	1
ddH_2O	-	6

The mixture was incubated in a Bio-Rad thermocycler at 37ºC for 30 minutes, 95ºC for 5 mins and then cooled to 25ºC at a rate of 5ºC per minute. The solution was diluted 1:200 in ddH_2O and the ligation reaction performed, one gRNA for each pair being cloned into PX461 and PX462.

Reagent		Volume (µl)
Diluted oligo duplex	-	2
Plasmid, 100ng	-	1
T4 DNA ligase HC	NEB	0.5
Tango buffer 10x	NEB	2
ATP 10mM	-	1
DTT 10mM	-	1
FastDigest Bbs1	Thermo Fisher	1
ddH_2O		6

The mixture was incubated as below:

Temperature	Time	Cycles
37ºC	5 minutes	x5
21ºC	5 minutes	

After ligation, plasmid mixtures were treated with ATP-dependent DNase to remove residual linearised DNA. The mixture below was incubated at 37ºC for 30 minutes and 70ºC for 30 minutes. The reaction was then transformed.

Reagent	Company	Volume (µl)
Ligation reaction	-	11
PlasmidSafe Buffer	Epicentre	1.5
ATP, 10mM	-	1.5
PlasmidSafe endonuclease	Epicentre	1

2.2.2.2 Transformation of gRNA cloned plasmids

Ligated plasmids were transformed into DH5α cells (Life Technologies). 50µl tubes of cells were thawed on ice and 2µl of sample was added to each tube and samples incubated on ice for 20 minutes. Samples were heat shocked at 42ºC for 50 seconds, before further incubation on ice for 2 minutes. The samples were transferred to 500µl of SOC media and incubated at 37ºC and at 200rpm for 1 hour to allow antibiotic resistance generation. 50µl of sample was then spread on agar plates with 100ug/ml kanamycin antibiotic. Plates were sealed and incubated at 37ºC overnight. After colony formation, ~10 colonies per condition were picked. These were grown for 24 hours at 37ºC in L-broth with 100µg/ml kanamycin. Samples were sent for miniprep and sequencing by the Human Genetics Unit technical services centre. DNA was sequenced using U6 sequencing primer (table 2.2 and table 2.3).

2.2.3 Transfections

2.2.3.1 Transfection of SH-SY5Y and HEK293T cells

Transient transfection of constructs was performed in both SH-SY5Y and HEK293T cells. Cells were seeded 24-48 hours prior to transfection, at a density no greater than 50%. 16-24 hours prior to transfection, media was substituted for serum free DMEM (Gibco). Cells were further incubated at 37ºC and 5% CO_2. Relative volumes of Turbofect (ThermoFisher) was mixed with appropriate

concentrations of DNA in serum free DMEM, according to the manufacturer's instructions. Tubes were left for 15 to 20 minutes at room temperature and the mix was applied to cells. Cells were incubated for 48 hours prior to collection for protein extraction.

2.2.3.2 Transfection of LUHMES cells with gRNAs

Transfections of gRNAs were performed by Dr Faith Davies using basic primary neuron nucleofection kit (Lonza) and Lonza Nucleofector II™. The method of transfection had been optimised for LUHMES cells previously (139). Proliferative LUHMES cells were harvested and added to transfection tubes at a density of $1x10^6$. 100µl of nucleofector solution was prepared for each sample as per the manufacturer's instructions. 1µg of each gRNA in the pair was added to the solution, along with 2µl of 10µM of repair template (table 2.4). Electroporation of cells was done on program D-33. Cell suspensions were then transferred to 650µl of pre-warmed RPMI and incubated at 37°C for 5 minutes. The mixture was then transferred to one 6 well plate for each condition. In tandem, non-transfected and GFP-only controls were performed. Cells were incubated for 48 hours, prior to fluorescent associated cell sorting (FACS) analysis.

2.2.4 Creation of CRISPR/cas9 edited cell lines

2.2.4.1 FACS analysis of transfected LUHMES cells

As PX461 plasmid contains GFP coding sequence, uptake of gRNAs could be measured using FACS. Pre-coated 96 well plates (Co-star) were washed, dried and had proliferation media added. Transfected cells were trypsinised, spun at 500 rpm for 9 minutes and resuspended in sterile filtered PBS. FACS analysis was then performed using FACSJazz cell sorter (BD Biosciences) to sort fluorescent cells into individual wells of 96 well plate (Co-star). Cells were incubated for 14 days at 37°C.

2.2.4.2 Maintenance of cellular stocks, collection of genomic DNA and PCR analysis of genotypes

After 14 days of growth, single cell colonies were transferred to pre-coated 24 well plates. Cells were removed by pipetting up and down harshly. The cell suspension was transferred and left to grow for 48 hours. After confluency was achieved, cells were further transferred using standard trypsinolysis to a 6-well plate. After reaching confluence, cells were frozen and stored in liquid nitrogen. A small portion of cell pellet was isolated and stored at -20^{o}C for genomic DNA extraction. Genomic DNA was extracted using the Qiagen cell/tissue DNA extraction kit as per the manufacturer's instructions. Genotyping of lines was performed using the primers in tables 2.2 and 2.3, and the following reaction mix and cycling parameters.

Component	Company	Volume (µl)
Forward Primer (10µM)	Sigma	1
Reverse Primer (10µM)	Sigma	1
Superfi buffer 10X	Thermo Fisher	1
dNTPS(10mM)	Invitrogen	0.4
Betaine	-	4
Superfi-Taq	Thermo Fisher	0.2
ddH_2O	-	9.15
DNA	-	1

Temperature (^{o}C)	Time	Step/cycles
98	5 minutes	Initial denaturation
98	5 seconds	8 cycles
68^{o}C -1^{o}C each cycle	10 seconds	
72	10 seconds	

98	5 seconds	22 cycles
60	10 seconds	
72	10 seconds	
72	5 minutes	Final Extension
10	∞	Storage

Products were mixed with 6x DNA loading dye (table 2.12) run on a 1.5% agarose gel containing SYBR safe (Invitrogen) with 100bp ladder (NEB) at 120V for 1 hour and visualised.

2.2.4.3 Sequencing of CRISPR/cas9 LUHMES cell lines

PCR fragments generated above were cleaned using ExoSapIT (Affymetrix). 5µl of PCR reaction was mixed with 2µl of ExoSapIT and incubated at 37ºC for 15 minutes and 80ºC for 15 minutes. Sequencing was then performed using general sequencing protocol (2.2.5) using primers described in tables 2.2 and 2.3.

2.2.4.4 TOPO cloning PCR fragments generated for testing genotypes of mutant LUHMES cell lines

To identify the sequence of individual alleles, PCR fragments generated in 2.2.4.2 were TOPO cloned using the Zero Blunt TOPO cloning kit (Invitrogen). PCR fragments were generated and cleaned as in 2.2.4.2 and 2.2.4.3. Reaction mixes were made as below:

Reagent	Volume (µl)
PCR product	2.5
Salt Solution	1
Zero Blunt TOPO™	1
ddH_2O	1.5

Samples were incubated at room temperature for 5 minutes. 2µl of reaction was then applied to a vial of One Shot© competent cells (Thermo Fisher). Tubes

were incubated on ice for 25 minutes and transformed as in 2.2.2.2. Colonies were picked, grown and sequenced as in 2.2.2.2, using the sequencing primer provided by the manufacturer.

2.2.5 General Sequencing protocol

Sequencing PCR products and plasmids was achieved using BigDye, (ThermoFisher). Mixture reactions were set up as below and run on the following parameters on a Bio-Rad C1000 Touch Thermal Cycler.

Reagent	Volume (µl)
Primer 3.2µM	1.5
Big Dye	1
Big Dye Buffer	1.5
ddH_2O	4
PCR reaction	1

Temperature (°C)	Time	Step/Cycles
96	1 minute	Initial activation
98	10 seconds	x30 cycles
50	5 seconds	
60	4 minutes	
10	∞	Storage

Clean up of sequencing products was achieved by adding 1µl of 125mM EDTA, 1µl 3M sodium acetate and 25µl of ethanol to each sample. The reactions were inverted and left at room temperature for 15 minutes. Tubes were centrifuged at 10,000rpm for 20 minutes. Supernatant was removed and replaced with 30µl of 70% ethanol. Samples were further centrifuged for 10 minutes

before supernatant removed. Tubes were dried and stored at -20ºC before being read on a 3130 or 3730 Genetic Analyser (Applied Biosystems).

2.2.6 eEF1A2-V5 construct preparation

2.2.6.1 eEF1A2-V5 construct library

eEF1A2-V5 construct was created by Justyna Jankiewicz by cloning the eEF1A2 cDNA sequence in to the backbone of the pcDNA3.1-V5 vector (Invitrogen). I introduced the D91N and E124K mutations using the Quik Change II site directed mutagenesis kit (Aligent Technologies); other mutant constructs were made by other lab members. The manufacturer's instructions were followed using primers in table 2.5. After ligation of the mutant PCR construct, samples were transformed into DH5α cells (Life Technologies) as in protocol 2.2.2.2. Zeocin (Thermo Fisher) 50mg/ml was mixed 1:150 with melted L-agar and plates left to solidify.

After overnight incubation, three colonies per mutant condition were picked and were grown in 150µg/ml Zeocin (Thermo Fisher) 2ml L-broth for 24 hours at 37ºC and 200rpm. The cell suspension was spun at 3000rpm for 3 minutes and the supernatant removed. The pellet was miniprepped using a Qiagen miniprep kit according to the manufacturer's instructions. Constructs were sequenced to assess for evidence of the correct point mutation using standard sequencing protocol described in 2.2.5 and primers in table 2.5.

Once the correct mutation had been identified, the DNA was transformed into DH5α cells (Life Technologies) as in 2.2.2.2 and grown in 500ml L-broth + 150µg/ml zeocin for 24 hours. The cultures were used both for glycerol stock generation and maxi prepped using the Qiagen maxi prep kit. Collected DNA was stored at -20ºC for use.

2.2.7 Affinity Purification mass spectrometry

2.2.7.1 Affinity purification mass spectrometry in SH-SY5Y cells

2.2.7.1.1 Cell preparation, transfection and lysis

SH-SY5Y cells were grown in flasks T75 (p12-14) until confluent. Cells were passaged when confluent and divided equally in to 4 flasks. Cells were left to proliferate for 24 hours and the media replaced with serum free DMEM (Gibco). Cells were transfected using the Turbofect (Thermo Fisher) protocol 2.2.3.1. 20µg of DNA (WT, G70S, D252H and pcDNA3.1) was transfected into separate flasks. Flasks were incubated for 48 hours, trypsnised and pellets were stored at -80^{o}C. This was repeated twice obtaining 3 biological repeats in total. Pellets had 500µl ice-cold RIPA buffer + protease inhibitor (Roche) (table 2.9) added and were lysed in a Bioruptor for 7 cycles of 30 seconds on and off at 4^{o}C. The lysates were then spun in centrifuge at 13300xg for 20 minutes. The supernatant was removed and taken for immunoprecipitation.

2.2.7.1.2 Co-immunoprecipitation using V5 tag

To isolate eEF1A2-V5 and binding partners, samples were incubated at 4^{o}C for 3 hours with V5 agarose magnetic beads (MBL international), using the KingFisher Duo II robot system. 120µl of beads were diluted 1:10 in PBS. 100µl of bead solution was added to each sample using the robot. After incubation, the robot washed the beads 3 times with 500µl of RIPA buffer (table 2.9) and a further 2 times in 500µl TBS. Finally, beads were deposited in trypsin working reagent made up as in table (2.10). Samples were left overnight to digest at 4^{o}C and peptide fragments were collected.

2.2.7.1.3 Peptide storage and LFQ mass spectrometry

Peptide storage and mass spectrometry was performed by Jimi Wills. In brief, peptides were transferred to storage in small pieces of membrane using a centrifugation method. Samples were then maintained at -20^{o}C until loaded on to Thermo-Q Orbitrap mass spectrometer for label free quantification.

2.2.8 Co-immunoprecipitation

2.2.8.1 *In vitro* co-immunoprecipitation of eEF1A2-V5 constructs

HEK293T and SH-Y5Y cells were cultured and transfected as in 2.2.3.1. After 48 hours cells were trypsinised, spun and pellets were lysed in RIPA buffer with protease inhibitor (table 2.9). Appropriate volumes of RIPA buffer for different cell numbers are reported below.

Flask size	Cell number	Volume of RIPA	Volume bead solution	Volume of IP dilute	Volume of wash buffer
6 well plate	$1.2x10^6$	50µl	5µl	10µl	100µl
T25 flask	$2.8x10^6$	100µl	10µl	30µl	300µl
T75 flask	$8.4x10^6$	200µl	20µl	50µl	500µl

Cells were sonicated using the Bioruptor as in 2.2.7.1.1. Lysates were spun and supernatant collected. A bead solution was made by diluting V5 agarose magnetic beads (MBL International) 1 in 10 in RIPA buffer. Appropriate volumes of bead solution (above) were added to lysates and samples incubated for 3 hours at 4^{o}C with rotation. Samples were spun in a centrifuge for 2 minutes at 8000 rpm. Using a magnetic Eppendorf rack (Active Motif), beads were isolated and lysate extracted. These lysates were diluted 1:1 in 2X Laemmeli buffer (table 2.13) and 10% 1M DTT, boiled for 10 minutes at 95^{o}C and stored at -20^{o}C as the 'input' fraction. Beads were washed in RIPA buffer (table 2.9) 3 times and with TBS twice using volumes described above. 2X Laemmeli buffer and RIPA buffer were mixed 1:1 at a total volume as referred in the table above. This mixture was added to beads, and tubes were boiled for 10 minutes at 95^{o}C. Tubes were re-applied to the magnetic rack and supernatant collected. The sample was supplemented with 10% v/v 1M DTT and stored at -20^{o}C as the IP fraction.

For western blotting 15µl of IP fraction and 5µl of input fraction were used.

2.2.9 Western Blotting

2.2.9.1 Protein extraction

2.2.9.1.1 Protein extraction from tissue

Tissue samples were removed from -80ºC storage on dry ice, to prevent thawing. Slices of tissue were weighed and added to homogenisation tubes (Stretton Scientific). The appropriate volume of 0.32M sucrose plus protease inhibitor was added at a ratio of 100µl/mg. Samples were homogenised using a Precellys®24 shaker (Precellys) for 1 minute. Samples were transferred to centrifuge tubes and spun at 13300 rpm for 15 minutes at 4ºC. The supernatant was extracted and either had protein concentration determined in 2.2.9.2, or directly prepared for western blot in 2.2.9.3.

2.2.9.1.2 Protein extraction from cells

Cells were removed from culture flasks using trypsin (Life Technologies) and spun as reported previously. Cells were diluted in RIPA buffer and sonicated at concentrations as reported in 2.2.8.1. Samples were spun at 13300 rpm at 4ºC for 15 minutes. The supernatant was removed and either had protein concentration determined in 2.2.9.2, or directly prepared for western blot in 2.2.9.3.

2.2.9.2 Protein quantification

To achieve equal loading of total protein in western blot analysis, protein concentration was measured using Pierce Bradford colorimetric analysis (Thermo Fisher). A standard curve of known protein concentrations was made using 2mg/ml BSA with 8 1:1 dilutions and a negative control. Tissue samples were diluted 1:100 and cell extracts 1:50, to a total volume equal to the standard curve. Colorimetric detection reagents A and B were diluted 50:1 and 1ml of detection reagent added to each sample. Tubes were incubated at 37ºC for 30 minutes. 100µl of samples was added in triplicate to a clear 96 well plate (Co-Star). Absorbance was measured at 562nm wavelength on a Fluostar Omega plate reader.

2.2.9.3 Sample preparation

Samples were diluted in lysis buffer to normalise protein concentration based on BCA analysis. After normalisation, samples had 2X Laemmeli buffer added. Tubes were boiled at 95^{o}C for 10 minutes and had 10% v/v 1M DTT added. Samples were either added to gels immediately or stored at -20^{o}C for later analysis.

2.2.9.4 Acrylamide gels

Acrylamide gels for protein separation were made by creating a 10% separating gel, with 4% stacking gel atop. Bio-Rad glass plates were assembled and secured tightly in a gel assembly holder. Separating gel was composed as below:

Reagent	Company	Volume for 4 gels
30% Acrylamide/Bis	Bio-Rad	10.4ml
1.5M Tris pH8.8	-	8ml
dH_2O	-	13.4ml
20% SDS (w/v)	-	160µl
TEMED	-	20µl
25% AMPS	-	80µl

Separating gel was added to assembled glass plates. A layer of isopropanol was added on top to remove bubbles and achieve an even distribution. After 20 minutes at room temperature, the isopropanol was poured off. Stacking gel was then composed and added on top.

Reagent	Company	Volume for 4 gels
30% Acrylamide/Bis	Bio-Rad	2.9ml
0.5M Tris pH6.8	-	5ml
dH_2O	-	11.9ml

20% SDS (w/v)	-	100µl
TEMED	-	10µl
25% AMPS	-	100µl

A 10- or 15-well comb (Bio-Rad) was added to the top and the gel left to set. Gels were either used immediately or wrapped in moist paper and stored at 4^{o}C for a maximum of a week.

2.2.9.5 Gel Running

Gels were assembled in Bio-Rad gel tank. 1 litre of running buffer was prepared by diluting 100ml of 10x TGS (Bio-Rad) in 900ml of dH_2O. Running buffer was added to the tank, ensuring gels were immersed. Samples were loaded into individual wells, with one well reserved for 5µl of High-Range Rainbow Ladder (GE Healthcare). Except for Co-IP samples (specified separately), 12.5µl of samples were loaded into gels. Gel was run at 120V for ~2 hours, until loading dye could be seen at the bottom of the gel.

2.2.9.6 Gel Transfer

After samples had separated sufficiently, gels were removed from the tank and prepared for transfer. Transfer buffer was made by combining 700ml of H_2O with 200ml of methanol and 100ml of 10X TGS. Hybond-P PDVF membrane (GE Healthcare) was cut to the size of gel. The membrane was transferred to methanol for 1 minute to activate it, before being stored in transfer buffer for 3 minutes for equilibration. For each gel 2 sponges and 2 pieces of Whatman filter paper (cut to size) were assembled in a cassette (starting with the black side), along with gel and activated membrane in the following order: sponge, filter paper, gel, membrane, filter paper, sponge. Cassettes were pressed tightly to ensure the removal of air bubbles from samples. Cassettes were sealed and placed in transfer tank (Bio-Rad), along with an ice pack and transfer buffer. Transfer was set at 100V for 1 hours at 4^{o}C.

2.2.9.7 SYPRO Ruby

After transfer, membranes were removed from transfer cassettes using forceps. Membranes were placed on a sterile plastic film and dried at room temperature. Membranes were re-activated by being immersed in methanol. To measure total protein membranes were incubated in SYPRO Ruby prewash solution (7% Acetic Acid, 10% Methanol, ddH_2O) for 15 minutes. Blots were then washed 4 times for 5 minutes in ddH_2O. Finally, blots were incubated for 15 minutes with SYPRO Ruby solution (Thermo Fisher) in the dark. Blots were washed for twice for 1 minute in ddH_2O to remove excess stain and then were imaged by a LI-COR imaging system on channel 600 for 2 minutes. This provided an image of total protein transferred to the membrane.

2.2.9.8 LI-COR immunostaining

The LI-COR system uses fluorescent secondaries for western blot detection. Blots were blocked in Odessy™ LI-COR blocking buffer for 1 hour at room temperature whilst rocking. Primary antibodies (one mouse, one rabbit) were diluted in LI-COR blocking buffer and incubated either at room temperature for 1-3 hours or overnight at 4^{o}C whilst rocking (see table 2.17). Blots were washed in TBS with 0.2% Tween20 (TBS-T) 3 times for 15 minutes each, at room temperature. LI-COR secondary antibodies (table 2.18) were diluted 1:5000 in LI-COR blocking buffer and incubated in the dark at room temperature for 1 hour whilst rocking. After 3 15-minute washes with TBS-T, blots were imaged in the LI-COR imaging system at channel 700 for rabbit and 800 for mouse or goat (2 minutes per channel).

2.2.9.9 HRP immunostaining

For some antibodies LICOR staining did not work. In those instances, HRP-conjugated secondaries were used. Further, co-immunoprecipitation samples required light-chain secondary antibodies, these were HRP conjugated.

After SYPRO Ruby staining, membranes were blocked in blocking solution (5% milk powder in 0.2% Tween20 in TBS) for 1 hour at room temperature.

Antibodies were diluted in blocking solution and applied to membranes overnight at 4^{o}C with agitation (table 2.17). Membranes were washed with TBST for three 15-minute washes. All HRP-conjugated secondaries were diluted 1:1000 in blocking solution and incubated on membranes, whilst rocking, for 1 hour at room temperature (table 2.18). Blots were washed as previously described. Clarity™ ECL detection reagent (Bio-Rad) was made by diluting reagents A and B in a 1:1 ratio. Solution was applied to the membrane for 5 minutes in direct light. Membranes had the solution removed and sealed in plastic film. Blots were placed in a cassette and exposed in a dark room using autoradiography film.

As only one antibody could be tested at a time, blots were stripped after exposure using stripping buffer. Stripping buffer was applied to membranes twice for 10 minutes each, TBS was then used to wash blots twice for 10 minutes and finally two washes with TBS-T were performed. Blot was then ready for further blocking and immunostaining, as above.

2.2.9.10 Densitometry analysis

HRP-Blots were scanned, and images were subjected to densiometric analysis using ImageJ software. Pixel intensity for each band in western blot was measured. These were standardised either against loading control protein or total protein. LI-COR images were taken from LI-COR imaging system and the same analysis was performed.

2.2.10 *In vitro* protein synthesis treatment

2.2.10.1 Puromycylation treatment for western blot analysis

To assess nascent protein synthesis, HEK293T and LUHMES cells were treated with puromycin before immunoblot analysis.

HEK293T cells were transiently transfected with eEF1A2-V5 constructs as with in 2.2.3.1.

Cells were grown in 6 well plates for HEK293T and T25 flasks for LUHMES cells. Control cells were pre-treated with 150µM cycloheximide for 20 minutes. Cells were then treated with 100µg/ml puromycin for 15 minutes. A vehicle condition was added as a negative control. Cells had media removed immediately after treatment and trypsinolysis was used to extract cells and centrifugation at 5000rpm for 5 minutes pelleted cells. Cell lysis and protein extraction, BCA analysis and western blot was then performed as in 2.2.9.

2.2.10.2 Immunocytochemistry of puromycin staining

Differentiated and proliferative LUHMES cells were cultured on glass 24 well coverslips (Costar). Puromycin treatment was performed as above, including cycloheximide and vehicle treatments. Treatments were staggered to ensure equal incubation lengths, matching genotypes in each staggered repeat. After treatment was finished, media was removed and cells washed once with PBS. Cells were then fixed in 4% PFA for 15 minutes. Cells were washed twice with PBS and stored in PBS overnight at 4^{o}C.

Cells were permeabilised using 0.1% Triton-X100 for 5 minutes before a further washing step with PBS. Cells were blocked in 5% BSA in PBS for 1 hour at room temperature. Cells were then incubated with puromycin and eEF1A antibodies diluted in 5% BSA 0.1% PBST. A ‘no primary’ control was added for background fluorescence control. This was incubated in PBST. Slides were incubated for 1 hour at room temperature. Cells were washed 3 times with PBST for 10 minutes each. Afterwards, fluorescent secondary antibodies, diluted in 5%

BSA 0.1% PBST, were applied to slides for 30 minutes in the dark. After further washing 3 times with PBST, slips were removed from wells and were fixed to slides using ProLong gold Antifade mounting media with DAPI (Thermo Fisher). Slides were left at 4ºC covered from light for 18 hours to allow mounting media to solidify.

Cells were imaged on a Zeiss epifluorescence microscope at x63 objective and analysed using ImageJ software with blinding.

2.2.10.3 AHA click-it protein synthesis

Proliferative and differentiated LUHMES cell lines were cultured in a 96 well plate. Cells had media replaced with pre-warmed artificial cerebrospinal fluid (aCSF) (table 2.14). Cells were left for 2 hours at 37ºC to allow methionine depletion. Anisomycin (Sigma) was used to treat control cells to inhibit protein synthesis at a concentration of 250μM.

Click-it™ AHA protein synthesis kit (Invitrogen) was used as per the manufacturer's instructions. Wells were imaged on a Zeiss live inverted epifluorescence microscope at x4 objective.

2.2.11 *Eef1a2* mouse lines

2.2.11.1 Generation and *Eef1a2*/D252H, *Eef1a2*/del22ex3 and *Eef1a2*/G70S mouse lines

CRISPR/Cas9 was used to generate missense mutations and deletions in mice. This work was done by other members of the lab and mouse lines have been extensively characterised previously, both in published work and other theses in the lab (121,140,141). In summary, nickase technology was used to edit missense mutations and deletions in C57BL/6 mice. Genetic editing resulted in mice with G70S missense mutations, but no surviving founders to generate a breeding line. Surviving founders were generated for *Eef1a2/*D252H and *Eef1a2*/del22ex3 lines. Table 2.21 summarises all mouse lines used during this thesis.

Table 2.21: Description of mouse lines used in thesis.

Line name	Mouse line
Eef1a2/D252H	Line generated using CRISPR/cas9. Two founder mice with *Eef1a2*$^{D252H/+}$ genotypes were used to generate breeding lines.
Eef1a2/G70S	Line generated using CRISPR/cas9. Founder mice only were generated: *Eef1a2*$^{G70S/G70S}$, *Eef1a2*$^{G70S/-}$ and *Eef1a2*$^{-/-}$.
Eef1a2/wst	Mouse line with 15kb deletion including promoter of *Eef1a2* gene. Homozygote mice have a *Eef1a2*$^{-/-}$ genotype.
Eef1a2/del22ex3	Line with 22bp deletion in exon 3 resulting in loss of expression of the allele. Homozygote mice have an *Eef1a2*$^{-/-}$ genotype.

2.2.11.2 Genotyping

2.2.11.2.1 *Eef1a2*/D252H genotyping

Ear notches were taken by animal technicians at the BRF Unit, Western General Hospital. DNA was extracted by boiling for 10 minutes in 300µl 15mM NaOH. 25µl of Tris 1M pH8 was added to samples and tubes were shaken. DNA extracts were stored at -20^{o}C until PCR analysis. A combination of PCR and restriction digest was used to characterise Eef1a2/D252H mice. PCR amplified a 442bp product using primers in table (table 2.6). PCR was composed of the below components and run on cycling parameters on a Bio-Rad C1000 Thermal Cycler.

Reagent	Company	Volume (µl)
5x Platinum Superfi buffer	Thermo Fisher	4
Platinum Superfi polymerase	Thermo Fisher	0.2
10mM dNTPs	Invitrogen	0.4
10µM forward primer	Sigma	1
10µM reverse primer	Sigma	1
Betaine	-	4

ddH_2O	-	9.15
DNA	-	0.25

Temperature	Time (seconds)	Step/cycle
98ºC	60	Initial denaturation
98ºC	5	X30 cycles
58ºC	10	
72ºC	15	
72ºC	10 minutes	Final extension

After PCR amplification, samples were subjected to restriction digest by Hin1II (Thermo Fisher). Reactions were set up as follows:

Reagent	Company	Volume (µl)
Fast digest green buffer	Thermo Fisher	2.5
Hin1II	Thermo Fisher	0.5
PCR product	-	15
ddH_2O	-	7

Samples were incubated at 37ºC for 5 minutes in a Bio-Rad C1000 Touch thermal cycler. Products were run on a 2% agarose gel for 1 hour at 130V with 100bp ladder (NEB). Restriction digest resulted in either 300bp and 122bp fragments for A WT allele, or a 202bp, a 128bp and a 122bp fragment pattern for D252H allele.

2.2.11.2.2 *Eef1a2*/del22ex3 genotyping

Ear notches were obtained, and DNA extracted as in 2.2.11.2.1 from the *Eef1a2*/del22ex3 mouse line (table 2.21). PCR amplification around exon 3 using primers in table 2.7 produced a 208bp band for a WT allele and a 186bp band for a mutant. Reactions were set up as below and cycling parameters in 2.2.4.2 were

used on a Bio-rad C1000 Touch thermal cycler. Samples were diluted with 6x DNA loading buffer and run at 130V on a 2% agarose gel with SYBR safe (Invitrogen) with 100bp ladder (NEB).

Reagent	Company	Volume (µl)
10x PCR Buffer	Invitrogen	2.5
$MgCl_2$	Invitrogen	1
Taq DNA polymerase	Invitrogen	0.2
10mM dNTPS	Invitrogen	0.5
10µM forward primer	Sigma	1
10µM reverse primer	Sigma	1
Betaine	-	7.5
ddH_2O	-	10.3
DNA	-	1

2.2.11.2.3 Genotyping *Eef1a2*/wst mouse line

After it became impossible to breed del22ex3 homozygote mice for welfare reasons, I used the older more established *Eef1a2*/wst line (table 2.21) which had been well characterised previously (13,62) as control mice in protein synthesis experiments. Samples from the 'wst' mouse line were genotyped using two standard PCR amplifications with primers in table 2.8. Reagent mix was composed as in 2.2.11.2.2 and the samples were run on a Bio-rad C1000 Touch thermal cycler using the following cycling parameters.

Temperature	Time (minutes)	Step/cycles
95°C	3	Initial denaturation
95°C	1	X30 cycles
62°C	1	
72°C	1	
72°C	5	Final Extension

PCR products were diluted with 6x DNA loading buffer and run on a 1.5% agarose gel at 130V. WT allele PCR amplification resulted in 452bp product (62) and null allele PCR created a 200bp product (119).

2.2.12 Animal phenotyping

WT, heterozygous and homozygous littermates from *Eef1a2*/D252H and *Eef1a2*/del22ex3 lines were subjected to phenotyping analysis from postnatal days 16 to 24. Phenotype assessments were carried out according to the method of Guyenet and colleagues (142). In brief, mice were subjected to 4 measurements and scores recorded daily; gait, degree of kyphosis, hind limb clasping and ledge test. Scores on severity were agreed between all three experimenters. To ensure consistency, a training period was undertaken where experimenters scored the same mice at the same time, but independently of one another to ensure scores were consistent. All experimenters were blind to mouse genotypes during phenotypic analysis. A training day at p15 was also undertaken, this was because artificially high scores on ledge test were being recorded for all mice, who were unable to perform the task straight away owing to their age.

In addition to phenotype, weight of mice in grams was recorded daily.

2.2.13 Animal treatments with puromycin

Protein synthesis experiments were performed using SUnSET which had been adapted for *in vivo* usage, as reported previously (143). Mice were housed in the BRF animal unit of the Western General Hospital. Injections were performed by licensed animal technicians. Stock drug solution was prepared by solubilising Puromycin Dihydrochloride (Millipore) in sterile filtered PBS and aliquoted. Aliquots were stored at -20^{o}C and thawed on ice. Mice were weighed and drug concentration of 0.04µmols/gram in 100µl sterile filtered PBS was made up. After successful anaesthetisation, mice had the drug solution administered subcutaneously. Animals were left under anaesthetic for exactly 30 minutes before culling by cervical dislocation. Heart, liver, skeletal muscle, brain and spinal cord were extracted. These were flash frozen in liquid nitrogen, before

being transferred to -80°C and stored for later analysis. Mice were treated consecutively to allow for exactly 30 minutes of treatment each.

Muscle and liver samples were prepared using the method in 2.2.9.1.1. The subsequent protocol described in 2.2.9 was then followed including BCA analysis and using HRP-conjugated immunostaining technique. An IgG2a secondary antibody was used to remove non-specific background staining (143).

Protein synthesis was measured by normalising relative puromycin signal to total protein concentration using densiometric analysis performed on ImageJ software.

2.2.14 RNA extraction

RNA for qPCR analysis was extracted from cells and tissue using the RNeasy Qiagen kit as per the manufacturer's instructions.

Cell pellets were stored at -80°C. Pellets were collected on ice and lysed in RLT buffer using a Bioconductor for 7 cycles of 30 seconds on and 30 seconds off at 4°C. Tissue was removed from -80°C on dry ice, sliced and weighed. Appropriate weights of tissue were added to specific volumes of RLT buffer as per the manufacturer's instructions. These samples were lysed in homogenisation tubes (Stretton Scientific) on a Precellys®24 homogenisation shaker for 1 minute and returned to ice. RNA extraction using Qiagen kit was then followed for both sample types. On column DNAse digestion was performed using the Qiagen DNAse digestion kit, as per the manufacturer's instructions. After RNA extraction, a second DNAse digestion step was performed using DNA-free DNAse removal kit (Invitrogen). 0.1 volumes of DNase I Buffer and 1µl of rDNase was added to the RNA. Samples were incubated at 37°C for 20-30 minutes. 0.1 volumes of DNAse inactivation reagent was added and tubes were mixed. A further 2-minute incubation at room temperature was performed before tubes were centrifuged at 10000 x g for 2 minutes at 4°C. Supernatant was removed and stored as RNA. RNA quality and concentration were measured using the Nanodrop Optical Imager. RNA was stored at -80°C.

2.2.15 cDNA synthesis

To convert RNA to cDNA, Aligent cDNA synthesis kit was used following the manufacturer's instructions. All samples of RNA were diluted to a standard concentration (typically 1µg) in RNAse free water. Negative controls were also performed; -RT sample contained 1µl of RNA from all samples, but no reverse transcriptase (allowing for a genomic DNA contamination check), whilst a no RNA condition checked for contamination with PCR products

2.2.16 qPCR

qPCR was used to measure *EEF1A2* mRNA concentrations in LUHMES cells. First, cDNA was diluted 1:100 in ddH_2O. qPCR experiments were performed using Brilliant II SYBR Green qPCR master mix (Aligent) with the following reaction mix:

Reagent	Volume (µl)
2x Brilliant II SYBR green	6
6µM primer mix	0.5
ROX reference dye (1:50 ddH_2O)	0.375
RNAse free water	1.125
cDNA	4

Reactions (triplicates per sample) were added to an opaque 384 well plate (Co-star), spun in a plate spinner for 1 minute and run on the Light Cycler HT7900 (Roche) using below cycling parameters, with dissociation curve step added post amplification.

Cycles	Temperature	Time
1	95°C	10 minutes
40	95°C	3 seconds
	60°C	1 minute

Negative control samples were also added to check for RNA or genomic DNA contamination. Results are presented as ΔΔCT values. These are a measure of how many cycles it took within the PCR for amplification of the product to reach a specific threshold and inversely correlate to RNA concentration.

To establish the number of, and optimal, housekeeping genes for normalisation, GeNorm™ analysis was performed (144). This allowed for comparison of sample variability across different housekeeping genes. At least ten samples were added in triplicate to a plate and tested against six housekeeping genes. These were run as above and the GeNorm™ software was used to analyse the samples. This allowed for the selection of an appropriate number of genes which had the lowest inter-sample variability

EEF1A2 and selected housekeeping genes were subjected to qPCR as above. In addition, standard curve of DNA was made for all primer pairs. One WT RNA sample was diluted 1:10 and then five subsequent 1:1 dilutions were performed. These standard curves were used to quantify ΔΔCT values.

Samples were analysed by comparing ΔΔCT values to standard curve. The anti-log of samples was taken and the GEOMEAN function in excel was used to gather an average of housekeeping genes. The *EEF1A2* values were then divided by this value in each respective sample. These values provided relative *EEF1A2* mRNA quantification values for all samples.

2.3 Computational analysis

2.3.1 Analysis of AP-mass spec

Mass spectrometry results supplied a list of proteins identified in the pulldown along with label-free quantifications in each condition. Filtering analysis was performed in R using ‘dplyr’ package. Proteins with a unique peptide value less than 1 were omitted. Proteins with a mode of zero were also removed. The minimum value above zero was found for each protein and used to replace zero values. Average $\log_2$ fold change of all conditions as compared to empty vector was calculated. Proteins which showed a 3-fold greater increase in any condition

as compared to empty vector were kept. Z-scores for filtered protein set were obtained and 'pheatmap' package was used to visualise variance. Once background filtering was complete several normalisation analyses were performed.

2.3.1.1 Bait normalisation

eEF1A2 label free quantification (LFQ) values for all repeats were normalised against the first WT sample. The resulting ratio was then used to adjust all other proteins in the sample. Log_2 fold change for mutations compared to WT for each protein were calculated. t-tests for every protein in mutant versus WT were also performed. P-values were adjusted owing to multiple testing using a 1% false discovery rate. Negative log_{10} of p-values was calculated and plotted against the log_2 fold change for respective proteins using R package 'ggplot2' to create volcano plots.

2.3.1.2 Total Area Sums normalisation

The sum of all LFQ intensities in each sample (post background filtering) was obtained. These sums were divided against the sum of one WT repeat and a relative score for each condition obtained. These scores were used as a normalisation factor for all proteins in respective condition. Heatmap and volcano plots were visualised as previously.

2.3.1.3 Most-Likely Ratio normalisation

To counteract variable bait levels, most-likely-normalisation ratio (MLR) was performed as reported by Lambert and colleagues (145). The most representative sample of each technical repeat was determined by comparing the log_{10} of ratio of respective proteins with all other technical repeats in the genotype. The density of these values was plotted using 'ggplot2'. Delta and histogram width were calculated and used as a measure of global data similarity. Comparing all these repeats allowed for determination of the most representative sample within each genotype. All other samples were then adjusted using the appropriate apex ratio to the 'representative' sample. This was termed the 'technical normalisation step'

This process was then repeated comparing all mutant repeats with all WT technical repeats. Again, using histogram analysis the most representative WT sample was identified and appropriate apex ratio was used to adjust all other samples. Density and volcano plots were visualised using 'ggplot2' and heatmap was prepared using 'pheatmap' package.

2.3.2 Protein network analysis

2.3.2.1 eEF1A2 AP-mass spectrometry

Advice on the appropriate filtering and normalisation techniques for AP-MS was supplied by Dr Alex von Kriegsheim (ECRC, IGMM). I went on to explore further normalisation techniques, in addition to his advice, using the scientific literature as a guide, settling on Most-Likely-Ratio normalisation.

To generate biological networks, all proteins identified after background filtering were inputted into the String database to obtain functional interaction scores. The interactions were added to Cytoscape. The ClusterONE plug-in was used to create clusters based on the edge weighted scores obtained in string database. Significantly identified clusters were then subjected to gene ontology analysis to identify functional enrichment using the GOrilla software.

2.3.3 Statistical testing

Statistical testing was performed in R and GraphPad software V8. t-tests, multiple correction calculations, one-way ANOVAs and 2-way mixed ANOVAs and non-parametric alternatives were used where appropriate.

Chapter 3: eEF1A2 interactome analysis and mutation consequences

3.1 Introduction

Analysis of the 'interactome' (everything a protein interacts with) is a powerful way of examining mutations and their consequences. Two common approaches used to assess the global protein interaction network are yeast-two-hybrid assays and affinity-purification mass spectrometry (AP-MS) (Figure 3.1**A**). Yeast two hybrid assays are practical for establishing binary interactions between two proteins (146). AP-MS, meanwhile, uses bait-pulldown followed by identification and quantification of interacting protein partners. This allows for the identification of protein interaction networks based on direct and indirect association (147). The second advantage to using AP-MS is the ability to use mammalian cells. All protein interactions are measured within the desired cell type. Unlike yeast two hybrid assays, which can induce artificial interactions which would normally not occur in a cell type, this is does not occur using AP-MS.

AP-MS has been an insightful tool for other neurological conditions in both human and mouse studies. Using a multiple sclerosis mouse model LRP1 interacting proteins were established (148). The mutant form of the protein huntingtin, the causative mutation in Huntington's disease, showed altered protein interactions including translation apparatus. (149).

The analysis of interactome changes is termed 'Edgotyping'. Edgotyping uses network analysis to examine the impact of mutations on the interactome. Proteins are represented as nodes and their interactions are mapped as interconnecting edges. Zhong et al argued that edgotyping analysis is essential for understanding a complex array of pleiotropic phenotypes, resulting from different mutations in the same gene (150). Sahni et al discovered that whilst some missense mutations disrupt protein stability resulting in a 'quasi-null' protein, the vast majority of point mutations did not result in total loss of binding to all interactors, but instead edge specific changes (edgetic perturbations) (151). Different mutations in the same protein perturbed different edges, resulting in diverse phenotypes.

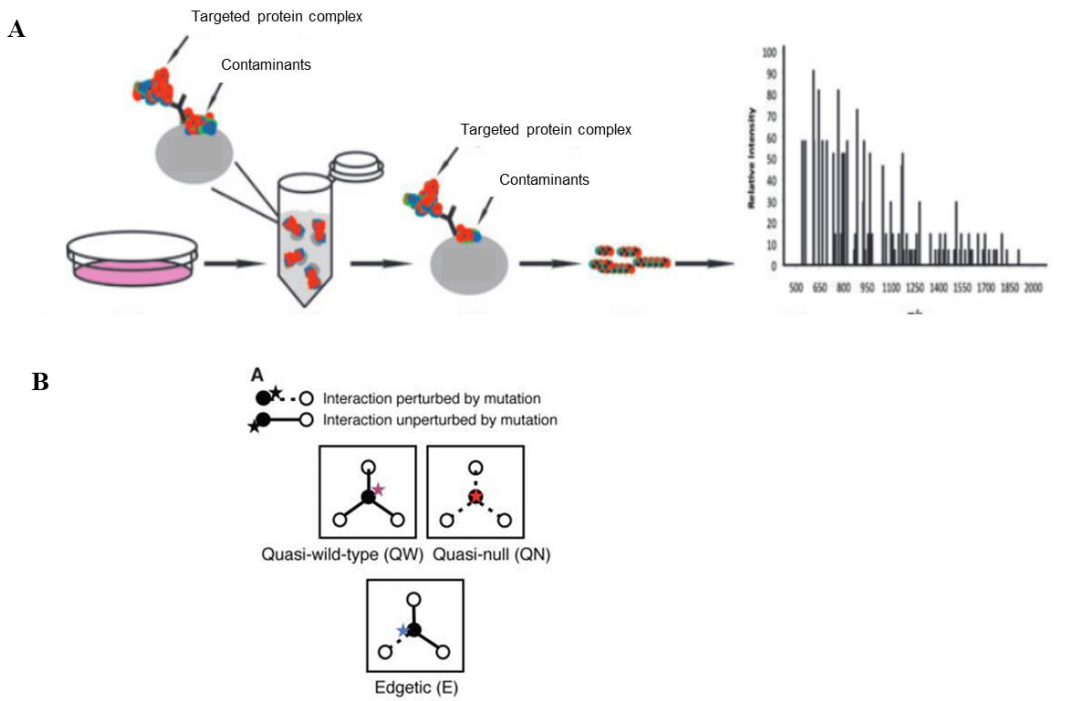

Figure 3.1: AP-MS to establish eEF1A2 interactome. ***A****, schematic diagram of AP-MS process. Figure adapted from Dunham et al 2012 (152).* ***B*** *highlights the possible protein interaction disruptions which result from mutations. In some instances, mutations can result in no changes to binding partners (Quasi-wild-type). In some cases, the opposite can happen, with mutations causing perturbations to all interactors (Quasi-null). Sahni and colleagues demonstrated that in many mutations a third consequence, edgetic perturbations, occurs Edgetic perturbations result disruption of specific interactors due to mutations. Location of disruption can impact which interactions are perturbed and mediate the severity of the condition. These have been displayed in figure* ***B*** *(adapted from Sahni et al (151)).*

I used AP-MS to isolate eEF1A2 and its binding partners. This allowed me to study the interactome of eEF1A2, and how it was disrupted with mutations. Any changes in interactions, as a result of mutations, might shed light on the molecular consequences. Firstly, the key interactors might illuminate the non-canonical functions of eEF1A2. Secondly, mutations may disrupt or enable binding proteins suggesting a loss or gain of function, and the molecular mechanisms implicated.

3.2 Aims of chapter

1) Identify the interactome of eEF1A2

2) Identify interactome perturbations resulting from mutations eEF1A2^{D252H} and eEF1A2^{G70S}

3.3 Identify the interactome of eEF1A2

3.3.1 Experimental workflow of mass spectrometry experiment

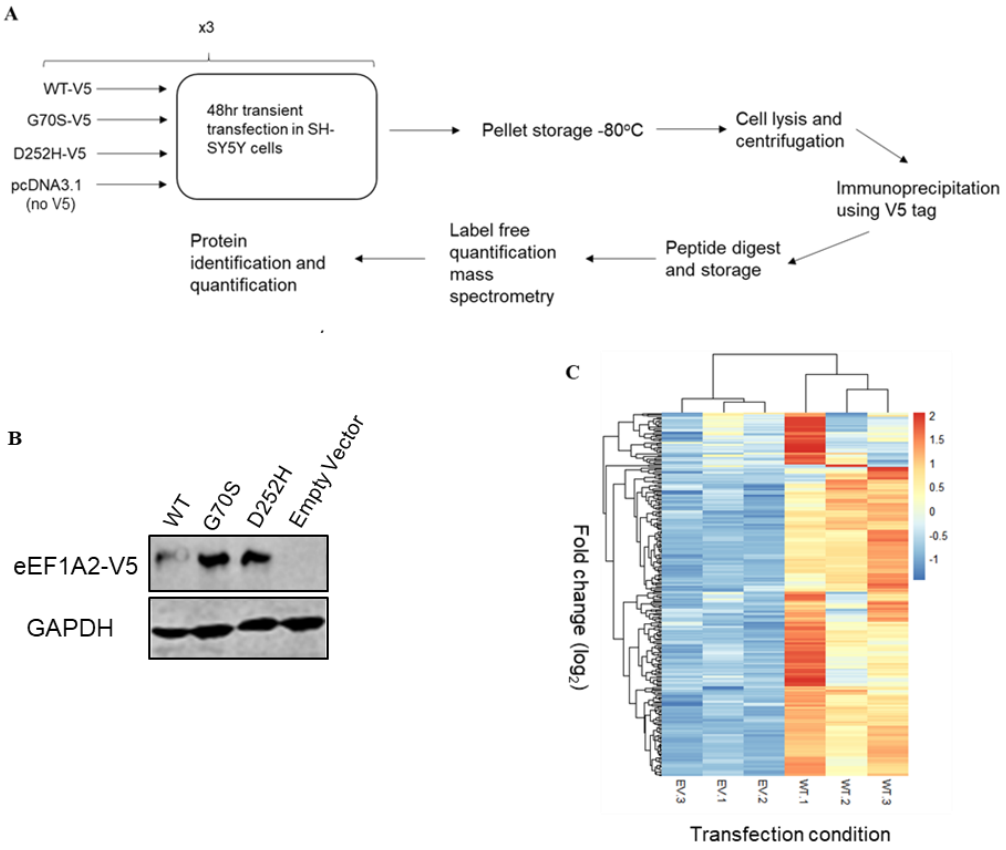

Figure 3.2: ***Affinity purification mass spectrometry experiment to assess the eEF1A2 interactome. A,*** *Experimental workflow of the mass spectrometry experiment.* ***B,*** *An example western blot of transfected eEF1A2-V5 constructs in SH-SY5Y cells. V5 staining is shown at the correct size for eEF1A2-V5 (52kDa). GAPDH staining is shown at 38kDa.* ***C,*** *a heatmap of z-scores for all proteins identified as 'confident interactors' (above empty vector filtering). Hierarchical clustering groups background (EV) and WT repeats together, showing higher intensity in WT compared to EV.*

No commercial antibody can discriminate between endogenous eEF1A1 and eEF1A2 in cultured cell lines, and all immortalised cell lines express eEF1A1. Consequently, I used a tagged form of eEF1A2 with a C-terminal V5 tag. Exogenously expressing eEF1A2-V5 resulted in a band at 52kDa, identified with a

V5 antibody (Figure 3.2B). Before filtering, 1081 proteins were identified by AP-MS. After contaminants, low expression and background proteins were filtered, 288 proteins were identified as high confidence interactors (a 27% identification rate). A heatmap of LFQ intensities for high confidence interactor in the empty vector and WT conditions shows successful filtering of background contaminants (3.2C). In this experiment, the whole cell lysate was applied to AP-MS. In future experiments a small volume of lysed sample was taken before immunoprecipitation, to assess transfection efficiency. As all cells were seeded equally and transfected at the same time for each biological replicate, endogenous levels of eEF1A2 are likely to be relatively consistent. Therefore, looking at the LFQ intensities of eEF1A2 provides an insight into exogenous levels of eEF1A2-V5. It was clear from label-free quantities, that one G70S sample was an outlier and therefore discarded (see Appendix A.1).

3.3.2 Gene Ontology and network analysis of eEF1A2 interacting partners

I assessed the interactome of eEF1A2, which has never been examined before, to gain insight into the functions of eEF1A2.

Functional enrichment analysis identified key areas consistent with previous knowledge of eEF1A2 function. Translation elongation factors from the eEF1 complex and ribosomal subunits display the most significant enrichment of the cellular component (3.3A). Similarly, RNA binding and ribonucleoside binding proteins featured highly in the molecular function gene ontology (GO) terms (3.3A). Results supported the hypothesis that the role of eEF1A2 in protein synthesis would feature as the dominant pathway affected.

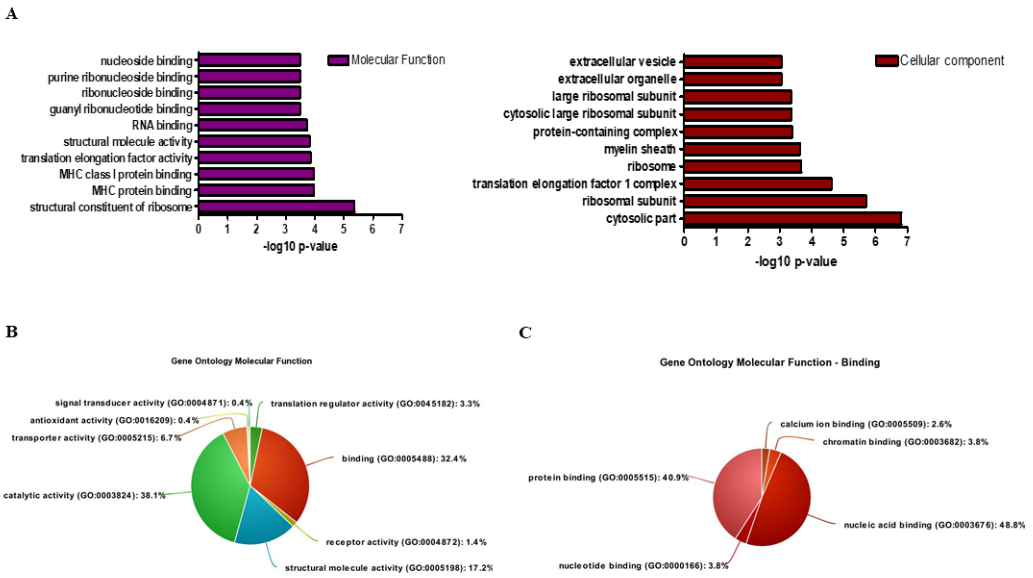

Figure 3.3: Gene ontology analysis of the eEF1A2 interactome. *Using DAVID functional annotation software, the ten most significant GO terms in both molecular function and cellular component were identified (**A**). Significance of each of these GO terms is demonstrated by the negative log10 p-value score. **B** PANTHER functional enrichment of all proteins in eEF1A2 interactome. **C** is an examination of the GO terms included in the overall term 'binding' in figure **B**.*

Gene ontology analysis identified interactors associated with functions which were conceivably linked to eEF1A2. The GO term 'binding' contributed to nearly a third (32.4%) of eEF1A2 interactions (3.3B). When examined in closer detail, this term can be subdivided, with nucleic acid and protein binding genes responsible for interactions in this category (49% and 41% respectively). The nucleic acid term is largely taken up by mRNA binding proteins, mostly associated with RNA splicing prior to protein synthesis and RNA transport. The protein binding category includes cytoskeletal modifications (60% of the category), which is solely accounted for by actin binding proteins. The extent to which each isoform is involved in actin bundling is of particular interest, as actin bundling is the central hypothesis behind the conserved expression of two isoforms (28). Evidence is emerging that the pair have differing actin bundling properties (21). These results highlight that eEF1A2 at the very least interacts with actin and actin bundling proteins, although no insight

is provided as to whether the two isoforms bundle actin to different degrees or in different ways.

3.3.3 Mapping the eEF1A2 interaction network

More information is determined on the eEF1A2 interactome by mapping protein interactions in a network. Clustering proteins into a network using prior knowledge of protein interactions can provide biological context to interactome data. To generate a network, topological analysis of the mass spectrometry data was performed. Topological analysis can either be performed using node centrality or clustering methods (153). Node centrality measures the importance certain proteins (nodes) play in a network. Given my network was centred around a bait protein, this was not the most appropriate method. A more appropriate technique was clustering analysis. This method grouped proteins based on previous knowledge of interactions. Clustering analysis simplified data by creating 'clusters' of proteins (nodes) and measured their interconnectedness (edges). Clusters could then be examined for biological functions to glean insight into the proteins associated with eEF1A2.

I analysed the proteins identified in the AP-MS experiment by obtaining the known protein interaction scores from the String database (edge scores). Using edge-weighted clustering analysis, protein complexes were identified, and the network was visualised in Cytoscape (Figure 3.4).

Nine clusters of proteins were reported as significant in this analysis ($p<0.05$). These clusters were subjected to gene ontology analysis to identify functional enrichment (table 3.1). Functions identified both supported the previous enrichment results and helped identify smaller clusters of proteins with which eEF1A2 might interact. By far the most substantial cluster was cluster '*a*' (Figure 3.4 ($p<0.0001$)). This cluster includes all the ribosomal subunits and other proteins involved in translation. It was unsurprising this would be the largest and most significant cluster, given the role eEF1A2 plays in protein synthesis. Other functions in which eEF1A2, or more generally eEF1A are implicated in have also been reported. eEF1A mediates the processing of unfolded or misfolded nascent polypeptides to

the proteasome (29). Cluster '*b*' in Figure 3.4 ($p<0.0001$), identifies heat shock proteins and chaperones (table 3.1). eEF1A1 but not eEF1A2 has been implicated in the induction of the heat shock response (30). Heat shock proteins have been shown to regulate translation at the elongation phase, especially during an augmented stress response, by interacting with elongation factors including eEF1A2 (154). This binding to heat shock factors likely reflects a different function of eEF1A2. Another cluster related to a previously acknowledged function of eEF1A2 is protein transport. Interacting proteins were identified clustered in a group associated with protein transport, specifically ER-Golgi (green cluster Figure 3.4 & table 3.1). There is some, but limited, work on eEF1A and its role in protein transport, but the isoforms responsible have not been identified. These results speculate eEF1A2 may have a role in both protein transport and the proteolysis of malformed peptides.

One cluster identified as significant was less expected: a complex of proteins which included transcription factors (turquoise (*d*); $p<0.0001$). eEF1A is predominantly a cytoplasmic protein, with little to no nuclear expression. There is evidence of eEF1A having a role in nuclear export (31–33). However, in the reported instances, eEF1A binds to the nuclear export machinery to facilitate the removal of components of the translational apparatus. To do this eEF1A interacts with Exportin 5 and Snail transcription factors. Neither of these were identified in the AP-MS experiment. Instead, proteins reported in the 'Turquoise' cluster include DNA replication licensing factors (MCM2, MCM3, MCM4, MCM5, MCM6 and MCM7). Immunostaining provided no evidence that transfected eEF1A2-V5 was expressed in the nucleus (see appendix A.2). However, the MCM complex and eEF1A2 have previously been linked as interactors. eEF1A2 was pulled-down as an interacting partner of the MCM complex in a mass spectrometry experiment (155).

RNA binding proteins were unsurprisingly identified in clusters (*f* & *h*, $p<0.01$, Figure 3.4). eEF1A has previously been associated with RNA binding proteins, likely relating to its canonical function and RNA transport (48,49). If valid, this

result would be the first evidence for the involvement of the eEF1A2 variant in these interactions.

After filtering, the protein interactors in the AP-MS sample were a densely clustered group of proteins associated with both reported canonical and non-canonical functions of eEF1A2 including protein synthesis, RNA binding, protein transport and actin bundling.

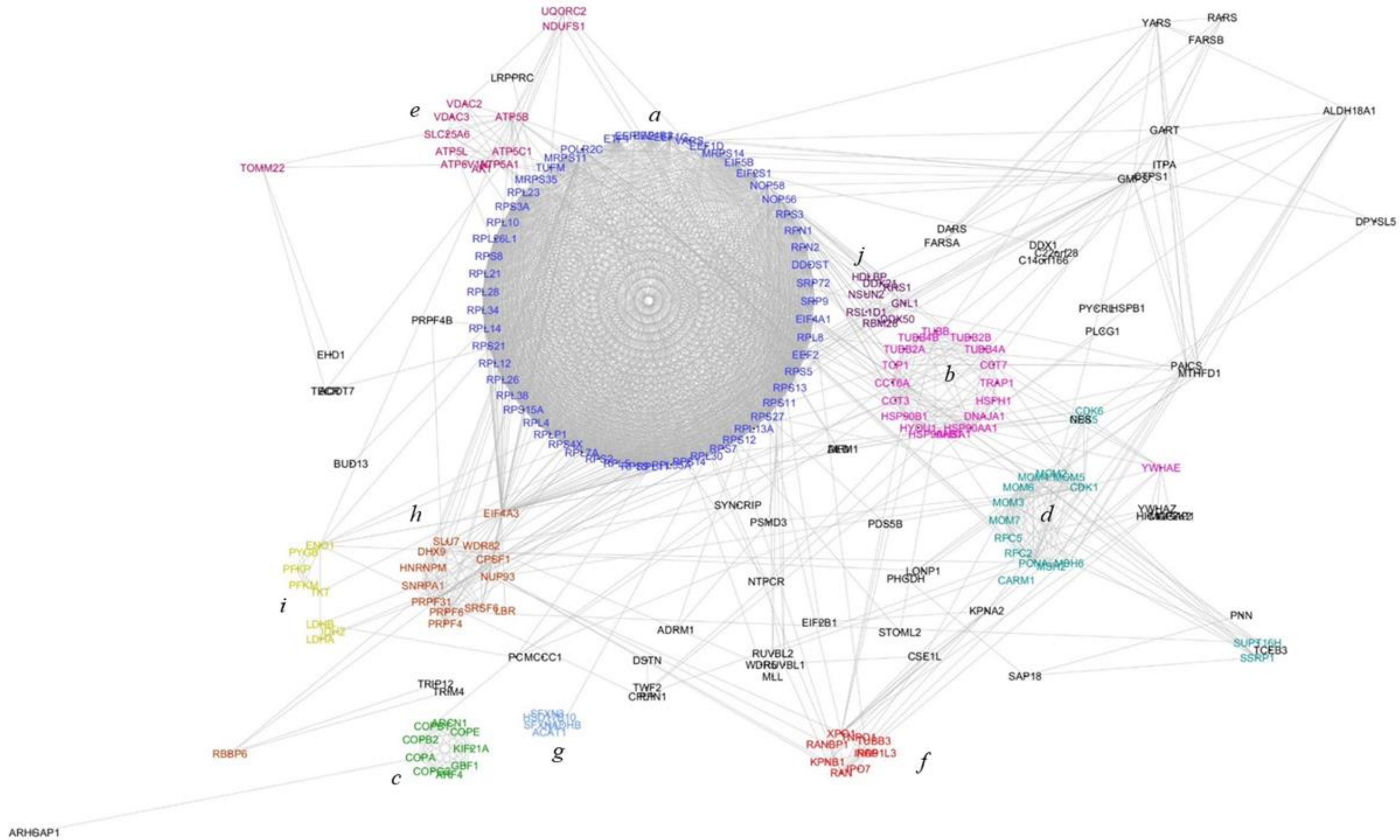

a
b
c
d
e
f
g
h
i
j
UQORC2
NDUFS1
LRPPRC
VDAC2
VDAC3
ATP5B
SLC25A6
ATP5L
ATP5C1
TOMM22
YARS
RARS
FARSB
ALDH18A1
GART
ITPA
DPYSL5
DARS
FARSA
DDX1
PYCRL
HSPB1
PLCG1
PAICS
MTHFD1
POLR2C
MRPS11
TUFM
MRPS35
EEF1D
MRPS14
EIF5B
NOP58
NOP56
RPS3
RPN1
RPN2
DDOST
SRP72
SRP9
EIF4A1
RPL8
EEF2
RPS5
RPS13
RPS11
RPS27
RPL13A
RPS12
RPS7
RPL30
RPL23
RPS3A
RPL10
RPS8
RPL21
RPL28
RPL34
RPL14
RPS21
RPL12
RPL26
RPL38
RPL4
RPS4X
PRPF4B
EHD1
BUD13
HDLBP
NSUN2
GNL1
TUBB2B
TUBB2A
TUBB4A
TOP1
CCT6A
CCT3
CCT7
TRAP1
HSPH1
HSP90B1
DNAJA1
HSP90AA1
CDK6
YWHAE
MCM3
MCM7
RFC5
RFC2
CDK1
CARM1
YWHAZ
PNN
SSRP1
TCEB3
SAP18
KPNA2
STOML2
CSE1L
LONP1
PHGDH
PDS5B
PSMD3
SYNCRIP
NTPCR
EIF2B1
ADRM1
RUVBL2
MLL
DSTN
PCMCCC1
EIF4A3
SLU7
WDR82
DHX9
CPSF1
HNRNPM
NUP93
SNRPA1
PRPF31
PRPF6
LBR
PRPF4
ENO1
PFKP
PFKM
TKT
LDHA
TRIM4
COPE
COPB2
KIF21A
COPA
GBF1
ARF4
ACAT1
RANBP1
TUBB3
KPNB1
IPO7
RAN
RBBP6
ARHGAP1

.

Figure 3.4: eEF1A2 protein interaction network. *eEF1A2 and interacting partners were added to the string database, to gain functional interaction scores. Clusters were generated using edge-weighting analysis in Cytoscape based on interaction scores*

Table 3.1: Gene ontology analysis of interactome clusters identified in network analysis. *Clusters from Figure 3.4 had gene ontology analysis applied, clusters with significantly enriched GO terms are reported.*

Cluster		Letter	Gene Ontology classification		log10 P-value
Colour	p-value				
Dark Blue	p<0.0001	*a*	GO:0003735	Structural constituent of ribosome	30.2
			GO:0003723	RNA binding	12.3
			GO:0008135	Translation factor activity, RNA binding	5.95
Pink	p<0.0001	*b*	GO:0051082	Unfolded protein binding	11.0
			GO:0032553	Ribonucleotide binding	6.75
			GO:0017076	Purine nucleotide binding	6.66
Green	p<0.001	*c*	GO:0015031	Protein transport	3.77
			GO:0016192	Vesicle-mediated transport	6.46
			GO:0006888	ER to Golgi vesicle-mediated transport	12.0
Turquoise	p<0.0001	*d*	GO:0005524	ATP binding	5.46
			GO:0008094	DNA-dependent ATPase activity	6.81
			GO:0003677	DNA binding	9.83
Magenta	p<0.001	*e*	GO:0022804	Active transmembrane transporter activity	7.77
			GO:0005215	Transporter activity	8.09
			GO:0022857	Transmembrane transporter activity	10.4
Red	p<0.001	*f*	GO:0008380	RNA splicing	7.88
			GO:0051028	mRNA transport	5.33

			GO:0006396	RNA processing	4.87
Light Blue	p<0.05	*g*	GO:0003988	acetyl-CoA C-acyltransferase activity	
Orange	p<0.01	*h*	GO:0006397	mRNA processing	10.6
			GO:0051028	mRNA transport	6.03
			GO:0008380	RNA splicing	8.39
Yellow	p<0.01	*i*	GO:0048037	Cofactor binding	5.61
			GO:0006732	Coenzyme metabolic process	9.16

3.3.4 Comparison of experimental results with previously reported interactors of eEF1A2.

As a first step to validate the identified proteins in my AP-MS, I compared experimental results to previously published interactors of eEF1A2. I compiled an interactome network of eEF1A2 from protein interaction databases String, BioGrid, GPSprot and IntAct. I then compared these proteins with the AP-MS hits to assess overlap. Figure 3.5A shows that only 5% of the proteins pulled down in my experiment had previously been associated with eEF1A2. Proteins in common include ribosomal constituents, eEF1B subunits and DNA replication factors, all constituents of statistically significant clusters in my own analysis. The overlap overall is disappointingly low and suggests there is an overestimate of interaction partners in this network.

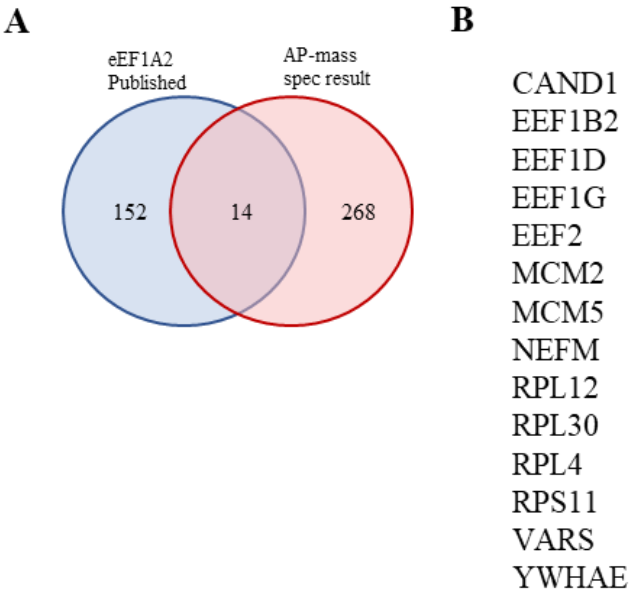

Figure 3.5: Comparison of AP-MS and published eEF1A2 interactions. ***A*** *Overlap between previously reported interactions (eEF1A2-pub) and proteins identified in the mass spectrometry experiment (AP-MS).* ***B*** *list of overlapping genes.*

Proteins which do share an overlap are of particular interest, however. The list of genes identified in Figure 3.5B includes subunits of the eEF1B complex, ribosomal protein subunits and molecular chaperone proteins. It can be concluded that these

proteins likely are true interactors. These proteins were, therefore, noted to be of most interest and were prominent in follow-up validation.

Cao and colleagues established that eEF1A2 interacts with the eEF1B complex just as eEF1A1 does (71). eEF1A is known to interact with the ribosome (156,157), presumably during its role in translation. eEF1A2 was identified as an interacting partner of 14-3-3 epsilon in a similar AP-MS experiment as part of a larger translation complex (158). The MCM complex has also been previously associated with eEF1A2 (155). The role these interactors may have when interacting eEF1A2 has been discussed in detail in Section 3.5.1.

Furthermore, all published interactions come from pull-downs where eEF1A2 was the identified interactor. eEF1A is known to be one of the most common contaminants in mass spectrometry experiments due to its prevalence. Whilst several papers have reported using yeast-two-hybrid assays to confirm the interaction of eEF1A2 with specific proteins (70,159,160), there has never been an AP-MS pulldown of full-length eEF1A2. One AP-MS experiment using the M-domain of eEF1A1 as bait has been reported. This research aimed to examine the non-canonical functions of eEF1A1 by isolating the domain not responsible for translation (161). However, there is a limited amount of research on interactors of eEF1A2 and my results supply the first known interactome using eEF1A2 as the bait pulldown protein.

In summary, the interactome I identified using affinity purification mass spectrometry supports eEF1A2 in protein synthesis as well as its non-canonical functions, including protein transport, actin bundling and unfolded protein mediation. Whilst there is little overlap between my results and published interactions, the interactions which do overlap are high confidence, and little published work focusses on eEF1A2 as the primary target.

3.4 eEF1A2 mutations alter eEF1A2 protein interactome

To establish the possible functional consequences of mutations in eEF1A2, I examined how mutations affected protein interactions. To do this, two mutations were selected and I examined their interactome in comparison with WT eEF1A2 (see experimental workflow in 3.1**A**). Any loss or gain of binding might explain possible loss or gain of functions. If mutations also yielded different interactome profiles, this might explain the severity variation between eEF1A2 mutation cases. Two mutations (D252H and G70S) were selected because experimental data in the lab had suggested they did not result in protein instability and because they were also being studied in mouse models. Work on the G70S mutation included a trial CRISPR mouse model attempt, in which I showed that the protein was expressed *in vivo* at levels similar to that of WT age-matched mice (140). These mutations, therefore, were deemed good candidates to test interaction analysis on, as they would not simply degrade, acting as a quasi-null protein.

3.4.1 Normalisation techniques for AP-MS data

For comparison of label free quantification intensities (LFQs) between genotypes, background filtering and normalisation of the dataset was required. Normalisation of label free quantification (LFQ) intensities was required to compare against different experimental conditions. Different normalisation strategies can be applied to affinity purification mass spectrometry (145). Normalising data correctly is imperative for proper interactome analysis, because each normalisation technique can manipulate the data in different ways, yield slightly different results and introduce bias. I examined different normalisation strategies appropriate to affinity-purification mass spectrometry, including bait normalisation, total area sums (TAS) and most likely ratio. Figure 3.6 displays the bait and TAS normalisation strategies. Whilst bait normalisation is the most established normalisation technique for AP-MS, variable levels of bait protein can skew results, by boosting contaminants in samples with low bait expression. Samples had a much higher intensity of eEF1A2 peptides in WT compared with G70S or D252H (0.07 and 0.1 $\log_2$ fold higher respectively) (Figure 3.6**D**). This discrepancy, although small sounding, can have a greater global impact,

as shown in the boxplot and heatmap in Figure 3.6**B** & **H**. eEF1A2 normalisation greatly reduced signal intensity of all proteins in the WT condition, augmenting what is likely background contamination in the mutant conditions. This normalisation strategy is the most appropriate for the experimental design, and true interactors should express in a linear fashion with bait proteins. However, an examination of the fold change analysis of each mutant when compared to WT showed how much this analysis technique biased data. Volcano plots for both D252H and G70S mutants showed a significant data bias to a greater fold change (when compared with the respective WT condition) instead of a normally distributed data set (Figure 3.7 C & D). This is likely to lead to the identification of false positive differential interactions.

Another technique employed to analyse data for AP-MS experiments is 'total area sums' (TAS) normalisation. In this technique, LFQ intensities for all interactors in a dataset are summed for each repeat. A ratio between the sum of the condition with the largest total and all other condition sums is produced. This ratio is then used as a normalisation factor for each respective condition. Whilst this analysis did result in the clustering of replicates by genotype in hierarchical clustering, analysis of TAS normalised data, between genotype differences were greatly amplified. The principal of affinity purification mass spectrometry dictates that unless a protein acts as a quasi-null, changes resulting from mutations will only result in interaction differences for a small number of proteins (162). Again, analysis resulting from TAS demonstrated a shift of mutant protein interactions towards the right, leading to a higher number of significantly greater interactions (green data points) than would be anticipated (Figure 3.7 A&B).

It is worth noting that in both normalisation techniques, a cluster of proteins has been found to be significantly reduced in the D252H condition when compared to WT (the eEF1B subunits). This consistency between different normalisation techniques is encouraging, and suggests this result is so strongly significant that it is not influenced by manipulation of the data. However, normalisation clearly

introduces great bias into this data set, and may occlude the discovery of smaller interaction changes, which may nonetheless be of interest.

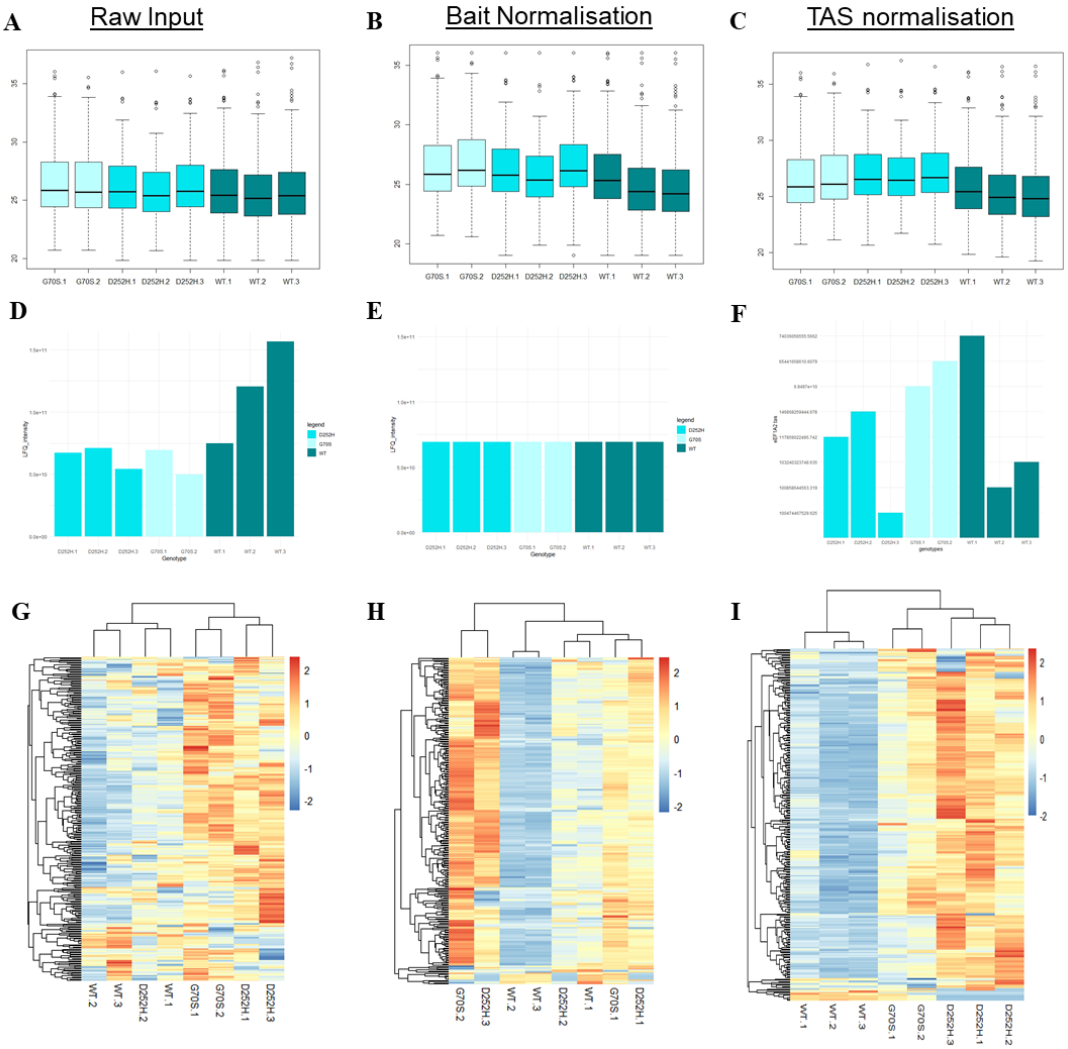

Figure 3.6: Normalisation strategies of AP-MS experiments. *A comparison of raw data (**A**, **D** and **G**), bait normalised data (**B**, **E** and **H**) and total area sums normalisation (**C**, **F**, and **I**). **A**-**C** highlights box plots demonstrating log2 data distribution for each sample with noted normalisation. **D**-**F** shows LFQ intensity values for eEF1A2 pre-normalisation (**D**), bait normalised (**E**) and TAS normalised (**F**). Heatmap of z-scores for each protein in raw, bait and TAS normalised samples is shown in **G**-**I**.*

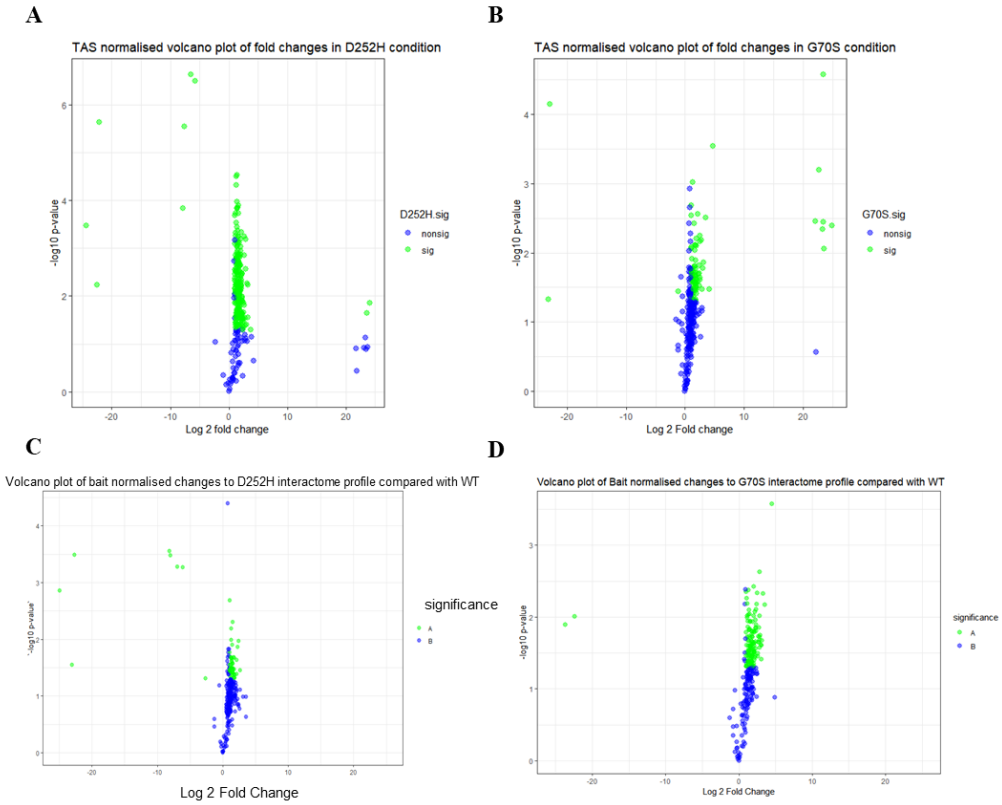

*Figure 3.7: Volcano plot for both TAS (**A** & **B**) and bait (**C** & **D**) normalisation for both mutations. Log fold changes for each mutation compared to WT for individual proteins are compared to the negative log 10 of their respective p-values. P-values were calculated using one t-test per protein with a 1% FDR correction for multiple testing. Blue points represent non-significant differences. Significant differences (defined as a log fold change greater than a log fold change of 1, and p <0.05) were displayed as green points.*

I examined an alternative normalisation strategy, developed by Lambert and colleagues (145), specifically for AP-MS when bait levels are deemed too variable for standard bait normalisation techniques. Called the Most-Likely Ratio normalisation (MLR), it is based upon the theory that there will be fewer proteins changing than remaining constant and uses this rationale to scale the data accordingly. The analysis works by comparing the $\log_{10}$ of ratios between replicates, with the understanding that replicate comparisons with minimal variance will display

normal distribution, with small kurtosis and peak around zero. Distributions are visualised and scaled appropriately based on the sample which is deemed most comparable with all other samples. There are two stages to scaling, firstly, technical repeats are compared, and scaled within their groups. Then biological replicates are compared, and an appropriate WT sample which varied least with both G70S and D252H was used for scaled normalisation. The full results of each step in the MLR analysis pathway are in appendix A.2. Figure (3.8A) displays an explanation of most likely ratio normalisation adapted from Lambert et al. **B**-**D** show the normalisation stages. Intensity ratios are compared to one WT sample in each instance to show how they vary. In raw input (**B**), variance is at its highest, with the data in most mutant conditions showing a density peak greater than zero, highlighting the overall higher intensity in data of mutant proteins. The first step of normalisation (**C**), scales and normalises technical repeats. Here closer alignments can now be seen between technical repeats when compared to one WT sample. Whilst this step of replication reduced the bias in D252H samples, aligning them better to WT, G70S samples still show a higher expression compared with WT. Biological normalisation (**D**) corrects this, shifting all values into normally distributed density plots which centre around zero, indicating that most protein intensity distributions have been normalised. This normalisation does appear to have made an impact of the global average protein expressions (**E**), however eEF1A2 levels still appear higher in two of the WT samples. Globally, however, the sample appears more normalised, with two of every genotype clustering together, although one WT and one D252H do not cluster. Importantly, this is more than with bait normalisation, and MLR appears to have corrected the distribution issue, which was likely boosting background contaminants in the mutant conditions.

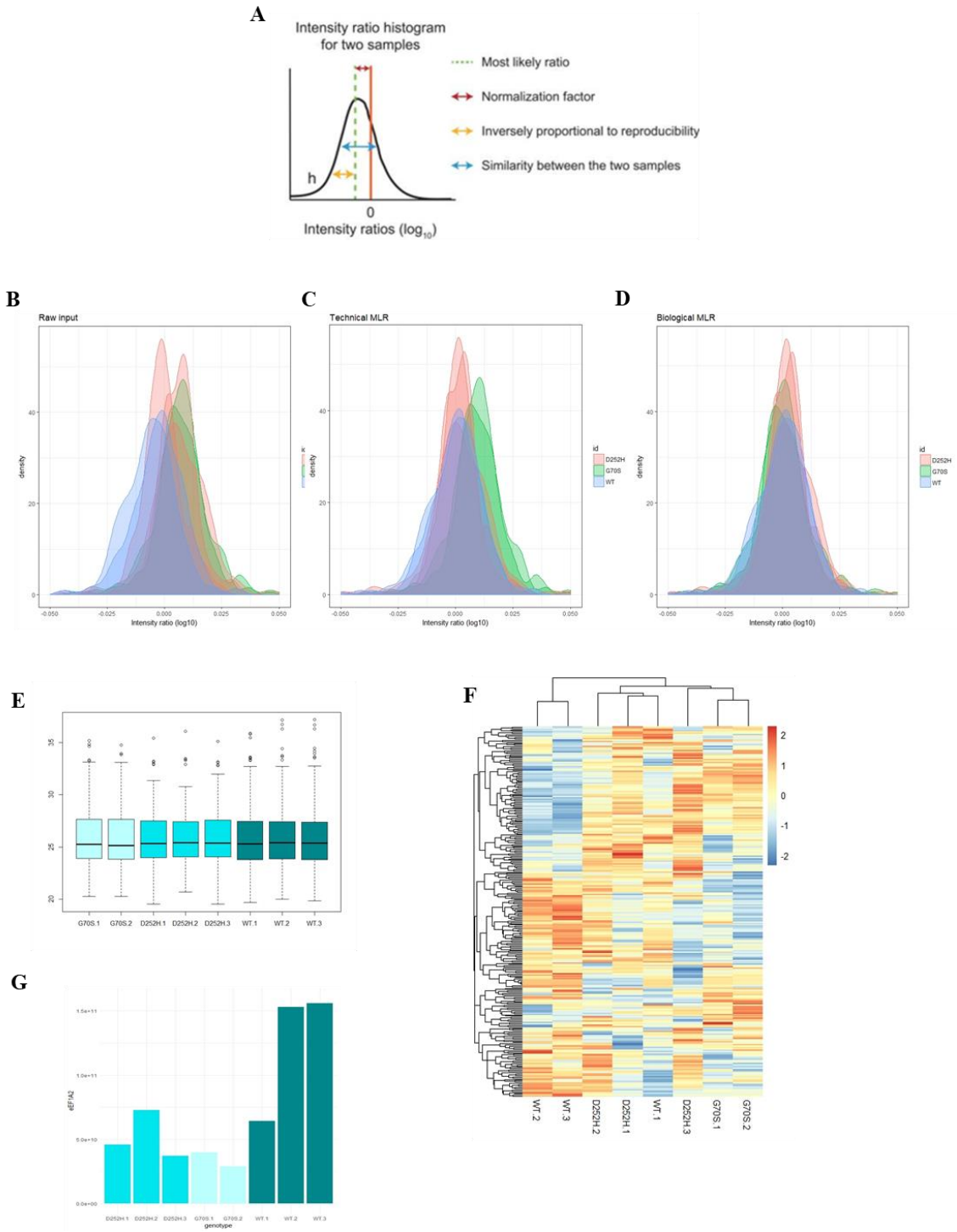

Figure 3.8: Most likely ratio normalisation analysis of the AP-MS data. ***A***, *an explanation of how MLR analysis adjusts replicates in data sets to minimise global variance and identify outlying interactors which are likely to be most affected.* ***B*** *demonstrates the distribution of raw* log_{10} *intensity ratios between respective*

proteins for each replicate compared with one WT sample. Each density peak represents an individual repeat compared to one WT repeat, with peaks coloured by genotype. ***C*** *highlights comparison of each replicate to the same WT sample post technical repeat normalisation.* ***D*** *shows the same intensity comparisons once biological-repeat normalisation.* ***E*** *is a boxplot displaying data distribution once MLR normalisation is complete, and* ***F*** *highlights a heatmap of z-scores for each protein across technical and biological repeats.*

Using MLR normalised data, both mutations show a normal distribution of fold changes with some significant interactors, making these proteins likely of most interest to study. Mutations do not appear to display identical interactome disturbances, indicating that changes in the interactome profiles may be specific, depending on the location of a given mutation. This result is the first evidence that protein interaction changes might illuminate which biological mechanisms are affected or the extent to which this happens. Of most note in the G70S mutation condition was an enhanced interaction with a cluster of ribosomal subunits (Figure 3.9B), whilst in the D252H condition by far the most significant result was a $\log_2$ ~9-fold decrease in the subunits of the eEF1B complex - *EEF1B2*, *EEF1G*, *EEF1D* and *VARS*, (Figure 3.9A). Additionally, a gain of interactions to a group of ribosomal subunits is seen, although, a smaller number than is seen for G70S.

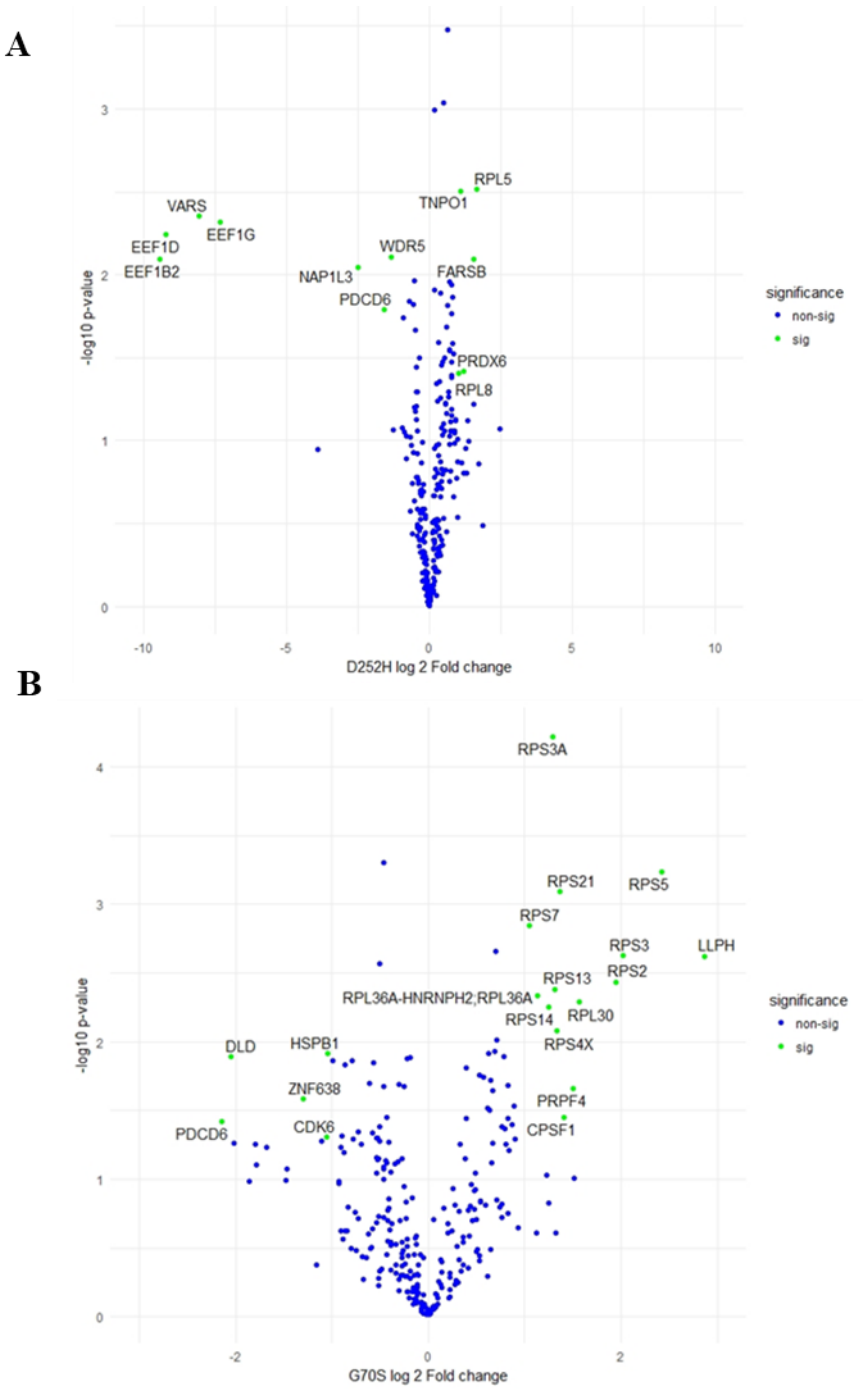

Figure 3.9: Volcano plots show distribution changes of D252H (A) and G70S (B) mutations after MLR normalisations. *Log_2 fold change of each mutation compared to WT was plotted against the corresponding -log_{10} p-value. P-values were calculated using one t-test per protein with a 1% FDR correction for multiple testing. Proteins were defined as significant (green) when there was a log_2 fold*

change greater than 1 and $p < 0.05$. These proteins have been annotated with their respective gene names for identification. Non-significant proteins were identified in blue.

MLR is probably over-conservative in its assessment of differential interactors, however the normalisation strategy managed to shift data towards a more normal distribution reducing the influence of background contaminants in the sample.

3.4.2 Interactome mapping differences resulting from mutations

Whilst 'top hits' can be identified in investigations such as volcano plots, more subtle protein complex changes could be overlooked. I further explored how interactions changed within the context of the eEF1A2 interactome. Log_2 fold changes for each mutation were mapped onto the interactome using a coloured scale to represent loss and gain of interaction. Figure 3.10A and B are the interactome disruptions for most-likely ratio normalised interactomes for $eEF1A2^{D252H}$ and $eEF1A2^{G70S}$ respectively.

Figure 3.10B displays MLR normalisation induced changes to the eEF1A2 interactome as a result of the G70S mutation. There is no significant difference in eEF1B subunit interactions in AP-MS between WT and G70S conditions. Validation experiments also show that there is no discernible difference between binding of WT and G70S to eEF1B subunits (Section 3.5.5). This casts some doubt on solely relying on the MLR normalisation technique to identify changes. I decided to compare changes resulting from both MLR and bait normalisation techniques. Examining changes mirrored in the two normalisation techniques is the most likely strategy for determining real proteins of interest. Log_2 fold changes after bait normalisation were determined and mapped using a colour scale to the eEF1A2 interactome (Figure 3.10C and 3.10D). Because of the bias towards increased interactions, a higher fold change score was set identifying a protein as having an increased interaction (see legends of Figure 3.10C and 3.10D). This allowed for an examination of the most extreme changes and increased the likelihood of finding clusters with meaningful differences.

In Figure 3.10D the down-regulation of eEF1 subunits in cluster *a* is not present, but there is still an increase to all ribosomal subunits. Other clusters showing the same increased interaction pattern in both normalisation techniques, were clusters '*h'* and '*i'*. Cluster '*h'* demonstrated increased interaction to RNA binding proteins. GO terms associated with mRNA '*i'* functional enrichment identified proteins associated with cofactors. Along with the enriched association to translation proteins, these

results provide insight into two molecular functions potentially impacted by the G70S mutation.

Figure 3.10C expands upon the results of the most significantly different interactors resulting from D252H identified in Figure 3.9A. The clear loss of eEF1B subunits is apparent within the network (cluster '*a*'), however this phenomenon does not extend to the rest of the proteins in this cluster, which showed up-regulation. All proteins identified were associated with translation. The cluster is primarily composed of ribosomal subunits and translation initiation factors. The cluster is significantly enriched, and all subunits (excluding the eEF1B subunits) show the same increase in association, meaning it is likely that the D252H mutation influences interactions with the ribosome and translation initiation factors.

As with G70S, two clusters which show the same pattern of increased binding in both normalisation strategies are clusters '*h*' (RNA binding) and '*i*' (co-factor binding). Because all 3 of these clusters show the same pattern of increased association in both mutations regardless of normalisation strategy, these results identify proteins of interest which are likely to be implicated in molecular dysfunction. Both normalisation strategies show an increase in binding in cluster '*j*' in mutant D252H relative to WT. Functional enrichment analysis resulted in no identification of relevant GO terms (likely owing to the size of the cluster). Proteins included involved more ribosome associated proteins (RSL1D1, RRS1 and RBM28) and RNA binding proteins (DDX21, DDX50, NSUN2 and HDLBP).

A

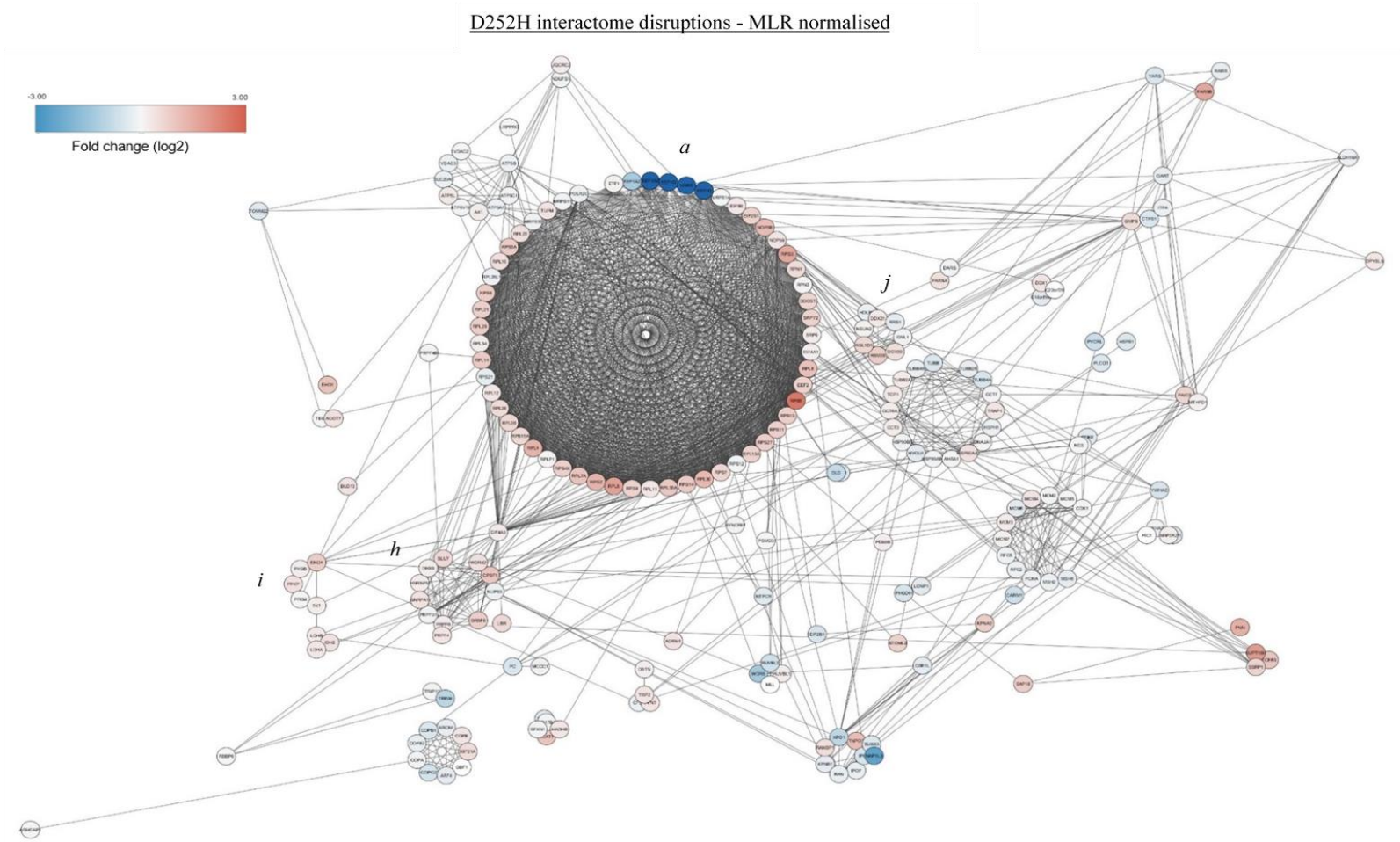
D252H interactome disruptions - MLR normalised
-3.00
3.00
Fold change (log2)
a
h
i
j

B

G70S interactome disruptions -MLR normalised

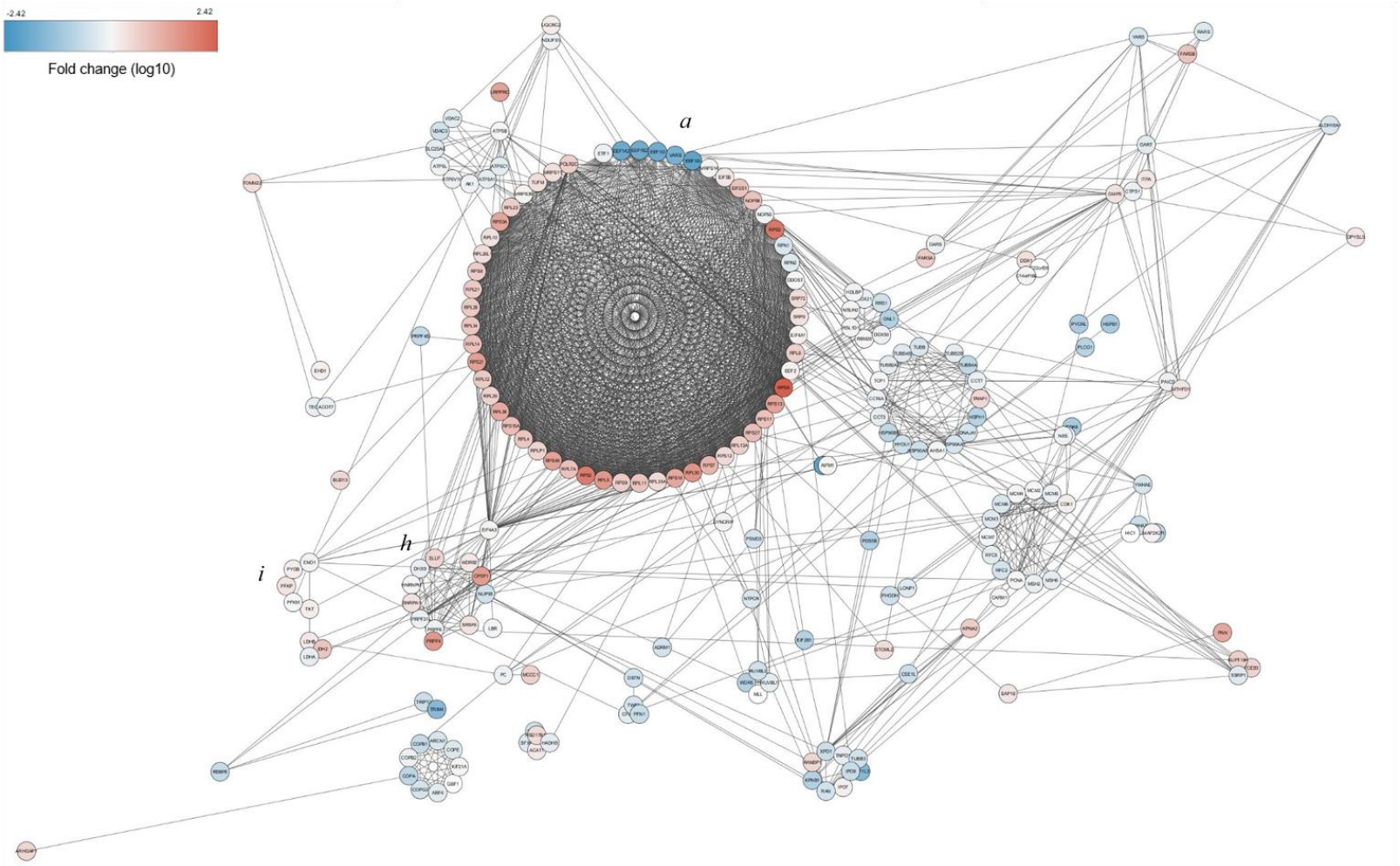

C

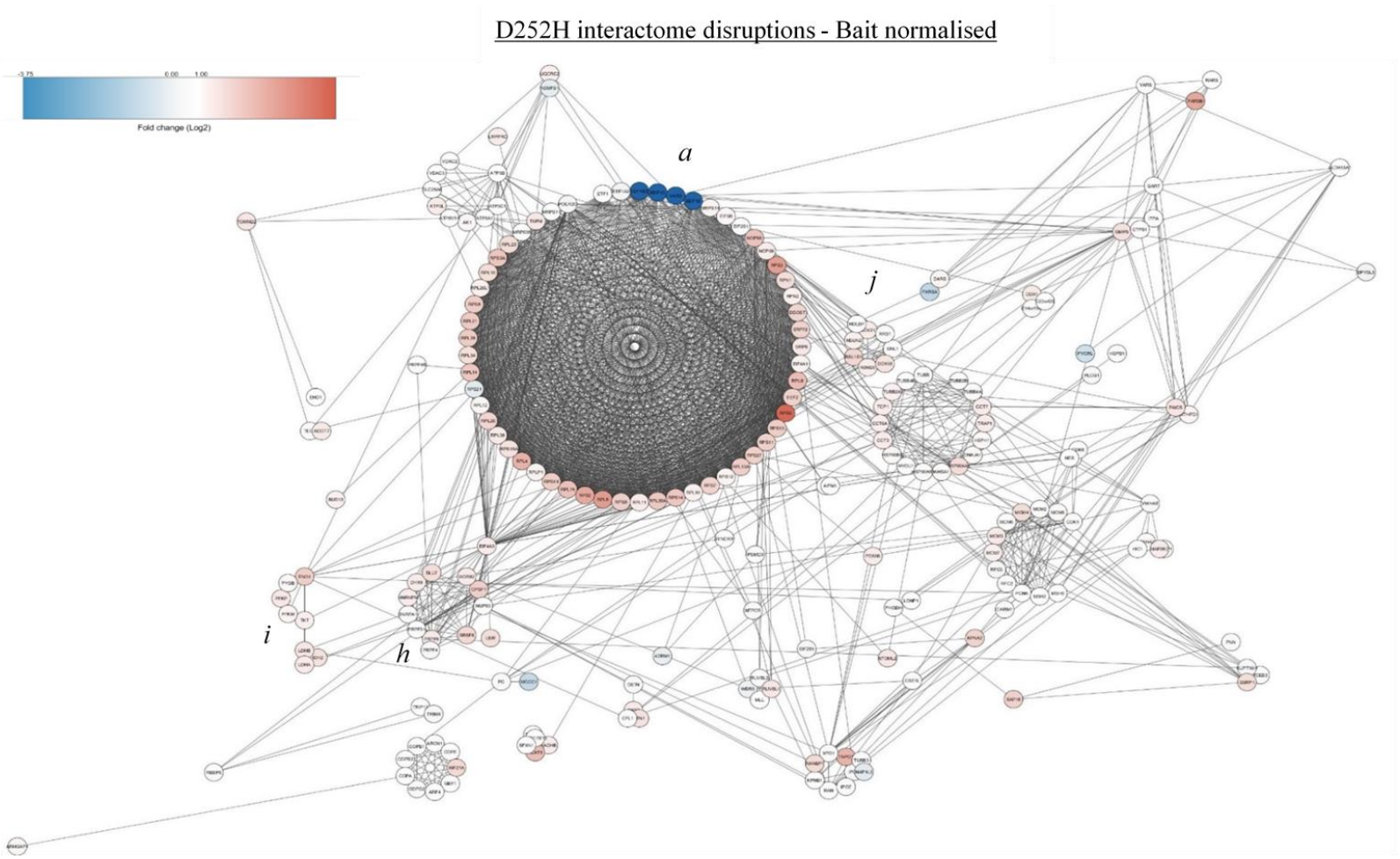
D252H interactome disruptions - Bait normalised
-3.75
0.00
1.00
Fold change (Log2)
a
j
i
h

D

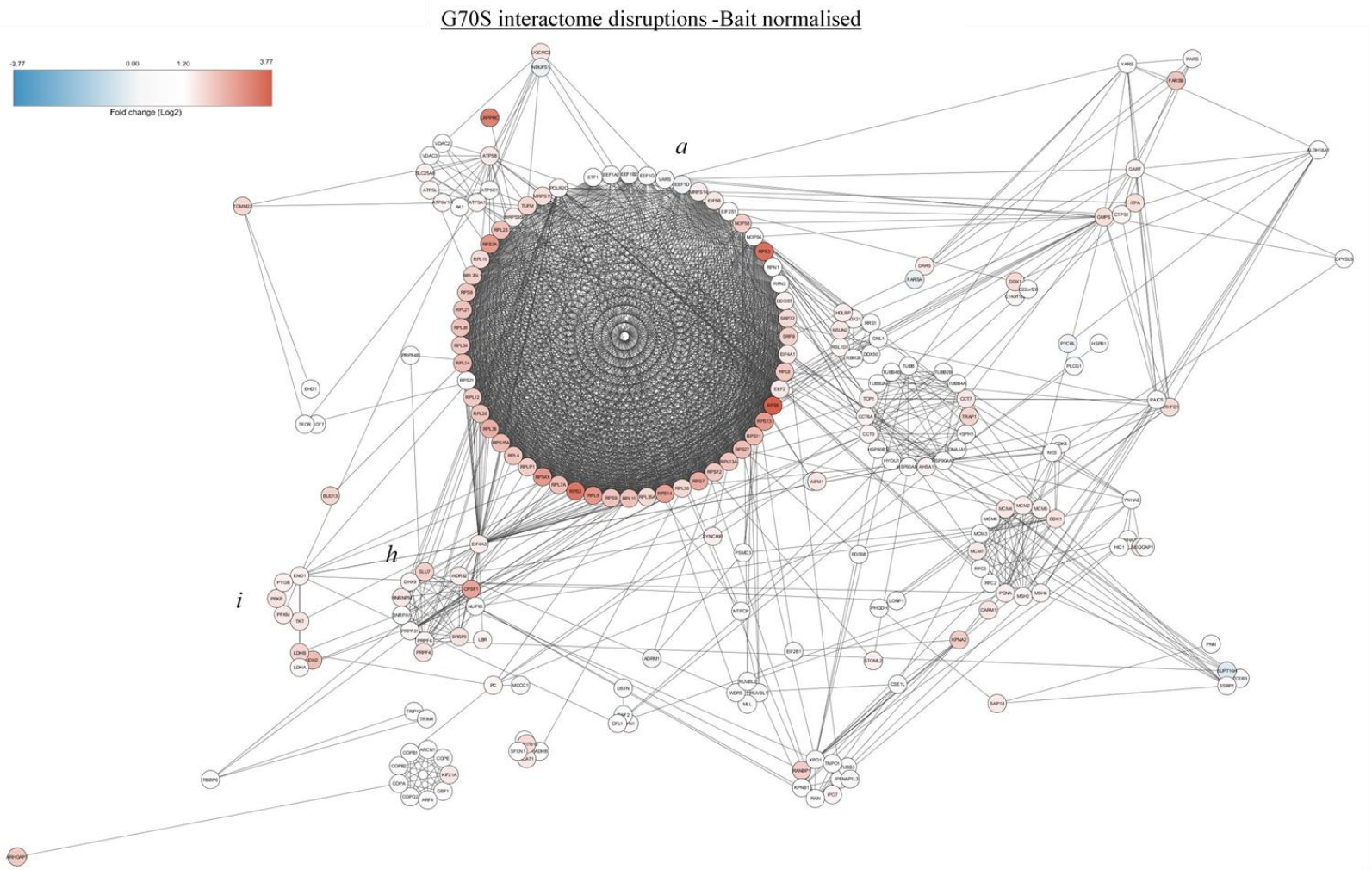
G70S interactome disruptions -Bait normalised
-3.77
0.00
1.20
3.77
Fold change (Log2)
a
h
i

Figure 3.10: Colour mapping of Log_2 fold changes of mutant versus WT LFQ intensities in AP-MS. ***A****, eEF1A2 interactome (MLR normalised) with colour mapping of log_2 fold changes in the D252H conditions compared with WT. Because fold changes for the eEF1B subunits were so extreme, using a full range scale resulted in under amplification of more subtle changes in interaction. Therefore, the fold change scale was set between -3 to 3 (log_2), this scale covered the fold change scores for all proteins excluding the eEF1B subunits, which are displayed as saturated (see Figure 3.4).* ***B****, eEF1A2 interactome (MLR normalised) with colour mapping of log_2 fold changes in the G70S condition compared with WT.* ***C****, eEF1A2 interactome (bait normalised) with colour mapping of log_2 fold changes in the D252H condition compared with WT. Because fold changes for the eEF1B subunits were so extreme, using a full range scale resulted in under amplification of more subtle changes in interaction. Therefore, the fold change scale was set between -3.75 to 3.75 (log_2). This scale covered the fold change scores for all proteins excluding the eEF1B subunits, which are displayed as saturated. To reduce influence of data normalisation bias (discussed kin Section 3.5.1), a 1-fold (log_2) score was set at minimum for identification as an increased interactor.* ***D****, eEF1A2 interactome (bait normalised) with colour mapping of log_2 fold changes in G70S condition compared with WT. To reduce influence of data normalisation bias (discussed in Section 3.5.1). A 1.2-fold (log_2) score was set as the minimum for identification of an increased interactor.*

In both instances, protein interactions which display the most dysregulation are associated with RNA regulation and protein synthesis. Critically, D252H shows altered protein interaction disruptions to eEF1B subunits, a binding disruption not seen in G70S. Altered interactions due to location of the mutation within the protein is the principle of Sahni and colleagues edgetic interactions theory (163). It is key to explore this discrepancy between mutations in greater detail, as it might underpin the variation in severity seen between cases (see Chapter 4).

3.4.3 Loss of binding to guanine cognate exchange factor

By far the most significant result, regardless of normalisation strategy, was the loss of binding to eEF1B subunits in the D252H mutation but not G70S (Figure 3.11B). eEF1B is composed of guanine exchange factors eEF1Bα and eEF1Bδ which are anchored by structural subunit eEF1Bγ. Valine tRNA synthetase (ValRs) is not a component of the eEF1B complex but is associated via an interaction with eEF1Bδ (Figure 3.11A) (85). All subunits were identified in the mass spectrometry and displayed a consistent pattern of interaction in each mutation (Figure 3.11B). Transiently transfected eEF1A2-V5 in a co-immunoprecipitation assay validated this finding (Figure 3.11C). All four subunits associated with eEF1B, show no signal in the eEF1A2^{D252H} condition, despite equal expression of the proteins in the unbound (input) fraction, and the presence of eEF1A2-V5 in the bound (IP) fraction. As with the AP-MS, the eEF1A2^{G70S} mutation displayed no difference in binding to any eEF1B subunits (Figure 3.11D). It also appears that WT eEF1A2 interacts with eEF1B subunits in a stoichiometric manner, as one WT sample shows less eEF1B subunit signal in response to less V5 (bait) staining. Taking stoichiometry into account is one of the key ways of identifying valid and important interactors within a mass spectrometry experiment (164).

A loss of binding to its cognate guanine exchange factor would likely hinder eEF1A2 in GDP recycling and consequently impair protein synthesis. It seemed imperative to explore this discovery further. Possible loss of protein synthesis in the D252H mutation would indicate a loss-of-function mechanism. I therefore expanded upon these results (Chapter 4 and Chapter 5).

For eEF1A2^{G70S}, the most significant result was an increased interaction with ribosomal subunits compared to WT. This result was investigated further by testing these interactions using co-immunoprecipitation (Figure 3.11D). Co-immunoprecipitation failed to find an interaction of eEF1A2-V5 with ribosomal subunits in any condition. This suggests that either the differential interactions identified in the AP-MS are false positives, or the interactions are too transient, weak or infrequent for co-immunoprecipitation to identify. It has been previously

established that eEF1A2 interacts with the ribosome (156,157). It may be the case, however, that any interaction is not observable using co-immunoprecipitation. It may be of interest to examine changes to ribosome function as a consequence of the mutation eEF1A2^{G70S} using an alternative method (such as ribosomal profiling). Given the negative co-immunoprecipitation results, I focussed my follow-up research on the loss of binding to the eEF1B complex in eEF1A2^{D252H}.

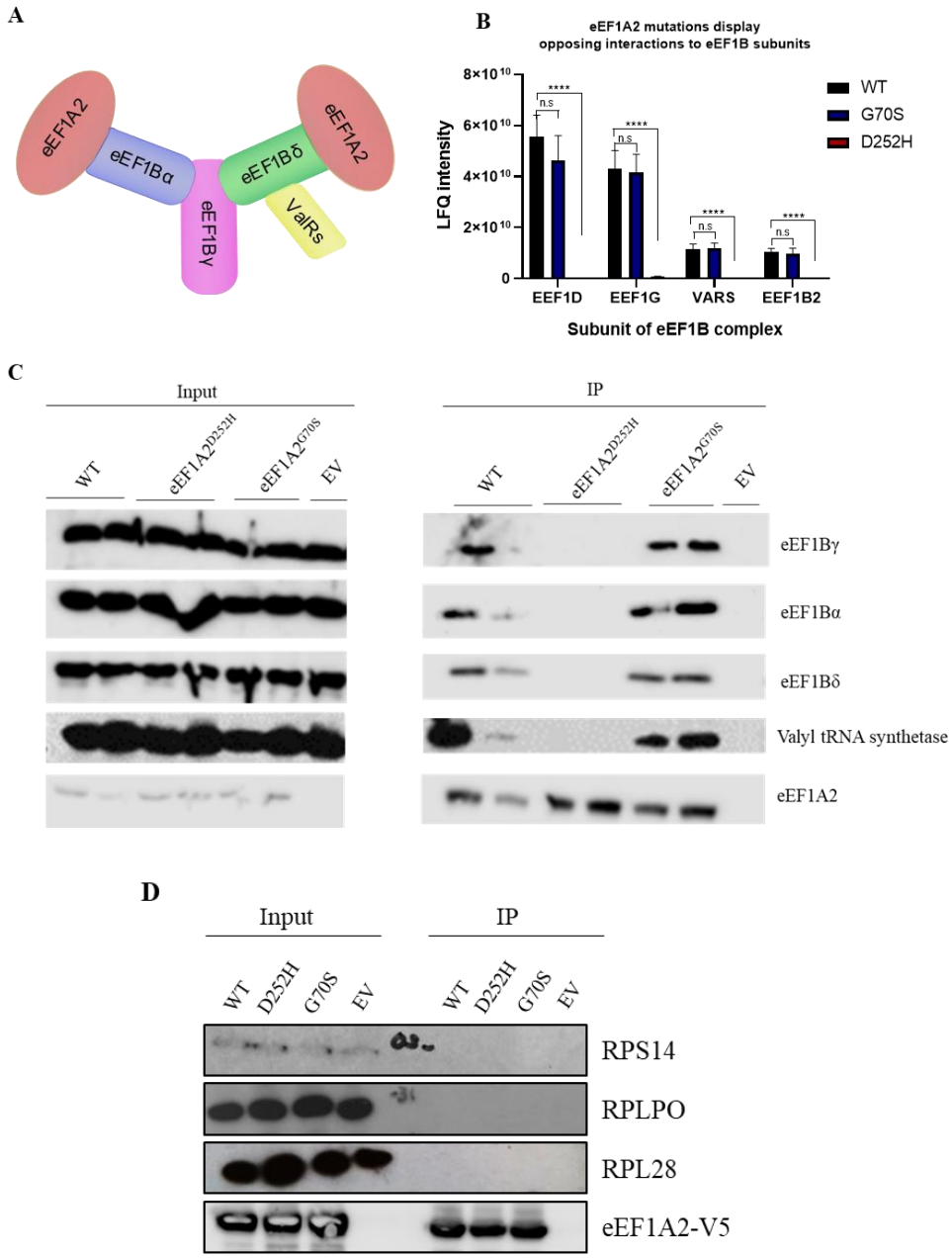

Figure 3.11: eEF1A2 mutations and their respective interactions with components of translation machinery. A*, a schematic of the eEF1 complex, including eEF1A2, and the subunits (and associated proteins).* ***B****, the LFQ intensities of each subunit in WT and mutant eEF1A2 conditions. P-values were identified using one-way ANOVA per protein comparing WT, G70S and D252H mutations. Tests for all subunits reported a significant interaction: eEF1Bα F(2,5)=84.81, p<0.001, eEF1Bδ F(2,5)=191.9, p<1x10^{-4}, eEF1Bγ F(2,5)=119.4, p < 1x10^{-4}, VARS p<1x10^{-5}. Post-hoc analysis was performed using Tukey tests. '****' refers to p<0.0001.* ***C*** *displays*

the co-immunoprecipitation experiments in SH-SY5Y cells. eEF1A2-V5 was isolated using the V5 tag. Subunits were then probed for using western blot. Input fraction (1/8th concentration of IP loaded) is displayed on the left, with the IP fraction on the right. Subunits were probed for using protein-specific antibodies. eEF1A2-V5 bait was confirmed with V5 staining ***D*** *demonstrates co-immunoprecipitation experiments to examine the interaction of eEF1A2-V5 and ribosomal subunits.*

3.5 Discussion

In this chapter, I examined the protein interaction network of eEF1A2 using affinity purification mass spectrometry. As the interactome of eEF1A2 had not previously been studied using this technique it was a useful tool for examining the possible functions of eEF1A2 and the effect specific mutations in eEF1A2 have on the interactome.

3.5.1 The eEF1A2 interactome

I used AP-MS to assess the protein interactions of eEF1A2. After background filtering, functional enrichment analysis was used to assess the make-up of the interactome. GO terms associated with eEF1A2 interactors were, in the main, associated with known functions of eEF1A2. Structural constituents of the ribosome and translation elongation factor subunits were identified, as would be expected. It has previously been established using the proximity ligation assay that eEF1A2 binds to eEF1B subunits (71). It is also unsurprising that ribosomal associated GO terms are enriched. eEF1A2 has previously been found to co-complex with a number of ribosomal proteins (156).

Principally, eEF1A2 interactors could be categorised as involved in catalytic activity, translation or protein binding. Whilst the first two could be attributed to its role in protein synthesis, it was worth examining the 'binding' category in more depth. In this category the majority of proteins are responsible for protein and nucleic acid binding. The nucleic acid binding term highlighted the number of RNA binding proteins eEF1A2 interacts with. It is unsurprising that eEF1A2 should co-complex with so many proteins in this category, given its ability to bind to aminoacylated tRNAs. Not only is it associated with tRNA delivery, but it has also been identified as a component of RNA granules (165). eEF1A, more generally, has been identified as a constituent part of RNA granules in both axons (166) and dendrites (48,49). Although the isoform is not specified in these publications, as the experiments are performed in developed neurons it is likely eEF1A2 is involved. RNA transporting granules are of particular importance in neurons, as RNA must be transported to distal parts of the neuron for rapid local protein synthesis.

The protein binding category contained proteins involved in cytoskeletal function. Actin bundling is one of the most discussed functions of eEF1A (29). It is hypothesised that the differences in actin bundling properties is the reason for the conserved presence of two isoforms in vertebrates. Abbott et al argued that in terminally differentiated cells, where cytoskeleton may require a more stable cytoarchitecture. The isoform switch may occur to spare terminally differentiated cells, such as neurons, from the same actin bundling activity as in proliferating cells (21,28).

AP-MS results isolated actin and several actin binding proteins (profilin, cofilin and destrin) from the eEF1A2-V5 complex. The experiment cannot determine whether this interaction represents an actin bundling property of eEF1A2, or whether there are differing actin bundling properties in eEF1A2 compared to eEF1A1. Actin and profilin concentrations have been shown to correlate with relative expression of eEF1A in maize endosperm. Suggesting there is a relationship between the proteins (167). If this is the case, eEF1A2 might share this interaction with eEF1A1.

One interesting difference between the two isoforms is their reported differing interactions with Ca^{2+}-calmodulin, and how this might influence the actin bundling properties of the proteins. Computationally it was predicted that amino acid variance between eEF1A1 and eEF1A2 would alter the flexibility of the putative calmodulin binding region Asn311-Gly327. Less flexibility of this region in eEF1A1 suggests it has an increased affinity for calmodulin than eEF1A2. These results were confirmed experimentally using ELISA analysis (168). Novosylna expanded on this research, confirming that eEF1A1 but not eEF1A2 results in interaction with Ca^{2+}-calmodulin. The authors expanded upon this result, demonstrating that the interaction of eEF1A1 with Ca^{2+}-calmodulin blocked both its actin and tRNA binding sites, negatively influencing ability of eEF1A1 to bundle actin. The authors suggest that eEF1A1 and eEF1A2 have different Ca^{2+}-modulated actin bundling properties (21). It is worth noting that in my AP-MS results, no evidence of calmodulin binding was found. My results, therefore, support the growing evidence that calmodulin interactions differ between isoforms, which may consequently mediate differences in actin bundling.

Overall, although specific protein interactions require validation, my results provide the first networked example of the eEF1A2 interactome. By clustering proteins using functional interaction scores, groups of proteins associated with canonical and some known non-canonical functions of eEF1A2 have been identified.

3.5.2 Analysing changes in the interactome due to mutations

My results identified protein interaction dysregulation in both the D252H and G70S mutations. These altered interactions were, however, not the same in both mutations. Sahni and colleagues studied edgotype disruptions resulting from missense mutations. They found mutation location to be the biggest predictor of how the edgotype would be disrupted (163). It is possible the differing level of severity in clinical cases is due to the varying locations of mutations in the protein. eEF1A2^{D252H} is located within the eEF1B binding site, whilst eEF1A2^{G70S}, although close to the binding site, is not. Most mutations on the surface of the protein cluster near sites of known functions of eEF1A2 (eEF1B and GTP binding). It was important to expand upon these results, to determine whether edgetic disruptions control clinical case severity. One caveat to be considered is the level of mosaicism in patients. In most cases, no mosaicism is detected, however the degree of mosaicism is not known for all patients and, if present, could greatly moderate the severity of any phenotype. Spatial analysis of mutations and how they might affect protein function is further examined in Chapter 4. It is interesting however, that preliminary experiments show a difference in interaction profiles, disruptions which can be directly correlated with location in the protein structure. This may serve as a useful predictor of eEF1B binding disruptions in other mutations.

One differential interaction between mutations identified in the AP-MS experiment was the increased affinity for ribosomal subunits in eEF1A2^{G70S} as compared with WT. This result was not reported to such an extent in the eEF1A2^{D252H} condition. Upon validation with co-immunoprecipitation, no interaction with ribosomal subunits could be found in any IP fraction. It is well established that eEF1A2 delivers amino-acylated tRNAs to the ribosome in protein synthesis. The exact nature of the interaction between eEF1A2 and the ribosome is

not fully elucidated, however. It is not known whether eEF1A2 interacts with the ribosome during tRNA delivery, or if eEF1A2 interacts with the ribosome in another capacity. Given the negative co-immunoprecipitation results, it is entirely possible that these interactions were false positives. It is also possible that the transience or weakness of these interactions makes studying the eEF1A2-ribosomal relationship impossible using co-immunoprecipitation. Given that these results were not able to be validated, I focussed follow-up experiments on the functional impact of the loss of eEF1B in eEF1A2^{D252H}.

In artemia, it has been shown that the loss of eEF1B results in a 1000 fold decrease in spontaneous GDP release (69). The yeast eEF1B equivalent, EF-Tu, is required for proper protein synthesis. Mutation E122K (interestingly - the same amino acid residue as one of the reported clinical cases) leads to greater translational infidelity and growth deficits (169).

Although less dependency on eEF1B is expected in the metazoan complex (23), loss of binding would still likely impact the ability of eEF1A2 to function in protein synthesis. Cao and colleagues found knocking down eEF1B subunits using siRNA did not impact cell growth or viability in the short term (71). However, due to the nature of the experiment, it was not possible to examine the long-term effects of these knockdowns. Furthermore, only one subunit was knocked down at a time, something which could potentially cause a less severe phenotype than loss of binding to all subunits.

There is certainly clinical evidence to support the requirement of eEF1B function in neurons. Mutations in other eEF1B subunits (as discussed in Section 1.4.3) have been found in individuals with neurodevelopmental disorders (170). Unlike eEF1A2 these mutations are homozygous, often the result of consanguineous parents. In eEF1Bδ mutation cases, reported mutations affect only the neuronal specific isoform (103). Whether this impacts just the heat-shock element or impacts global translation elongation rates is still under investigation. Recently Kaitsuka and colleagues demonstrated results to the contrary, suggesting the knock-out of the eEF1BδL isoform resulted in increased global translation as measured both by puromycin and

35S methionine labelling. However, the protein synthesis assays were not carried out on untreated mice, so background levels cannot be determined. My results in chapter 5 suggest that larger samples of mice for protein synthesis measurements *in vivo* would be required to detect differences, with only 3 for each sample being presented by Kaitsuka and colleagues. Further study must be done to determine whether eEF1BδL plays a role in protein synthesis. The authors did argue that the loss of eEF1BδL resulted in phenotypic differences between WT and knock-out mice. It is possible therefore that the intellectual disability displayed in the terminating mutation of the long isoform is a result of disruption to heat shock response and not translational imbalance.

A homozygous deletion in chromosome 2 which included half of the *EEF1B2* gene (gene encoding the eEF1Bα subunit) has been reported in a consanguineous family. Individuals present with a neurodevelopmental disorder including intellectual disability (102). It is surprising that such a homozygous deletion would be compatible with life and provides a suggestion that eEF1A can function partially without its cognate GEF. However, the individuals are still affected by the loss of the gene. Similarly, a recently reported mouse model with homozygous deletion in *Eef1b2* resulted in a viable mouse model which presented with neurological deficits (http://www.mousephenotype.org/data/alleles/MGI:1929520/em1(IMPC)J). This evidence, in conjunction with the reports of mutations in *EEF1D*, suggests that impacting the function or interaction with eEF1B could impact upon neuronal protein synthesis rates. It would be interesting to determine whether this is because neurons have a higher homeostatic requirement for protein synthesis than other cell types, or because eEF1A2 relies upon the action of eEF1B more than eEF1A1.

This is not the first evidence that disrupted protein synthesis would impact upon neurological function. Mutations in many other proteins associated with translation have been implicated in similar neuronal disorders. In some cases, like eEF1A2 and mutations in eEF1BδL these have been found in neuronal specific isoforms. However, this is not always the case. There are many cases of amino-acyl synthetase mutations which cause neurological disorders. An explanation for why these might

disproportionately affect neurons is provided in the introduction of this thesis (Section 1.4.3).

If loss of binding to eEF1B causes impaired protein synthesis, then D252H mutation causes a functional null, in terms of canonical function at least. Another possibility is that all the mutations render the protein non-functional. The discrepancy between G70S and D252H interactome profiles implies that D252H but not G70S would result in protein synthesis disturbances. This should result in a more severe phenotype for the D252H mutation than the G70S, if the mutations were operating under a loss-of-function mechanism alone. This, however, appears not to be the case. There are two possible reasons for this; 1) all clinical mutations render eEF1A2 non-functional and therefore binding to the guanine exchange factor is irrelevant, 2) an additional or other function of the protein is impacted by mutations. This leads to the question do mutations simply act as loss of function mutations or is there an additional toxicity element?

3.6 Conclusions

AP-MS proved an insightful technique for establishing the interactome of eEF1A2. Comparison of WT and mutant forms of eEF1A2 demonstrated protein interaction disruptions in both G70S and D252H conditions. These disruptions were not uniform between mutants, supporting the edgetic perturbations theory proposed by Sahni et al. In D252H, binding analysis results, indicate that protein synthesis would be impacted.

Chapter 4: Further analysis of interactome disruptions

4.1 Introduction

AP-MS analysis created a possible interaction network for eEF1A2 and enabled me to examine changes resulting from mutations (Chapter 3). The most significant finding demonstrated a loss of binding of mutant eEF1A2^{D252H} to the subunits of cognate guanine exchange factor (GEF) eEF1B. Mutation eEF1A2^{G70S} however, did not display the same interaction disruption. These findings were validated *in vitro* in SH-SY5Y cells by exogenous tagged IP-pulldown. Disruption of binding to the GEF would likely result in lower rates of GDP recycling, impacting upon the ability of the protein to perform protein synthesis. An assessment of the impact of mutation eEF1A2^{D252H} on protein synthesis is examined in Chapter 5. The disparity between eEF1A2^{D252H} and eEF1A2^{G70S} interaction profiles suggests several possibilities. 1) As both D252H and G70S mutations result in a clinically severe phenotype, mutations render the protein non-functional. 2) eEF1B interaction is not required for efficient protein synthesis by eEF1A2, and an additional causal mechanism is responsible for the protein malfunction. 3) Mutations impact upon the proteins ability to perform protein synthesis, but this is not the only effect of mutations, meaning an additional gain-of-function, in combination with a loss-of-function mechanism is at play. I explored these possibilities further using both *in vitro* and *in vivo* experiments.

Firstly, the interaction profile disparity of mutant forms of eEF1A2 was explored in greater detail. Computational analysis was performed to assess whether online tools could predict disruption in mutants. An array of mutations located throughout the protein were subsequently tested for interaction with eEF1B subunits to see if any pattern between interaction disruption and phenotype or amino acid localisation could be identified.

Secondly, using *Eef1a2*$^{D252H/D252H}$ and *Eef1a2*$^{-/-}$ mouse models, an assessment of phenotype was performed. If the loss of binding to cognate guanine exchange factor eEF1B in the case of eEF1A2^{D252H} led simply to a reduction in protein synthesis, then mice should demonstrate a partial or complete functional null phenotype.

However, a more severe phenotype in mutant mice than *Eef1a2*$^{-/-}$ would implicate an additional molecular consequence.

These experiments were designed with the aim of further identifying the consequences of eEF1A2 missense mutations on neuronal function.

4.2 Aims of chapter

1) Identify whether interaction profiles can be predicted.
2) Experimentally test eEF1B interactions with more eEF1A2 mutations.
3) Assess the phenotype of *Eef1a2*$^{D252H/D252H}$ mice to see if it is consistent with a loss- or dominant negative/gain-of-function mechanism.

4.3 Determine interaction profiles of other mutants

4.3.1 Computational analysis of interaction profiles of eEF1A2 mutations

Given the disparity between D252H and G70S interactome profiles, I performed analysis of the relationship between eEF1B and other mutations in the eEF1A2 protein. I wanted to ascertain if either D252H or G70S was an outlier in its interaction profile, or whether mutations could be grouped based on the relationship with interacting proteins. Initially predictive analysis of all mutations was implemented in several software prediction programmes. Given the array of mutations, experimental validation would be a labour intensive and costly task. Predictive analysis programmes claim to be a method of circumventing this experimental step, using calculations based on known interactors, changes in charge, structural alterations and internal bond disruptions. Many methods have been developed to use data and experimental knowledge to provide insight in to possible outcomes of mutations on binding (171). I used predictive analysis to see if consistency in predicted disruptions was found between different computational methods, and whether computational analysis would mirror experimental results, making it a good predictor for all mutations.

Prediction software assessing protein interactions can rely on several different sources of information to assess potential disruptions. These include, but are not limited to, conservation of the gene, whole gene order, evolutionary relationship, 3D protein structure, domain information and primary protein structure (172). I chose three protein interaction tools to identify whether the predictions they gave would match experimental results. Table 4.1 shows results from software tools which assessed structure and interactions of eEF1A2 missense mutations.

ELAPSIC is a computational pipeline which works to identify protein interaction disruptions by identifying the pfam domain boundaries of the protein, modelling domain-domain interactions and using this information to predict the energetic impact of mutation on a single domain or the affinity between two domains. The main output of the program is a predicted change in Gibb's free energy ($\Delta\Delta G$) of folding or binding for every domain affected by the mutation. This allows ELAPSIC

to predict whether changes are likely to affect interfaces responsible for protein interactions or the core stability of the protein (173). ELAPSIC analysis identified a cluster of mutations predicted to disrupt binding to eEF1B. These were grouped together and located near the eEF1B binding site. Although this would make sense, experimental results prove this prediction analysis to be incorrect. Results 3.4.2, show that contrary to the predictions of interactions with the G70S and D252H mutant forms of the protein (Table 4.1), the reverse is true. Section 4.2.2 provided further results which differ to computational findings. Mutations which demonstrate a reduction in eEF1B interaction in co-immunoprecipitation experiments have been highlighted in blue, whilst those which retain their interaction with the guanine exchange factor have been shown in red (Table 4.1).

A second prediction software, BeAtMUsIC also calculates the change in binding free energy (ΔΔG) and predicts the effect on binding intensity changes (174). ΔΔG values were calculated for all mutations and resulting predictions made by the program are summarised in Table 4.1. In addition, BeAtMUsIC enables the user to calculate the potential binding disruptions of all amino acid residues in the protein. The top 25 mutations which resulted in the greatest increase and decrease in binding affinity were calculated. These have been reported in appendix B.1. I highlighted these residues on the protein structure using Chimera software (Figure 4.1).

Many of the residue changes which resulted in the greatest increase or decrease in ΔΔG were where mutations occurred (Asp.252 and Ile.71). Furthermore, examining these residues on the 3D structure identifies that the most affected area is the ‘conserved face’ (4.1A), where aminoacyl-tRNA and eEF1B interactions occur. The individual predictions about changes in affinity for each specific mutation do not agree with experimental findings, however (Table 4.1), with increases in affinity predicted in D252H and P333L. Although BeAtMUsic did not predict the binding affinity changes for mutations accurately, it did identify the area of the protein in which ΔΔG changes, as a result of mutations, would have the greatest impact. This area aligns with the location of many of the mutations, and key eEF1B interaction sites.

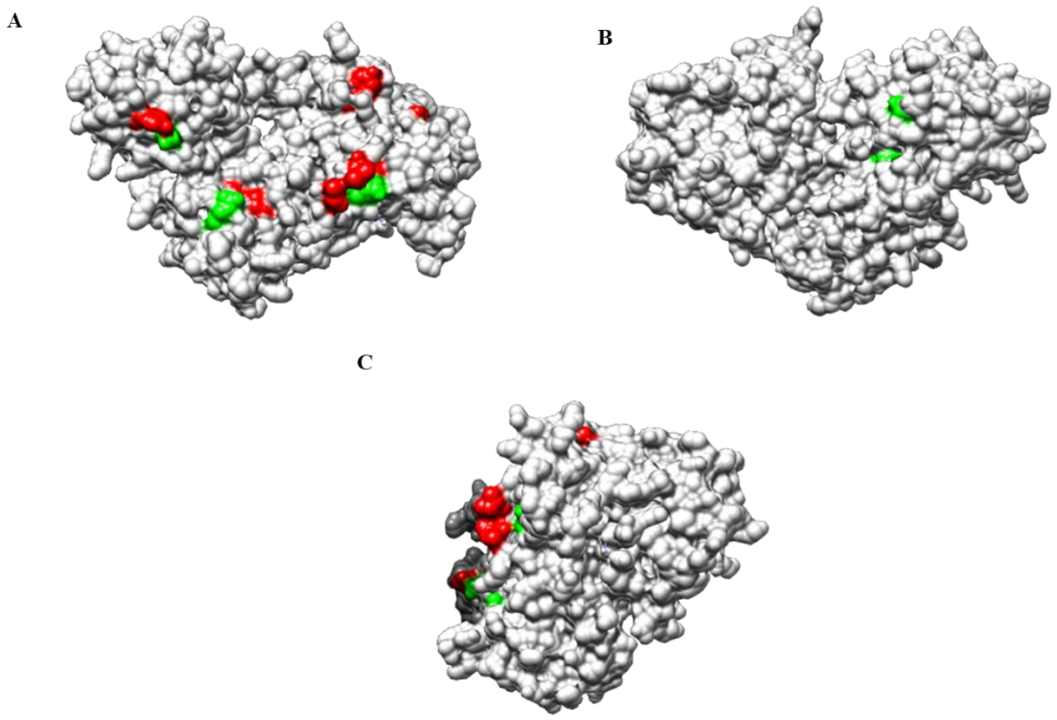

Figure 4.1: Structural modelling of eEF1A2 protein with the top changes in binding affinity demonstrated, as measured by BeAtMUsic *(174). Green amino acids highlight the greatest increase in binding affinity. Red amino acids represent the greatest decrease in binding affinity. The 3D structure is rotated to demonstrate the 'conserved face' of the protein where amino-acyl tRNA and eEF1B binding occurs (**A**), the 'variable face' of the protein, where amino acids differ from eEF1A1 (**B**) and the GTP binding site (**C**).*

A final interaction programme, MutaBind, was also used. This programme uses a combinatory approach to assess ΔΔG, including calculations on solvent accessibility, conservation score, changes to atomic forces and differences in unfolding free energy. Again, this prediction software was unable to accurately determine which mutations resulted in loss of eEF1B binding.

Computational analysis software did not serve as an accurate predictor of whether mutations would interact with eEF1B. Instead, co-immunoprecipitation experiments were performed on a range of mutations.

Table 4.1: Predicted binding interactions of eEF1A2 missense mutations. *Mutations in bold and blue were identified significantly decreased eEF1B interactions in co-immunoprecipitation assays. Mutations in italics with red shading are proven to have no significant difference in eEF1B binding affinity.*

Mutation	ELAPSIC (173)	BeAtMUsic (174)				MutaBind (175)
		ΔΔGBind (kcal/mol)	ΔΔG	Binding Affinity change	Interface	Binding site affected
H15D	Core, eEF1Bα	0.15	0.68	Decrease	No	Ntox46
G19R	Core, eEF1Bδ, eEF1BδL	0.93	1.38	Decrease	No	No binding site
T24M	Core	-1.30	0.44	Increase	No	No binding site
A65V	Core	0.50	1.06	Decrease	Yes	eEF1Bα
R69C	eEF1Bα, eEF1Bδ, eEF1BδL	2.02	-0.06	Decrease	No	eEF1Bα HBS1 eRF3
G70S	Core, eEF1Bα, eEF1Bδ, eEF1BδL	1.72	1.16	Decrease	Yes	No binding site
I71L	Core	0.33	1.03	Decrease	Yes	eEF1Bα
D91N	Core, eEF1Bα, eEF1Bδ, eEF1BδL	-0.65	0.59	Increase	No	eEF1B
A92T	Core, eEF1Bα, eEF1Bδ, eEF1BδL	-0.33	0.35	Increase	No	eEF1B

D97N	Core, eEF1Bα, eEF1Bδ, eEF1BδL	-0.48	-0.31	Increase	No	eEF1Bα eRF3 HBS1
F98C	eEF1Bα, eEF1Bδ, eEF1BδL	0.96	0.92	Decrease	No	eEF1Bα eEF1B eRF3
F98L	Core, eEF1Bα, eEF1Bδ, eEF1BδL	0.28	0.59	Decrease	No	eEF1Bα eRF3 eEF1B
M102V	Core, eEF1Bα, eEF1Bδ, eEF1BδL	0.19	0.3	Decrease	No	eEF1Bα eRF3
T104R	Core	0.42	0.91	Decrease	Yes	eEF1Bα eRF3
E122K	Core	-0.12	0.08	Increase	No	No binding site
E124K	Core	-0.09	0.12	Increase	No	No binding site
A125E	Core	0.16	0.08	Decrease	No	No binding site
E169K	Core	0.15		Decrease		
D252H	Core	-1.26	0.39	Increase	Yes	No binding site
R266W	Core	-0.40	0.99	Increase	Yes	No binding site
G275R	Core	0.90	0.57	Decrease	No	No binding site
N314K	Core	0.33	0.36	Decrease	No	No binding site
P333L	Core	-0.08	0.25	Increase	No	No binding site
R382H	Core	0.02	-0.29	Decrease	No	No binding site
G384R	Core	0.66	0.98	Decrease	No	No binding site
R423C	Core	0.33	0.66	Decrease	No	No binding sites
T432M	Core	-0.09	1.0	Increase	Yes	No binding sites

4.3.2 Defining the relationship with mutant eEF1A2 and eEF1B

To assess the relationship between eEF1B and eEF1A2 mutants, co-immunoprecipitation experiments were performed. This work was performed by Ningyuan Sun (a MSc student in the lab) and myself. I designed experiments, carried out cell culture and transfections, performed co-immunoprecipitation and western blot experiments for several subunits. Ningyuan Sun performed cell culture, transfections, co-immunoprecipitation and western blot experiments following my experimental design and instruction. Results are displayed collated together in Figure 4.2. Owing to the low transfection efficiency of SH-SY5Y cells and the consequential high sample volume required, experiments were performed in HEK293T cells. HEK293T cells, unlike SH-SY5Y, do not express endogenous eEF1A2. However, both cell lines express all eEF1B subunits. HEK293T cells were easier to transfect, requiring less sample volume. To confirm that cell type did not influence the interactions between exogenous eEF1A2 and the eEF1B subunits, both D252H and G70S mutations were included to affirm their eEF1B relationship did not change. Co-immunoprecipitation analysis (Figure 4.2) confirms the same results for D252H and G70S in both HEK293T and SH-SY5Y cells, enabling me to be confident that the cellular background did not influence the relationship of eEF1B interactions with transfected eEF1A2.

A

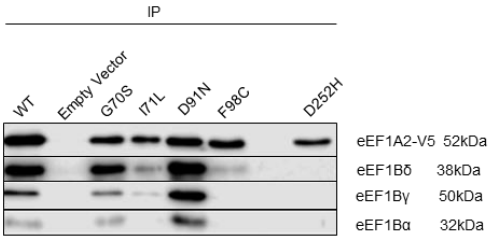
IP
WT
Empty Vector
G70S
I71L
D91N
F98C
D252H
eEF1A2-V5 52kDa
eEF1Bδ 38kDa
eEF1Bγ 50kDa
eEF1Bα 32kDa

B

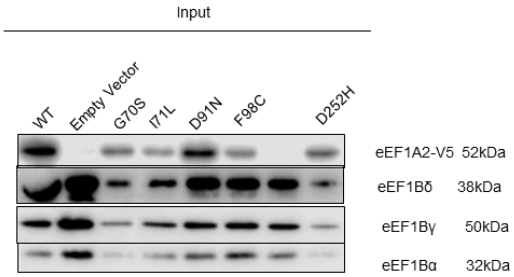
Input
WT
Empty Vector
G70S
I71L
D91N
F98C
D252H
eEF1A2-V5 52kDa
eEF1Bδ 38kDa
eEF1Bγ 50kDa
eEF1Bα 32kDa

C

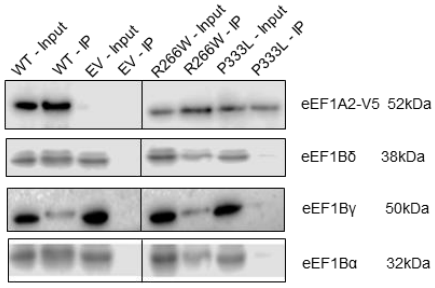
WT - Input
WT - IP
EV - Input
EV - IP
R266W - Input
R266W - IP
P333L - Input
P333L - IP
eEF1A2-V5 52kDa
eEF1Bδ 38kDa
eEF1Bγ 50kDa
eEF1Bα 32kDa

D

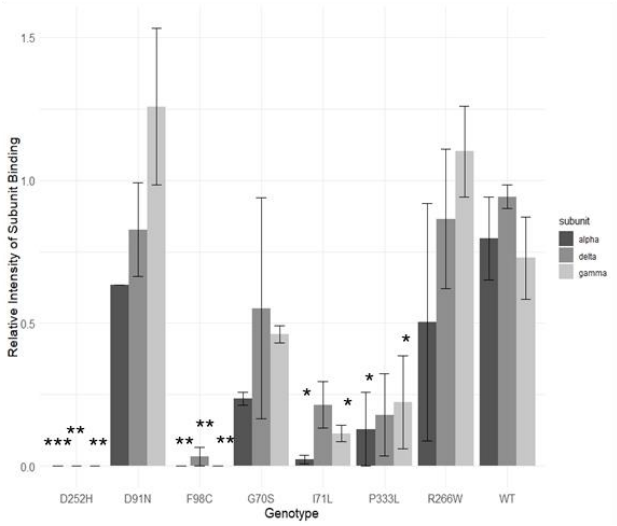
Relative Intensity of Subunit Binding
1.5
1.0
0.5
0.0
D252H
D91N
F98C
G70S
I71L
P333L
R266W
WT
Genotype
subunit
alpha
delta
gamma

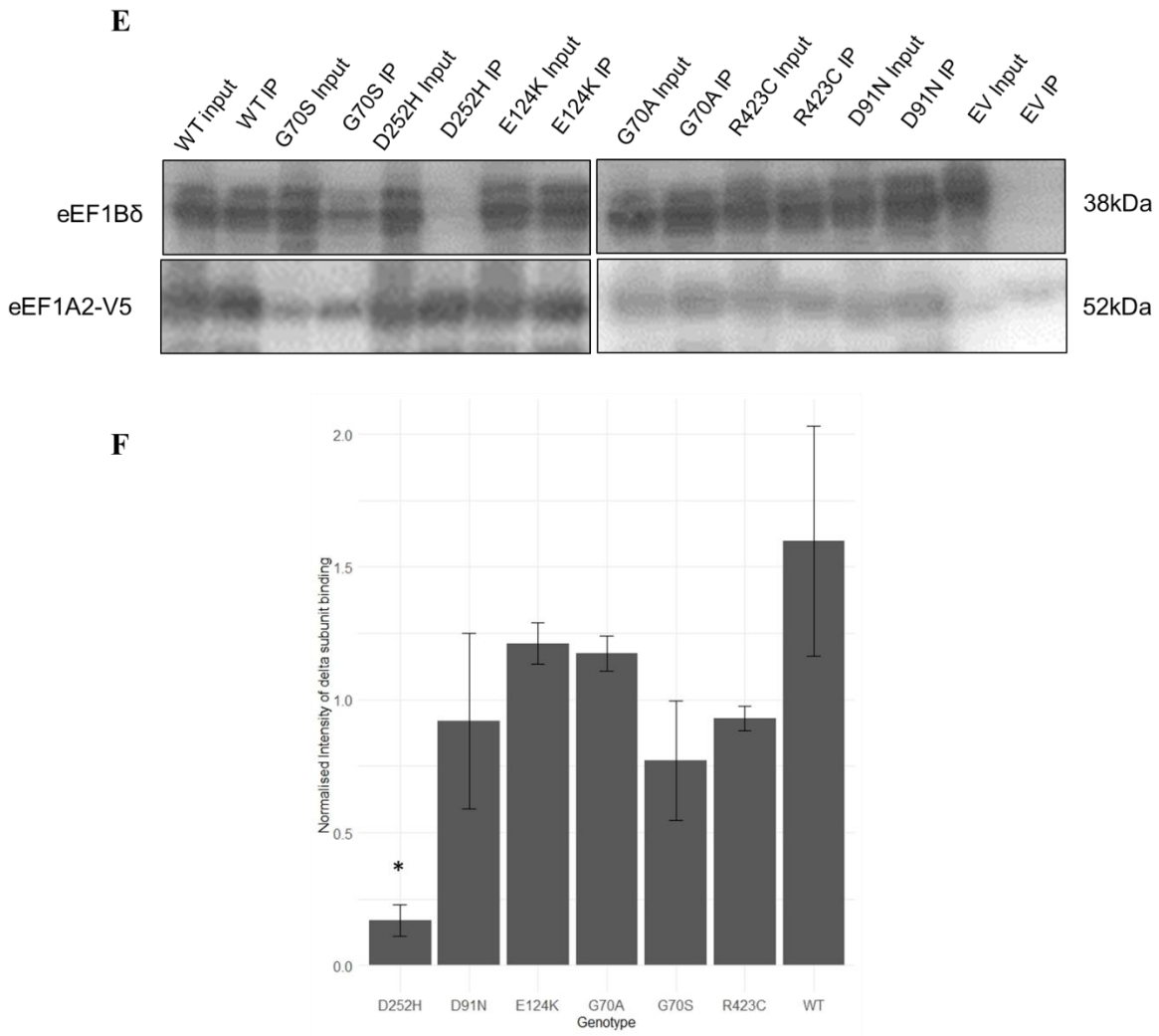

Figure 4.2: Co-Immunoprecipitation of eEF1A2-V5 constructs expressed in HEK293T cells performed in biological triplicate. *Staining for eEF1B subunits and eEF1A2-V5.* ***A****, IP fraction of pulldown and* ***B*** *input fraction (15% fraction of IP).* ***C*** *shows a separate experiment following the same design as above with IP and input fractions combined on the same blot. Experiments were performed in triplicate biological repeats (performed by Ningyuan Sun).* ***D*** *shows quantification of eEF1B subunit binding in* ***A-C*** *normalised to bait level (V5 staining) (for clarity, image of blots in C have been segmented, however all samples were run on the same gel and all images are of the same blot). Graph shows mean +/- SEM. As data was not parametric, results for each eEF1B subunit were subjected to Kruskil-Wallis testing, comparing the relative band intensities of mutant and WT conditions. Analysis predicted a significant interaction in all subunits (eEF1Bα; chi-squared =12.575, df*

=7, p <0.05, eEF1Bδ; chi-squared =13.535, df = 7, p <0.05, eEF1Bγ; chi-squared =14.314, df =7 , p<0.05). Post-hoc analysis was performed on all subunit data using the Dunn test; '' indicates p<0.05, '**' p<0.02 and '***' p<0.01 when compared with WT. A smaller experiment testing other eEF1A2 mutations in HEK293T cells only examined the interaction of mutant and WT eEF1A2 with subunit eEF1Bδ (**E**) (performed by Fiona McLachlan). Quantification for this and significance testing is provided in figure **F** (mean +/- SEM). This data met the parametric requirements and was subjected to ANOVA (F(6, 14) = 3.76847, p <0.02). Tukey post-hoc analysis was performed with '*' representing p<0.05 compared with WT.*

Results from experiments testing all subunits of the eEF1B complex (**A**-**C**) showed subunits interacted in the same pattern within each mutation. This gave me confidence to test a wider range of mutations, only probing for eEF1Bδ (**E**) and conclude that other subunits likely interact in a similar manner.

Analysis revealed two clusters of mutations which mirrored the results of D252H and G70S. Mutations D252H, I71L, F98C and P333L all showed significantly lower interactions with eEF1B subunits (p<0.05) whereas all other mutations tested showed no significant difference when compared with WT binding intensities. No obvious differences in clinical phenotype could be identified between mutations with or without their eEF1B interaction. Two mutations – D252H and I71L – are both published and are reported to be severely impactful. Patients have severe intellectual disability and, in the case of D252H, autism. Care must be taken with autism diagnoses as they are more readily reported in some countries than others. Further, some cases are too severe for autism to be detected (129,176). Conversely, mutation F98C is reported to present with only intellectual disability and no seizures (141). There is very little clinical information known about this case, making it difficult to discern how much this mutation differs from D252H and I71L. More is known about mutation P333L. A published report detailed the case of 2 homozygous children who passed away before aged 3. The children presented with severe epilepsy and intellectual disability. As a homozygous case, this mutation is severe. However, both

parents (i.e. the heterozygous cases) do not present with severe phenotypes. It is reported that the father "was unable to make eye contact and would smile inappropriately during medical encounters" but no official diagnosis of a neurodevelopmental disorder was reported. Three other children between the father and another woman were reported to exhibit significant speech delay, but genotype was not determined (122). In heterozygous cases, P333L appears to be a very mild mutation as compared to D252H and I71L. No link between clinical symptoms or severity and the loss of binding to eEF1B can be discerned. Similarly, some of the mutations which retain binding to eEF1B are severely affected. Mutation G70S is more severely affected than D252H. R423C has been published reporting severe seizures and developmental delay (123).

As no correlation was seen between mutation eEF1B interaction and clinical severity, the loss of eEF1B binding proposes several hypotheses. 1) eEF1A2 can function independently of its guanine exchange factor in protein synthesis, making this binding disruption obsolete. 2) The protein is a functional null in all cases. 3) There are elements of loss-of-function and gain-of-function mechanism which result from mutations, with the additional toxic effect enough to cause clinical symptoms.

To see if the 3D structure of eEF1A2 predicted the relationship between eEF1B and eEF1A2 for respective mutations, mutations were plotted with eEF1B and GTP binding sites (Figure 4.3). Most mutations cluster around sites associated with specific functions. Mutations P333L, D252H, I71L and F98C all lie close to, or are residues involved in eEF1B binding. Although this suggests that spatial location of mutations would be a good predictor of eEF1B interaction disruption, there are several mutations near the same binding site residues which do not demonstrate the same disruption. For example, G70S and I71L show opposing eEF1B relationships despite being consecutive amino acids. In addition, proximity to binding site residues does not completely predict severity of clinical cases. E122K is one of the most severe cases and the mutation lies within the GTP binding site. However, E124K (whilst not in the GTP binding site) demonstrates a drastically less severe phenotype, despite being only 2 residues away.

Although mapping the location of mutations on the 3D structure of the protein provides information which at times agrees with experimental data, and location of mutation in relation to binding sites might influence interaction profile, it is not the case in every instance.

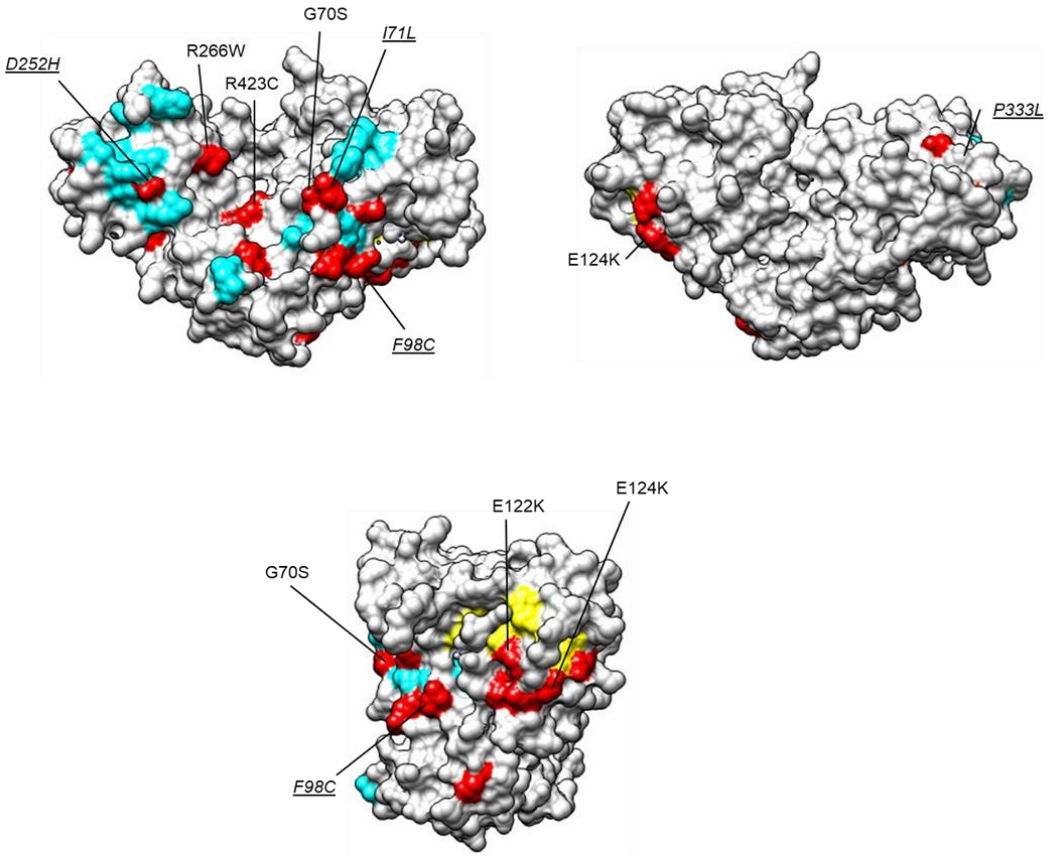

Figure 4.3: Spatial representation of mutations on eEF1A2 protein. *Mutations (red) were plotted on the eEF1A2 protein structure, along with eEF1B (blue) and GTP binding sites (yellow). Mutations which resulted in loss of binding have been italicised and underlined. Unaffected mutations remain in normal text.*

Overall computational analysis was not insightful in predicting protein interaction changes. Experimental testing revealed a cluster of mutations which lost binding to eEF1B. No discernible clinical presentation or severity could be gleaned from comparing these mutations. Secondly, spatial analysis did not completely reveal a distinct connection between location of mutations and prediction of interaction disruptions.

4.3.3 Summary of eEF1A2 mutation interactomes

Expanding upon the interaction analysis of D252H and G70S in Chapter 3, a group of eEF1A2 mutations with disrupted interactions to eEF1B were found. Despite this, no discernible clustering could be made to sort mutations by relationship to eEF1B. One possibility for these differing interactions is all mutant forms of eEF1A2 are non-functional, not performing protein synthesis – in essence, acting as null proteins. Phenotype testing to answer this hypothesis is reported in Section 4.3.

4.4 Assessing the phenotype of *Eef1a2* mutant mice

4.4.1 Summary of the *Eef1a2*/wst mouse line

The use of mouse models to explore the function of eEF1A2 began when a spontaneous deletion of a genetic region which included the *EEF1A2* promoter occurred in Jackson laboratory mice. The deletion resulted in a loss of expression of eEF1A2. Breeding of this mouse to develop a mouse line (termed *Eef1a2*/wst in this thesis), resulted in homozygote null mice. $Eef1a2^{-/-}$ mice develop normally until p21 when eEF1A1 down-regulation in terminally differentiated cells begins; death occurs before p28. eEF1A1 expression is undetectable in neurons and muscle after p24. This down-regulation is accompanied with a muscle tremors, gait abnormalities, ataxia and weight loss in the mice. Pathology shows muscular atrophy, and spinal cord and brainstem motor nuclei neurodegeneration (56). This homozygote mouse was well-established as a loss-of-function model for eEF1A2.

4.4.2 Generation of *Eef1a2*/D252H and *Eef1a2*/del22ex3 mice using CRISPR/cas9

To examine the phenotypic effects of mutations, the Abbott lab used CRISPR/Cas9 genetic editing to create *Eef1a2*/D252H, *Eef1a2*/del22ex3 and *Eef1a2*/G70S mice. The generation of the *Eef1a2*/G70S mouse line resulted in the creation of several $Eef1a2^{G70S/-}$ mice and one $Eef1a2^{G70S/G70S}$ homozygote. This round of CRISPR yielded no $Eef1a2^{G70S/+}$ animals which would have reflected the human phenotype and would likely have led to a less severe phenotype, which might have established a breeding colony. Nonetheless, we gleaned useful information from this line which has been published previously (140). *Eef1a2*/D252H and *Eef1a2*/del22ex3 lines were designed and generated by Faith Davies. Line maintenance, genotyping and phenotyping analysis was performed by Faith Davies, Jilly Hope, Francis Nunez, Laura Dumont and myself. Figure 4.4 shows the information related to the generation of the *Eef1a2*/D252H and *Eef1a2*/del22ex3 mice including an example restriction digest results of genotypes (**A** & **C**) and example western blot analysis examining eEF1A2 expression (**B** & **D**).

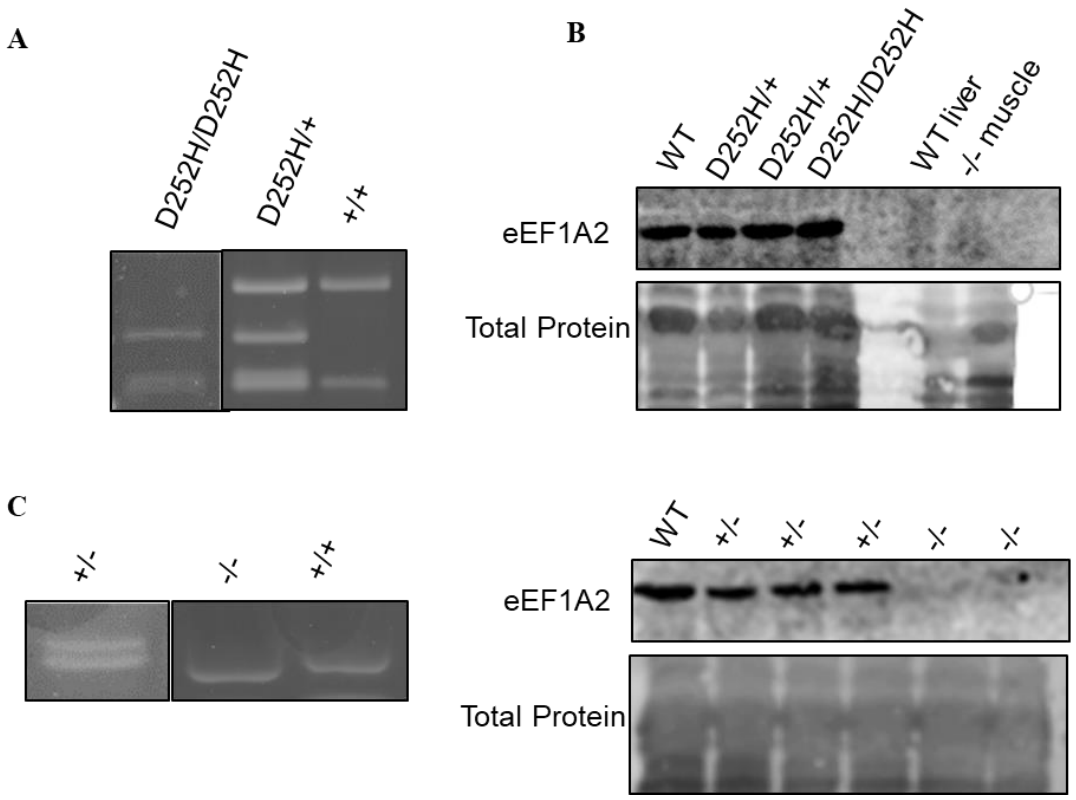

Figure 4.4: DNA and protein characterisation of Eef1a2^{D252H} and Eef1a2$^{-/-}$ mouse lines. *Example genotyping restriction digest (**A**) and protein expression analysis (**B**) for Eef1a2^{D252H} mouse lines. **A**, Hin1II restriction digest of PCR product resulted in digestion of a WT band into 330bp and 112bp bands, and D252H product into a 202bp and 128bp band. A heterozygous mouse therefore shows a combination of both digest fragments. **B**, Western Blot analysis of eEF1A2 expression and total protein concentration shows bands in all mutant Eef1a2^{D252H} skeletal muscle mouse samples. WT liver and -/- mouse muscle are both added as negative controls to confirm specificity of the eEF1A2 antibody. **C**, representative genotype analysis of del22ex3 mouse line. A 22bp deletion results in a smaller PCR fragment being generated (186bp) than WT (208bp). Heterozygote mice, again, show both PCR products. Western blot analysis shows complete ablation of eEF1A2 expression in skeletal muscle despite equal total protein concentrations (**D**).*

Of most note, D252H homozygote mice and D252H/+ heterozygote mice express eEF1A2. Western blot analysis of del22ex3 line (**4.4D**) also shows the complete ablation of eEF1A2 expression resulting from the deletion. More extensive analysis of protein and RNA expression of eEF1A2 in *Eef1a2*/D252H and *Eef1a2*/del22ex3 lines was performed by Jilly Hope as part of her doctoral thesis (121).

4.4.3 Phenotypic Analysis of *Eef1a2*/D252H and *Eef1a2*/del22ex3 lines

The aim of characterising the phenotype of these mouse lines was to provide a comparison of severity between the eEF1A2^{D252H} mutation and the complete loss of eEF1A2 (*Eef1a2*/del22ex3). If the phenotype was indistinguishable, it would suggest that the D252H mutation operated through a loss-of-function mechanism. By comparing *Eef1a2*/D252H and *Eef1a2*/del22ex3 lines (which were generated in the same CRISPR/Cas9 experiment in a C57/BL6 mouse), genetic background was controlled for. To assess phenotype severity, measurements of gait, hind-limb clasping, ledge balance and kyphosis were taken on a daily basis (142). In addition, the weight of each mouse was measured. Scores and weights for all genotypes in the *Eef1a2*/D252H and *Eef1a2*/del22ex3 lines were collated, compared and are displayed in Figure 4.5.

Assessment of the *Eef1a2*/del22ex3 line demonstrated a similar reported phenotype to that of the *Eef1a2*/wst line. Homozygote mice demonstrate no significant difference in phenotype severity or weight before p19 and p23 respectively (4.5**C** and **G**). The difference in phenotype severity also significantly increases in homozygotes compared to WT and +/- mice as days progress, suggesting a steady decline in health. This reported phenotype corresponds with the known information about the down-regulation of eEF1A1 in muscle and neurons. As with *Eef1a2*/wst line, heterozygous mice appear unaffected by deletion and are not significantly different from WT littermates in phenotype or weight profile.

In contrast to *Eef1a2*/del22ex3 mice, D252H/D252H mice show a significant difference from WT littermates substantially earlier in development (4.5**B** & **F**). Homozygotes weigh significantly less than WT littermates from p14, a difference which increases substantially over time (**F**). Mice also demonstrate a significantly

more severe phenotype from p16 (**B**) – 3 days earlier than the *Eef1a2*/del22ex3 mice. In addition, D252H/+ mice show a weight deficit as compared to WT mice. This begins at p14, just as with homozygote littermates. Unlike homozygote littermates, which fail to show an increase in weight during the period, heterozygous mice show a weight increase throughout development. Nevertheless, on each postnatal day heterozygous *Eef1a2*/D252H mice show a significant reduction in weight as compared with WT littermates (**F**).

The differences between the two mouse lines was directly compared by examining the weight and phenotype scores for *Eef1a2*$^{-/-}$ and *Eef1a2*$^{D252H/D252H}$ mice (**D**&**H**). D252H/D252H mice display a significantly more severe phenotype than -/- mice at several points throughout the postnatal testing window (**D**). This difference increases with age of the mice. Additionally, D252H mice show a significantly reduced weight at several points in the testing period compared to null mice (**H**). Unlike homozygote mice which show normal weight gain until p23, D252H mice fail to gain weight throughout the testing period.

The testing period was ceased at p23 as it was deemed necessary to cull *Eef1a2*$^{D252H/D252H}$ mice. After the testing period, it is of note that *Eef1a2*$^{-/-}$ mice show a rapid increase in phenotype severity and weight loss. They then die ~p26, a little earlier than the *Eef1a2*/wst mice.

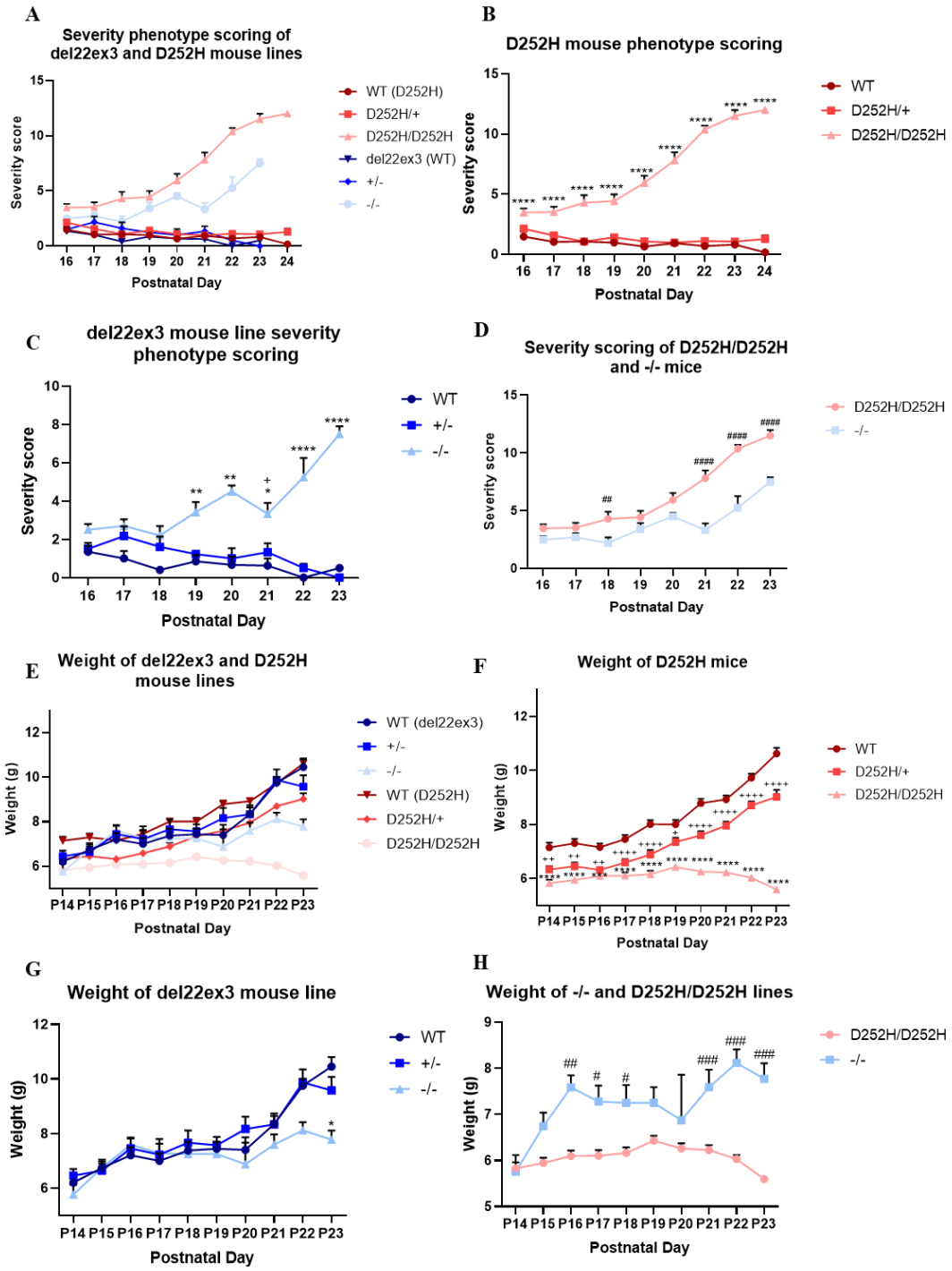

Figure 4.5: Phenotypic and weight analysis of Eef1a2/D252H and Eef1a2/del22ex3 mouse lines. *Analysis scoring severity of mouse phenotype was performed by experimenters (Faith Davies, Laura Dumont and Fiona McLachlan) who were blinded to genotype. Severity assessments for all lines are plotted in* ***A****. A*

*two-way mixed ANOVA with Tukey post-hoc analysis of all genotypes on each postnatal day was performed. ANOVA was found to have a significant interaction ($F(35,712) = 13.70$, $p<0.001$). Both postnatal day and genotype were deemed significantly responsible for this (Genotype; $F(5, 721) = 6.140$, $p<0.0001$, Postnatal Day; $F((7, 712)$, $p<0.0001$). Weights were taken for mice on each postnatal day. Two-way mixed ANOVA testing identified a significant interaction ($F(45, 1150) = 3.864$, $p<0.0001$). Both age ($F(9, 1150) = 34.40$, $p<0.001$) and genotype ($F(5, 1150) = 100.5$, $p <0.0001$) were responsible for this. Tukey post-hoc tests elucidated significant differences between genotypes on each day for both weight and phenotype severity. '****', '####' or '++++', $p<0.0001$, '***', '###' or '+++', $p<0.001$, '**', '##' or '++' $p<0.01$ and '*', '#' or '+' $p<0.05$). '*' reflects a significant difference between* $Eef1a2^{D252H/D252H}$ *and WT littermates, or,* $Eef1a2^{-/-}$ *mice and WT littermates. '+' reflects a significant difference between* $Eef1a2^{D252H/+}$ *and WT littermates, '#' reflects a significant difference between* $Eef1a2^{D252H/D252H}$ *and* $Eef1a2^{-/-}$ *mice.*

4.4.4 Summary of Eef1a2 mouse line phenotyping

Given the differences between null and D252H homozygotes, it is clear that the D252H mutation does not operate solely through a loss of function mechanism. After the down-regulation of eEF1A1 (~p21), both *Eef1a2*$^{D252H/D252H}$ and *Eef1a2*$^{-/-}$ mice health decline, however the deficit is clearly noticeable in D252H/D252H mice prior to the eEF1A1 down-regulation. This suggests an additional element of toxicity to eEF1A2 mutation in addition to the fact the protein is likely non-functional.

4.5 Discussion

4.5.1 Expanded edgotyping analysis for an array of mutants in eEF1A2

Given the disparate interaction profiles with eEF1B between mutations G70S and D252H tested in Chapter 3, it was imperative to explore how this difference would be reflected in other mutations. I wanted to expand upon these results and find out if the relationship with eEF1B correlated with severity of clinical presentation.

There is a wealth of structural analysis programmes available which use information on the location of a mutation in relation to functional domains, the charge of the substituted amino acid, and location in the 3D structure of the protein to calculate changes in binding energy (ΔΔG) which result from mutations. Given the ease of using these programmes, and the potential benefit of predictive analysis, I investigated whether computational prediction programmes would aid in classifying mutant proteins. Results from computational software and co-immunoprecipitation experiments were opposing, reporting many interactions as disrupted in mutants where no statistically significant difference was reported in either AP-mass spectrometry or co-immunoprecipitation. Computational predictions have proven to be insightful in the past, but my interaction analysis shows that in this case they do not predict results which agree with experimental data. The disparity between computational and experimental protein interaction analysis has been reported previously (177). Given this disparity, experimentally validating interactions with eEF1B in eEF1A2 mutants appears the most reliable course of action.

Structural analysis of all residues in the protein did identify that amino acids with the greatest changes in ΔΔG were associated around the ‘face’ of eEF1A2 – where eEF1B and aminoacyl-tRNA bind. Many mutations are located at or close to residues with the greatest ΔΔG. Clusters of likely pathogenic mutations can be identified by using ΔΔG energy modelling changes (178), and it would appear eEF1A2 fits with this phenomenon.

A brief review of clinical presentations was summarised in results Chapter 4.2.2. No association between severity and eEF1B affinity could be found. Subtle phenotypic differences would almost certainly be missed given the small sample

size, the limited clinical information and the possibility of undetected mosaicism. However, this initial overview with a small sample size does not suggest any obvious correlations.

The loss of eEF1B subunits in a cluster of mutations was identified in both the AP-mass spec results and co-immunoprecipitation experiments. The potential consequences of such disruptions are of significant interest and have been discussed further both in Chapters 3 and 5.

My results show that there is interaction profile variation from different mutations located throughout a single protein. Given the extreme variance in clinical severity reported within mutations, it was interesting to explore if mutation location within the protein, and resulting interaction differences, could be a factor influencing phenotypic severity. Differing phenotypes resulting from similar or identical mutations is widely reported (variable expressivity) (179). Variable expressivity is reported in a family presenting with autism caused by microdeletions in the MBD5 and NRXN1 genes (180). There are several mechanisms which can control phenotype severity. As mentioned previously, varying levels of mosaicism within patients with *de novo* mutations is likely to be a contributing factor which has not fully been accounted for. Genetic background will obviously be a contributing factor. Genetic background was found to be the driving force behind phenotypic variability in a mouse model of del22q11 syndrome (181). In patients of mendelian disorders genetic background and modifier genes are reported to play a significant role in phenotypic variability (182,183). Interestingly, Vu and colleagues explored identical genetic mutations in different strains of *c. elegans* to determine which genes were more susceptible to phenotypic variation. Their results showed that genes involved in protein synthesis and RNA binding were most likely to produce variable results in different genetic strains (184). Given these results, it is important to consider that the heterogenous background of individuals will have an influence. Another explanation for phenotypic variance in coding variants is alternative splicing (185). This is less likely to be a contributing factor as no alternative splice forms of eEF1A2 are known. Epigenetics is reported to play a role (186) and cannot be

excluded in our case. This work, however, supports the growing body of evidence to suggest that spatial location of the mutation can impact protein-interaction differences between mutants (150,151,163), resulting in phenotypic variation. Although no discernible clinical difference can be identified between mutant groups, more work and a greater sample size may unpick subtler differences.

4.5.2 Gain-of-function element of D252H mutation identified using phenotypic analysis of *Eef1a2*^{D252H} mouse line

Interactome results for the D252H mutation suggested that the most substantial interaction changes (loss of eEF1B binding) would result in impaired protein synthesis and a loss-of-function mechanism. The phenotypic severity and weight gain of mutant (*Eef1a2*$^{-/-}$ and *Eef1a2*$^{D252H/D252H}$) mice and their heterozygous and WT littermates was tested. Comparing a D252H with a null expression mouse line provided a key piece of evidence in evaluating the effect of missense mutations on eEF1A2 function. If, as interaction analysis had predicted, eEF1A2^{D252H} simply resulted in a non-functional protein, *Eef1a2*$^{D252H/D252H}$ mice should be phenotypically indistinguishable from *Eef1a2*$^{-/-}$ mice. Both weight and severity scoring proved this not to be the case. Having the eEF1A2^{D252H} mutation resulted in a gain-of-function or dominant negative element. This result agrees with reported structural analysis of eEF1A2 mutations. Mutations operating through loss-of-function mechanism are more likely to affect the structure of the protein, resulting in degradation and haploinsufficiency. Conversely, dominant negative or gain-of-function mutations are more likely to cluster around surface areas critical to protein function. Haploinsufficiency mutations can also cluster at critical domains, but this occurs less frequently than in gain-of-function mutations (187). eEF1A2 mutations are generally clustered with functional domains. Further, expression analysis in both *in vivo* (Section 4.3.1), *in vitro* (Section 5) and Hope (2018) (121) demonstrate that mutation eEF1A2^{D252H} is expressed at levels similar to WT. eEF1A2^{G70S} has also been shown to be expressed at concentrations not significantly different from WT (140). The mutations, therefore, do not cause structural disorganisation which results in complete protein degradation. Although the selected prediction software could not

accurately predict binding interaction disruptions resulting from specific mutations, structural analysis of the protein and mutation locations supports a gain-of-function or dominant negative mechanism.

Reported mutations are all heterozygous (except for the P333L homozygous lethal cases), which means that if mutations rendered proteins non-functional, haploinsufficiency would be responsible for the neurodevelopmental clinical presentation. *Eef1a2*$^{+/wst}$ mice do not display any form of the neurodegenerative phenotype seen in homozygotes, proving that haploinsufficiency does not result in the same neuronal degeneration. In the *Eef1a2*/D252H line, however, *Eef1a2*$^{D252H/+}$ mice do show significant differences from WT littermates. Although no difference in severity is witnessed, D252H/+ mice show a weight gain deficit as compared with WT mice. No such deficit is seen in +/wst mice, suggesting a difference in mechanism. This means that the protein must have, at least in part, an additional element of toxicity, causing neurodevelopmental/neurodegenerative damage.

Most reported gain-of-function mutations associated with epilepsy are channelopathies (188). Increased channel activity causes an imbalance in ionic influx and efflux, affecting the electrophysiological properties of neurons and resulting in seizures (189,190). Other neurodevelopmental disorders including intellectual disability have reported gain-of-function mutations as well (191,192). Gain-of-function mutations have also been reported in relation to protein synthesis. RNA binding protein FUS was reported in association with frontotemporal dementia (FTD). Gain-of-function mutations reportedly drive disease by causing up-regulation of the stress response resulting in suppression of axonal protein synthesis and resulting in neuronal death (193).

The unknown toxicity element which exacerbates mutant phenotype is unlikely the only consequence of the D252H mutation. Once eEF1A1 is completely down-regulated in both *Eef1a2*$^{-/-}$ and *Eef1a2*$^{D252H/D252H}$ mice, both mouse lines present with a similar neurodegenerative phenotype resulting in death. Therefore, when there is no compensatory elongation factor, eEF1A2^{D252H} is unable to sustain appropriate levels of protein synthesis. Consequently, mutations likely operate through gain and

loss-of-function mechanisms. Other combinatory loss- and gain-of-function mechanisms have been reported in neuronal dysfunction. Mutations in the TDP-43 gene demonstrated both a loss of canonical function and a toxicity which resulted in cytotoxic aggregations partly responsible for driving the disease in motor neurons (194).

4.5.3 Summary and conclusions

AP-MS was a highly insightful tool for identifying eEF1B interactions as disrupted in some mutations. Although no identifiable differences could be gleaned from the mutations based on their eEF1B interaction, this grouping should be studied in greater detail once more clinical cases and a greater depth of clinical information is reported. It is possible that subtle phenotypic differences could be reported between groups once confounding variables such as mosaicism are accounted for. Although the most significant result from mass spectrometry and co-immunoprecipitation experiments suggested a loss-of-function, phenotypic analysis of CRISPR generated *Eef1a2*^{D252H} mice suggests an additional gain-of-function or dominant negative element. I decided to follow up on the functional impacts of protein interaction disruptions by examining protein synthesis. The functional consequences of mutations is explored in Chapter 5.

Chapter 5: Functional implications for interaction disruptions in eEF1A2 missense mutations

5.1 Introduction

The results of Chapter 3 and 4 provide two conclusions and suggest several other possible hypotheses. Firstly, there is a class of mutations which result in significant loss of interaction to eEF1B. Although no correlation between this eEF1B interaction and clinical characteristics could be identified, it was by far the most significant disruption and was therefore important to follow up. Secondly, phenotypic analysis of the *Eef1a2*^{D252H} mouse line clearly shows, that in addition to a loss of function mechanism, mutations also operate through a gain of function/toxic element. Given the reported consequences of disrupted protein synthesis in neurons, and the clear non-functional element of the protein it was important to test the impact of the mutations on protein synthesis. Mutations in genes responsible for mRNA metabolism and protein synthesis predispose to neurodevelopmental disorders (195) Therefore, I carried extensive optimisation of protein synthesis experiments. I hypothesised that the loss of eEF1B interaction would result in reduced protein synthesis in *Eef1a2*^{D252H} mice and eEF1A2^{D252H} neurons.

5.1.1 Aims of chapter

1) Generate and characterise mutant eEF1A2 LUHMES lines for functional assays.

2) To establish whether global protein synthesis is impacted by eEF1A2 mutations *in vitro* and *in vivo*.

5.2 Generation and characterisation of mutant eEF1A2 LUHMES cell lines

5.2.1 Previous experimental results from eEF1A2^{D252H} CRISPR/Cas9

LUHMES cells are an immortalised neuronal precursor cell line, genetically edited to include the tetracycline system. This biological switch enables the differentiation of cells into dopaminergic neurons (137). The advantage of these cells over IPSCs is a shorter differentiation time and substantially lower cost. As all immortalised cells express eEF1A1, even when they would not *in vivo*, it was imperative to see if protein synthesis deficits would be detectable in LUHMES cells despite this confound. Pilot experiments to introduce eEF1A2$^{D252H/D252H}$ and eEF1A2$^{-/-}$ mutations into LUHMES cells were performed by Faith Davies as part of her doctoral thesis (141). Faith successfully generated one eEF1A2$^{D252H/D252H}$ and one eEF1A2$^{-/-}$ cell line. Owing to the limited sample availability, I created a greater number of cell lines to assess whether eEF1A2 mutations could result in a disrupted phenotype.

5.2.2 Generation of eEF1A2 mutant LUHMES cell lines

I aimed to generate LUHMES cell lines containing both eEF1A2^{G70S} and eEF1A2^{D252H} mutations. Figure 5.1A displays a schematic representation of genetic loci targeted in each CRISPR/Cas9 experiment. CRISPR/Cas9 was performed by Dr Faith Davies and myself. I was responsible for experimental design (jointly with Dr Faith Davies), gRNA cloning, genotyping, sequencing, RNA and protein expression analysis.

A

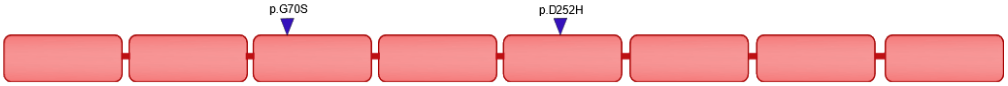

B

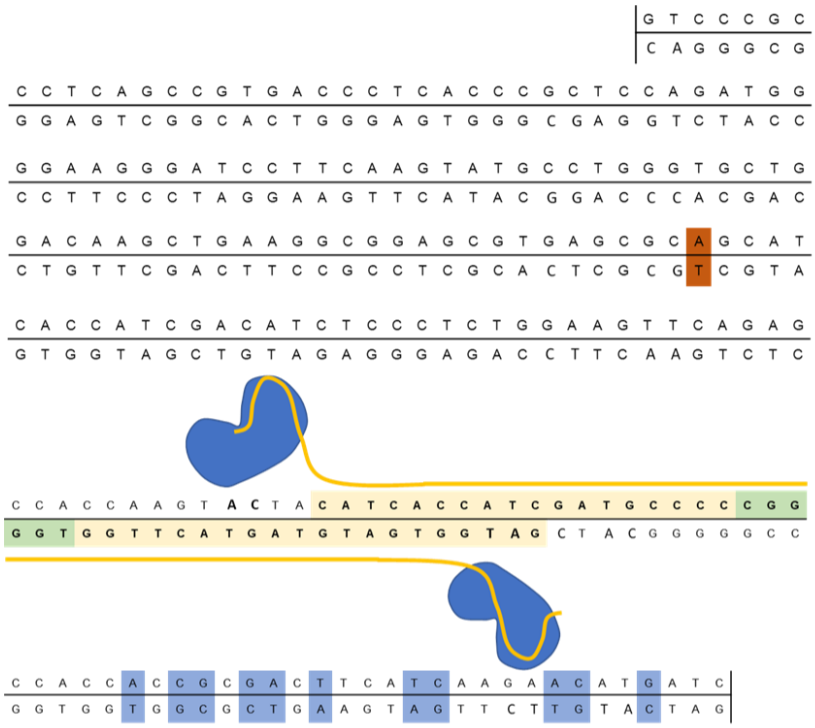

C

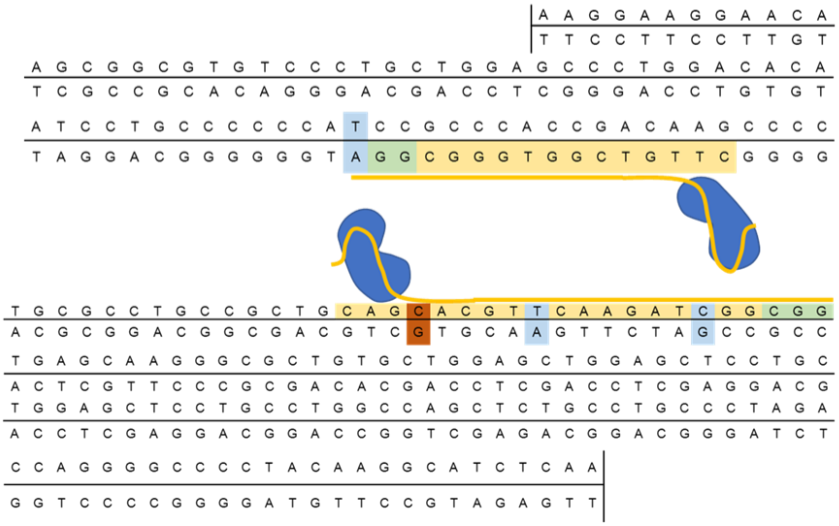

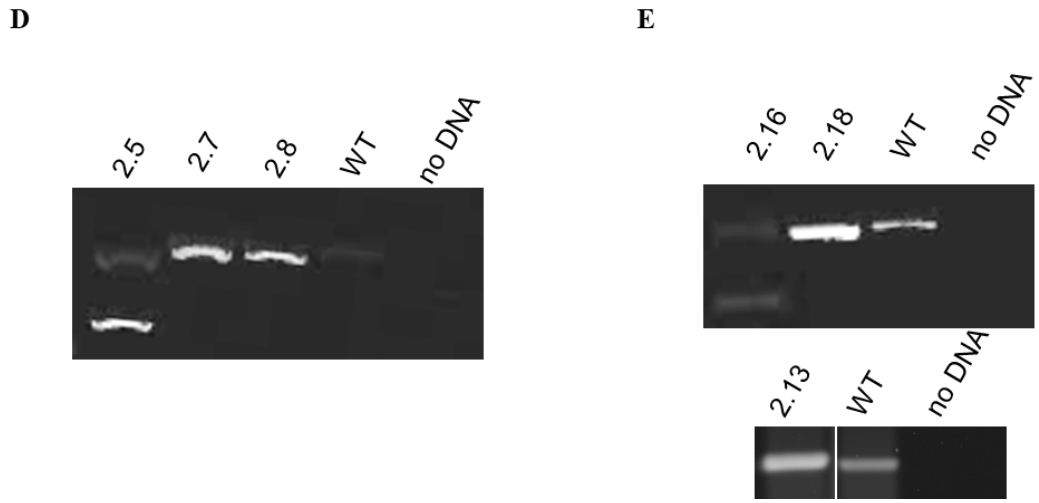

Figure 5.1: Induction of eEF1A2 mutations in LUHMES cells using CRISPR/Cas9. A, *schematic representation of the EEF1A2 gene exons with location of point mutations indicated above. Mutation p.G70S is in exon 3, whilst p.D252H is in exon 5.* ***B*** *and* ***C*** *schematic diagrams demonstrating the CRISPR/Cas9 targeting to induce missense mutations G70S and D252H respectively. The DNA sequence shown is the repair template in each instance. gRNA guide sequences are highlighted in yellow with adjacent PAM sites highlighted in green. Mutations are highlighted in orange and base pair changes to induce silent mutations in the repair template are highlighted in blue. PCR exon 3 (****D****) and 5 (****E****) in LUHMES lines which had undergone CRISPR/Cas9 genetic editing. PCR amplification of genomic DNA around the cut site was performed. PCR was used to establish genetic modification, and an initial assessment of whether lines were polyclonal. PCR amplification in* ***D*** *resulted in a 816bp fragment in the WT allele.* ***E*** *resulted in a 409bp product in the WT allele.*

Table 5.1 summarises the sequencing and TOPO cloning of lines obtained from CRISPR genetic modification. A full alignment of sequencing results for each line is reported in appendix C.1.

Table 5.1: Results of CRISPR/cas9 experiments in neuronal cell line LUHMES. *Attempts to generate G70S mutation (experiment 1) and D252H (experiment 2) created cell lines of varied genotypes. These were identified using sequencing and TOPO cloning of PCR fragments.*

Cell line name	Genotype	
	Allele 1	Allele 2
2.5	27 bp deletion	200 bp deletion
2.8	7bp deletion	Compound deletion/missense mutations
2.13	D252H missense mutation incorporation	D252H missense mutation incorporation
2.16	D252H missense mutation incorporation	125 bp deletion
2.18	WT	WT

Two rounds of CRISPR were performed, firstly in exon 3 to target amino acid p.Glu70. This failed to yield any Glu70Ser missense mutations but did succeed in generating eEF1A2 -/- and +/- lines. The second round of CRISPR targeted exon 5 to generate the Asp252His mutation. D252H was successfully introduced in two lines, one homozygote and one D252H/null. LUHMES lines were characterised in preparation of functional analysis. Figure 5.2 shows a schematic representation of the genetic editing which occurred in LUHMES clonal lines.

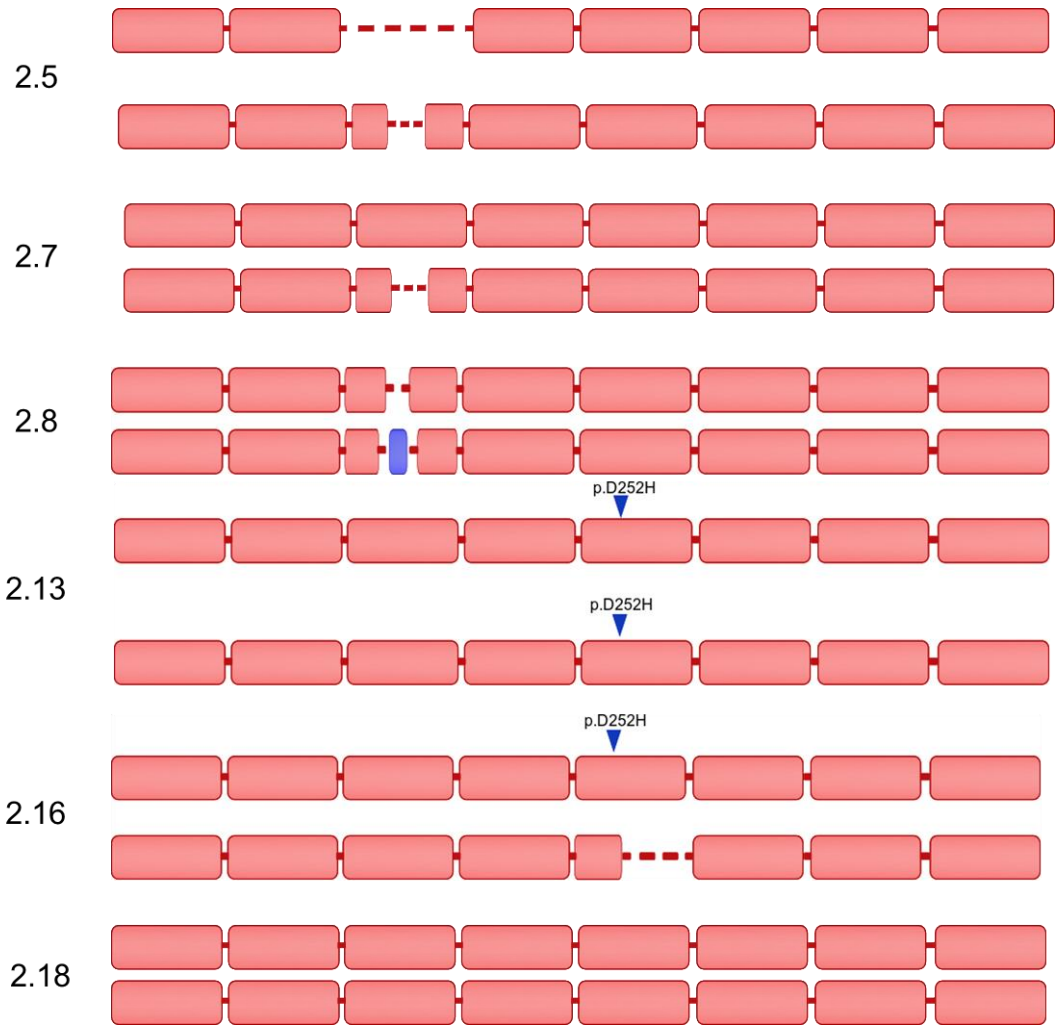

Figure 5.2: Schematic diagram of LUHMES lines generated through CRISPR/Cas9 experiments. *Shown are exons of eEF1A2 with deletions (red dotted line), random missense mutations (blue rectangle) and targeted missense mutations (blue triangles).*

5.2.3 Protein expression of LUHMES clones

All immortalised cell lines express eEF1A1, even when this would be down-regulated *in vivo*. As there is no commercial antibody which can differentiate the two eEF1A isoforms in cells using western blot, I stained for eEF1A (which could be either or both isoforms) in all lines. I tested eEF1A expression in all LUHMES cell lines both in a proliferative and differentiated state. Protein expression in proliferative extracts varied greatly, making quantification unreliable. Bands could

be seen in all conditions, as expected, given that the antibody detects both isoforms of the protein.

Differentiated protein extracts displayed more consistent total protein. Owing to low concentration of some samples, two protein extractions were performed (C and D). For quantification and analysis, the two blots were normalised to the same WT sample. A significant reduction of eEF1A expression in lines 2.5 and 2.8 could be seen when compared with WT CRISPR line 2.18. However, no significance between potential null lines and WT LUHMES was detected. eEF1A2$^{D252H/D252H}$ line 2.13 did not show significantly different expression of eEF1A as compared to WT. This is in agreement with the *in vivo* results showing that mutant D252H eEF1A2 protein is expressed and therefore relatively stable.

Expression of eEF1A in LUHMES cells had been previously tested by Faith Davies and showed a significant reduction of eEF1A staining in eEF1A2$^{-/-}$, but not eEF1A2$^{D252H/D252H}$ cells (1). As eEF1A1 is expressed in immortalised cells at a much greater concentration (~1000 fold) than eEF1A2, it was determined that protein analysis to detect significant levels of eEF1A2 was not reliable. To verify the concentration of eEF1A2 in LUHMES clones, I examined eEF1A2 mRNA.

A

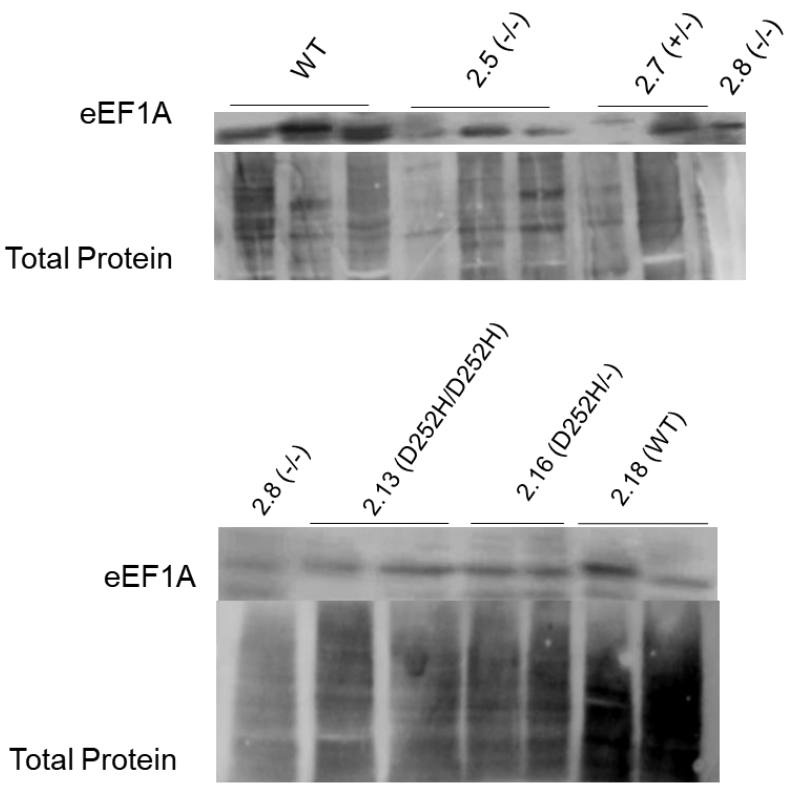
WT
2.5 (-/-)
2.7 (+/-)
2.8 (-/-)
eEF1A
Total Protein
2.8 (-/-)
2.13 (D252H/D252H)
2.16 (D252H/-)
2.18 (WT)
eEF1A
Total Protein

B

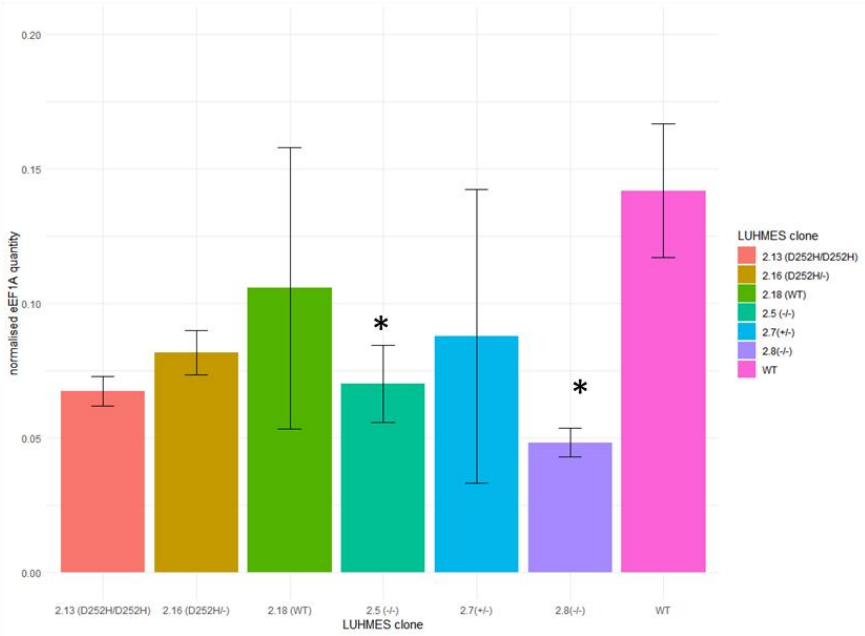
normalised eEF1A quantity
0.20
0.15
0.10
0.05
0.00
2.13 (D252H/D252H)
2.16 (D252H/-)
2.18 (WT)
2.5 (-/-)
2.7(+/-)
2.8(-/-)
WT
LUHMES clone
LUHMES clone
2.13 (D252H/D252H)
2.16 (D252H/-)
2.18 (WT)
2.5 (-/-)
2.7(+/-)
2.8(-/-)
WT

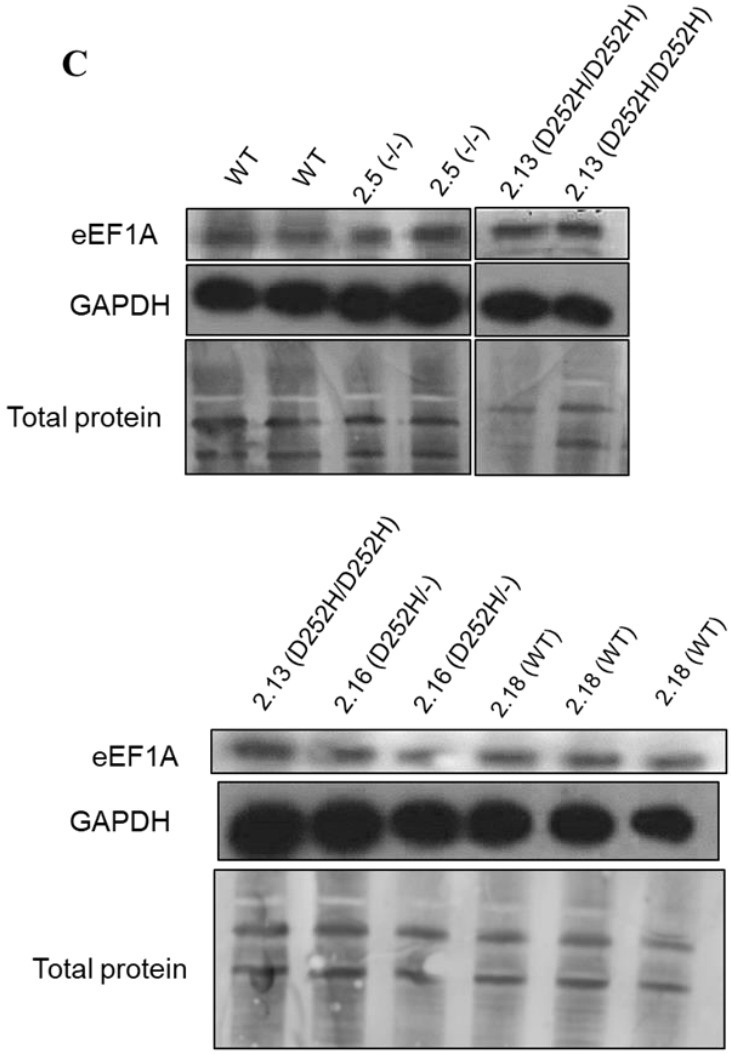
C
WT
WT
2.5 (-/-)
2.5 (-/-)
2.13 (D252H/D252H)
2.13 (D252H/D252H)
eEF1A
GAPDH
Total protein
2.13 (D252H/D252H)
2.16 (D252H/-)
2.16 (D252H/-)
2.18 (WT)
2.18 (WT)
2.18 (WT)
eEF1A
GAPDH
Total protein

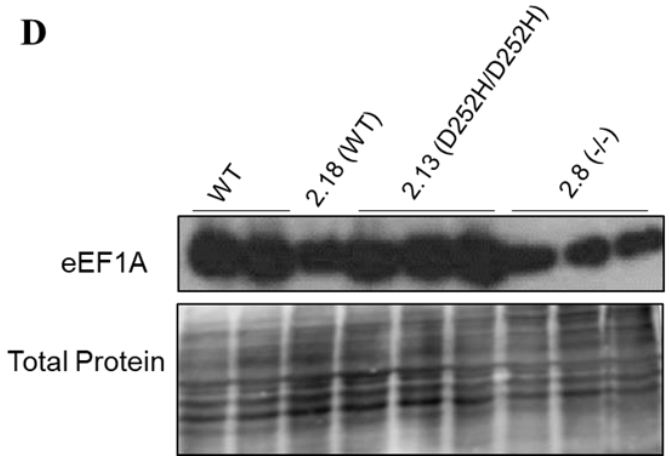
D
WT
2.18 (WT)
2.13 (D252H/D252H)
2.8 (-/-)
eEF1A
Total Protein

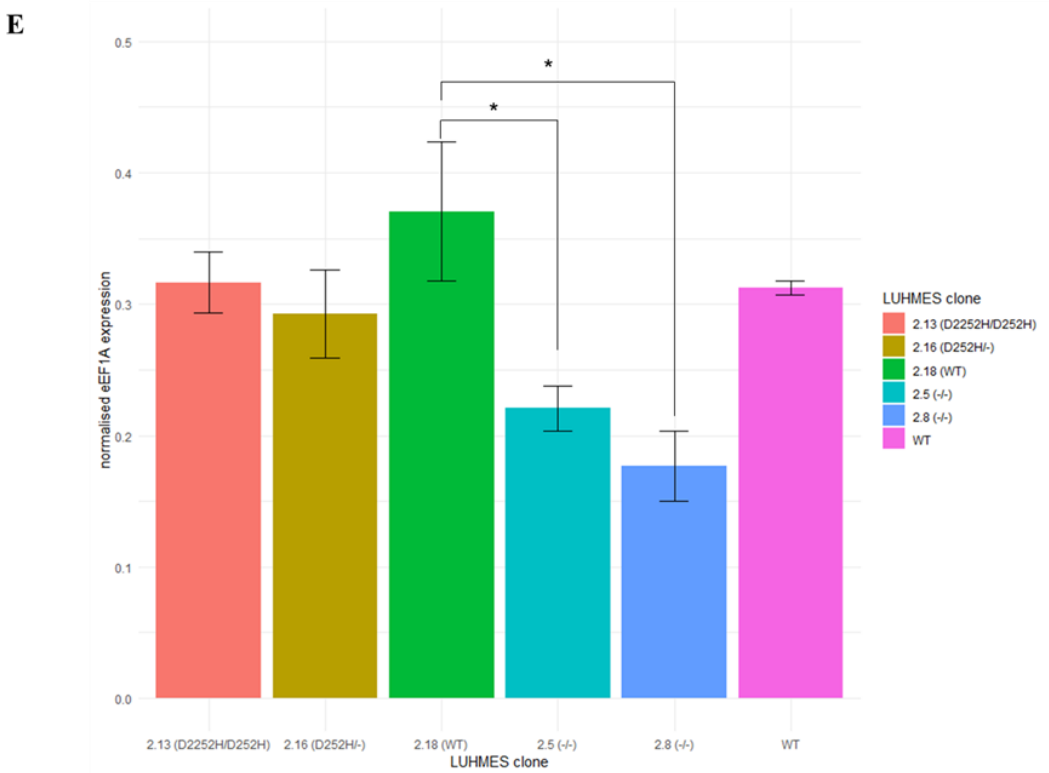

Figure 5.3: eEF1A expression in LUHMES cells. A, *shows the eEF1A expression of LUHMES lines in a proliferative state. The resulting quantification of normalised eEF1A expression is shown in* ***B****. The expression of eEF1A in differentiated LUHMES clones is shown in* ***C*** *and* ***D****. Quantification of this is presented in* ***E****. ANOVA analysis for differentiated LUHMES clones indicated a significant interaction (F(5, 15)=4.16, p<0.05. Tukey post-hoc analysis was performed and is indicated on the graph, with '*' reflecting p<0.05.*

5.2.4 RNA expression of LUHMES clones

As protein expression was inconclusive, I analysed RNA in order to see if mutations affected steady state eEF1A2 mRNA levels. GeNorm analysis performed to determine which housekeeping genes should be used for normalisation. Two housekeeping genes (TOP1 and RPL34) were selected. The melt curves and standard curves for these and eEF1A2 PCR reactions are in appendix C.2. A summary of RNA normalised expression values is provided in Figure 5.4A.

Because mutations had been engineered in different exons of the gene, I elected to perform a qPCR analysis on all lines by amplifying an area of exon 7-8 of eEF1A2 mRNA. This would not be affected by the location of any of the mutations I had made, and would allow an equivalent assessment of eEF1A2 mRNA expression in all lines. The results of the qPCR analysis are displayed in Figure 5.4**A**. A significant reduction in eEF1A2 mRNA was seen in proliferative cells in null lines 2.5 and 2.8 as compared to WT lines. 2.16 also showed a significant reduction with nearly no expression of eEF1A2 mRNA. Differentiated cell lines demonstrated no significant difference. 2.5 (-/-) differentiated mRNA appeared to show a reduction in mRNA but this did not achieve significance, perhaps owing to the low n number.

As it was important to establish mRNA concentrations of eEF1A2 in differentiated cell lines, further analysis was performed. To assess mRNA concentrations around the mutation site, RT-PCR was performed. In the case of exon 3 this was because the deletion in one allele in 2.5 line was so big (200bp), that any PCR spanning the deletion would be too large for qPCR analysis in an intact allele (**B**). Quantification of the results confirmed a significant reduction in eEF1A2 mRNA in line 2.5(-/-) as compared to both WT and 2.18 (WT), suggesting the line is a null (**C**).

In both qPCR and RT-PCR analysis no significant difference between line 2.13 (D252H/D252H) and WT was seen in either the proliferative or differentiated state. 2.16 shows a significant reduction in qPCR in the proliferative state (**A**). Given the drastic up-regulation of eEF1A2 mRNA in the differentiated cells and the presence of bands in the RT-PCR (**B**), it is likely that the PCR simply failed in some biological replicates in the proliferative qPCR.

Results confirm that lines 2.5 (-/-) and 2.8 (-/-) showed significantly down-regulated eEF1A2 mRNA based on analysis both at the mutation site and further down-stream. D252H mutations did not result in a genetic null, with lines expressing mRNA at the same concentration as WT.

A

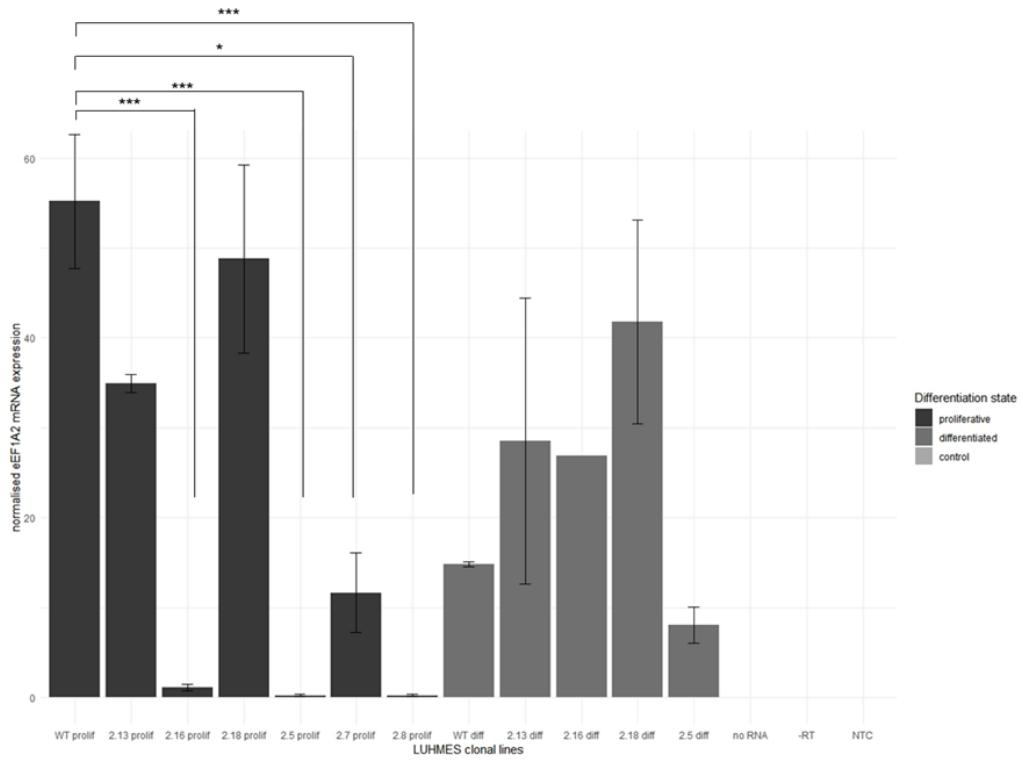
***
*
***
***
normalised eEF1A2 mRNA expression
60
40
20
0
WT prolif
2.13 prolif
2.16 prolif
2.18 prolif
2.5 prolif
2.7 prolif
2.8 prolif
WT diff
2.13 diff
2.16 diff
2.18 diff
2.5 diff
no RNA
-RT
NTC
LUHMES clonal lines
Differentiation state
proliferative
differentiated
control

B

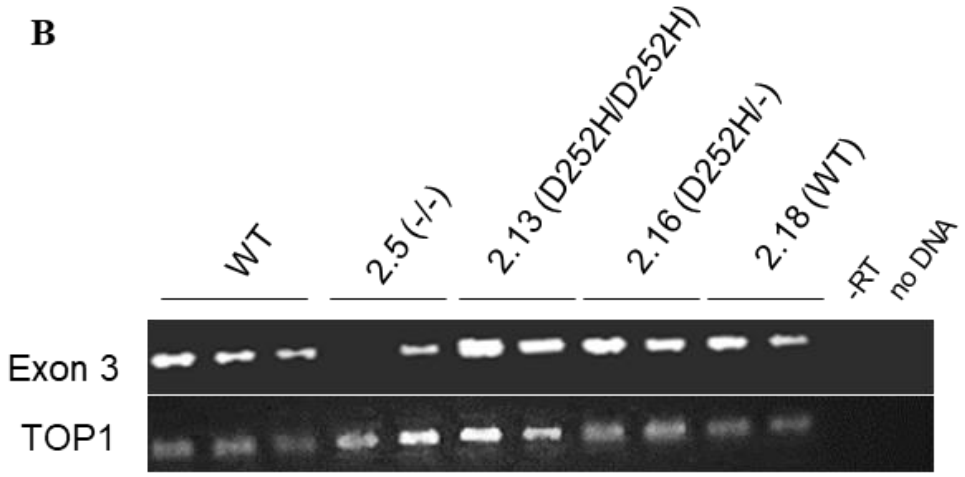
WT
2.5 (-/-)
2.13 (D252H/D252H)
2.16 (D252H/-)
2.18 (WT)
-RT
no DNA
Exon 3
TOP1

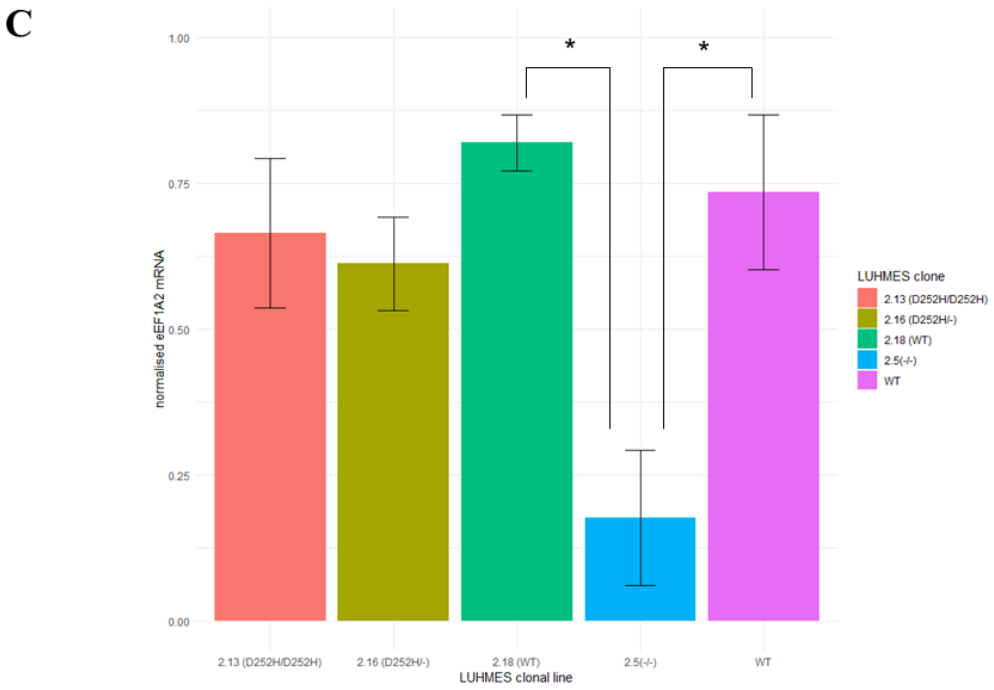

Figure 5.4: Analysis of eEF1A2 mRNA in LUHMES cell lines. A*, All LUHMES cell lines had RNA extracted and cDNA synthesised (2-3 biological repeats per genotype). After GENORM analysis for appropriate housekeeping gene selection, genes eEF1A2 mRNA was amplified using primers spanning the exon 7 – exon 8 junction. mRNA was normalised to housekeeping genes TOP1 and RPL34. Graph shows mean +/- SEM. One-way ANOVA analysis was performed on all lines. ANOVA demonstrated significant difference in levels of eEF1A2 mRNA F(12, 14) = 6.922, p<0.001. As only one biological replicate for each negative control was performed these were excluded from ANOVA analysis.* ***B****, RT-PCR of LUHMES differentiated samples at exon 3. RT-PCR of exon 3 generated an 310bp fragment. Housekeeping gene TOP1 was amplified to create a 224bp fragment. Normalised exon 3 samples were quantified (****C****) and an ANOVA analysis was performed. ANOVA indicated a significant interaction F(4, 6)= 4.22, p<0.05. Tukey post-hoc testing was performed for all ANOVAs. Significance values are displayed on graphs. '*' p<0.05, '**' p<0.01, and '***' p<0.001.*

5.3 Protein synthesis measurements in *in vitro* and *in vivo* conditions with mutant and loss of eEF1A2

Protein synthesis assays were conducted using a variety of methods *in vitro,* as well as *in vivo*. One technique reported recently was puromycylation, or the 'SUnSET' technique (196). This technique takes advantage of the amino-nucleoside properties of the antibiotic puromycin. At high concentrations the drug blocks nascent polypeptide chains and inhibits protein synthesis. At lower concentrations, however, puromycin is incorporated into nascent polypeptide chains. The use of a monoclonal puromycin antibody can then be applied to protein extracts/fixed samples to assess nascent polypeptide synthesis.

An alternative technique, AHA-click chemistry, was also used to assess protein synthesis. This technique uses fluorescent labelling, with a greater similarity to the classic radioactive metabolic labelling techniques used for protein synthesis measurements. In a methionine free environment, an amino acid analogue of methionine is incorporated into polypeptide chains. As this was not possible *in vivo*, this technique was used on LUHMES cell lines.

I hypothesised that loss of binding to guanine exchange factor eEF1B in mutation eEF1A2^{D252H} would impair protein synthesis. This was tested both *in vivo* and *in vitro*, comparing WT, eEF1A2^{D252H} and null LUHMES cells and *Eef1a2* mutant mice for protein synthesis disruptions.

5.3.1 Puromycylation of proliferative LUHMES cell lines

Initial experiments were performed in proliferative LUHMES cells to assess the effectiveness of puromycylation as a measure of nascent protein synthesis. Results demonstrated a significant reduction in nascent protein synthesis in line 2.13 (D252H/D252H) compared to WT cells (**A** and **B**). The same significance was not achieved when examining WT and null line 2.5 (**C** and **D**). Whilst this was a potentially interesting result, agreeing with the gain-of-function element discovered in phenotype analysis reported in Chapter 4, the method appeared crude and would likely produce variation in repeats. I therefore decided to optimise the puromycylation experiments for greater sensitivity.

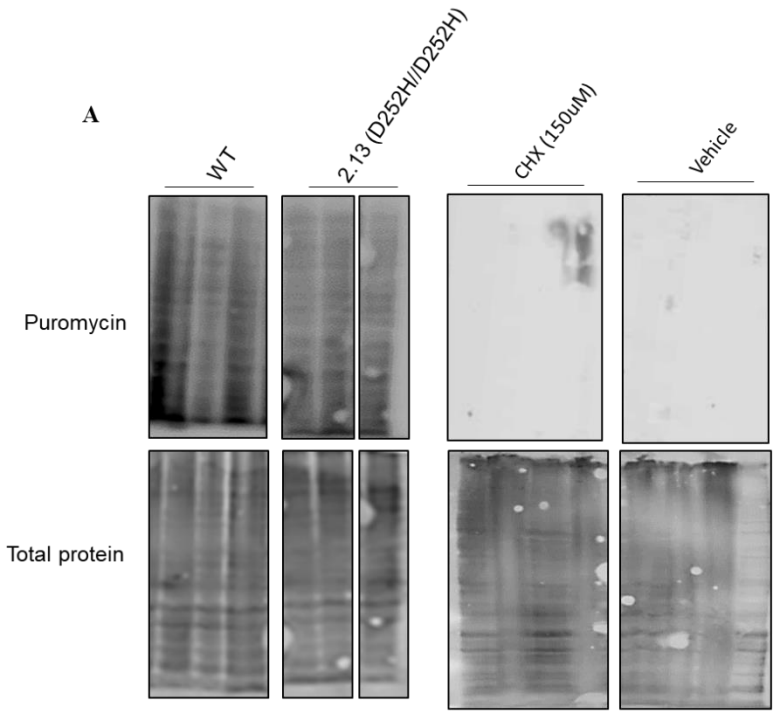
A
WT
2.13 (D252H/D252H)
CHX (150uM)
Vehicle
Puromycin
Total protein

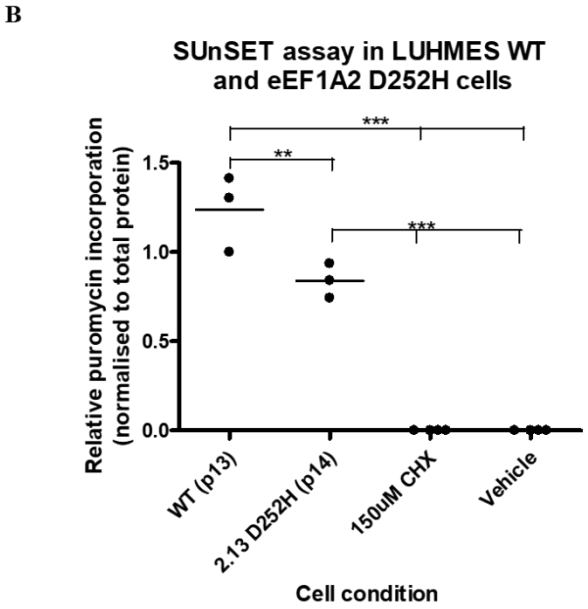
B
SUnSET assay in LUHMES WT and eEF1A2 D252H cells
Relative puromycin incorporation (normalised to total protein)
1.5
1.0
0.5
0.0
**
***
***
WT (p13)
2.13 D252H (p14)
150uM CHX
Vehicle
Cell condition

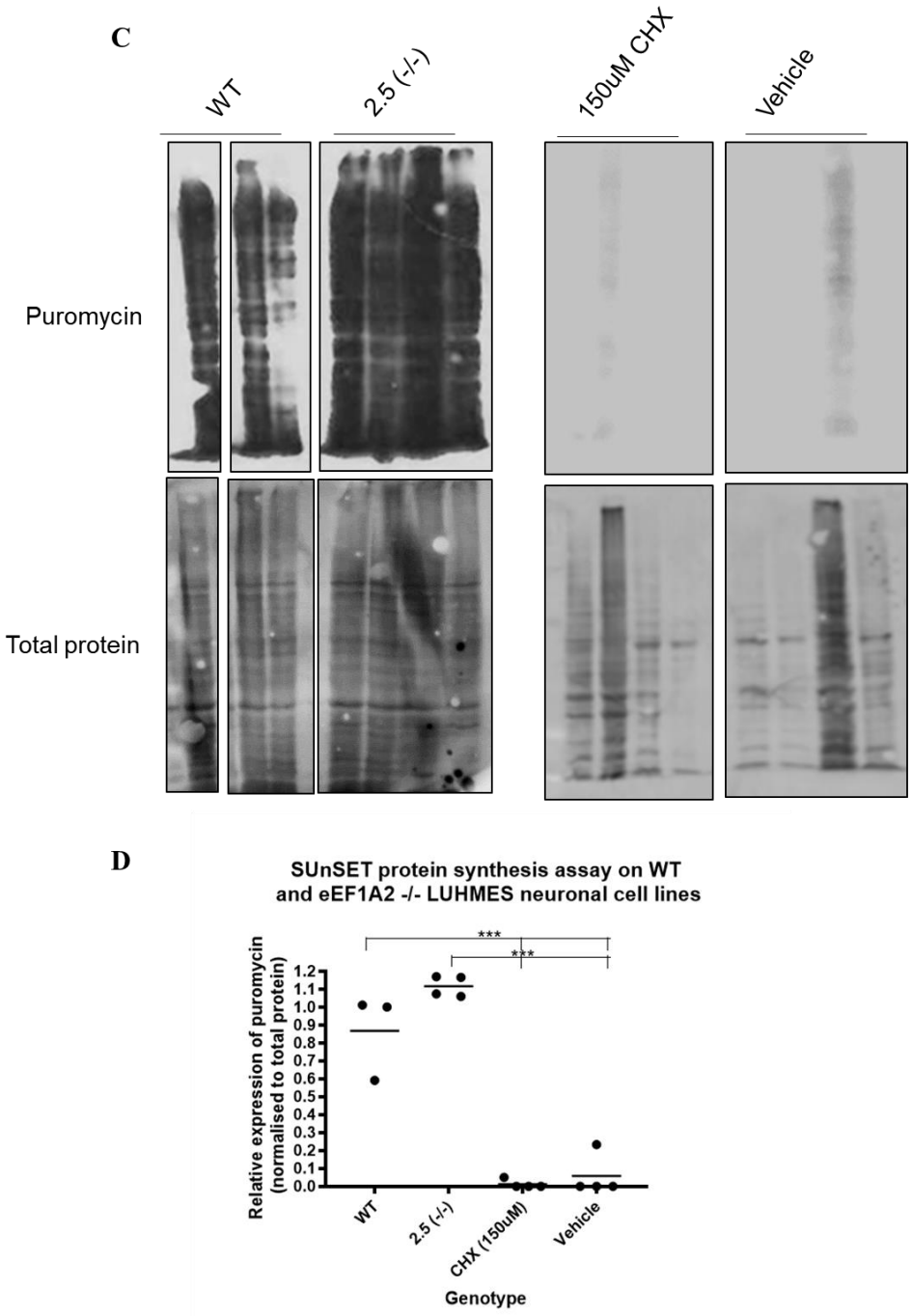

Figure 5.5: SUnSET assay in proliferative LUHMES cells to assess nascent protein synthesis. *Initial assays were run to assess whether puromycylation would be an appropriate measure of protein synthesis in LUHMES cells.* ***A****, shows the relative signal intensity of puromycin incorporated into nascent proteins with the*

total protein loaded into the experiment as a control. Positive control cells were pre-treated with 150µM cycloheximide (CHX) to inhibit protein synthesis. This and the negative control vehicle condition are displayed along with D252H and WT LUHMES lines. A quantification of relative puromycin signal intensity (normalised to the total protein signal for each repeat) is provided in ***B****. One-way ANOVA analysis reported a significant interaction F(3,12)=3.45, p<0.05. Tukey post hoc analysis was used to explore significant differences. The notation system for this is described below. A second experiment comparing eEF1A2 WT and null cell lines was performed as is shown in* ***C****. As above puromycin signal intensity, and total protein staining for WT, null and control conditions. The normalised puromycin signal intensity is reported in* ***D****. One-way ANOVA analysis reported a significant interaction, F(3,11)=3.657, p<0.05. Tukey post-hoc testing was performed for both experiments. Significant differences are marked on the respective graph. '*' p<0.05, '**' p<0.01 and '***' p<0.001.*

5.3.2 Immunostaining of puromycin treated LUHMES cells

Whole lysate analysis was a highly variable and crude method which did not yield reproducible results (Section 5.2.3). Other papers have reported using the puromycylation technique coupled with immunocytochemistry (193,197). I decided to visualise the distribution of protein synthesis in differentiated LUHMES cells. In addition to providing an increase in sensitivity, this technique enables visualisation of protein synthesis distribution. The principal behind this theory was to see if differences in axonal/synaptic or somatic synthesis could be examined between genotypes. The staining from four biological repeat experiments is reflected in Figure 5.6 (A-I).

Staining of puromycin identified that cell bodies produced a signal intensity far greater than in the neuropil. This agrees with the expected distribution of protein synthesis in neurons, the vast majority of which would be performed in the soma. Images have therefore been presented at two different contrast intensities for accurate representation of cell body and neuropil signal.

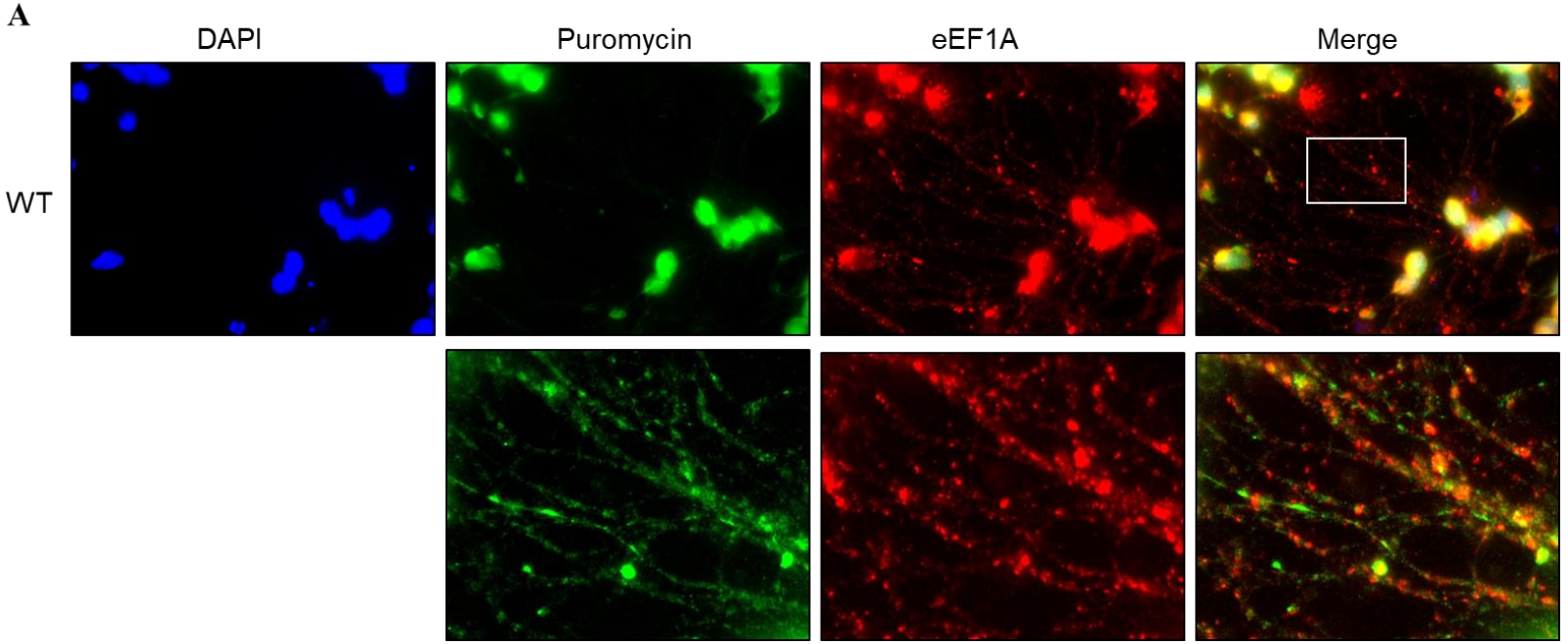
A
DAPI
Puromycin
eEF1A
Merge
WT

B

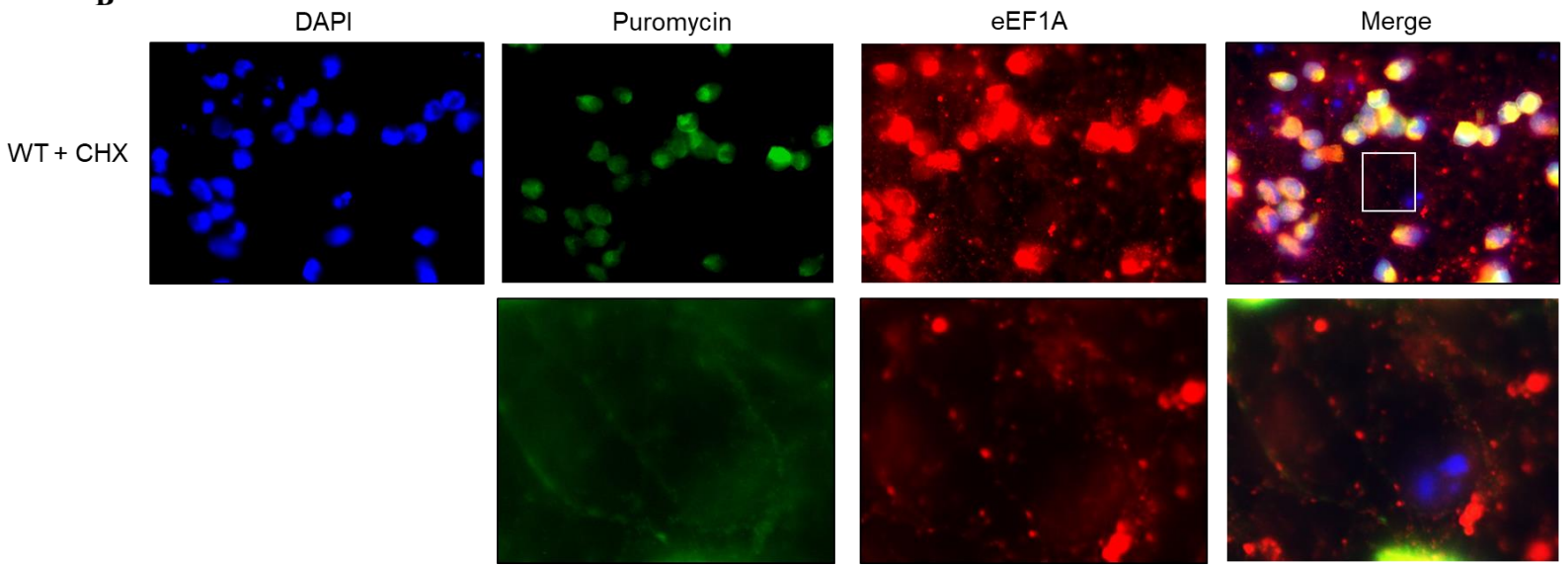

C

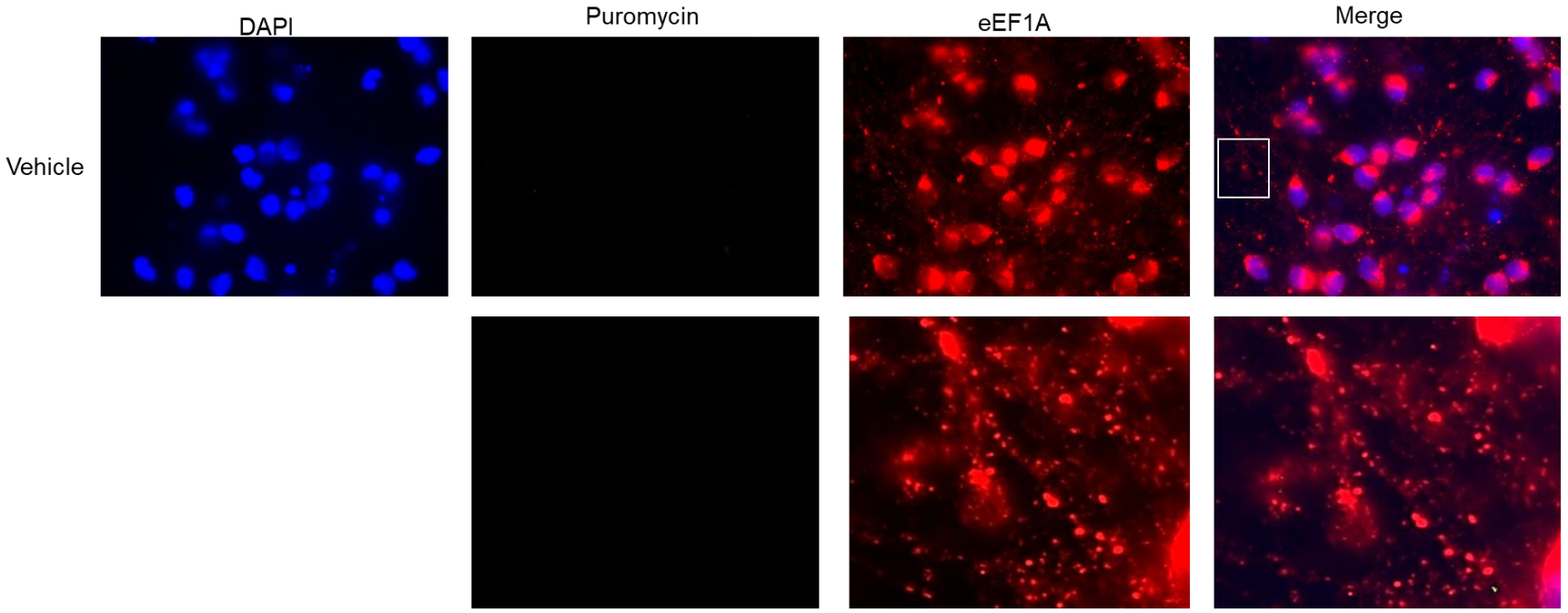

D

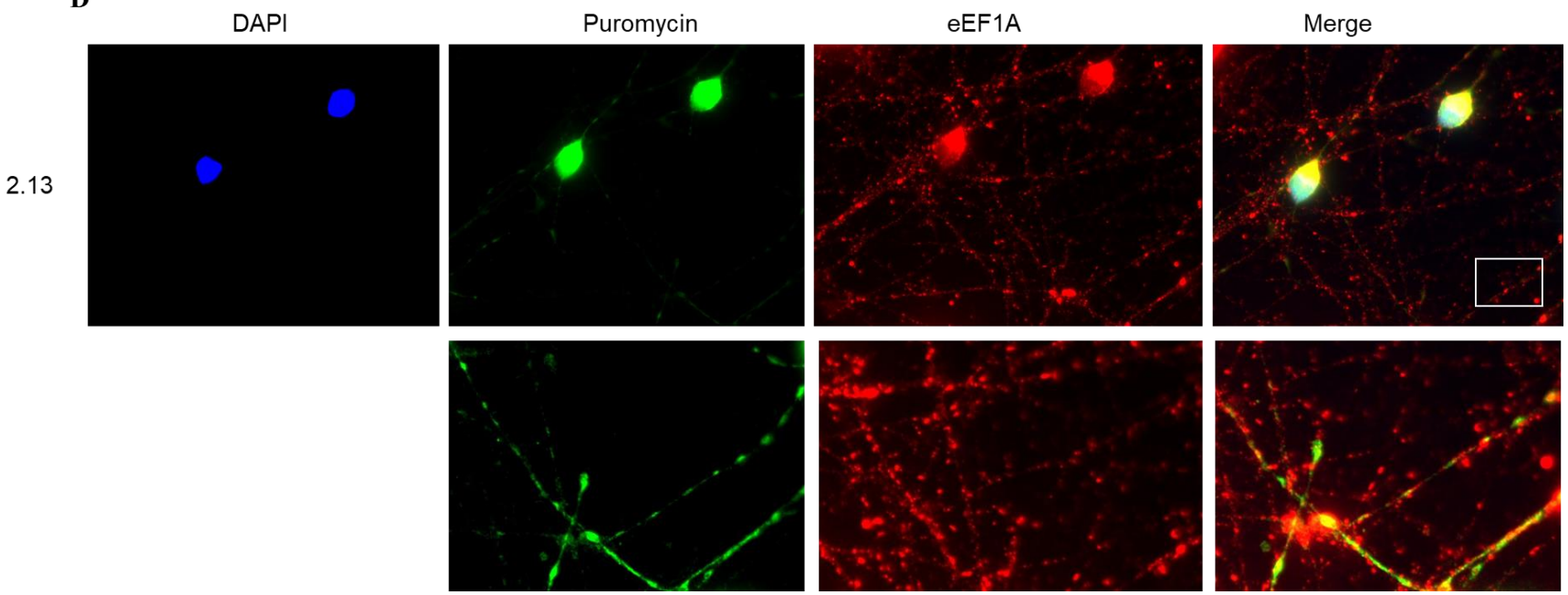

2.18

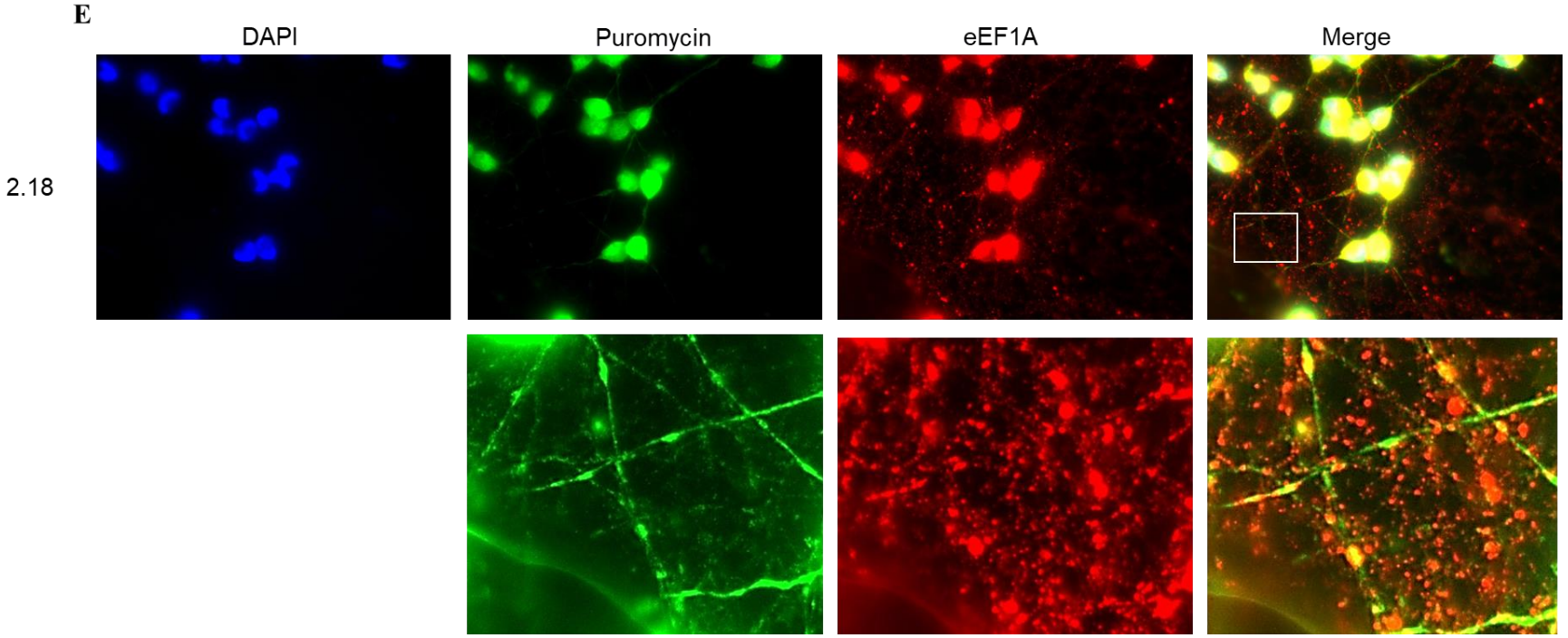

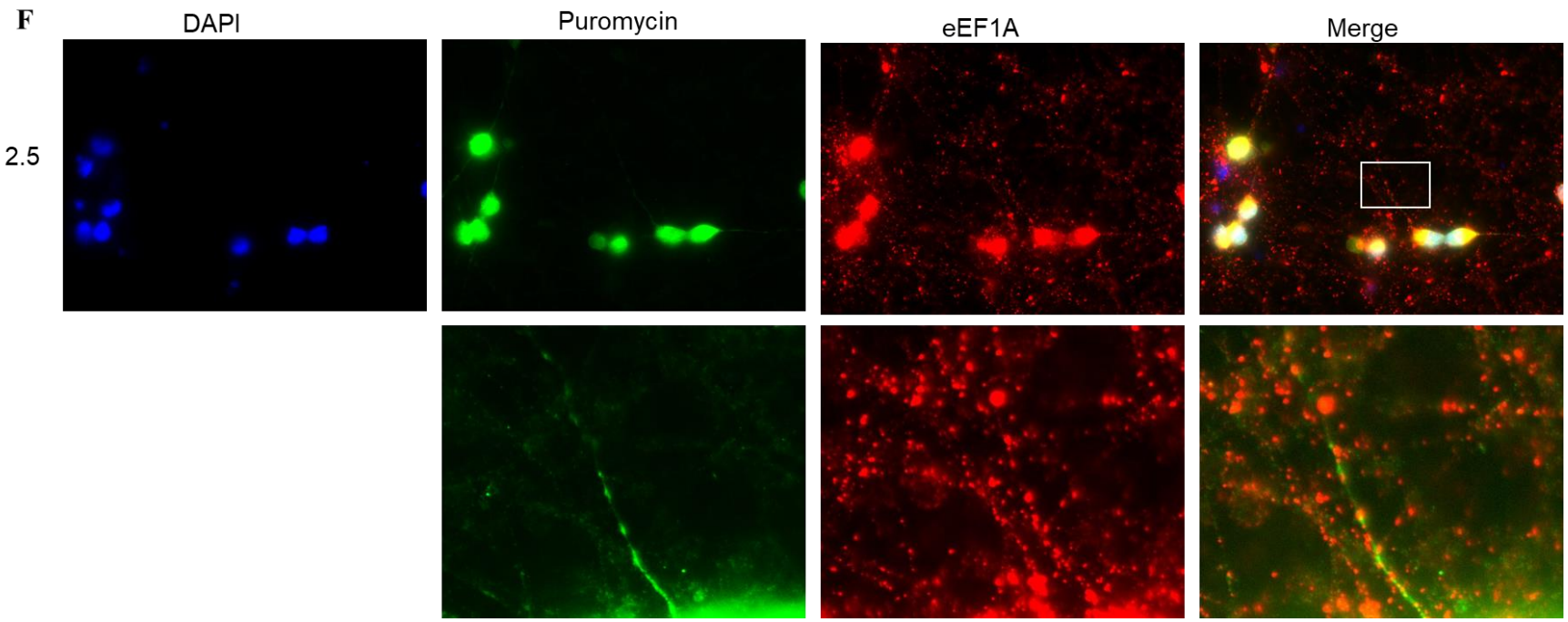
F
DAPI
Puromycin
eEF1A
Merge
2.5

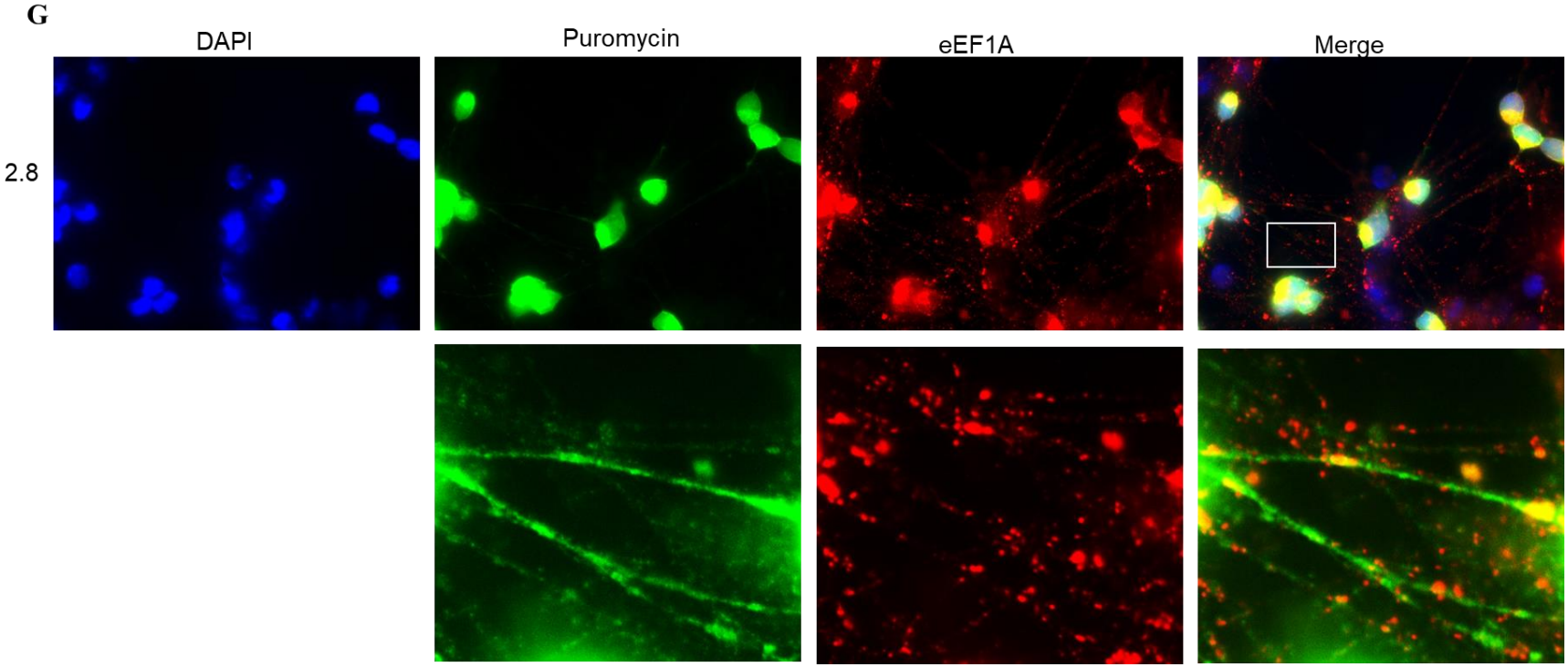
G
DAPI
Puromycin
eEF1A
Merge
2.8

H

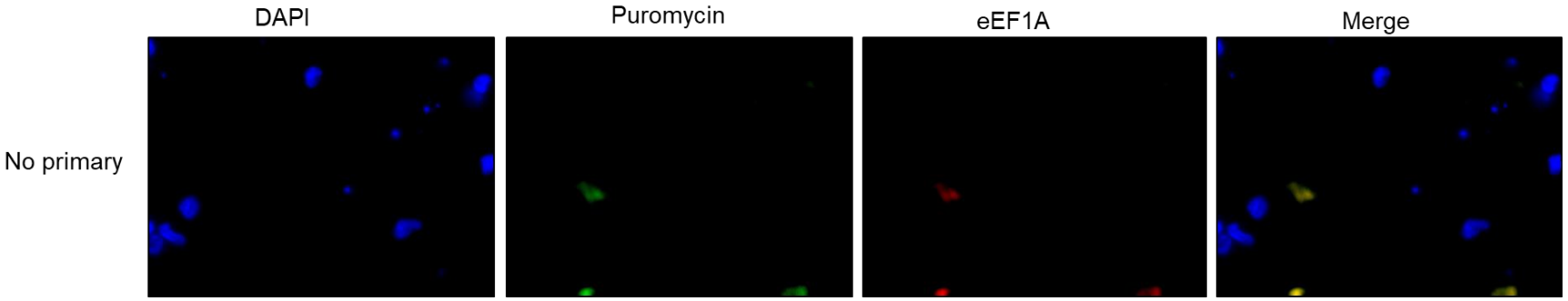

I

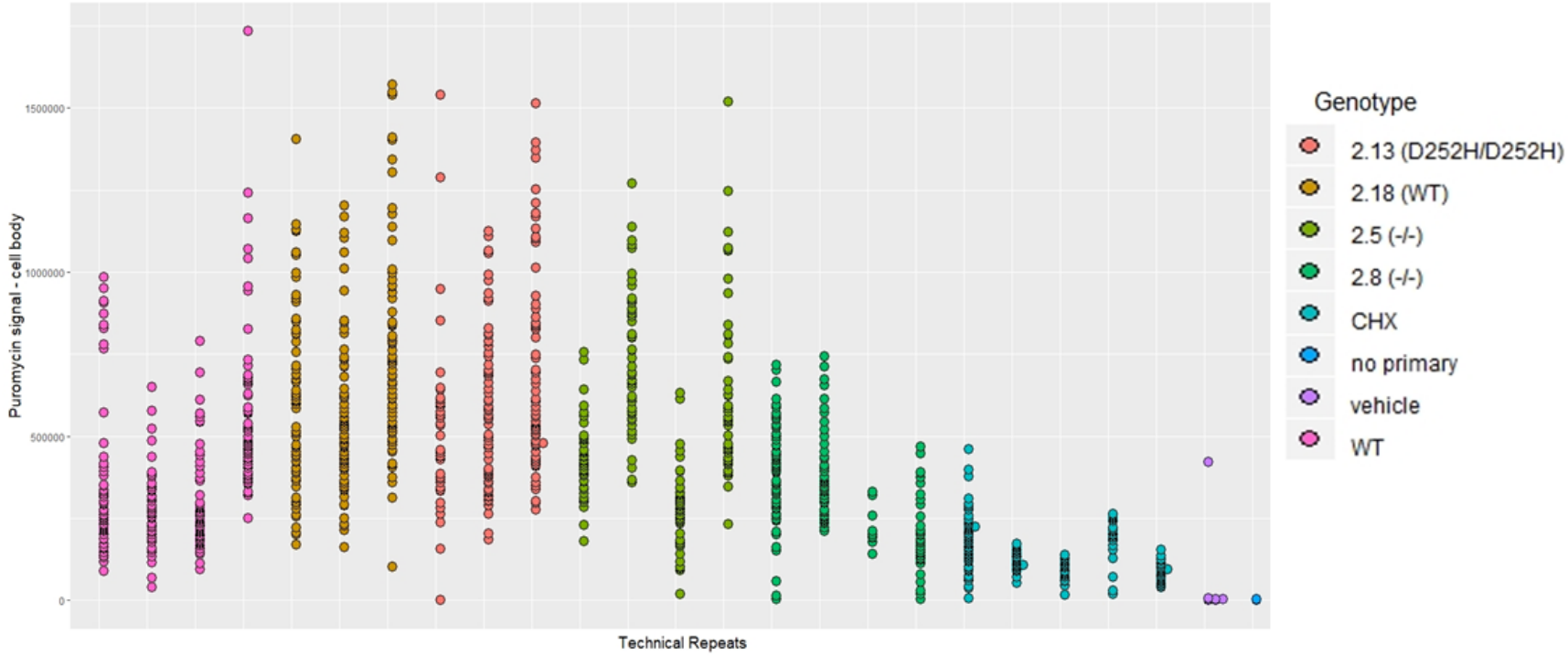
Puromycin signal - cell body
1500000
1000000
500000
0
Technical Repeats
Genotype
2.13 (D252H/D252H)
2.18 (WT)
2.5 (-/-)
2.8 (-/-)
CHX
no primary
vehicle
WT

J

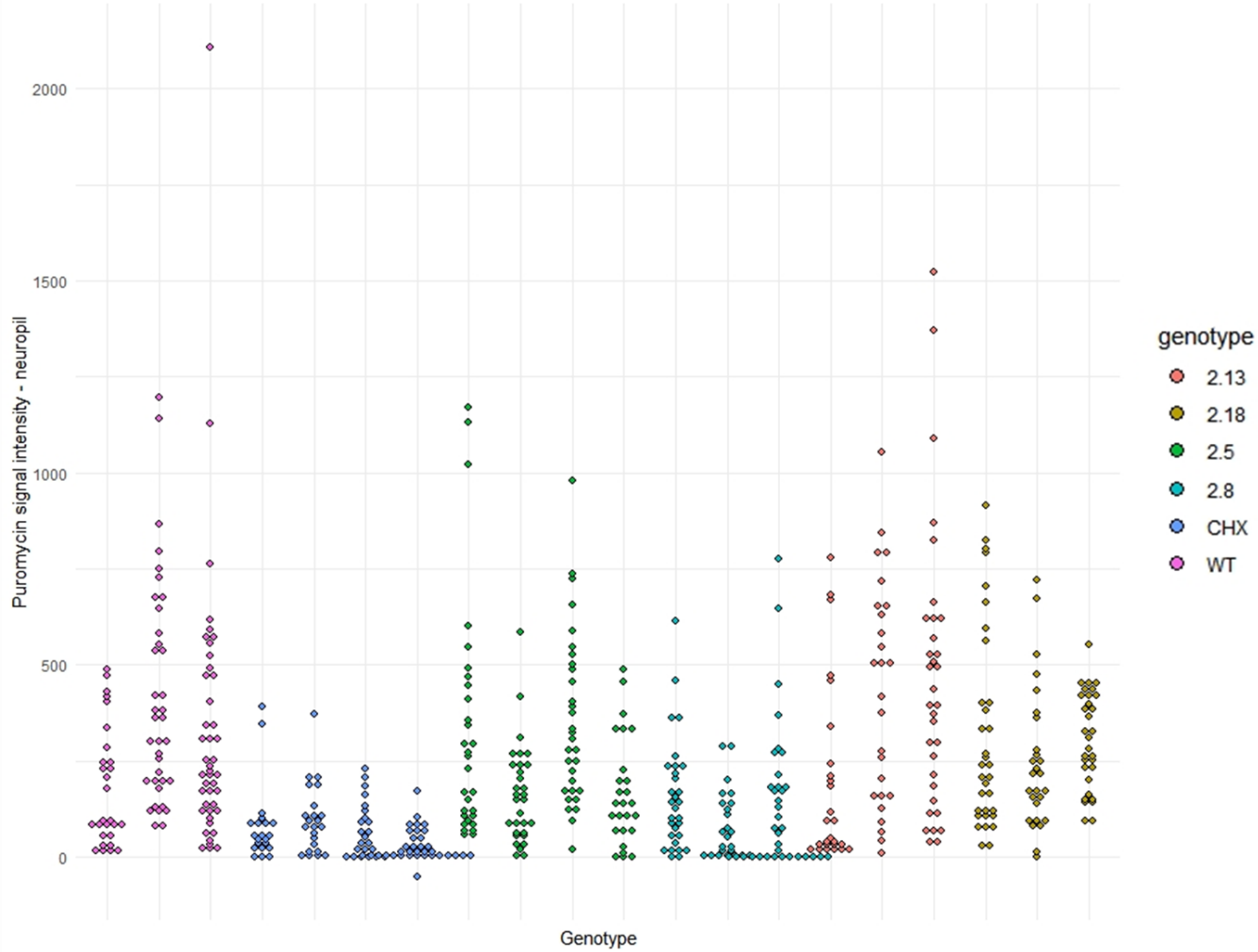
2000
1500
1000
500
0
Puromycin signal intensity - neuropil
Genotype
genotype
2.13
2.18
2.5
2.8
CHX
WT

K

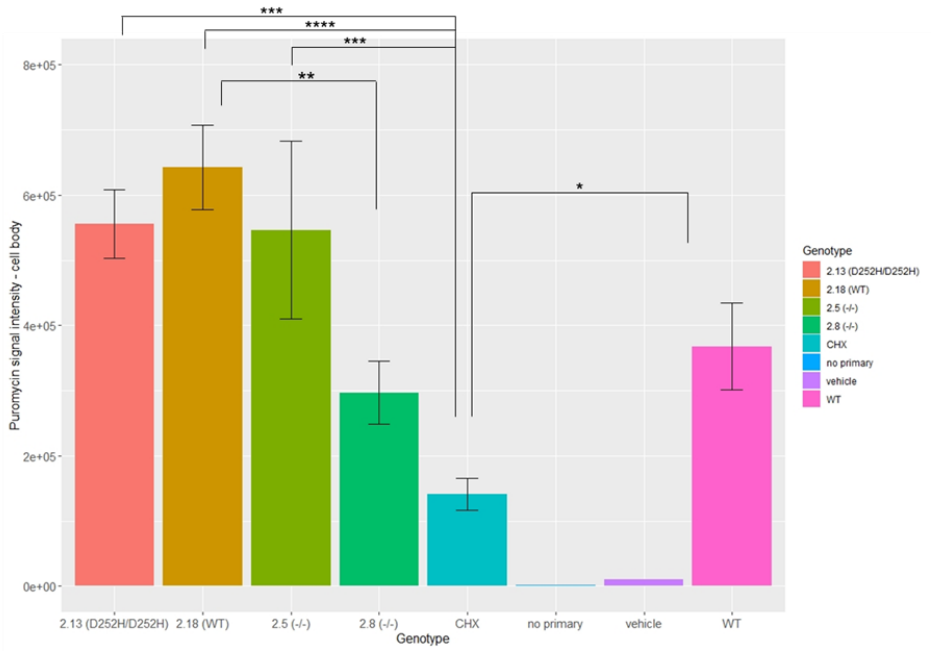
***
****
***
**
*
8e+05
6e+05
4e+05
2e+05
0e+00
Puromycin signal intensity - cell body
2.13 (D252H/D252H)
2.18 (WT)
2.5 (-/-)
2.8 (-/-)
CHX
no primary
vehicle
WT
Genotype
Genotype
2.13 (D252H/D252H)
2.18 (WT)
2.5 (-/-)
2.8 (-/-)
CHX
no primary
vehicle
WT

L

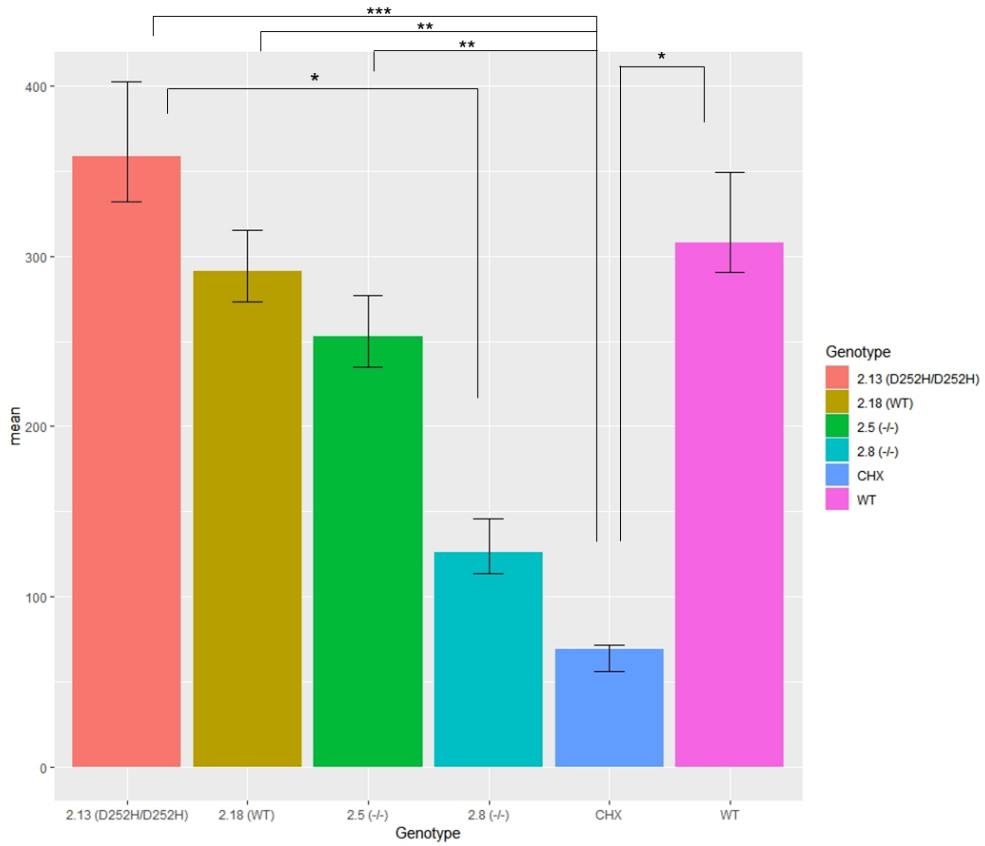
***
**
**
*
*
400
300
200
100
0
mean
2.13 (D252H/D252H)
2.18 (WT)
2.5 (-/-)
2.8 (-/-)
CHX
WT
Genotype
Genotype
2.13 (D252H/D252H)
2.18 (WT)
2.5 (-/-)
2.8 (-/-)
CHX
WT

Figure 5.6: Puromycin treatment to assess nascent protein synthesis in differentiated LUHMES cell lines. *A-H, are representative images taken from LUHMES cell lines as follows (WT, WT + Cycloheximide, WT + vehicle treated, 2.13 (D252H/D252H), 2.18 (WT which had undergone CRISPR), 2.5 (-/-), 2.8(-/-) and no primary control (WT cells). Images are shown both separated into channels and as a merged acquisition. As protein synthesis was far more prominent in the cell body, two different exposures were used to image cell body and axons. In each case, a portion of the imaged axons is shown at the higher exposure. This portion is identified by a white box on the merged image. Quantification of the signal intensity in cell bodies in all technical repeats is shown in I. Each point represents a cell body which was quantified. Quantification of puromycin signal in the neuropil in each condition was also measured. Technical replicates are shown in J as described previously. The technical replicates of cell body measurements (between 3 and 5 for each genotype) were averaged, plotted and statistical analysis performed using a one-way ANOVA (no primary and vehicle conditions were excluded from statistical analysis) (K). One-way ANOVA demonstrated significant interaction ($F(5, 17) = 9.299$, $p<0.001$). The mean and SEM of signal intensity in the neuropil for each genotype is reported in L. One-way ANOVA analysis determined a significant interaction ($F(5, 14) = 5.403$, $p<0.01$). Post-hoc Tukey multiple comparison testing was used in both cases to determine significant differences between conditions. Significance is denoted by '*' symbol. '*' $p<0.05$, '**' $p<0.01$, '***' $p<0.001$..*

The treatment of cells with cycloheximide prior to puromycin administration produced significantly lower levels of nascent protein synthesis as compared to all LUHMES cell lines (excluding 2.8(-/-)), validating the experiment (Figure 5.6K). Comparison of technical repeats for both cell body and neuropil demonstrated reasonable clustering within genotypes. No significant difference was found between technical repeats in all genotypes.

In both neuropil and cell body measurements, no significant difference could be seen between any lines and WT. In cell body quantification, 2.18 (WT CRISPR) was seen to be significantly increased compared to 2.8 (-/-). However, it was not different

from other null line 2.5, and WT cells did not achieve the same significance. In neuropil examinations, 2.13 (D252H/D252H) showed an increased protein synthesis rate compared with 2.8, likely suggesting the LUHMES cell line 2.8 shows lower protein synthesis than other lines and suggests the driving force behind changes in protein synthesis is clonal variability.

There is no significant difference between WT and line 2.13. It is possible that with more lines we may be able to conclude that there is no difference between D252H neurons and WT in terms of protein synthesis capacity. This result, however, is at odds with the preliminary results produced in 5.3.1. Given the clonal variability and discrepancy between methods of puromycylation, results suggest that LUHMES cells are not a viable model for measuring protein synthesis. This is likely owing to a mixture of the presence of eEF1A1 and clonal variability.

5.3.3 AHA click-it chemistry of LUHMES cell lines

Click-it chemistry experiments were performed in conjunction of puromycylation to ascertain if clones behaved in a similar manner using a different technique. This technique mirrored the more traditional radioactive labelling measurements but used a fluorescent analogue of methionine. As cycloheximide had not totally ablated protein synthesis signal in 5.3.2, I opted to use an alternative protein synthesis inhibitor, anisomycin. Compared with WT LUHMES cells, anisomycin and other negative control conditions showed a significant reduction in fluorescence intensity (5.5 **A**-**C**).

In this assay reduction in nascent protein synthesis between D252H/- line 2.16 and WT was observed. However, the deficit between WT and line 2.8 which had been seen in puromycin staining (5.3.2) was not reproduced. In addition to clonal variability, LUHMES cells may also show variability in protein synthesis levels based on experimental conditions. Taking all results together, it seems that LUHMES cells are not an appropriate model for testing protein synthesis as a result of eEF1A2 mutations/deletions.

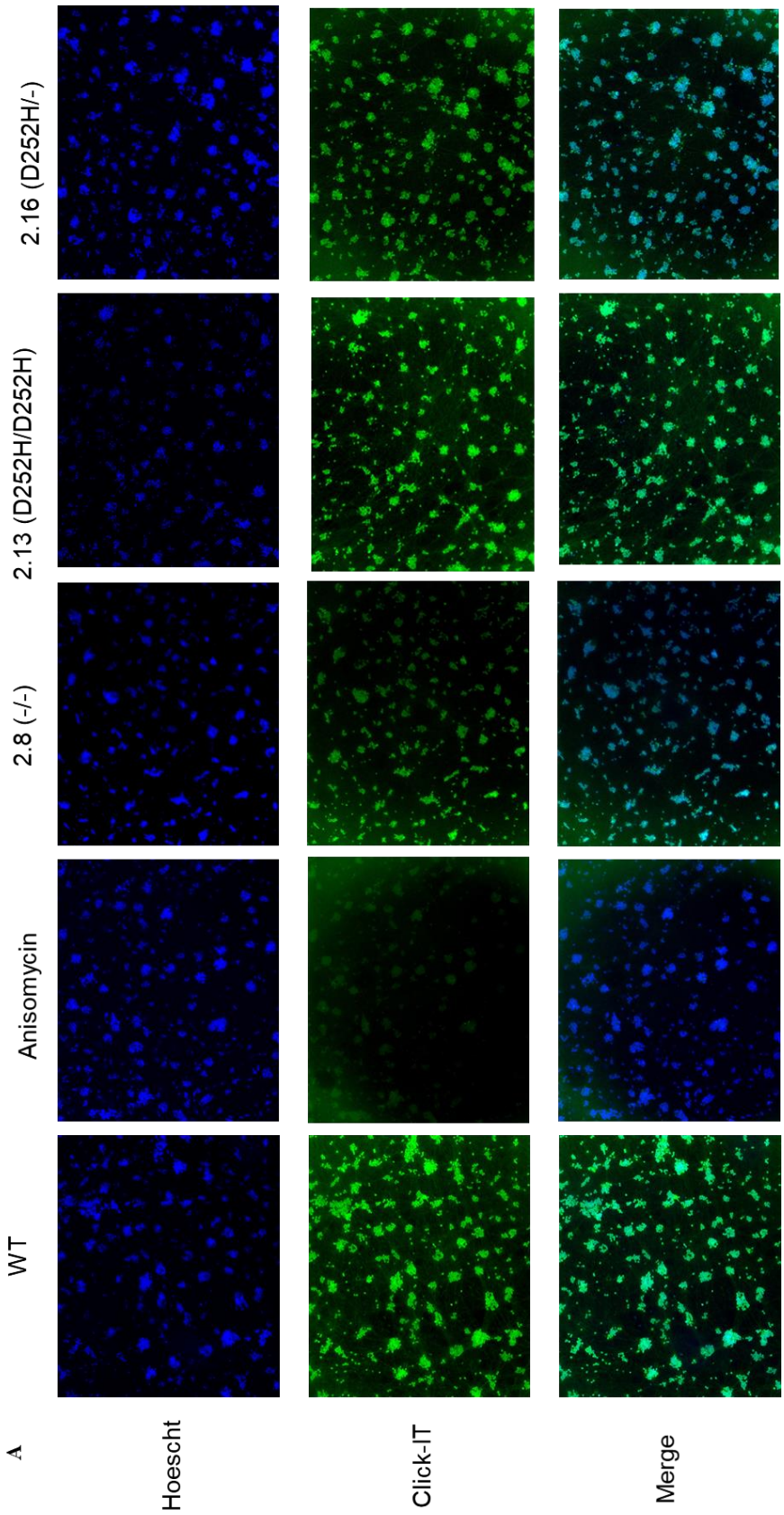
A
WT
Anisomycin
2.8 (-/-)
2.13 (D252H/D252H)
2.16 (D252H/-)
Hoescht
Click-IT
Merge

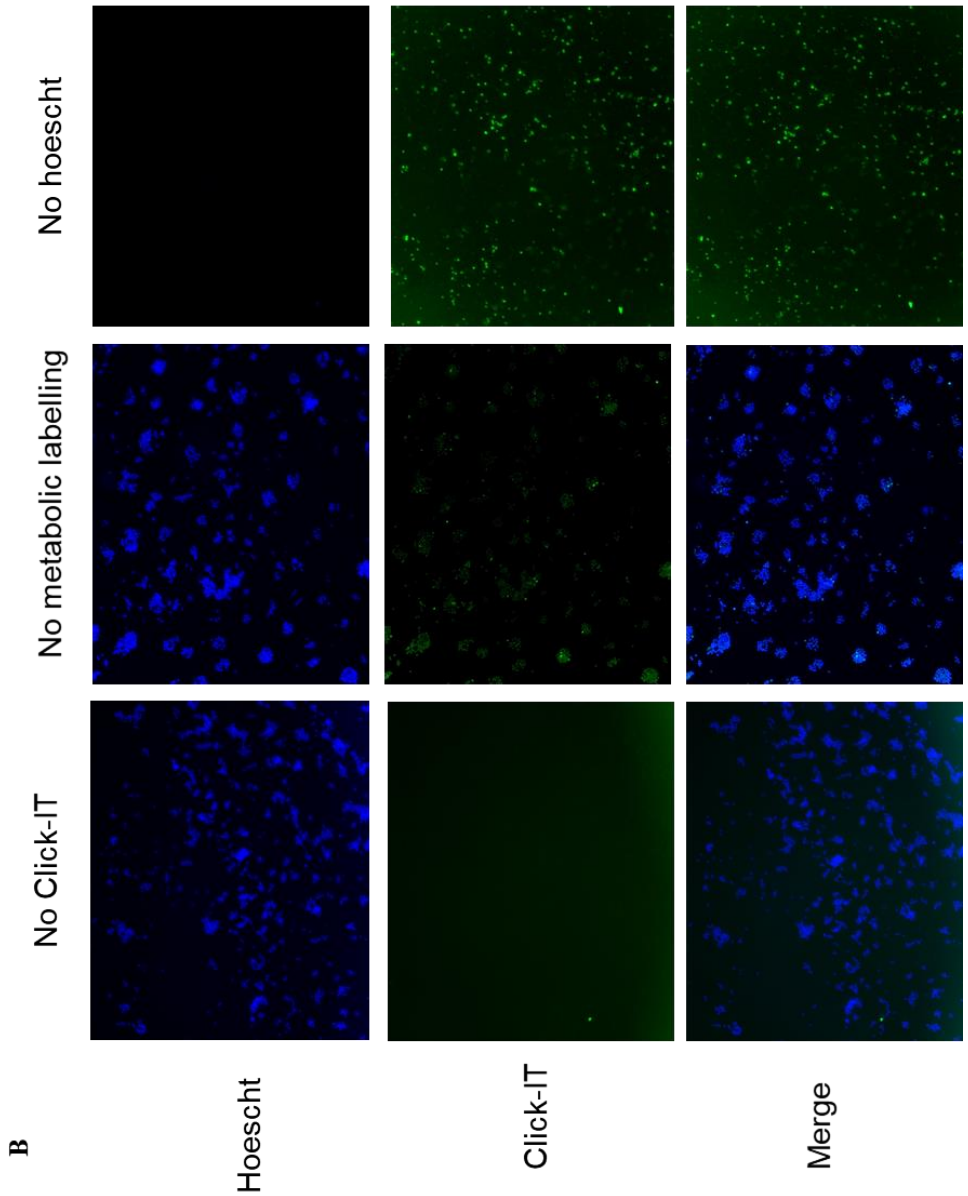
B
Hoescht
Click-IT
Merge
No Click-IT
No metabolic labelling
No hoescht

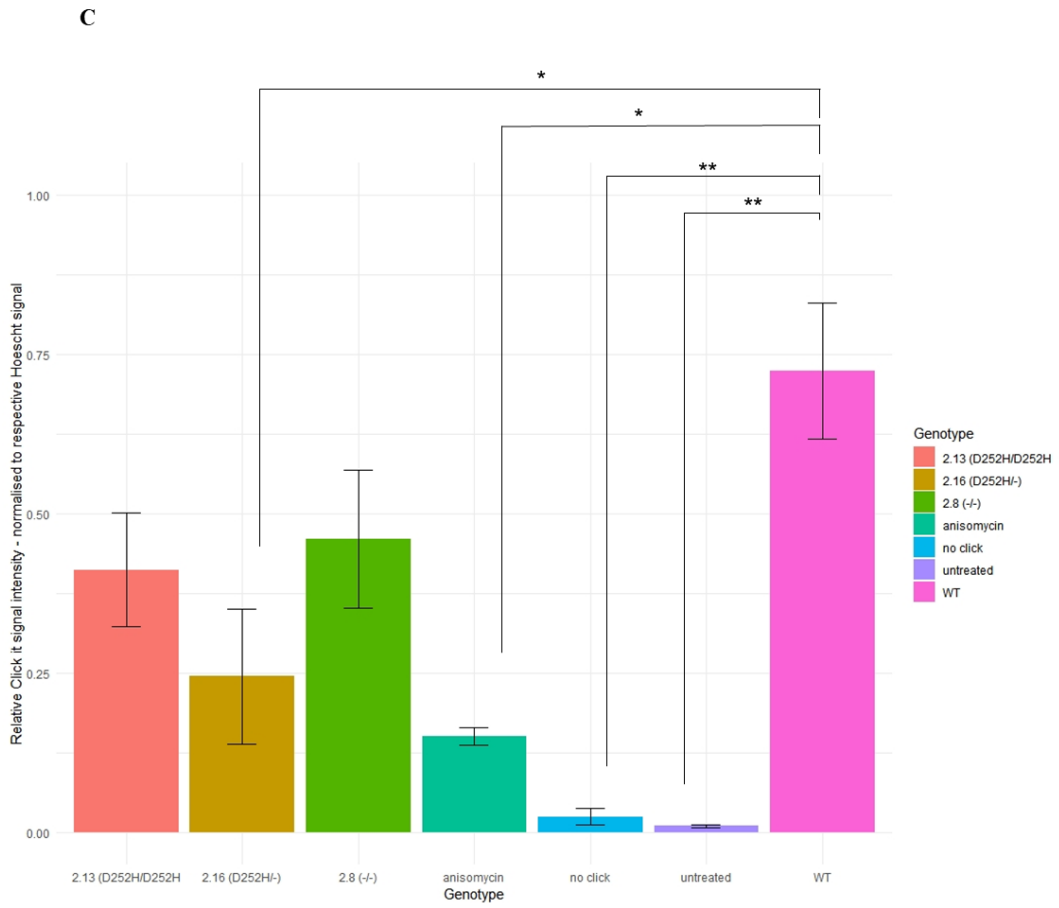

Figure 5.7: Click-IT AHA metabolic labelling to detect protein synthesis in differentiated LUHMES cells. *Using methionine analogue AHA, the Click-IT protein synthesis kit (Invitrogen) assesses nascent protein synthesis using a fluorescent reporter system. Fluorescence as a measure of protein synthesis was imaged using the FITC channel (488/519 excitation/emission). Cell number was controlled by staining for nuclei using Hoescht. Images for each condition are represented in* ***A*** *and* ***B****. After background correction in each channel click—it signal was normalised to respective Hoescht signal. The resulting levels of nascent protein synthesis are represented in* ***C*** *(mean +/- SEM). For control conditions n = 3 and for genotype lines n = 10-14. One-way ANOVA analysis demonstrated a significant interaction (F(6, 34) = 4.683, p<0.01. Tukey post hoc analysis was performed to assess which conditions significantly different. '*' represents p<0.05, '**' p<0.01.*

5.3.4 *In vivo* puromycylation to assess protein synthesis rates in Eef1a2^{D252H} and Eef1a2$^{-/-}$ mouse lines

As LUHMES cells were not a viable model to measure protein synthesis, attempts to assess protein synthesis were made *in vivo*. Puromycin can be administered at a very low dose to mice for a 30-minute period before tissue is collected and measured for puromycin signal intensity. As puromycin cannot pass the blood brain barrier, I tested skeletal muscle, as a representative tissue that exclusively expresses eEF1A2. To maximise the chance of detecting a deficit, I chose to test mice with severe phenotypic deficits and after the down-regulation of eEF1A1 (p21).

Initial experiments treated *Eef1a2*/D252H and *Eef1a2*/wst lines at p21-p24 when mice were available. Testing of these samples however determined that mice treated on different days were not comparable, with variation between treatments on different days making conclusions impossible. I was therefore only able to test a cohort of mice all born within one day of each other and had no control over the genotype distribution of samples. By chance, several large litters from *Eef1a2*/D252H and *Eef1a2*/wst were born within one day of each other. These were all tested at p22 / p23. Only one of the mice was a D252H homozygote.

Figure 5.8 shows puromycin signal intensity and total protein staining in skeletal muscle of mice (5.6**A**). Testing *Eef1a2* null mice provided a validation of the technique. eEF1A1 is down-regulated in skeletal muscle by p21 (56) and with no eEF1A2 to compensate, the mice would be expected to show a reduction in protein synthesis.

No significant difference between *Eef1a2*$^{-/-}$ mice was seen in comparison with heterozygous littermates. No significant difference is seen between WT and heterozygous mice from *Eef1a2*/D252H line either. Mice show a total down-regulation of eEF1A1 in muscle at p21 and are normally culled due to severity at p24 for *Eef1a2*/D252H and p26-p27 for *Eef1a2*/wst mice. Given this narrow time-window for testing, the *in vivo* SUnSET technique did not appear to be compatible with our model. Even when small cohorts of littermates are tested at the same time, no observable differences in puromycin signal intensity are seen. This is perhaps

owing to the sample numbers, but my results cast doubt as to whether the technique measures protein synthesis accurately.

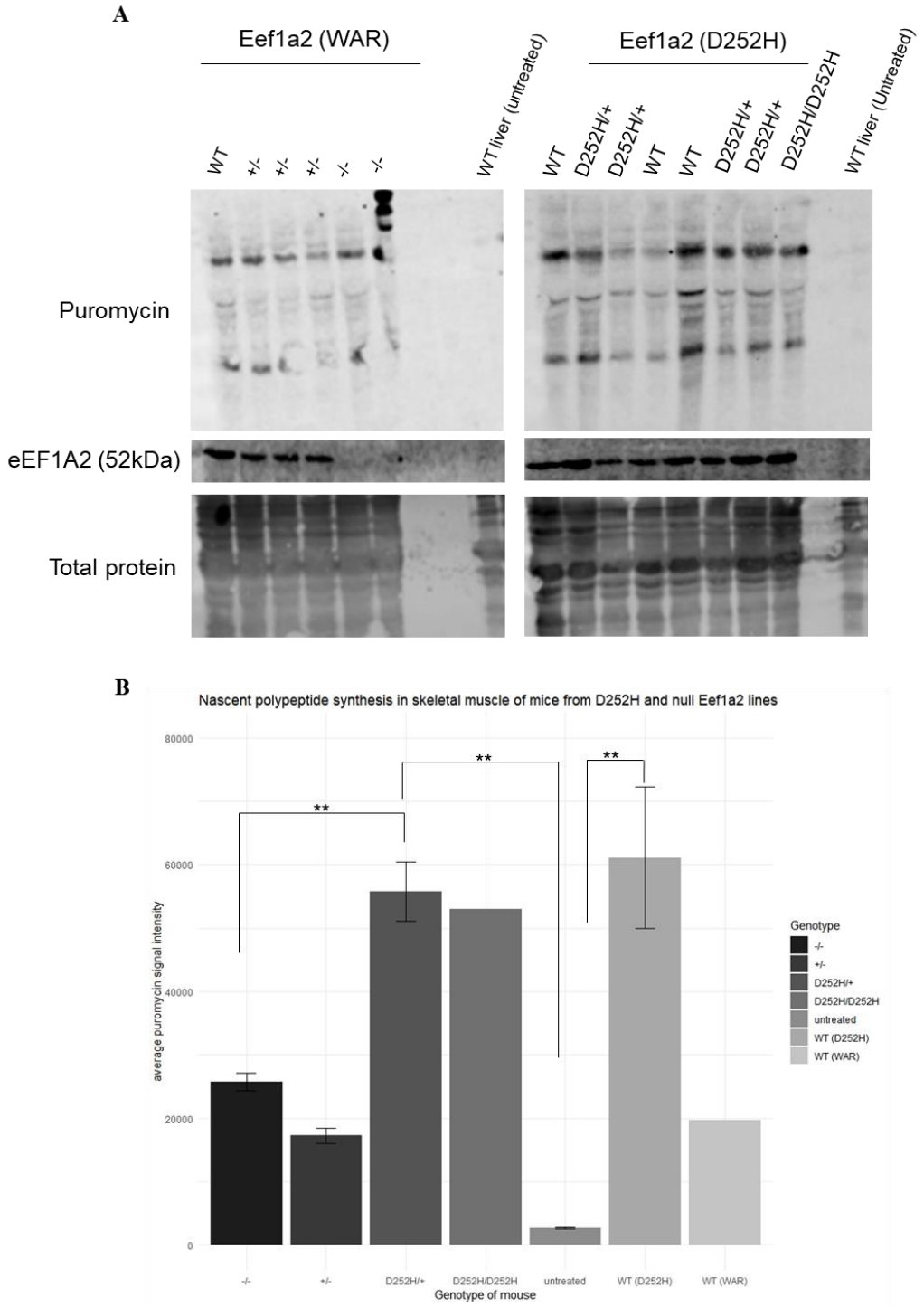

***Figure 5.8**: **In vivo measurements of nascent polypeptide synthesis using puromycin administration.** Skeletal muscle extracts from mice from Eef1a2/wst and Eef1a2/D252H lines treated with 0.04µmols/kg puromycin for 30 minutes. Puromycin staining is seen in **A.** eEF1A2 and total protein staining are below.*

*Quantification has been reported in **B**. Graph shows mean of normalised puromycin staining +/- SEM. One-way ANOVA analysis reported a significant interaction $F(6, 9)=10.69$, $p<0.01$. Tukey post hoc analysis was performed to assess which conditions were significantly different. '*' indicates $p<0.05$, '**' $p<0.01$.*

5.4 Discussion

5.4.1 Generation and characterisation of mutant eEF1A2 LUHMES cell lines

I aimed to generate both G70S and D252H mutations in CRISPR/Cas9 cells for functional testing. Although CRISPR/Cas9 activity was efficient and demonstrated genetic editing in nearly all lines, the number of surviving clones was limited, giving a smaller number of biological repeats than would be ideal for larger experiments. This is likely owing to the high mortality rate and low transfection efficiency of LUHMES cells during transfection. The optimal LUHMES transfection method, reported by Shah et al, was followed during the experiment (139). However, even with this optimisation, neuronal cell lines are renowned for being difficult to transfect and even using the optimised method, Shah et al only reported a 25-30% incorporation of CRISPR/Cas9 guides. As I aimed to test if LUHMES cells were a viable model, I continued with a smaller number of clonal lines. However, if LUHMES cells had been proven to be a viable model for testing protein synthesis, a larger number of clones would be required for conclusive testing.

The repair template including the D252H mutation was successfully incorporated in to two cell lines – 2.13 (D252H/D252H) and 2.16 (D252H/-). In contrast, the G70S experiment failed to yield homology directed repair and incorporation of the G70S mutation. One notable difference between the G70S and D252H repair templates was the incorporation of silent mutations into the PAM sites of the D252H repair template. This likely prevented further cutting of the PAM sites by gRNAs without affecting the protein coding sequence, enabling more efficient homology directed repair.

mRNA testing demonstrated a down-regulation of eEF1A2 mRNA in 2.5 (-/-) and 2.8 (-/-) cell lines, highlighting successful knock-down of eEF1A2 at the mRNA level. However, despite this, eEF1A2 mRNA and eEF1A protein concentration varied between different clones. Most notably, 2.18 (WT) showed a significant up-regulation of eEF1A2 mRNA compared to null clones at exon 7 when WT clones did not. Given there is no genetic difference between WT and 2.18 (WT) lines, the

variability in eEF1A2 mRNA may well be the driving force behind the clonal variation seen in protein synthesis assays.

Clonal variability has been reported in neuronal cell lines previously (198). If LUHMES cells were to be used in the future to assess impact of eEF1A2 deletions and missense mutations, an experimental design measuring basal levels and response to treatment/change in condition would likely be the most appropriate strategy.

5.4.2 Protein synthesis assays

Local protein synthesis impairments in axons and dendrites are sufficient to mediate neurological deficits (199). Fragile X syndrome (FXS) has been implicated as a result of local protein synthesis deficits in both dendrites and axons (200,201). Given the function of eEF1A2 in neurons and my interaction results, it was imperative to test global and local protein synthesis changes resulting from $eEF1A2^{D252H}$ and $eEF1A2^{-/-}$ mutations.

Several techniques are available for measuring protein synthesis. Two of the most utilised are metabolic labelling and puromycin tagging (202). These were both used *in vitro* and puromycylation was additionally used *in vivo*. In differentiated LUHMES cells, I used imaging-based methods of these treatments to enable the assessment of protein synthesis in both the neuropil and cell body. Neither technique managed to find a deficit in D252H neurons globally. Additionally, puromycin tagging revealed no deficit in neuropil puromycin staining. Although puromycin staining was reduced in one $eEF1A2^{-/-}$ line (2.8), this can likely be attributed to clonal variability, as line 2.5(-/-) did not share this deficit. It is very possible that the techniques were not sensitive enough to measure any deficit changes with so much eEF1A1 expressed and likely enabling normal protein synthesis. As all immortalised cells, even differentiated neuronal iPSCs produce eEF1A1, these results support the idea that measuring protein synthesis deficits as a result of eEF1A2 mutations and deletions is not possible *in vitro*.

Given the impossibility of measuring protein synthesis *in vitro* in our case, I looked at *in vivo* options. Several papers have reported using the puromycylation

technique *in vivo*, by treating mice with low doses of puromycin. This technique has been reported to successfully work in skeletal muscle (143) and cardiac muscle (203), both tissues expressing eEF1A2. On samples available for testing simultaneously, no deficit could be seen between genotypes from within the respective *Eef1a2*/D252H and *Eef1a2*/wst littermates. Given the high chance of a protein synthesis deficit in *Eef1a2*$^{-/-}$ muscle, my results throw in to question the accuracy of SUnSET using western blotting.

A recent study looked at protein synthesis rates in patient derived fibroblasts from FXS patients and determined a subset of individuals in which protein synthesis was increased compared to controls. The authors argued that this subset may respond to translational inhibition treatment, but that the variability in protein synthesis explains why other FXS individuals do not respond to the same treatment (204). This result would make biological sense given that FXS patients have reduced FMRP protein and consequently have a reduction in protein synthesis inhibition. However, the authors fail to identify what method they used for classifying FXS individuals into 'high' and 'low' protein synthesis groups. No testing was performed confirming that these 'high' and 'low' patient groups are statistically different from one another. Furthermore, the technical repeats shown suggested that the difference between 'high' and 'low' protein synthesis groups was mediated by technical repeat variability in the 'high' condition. The authors also demonstrate that this variation in protein synthesis rates between patients did not correlate with FMRP levels, suggesting this variance comes from a different source. This evidence lends credence to my theory that western blotting lysate of puromycin samples is too variable and crude a method between technical repeats and cannot detect subtle levels of changes in protein synthesis.

Another, albeit slim, possibility is that cells in *Eef1a2*$^{-/-}$ and *Eef1a2*$^{D252H/D252H}$ mice have undergone energy starvation due to dysregulation of protein synthesis. It has been reported that energy starved cells are not suitable for use in SUnSET experiments (205).

It is also possible that deficits in protein synthesis would be more noticeable in neurons than skeletal muscle. Wider research based around my results supports this hypothesis. D252H mutation results in a lack of eEF1B binding. eEF1B deletions in humans and mice show a neuronal specific phenotype. Deletion of an *Eef1b2* exon knocks-out eEF1Bα expression in homozygous mice. These mice are reported to show neurological deficits (http://www.mousephenotype.org/data/alleles/MGI:1929520/em1(IMPC)J). A recessive deletion of part of the *EEF1B2* gene was reported in a pair of siblings from consanguineous parents. These patients were reported to have intellectual disability (102). This suggests eEF1B is not required for protein synthesis in all but higher neuronal function. Given this evidence, the D252H mutation may impact more upon protein synthesis in neurons than in muscle.

Puromycin cannot pass the blood brain barrier, making subcutaneous administration impossible for testing neurons. Brain slices can be treated *ex vivo* with puromycin, however I decided against this, as brain contains a high level of glial cells which express eEF1A1 and would influence results (although immunofluorescence of fixed slices may overcome this). Another possibility is to measure puromycin incorporation in sciatic nerves. Successful staining of puromycin incorporation in sciatic nerves has been demonstrated by Lopez-Erauskin and colleagues (193). Given these approaches do not involve radiation, they should be examined as possibilities in the first instance. It might, however, be the case that measuring protein synthesis through radioisotope labelling is required for measuring deficits. This treatment can be applied to brain slices to measure protein synthesis rates (206), but as with *ex vivo* administration of puromycin, glial cells expressing eEF1A1 would be a confound.

In conclusion, I believe the immunostaining of puromycin treated *in vivo* neuronal samples (sciatic nerve or brain slices) is likely to provide the best technique for assessing protein synthesis in *Eef1a2*$^{D252H/D252H}$ and *Eef1a2*$^{-/-}$ mice.

5.4.3 Conclusions

LUHMES cells were successfully genetically modified to induce null and eEF1A2^{D252H} mutations. Although null cells demonstrated a knock-down of eEF1A2 mRNA, levels of eEF1A protein varied between clonal lines. This was likely the driving factor in clonal variability in LUHMES lines. No discernible difference in protein synthesis could be measured by puromycin incorporation *in vivo* in *Eef1a2*/D252H or *Eef1a2*/wst mouse lines.

Chapter 6: Discussion

6.1 Project Summary

Recent exome sequencing has identified heterozygous *de novo* missense mutations in eEF1A2 which result in epilepsy, autism and intellectual disability. This project aimed to expand upon the role of these mutations in causing neurodevelopmental dysregulation. By examining the protein-protein interactions of WT and mutant eEF1A2, protein clusters associated with canonical and non-canonical eEF1A2 functions were identified. Changes to this protein interaction network map as a result of specific mutations eEF1A2^{D252H} and eEF1A2^{G70S} were assessed.

The D252H mutation demonstrated a loss of binding to guanine exchange factor eEF1B. eEF1B mediates the GDP recycling after eEF1A delivers aminoacyl tRNAs to the ribosome. It is unclear the extent to which eEF1A2 relies upon eEF1B for GDP recycling versus levels of spontaneous GDP release. siRNA experiments knocking down eEF1B subunits showed no deficit in cell growth in the short term (71). However, eEF1A2 has a greater affinity for GDP than eEF1A1 (19), suggesting spontaneous release rates would be lower. Additionally, clinical mutations and knock-out mouse models support the theory that eEF1B is required for healthy neuronal function (72,102,103). Whilst the extent to which eEF1A1 and eEF1A2 rely on eEF1B still needs to be fully elucidated, these results would suggest the protein interaction is required, at least in neurons, for proper functioning.

The G70S mutation did not display loss of eEF1B binding. If the relationship with eEF1B mediated clinical severity, it would be hypothesised that the D252H mutation would be more severe than the G70S. Indeed, the opposite appears to be the case. Clinical reports demonstrate that all G70S patients develop early onset severe epilepsy, whilst the D252H cases do not report seizures until later in childhood. Given the number of patients this evidence is speculative, however it is an interesting observation. The results from the AP-MS experiment were validated and expanded upon by testing other mutant forms of eEF1A2 for interaction to eEF1B. Clusters of mutations which did and did not lose eEF1B binding were identified using co-

immunoprecipitation. More cases and clinical information would be required to see if a difference in severity/phenotype can be seen between these groups based on their eEF1B interaction. As interaction analysis implicated protein synthesis as possibly dysregulated in neurons, translation assays were optimised *in vivo* and *in vitro* to assess the impact of the D252H mutation on eEF1A2 canonical function. These protein synthesis experiments did not provide a conclusive result.

6.2 Aim 1: Protein interactome analysis of eEF1A2

This chapter aimed to establish the protein-protein interactions of eEF1A2 and how they varied when eEF1A2 was mutated. Any loss or gain of binding might elucidate a loss or gain of function and reveal the molecular mechanism underlying different mutations.

Interactome analysis of eEF1A2 generated a protein network with clusters of proteins involved in previously reported functions of eEF1A2. This thesis is the first work to examine the interactome of eEF1A2 using AP-MS.

After appropriate normalisation of the AP-MS data, dysregulation in binding to eEF1B subunits in the D252H, but not G70S, mutation was identified. The consequences of this altered interaction have been discussed extensively throughout this thesis, and the functional consequence was subsequently tested using protein synthesis assays. Further exploration of this finding seems vital to elucidate the role of specific mutations in the function of eEF1A2. Given the clinical reports of neurodevelopmental disorders arising from mutations in other eEF1B subunits, and the neuronal specific phenotypes displayed by eEF1Bα and eEF1BδL knock-out mice, recent evidence for the role of eEF1B suggests it is not essential in all but neuronal cells (72,102–105). Given this finding, it would be likely that disruption to eEF1B interaction in the D252H mutation would be more problematic in neurons than other cell types (i.e. skeletal and cardiac muscle). It was therefore imperative to assess the impact of eEF1A2 clinical mutations on protein synthesis.

Another result from the AP-MS analysis was the disruption of interactions with ribosomal subunits in both mutant forms compared to WT eEF1A2. Co-immunoprecipitation experiments failed to pull down ribosomal subunits, despite extensive testing, suggesting these interactions are too transient for co-immunoprecipitation. Other papers have reported successful immunoprecipitation experiments of ribosomal subunits (207). Dysregulation in ribosomal homeostasis has long been implicated in a range of clinical disorders – often with surprisingly specific phenotypes (208). Ribosomes are, unsurprisingly, critical for growth and maintenance in neurons. Impairments in ribosomal biogenesis in neurons lead to

translational inhibition, stress granule formation and neuronal outgrowth deficits (209). Given it has been previously established that eEF1A2 interacts with ribosomes (156,157), dysregulation of these interactions could compound any protein synthesis deficits resulting from eEF1A2 mutations. If mutations led to inappropriate interaction with the ribosome, this might even lead to 'stalling' of ribosomes which are prevented from functioning normally. If this was occurring prior to eEF1A1 down-regulation in *Eef1a2*$^{D252H/D252H}$, ribosomal stalling might impair eEF1A1 from performing sufficient translation elongation and could possibly be the cause for the gain-of-function element seen in D252H/D252H mice prior to p21. Indeed, ribosomal stalling was proven to be a contributing factor in similar neurodevelopmental disorder fragile X syndrome (FXS). Research shows that RNA-binding protein fragile X mental retardation protein (FMRP) binds to RNA and is transported to the ribosome. At the ribosome FMRP binds to ribosomal subunit RPL5 and prevents the interaction of other translational machinery with the ribosome. This action induces ribosome stalling and inhibits protein synthesis. This mechanism occurs under normal physiological conditions as a measure of controlling protein synthesis rates (99). In the case of FXS a 5'UTR 'CGG' expansion repeat results in loss of FMRP expression. Without FMRP to mediate ribosome stalling and control levels of protein synthesis, an excess of translation creates a homeostatic imbalance and consequently neurodevelopmental difficulties (210). Although in this instance, the consequence is an increase in protein synthesis, it is conceivable the reverse is happening in the case of eEF1A2. Research on protein synthesis deficits in neurodevelopmental disorders has previously shown that mutations resulting in either increases or decreases in synaptic protein synthesis result in a similar neurodevelopmental phenotype (211). If time constraints had not been an issue in the project, proximity ligation assay, assessing mutations and their effect on ribosomal subunits using a 'Ribosomal P' antibody and ribosomal profiling would have been insightful.

RNA binding proteins also showed an increased association with eEF1A2 in mutant conditions compared to WT. Again, my co-immunoprecipitation experiments for these proteins were inconclusive, likely because these RNA binding proteins are

associated with eEF1A2 at a much lower concentration than that of translation factor subunits. RNA binding proteins are critical to neuronal homeostasis, by regulating processes such as mRNA transport in axons and dendrites, RNA editing and local protein synthesis (212). Under stress-induced translational arrest, mRNA is freed from disassembled polysomes and interacts with RNA binding proteins in aggregates termed stress granules (SGs). SGs then trigger global translational silencing to help mediate cellular stress (213). RNA and associated binding proteins have been implicated in several neurodevelopmental, degenerative and psychiatric conditions, including FXS and FTD-ALS (212). Research on eEF1A and stress granules has focussed on eEF1A1. The cell type used in experiments (HeLa cells) does not express the eEF1A2 isoform, making it possible to conclude that the antibody is only detecting eEF1A1. Evidence suggests that the isoform does not associate with SGs during a translational inhibition stress response (214). It would be interesting to expand upon this research by examining if eEF1A2 associates with SGs during the cellular stress response and if this changes with mutant forms of the protein.

Interactome analysis, while not entirely conclusive in determining the mechanism behind eEF1A2 mutations, was insightful for providing potential avenues of exploration.

6.3 Aim 2: Further analysis of protein interactions and the mechanism behind mutations

The aim of this chapter was to expand on the disruption of eEF1B binding result identified in the D252H but not G70S mutation and to examine if *Eef1a2*$^{D252H/D252H}$ mice demonstrated a loss of function mechanism which would correlate with eEF1B binding disruption.

Eef1a2/del22ex3 and *Eef1a2*/D252H mouse lines were compared to assess whether the eEF1A2^{D252H} mutation resulted in a different phenotype from null mice. *Eef1a2*$^{D252H/D252H}$ mice exhibited an initially more severe phenotype than *Eef1a2*$^{-/-}$ mice. After the ablation of eEF1A1 expression both lines quickly succumb to a neurodegenerative phenotype which results in death. This rapid decline in the homozygotes from both lines suggests that eEF1A2^{D252H} cannot compensate for WT eEF1A2, resulting in a loss-of-function mechanism. However before eEF1A1 down-regulation, mutant eEF1A2^{D252H} exerts an additional gain-of-function or dominant negative mechanism.

One crucial question to ask is, do all mutations operate in the same manner as D252H? Given that protein interaction results vary between mutations, it is almost certain that mutations operate through different mechanisms. It appears from my results that *in vitro* analysis of mutations may not be able to identify functional deficits (owing to the confounding presence of eEF1A1 in cell lines). Therefore *in vivo* research may be required to determine the answer to this question. The only other mutant *Eef1a2* model generated by our lab was the *Eef1a2*/G70S mouse line which failed to generate any founder mice for breeding. Only one homozygote G70S mouse was created making any conclusion impossible. However, it is interesting to note that this homozygote mouse demonstrated a more severe phenotype and had to be culled days before any of the null or G70S/- mice (140). Although it would not be feasible to generate every eEF1A2 mutation in a mouse model, generation of more eEF1A2 missense mutations in mouse models may be vital for clarifying whether all mutations operate like D252H in both a gain- and loss-of-function mechanism.

Unlike *Eef1a2*$^{+/-}$ or *Eef1a2*$^{+/wst}$ mice, *Eef1a2*$^{D252H/+}$ mice show a weight deficit compared to WT during the p14-p23 testing period. Further testing of aged D252H/+ and WT littermates has confirmed this deficit is lifelong (personal communication with Professor Abbott). This suggests that the mutant copy of the protein is exerting a dominant negative/gain-of-function mechanism. Expanding upon this by examining D252H/+ mice in greater detail could provide an insight into this additional element to the mutation mechanism. Testing aged (1 year and older) D252H/+ mice for neurological deficits which might accrue over time would be interesting in helping determine what is happening in the heterozygous patients. Jilly Hope performed initial behavioural testing of these mice as part of her doctoral thesis (121). Although Jilly found no deficits in social cognition or increased anxiety behaviours, work on the novel object recognition test (a learning and memory assay) was inconclusive. It would be interesting to repeat these experiments in a bid to assess whether prolonged exposure of neurons to one copy of the D252H protein hindered the ability of eEF1A2 to perform in late-LTP formation.

Assessing neuron growth in D252H/D252H, or D252H/+ mice over an extended period could identify underlying deficits in neurodevelopment. Images of neuroanatomy could be measured in mice using micro-imaging magnetic resonance imaging (mi-MRI). mi-MRI in mice is a well-established technique which could be useful for in-depth analysis of structural differences between WT and D252H mutant mice (215).

Evaluating the electrophysiological properties of hippocampal slices from Eef1a2 mutant mice might identify aberrant neuronal activity. Mice which overexpress eIF4E have been shown to have an increase in protein synthesis. These mice consequentially show electrophysiological dysfunction, changes to dendritic spine density and altered synaptic plasticity which culminate in autism-spectrum like behaviours (216).

Neither *Eef1a2*$^{D252H/D252H}$ or *Eef1a2*$^{D252H/+}$ mice exhibit seizures. The clinical cases of eEF1A2^{D252H} do report epilepsy, however the onset is reported to be much

later than in other mutations (123). It would be interesting to see if seizures were more inducible in these mice than WT counterparts.

Given that *Eef1a2*$^{D252H/D252H}$ mice are far more severely affected than Eef1a2$^{D252H/+}$ littermates, it suggests mutations are disrupting the function of a mechanism other than the WT allele, making it unlikely the mutation operates through a classical dominant negative function. Crucially one of the main differences between *Eef1a2*$^{D252H/D252H}$ and *Eef1a2*$^{-/-}$ mice at p14-p21 is that eEF1A2 is present in D252H mice when eEF1A1 is still expressed. There is a possibility that mutant eEF1A2 is acting upon eEF1A1, forming an aberrant heterodimer which is analogous to a dominant negative effect. Homodimerisation (eEF1A2 – eEF1A2) and heterodimerisation (eEF1A2 – eEF1A1) have been reported (25,217,218). It would be important to assess whether mutant eEF1A2 acts upon eEF1A1, inhibiting its function. It may sequester the isoform and impede the normal function of the heterodimeric complex. Alternatively, as eEF1A is suggested to function in translation as a monomer (219), mutant eEF1A2 may sequester eEF1A1 in a dimer, reducing the rate of protein synthesis at an earlier time point than in the *Eef1a2*$^{-/-}$ mice. Identifying these dimers has not been proven using co-immunoprecipitation. Using more sensitive techniques such as FRET analysis may be insightful in answering this question (218).

It is vital that this additional mechanism in the D252H mutation is identified to ensure any treatment strategy does not exacerbate the toxic activity which the mutation exerts. Given that it is possible mutant eEF1A2 might act upon eEF1A1 when it is still present, but additionally cannot compensate for eEF1A1 when it is down-regulated, it is possible different treatment strategies would be required at different stages of development.

6.4 Aim 3: Functional analysis of disrupted protein interactions

In this chapter I aimed to generate eEF1A2 mutations in LUHMES cells and assess whether mutations impeded protein synthesis.

I used genetic editing technique CRISPR/Cas9 to introduce missense and deletion mutations into the *EEF1A2* gene in neuronal precursor cell line LUHMES. Although the G70S template was not successfully introduced, two lines showed D252H mutation incorporation with no indels. One line was a D252H/D252H homozygous line, while the other had the equivalent of the patient genotype D252H/+. These lines were instrumental in assessing whether LUHMES cells would be an appropriate model for measuring eEF1A2 mutations. Additionally, two eEF1A2 null lines, and a +/- line were generated. A line which had undergone CRISPR/Cas9 treatment but remained unedited (WT) was also examined to ensure there was no difference between this line and an unedited line. Using null lines for comparison was useful for determining whether eEF1A1 would mask any deficits seen by the eEF1A2 deletion. Comparing multiple lines in a more extensive pilot study than initially trialled before (141) also controlled for clonal variability which can be a factor in neuronal cell lines (220).

The most significant caveat to the use of immortalised cell lines is the ubiquitous expression of eEF1A1. RNAseq analysis of differentiated neuronal induced pluripotent stem cells (iPSCs) revealed that while eEF1A2 mRNA expression is upregulated as differentiation continues, eEF1A1 levels do not down-regulate substantially over time, and remain in excess of eEF1A2 (221).

A significant issue with protein expression analysis in LUHMES cells is the inability to detect eEF1A2 at the protein level. eEF1A protein and eEF1A2 mRNA analysis revealed that null cell lines showed significant reduction in expression. However, no antibody detecting eEF1A2 exclusively *in vitro* could be found. Without this, it would be difficult to fully validate LUHMES as an appropriate model for assessing eEF1A2 mutations. Nevertheless, the problem of eEF1A1 expression is not specific to LUHMES cells, and would occur in all *in vitro* testing.

Therefore, it was imperative to continue to see if deficits in protein synthesis or other mechanisms could still be seen regardless of the eEF1A1 confound.

Interaction analysis led to the discovery that eEF1B binding was disrupted, leading to the hypothesis that protein synthesis might be inhibited. It is highly likely that protein synthesis is disrupted by mutations, however this needs to be formally proven. Clonal variability was found to be an issue when measuring protein synthesis using either puromycin tagging or AHA click-it chemistry in LUHMES cells. Protein synthesis inhibitors cycloheximide and anisomycin verified that although the techniques were successfully measuring protein synthesis, LUHMES cells were not a viable model for functional testing, likely because of eEF1A1 expression.

Owing to this result, I aimed to test protein synthesis in *Eef1a2*/D252H and *Eef1a2*/WAR mouse lines. No deficit could be seen in the skeletal muscle of *Eef1a2*$^{wst/wst}$ mice at p22, demonstrating the lack of sensitivity of the puromycin tagging system. Puromycin tagging is reported to be one of the less sensitive techniques for measuring protein synthesis (202). Given the *in vitro* results of this thesis, assessing protein synthesis in neurons of *Eef1a2*/D252H and *Eef1a2*/WAR mice (using a different method to puromycin tagging) is the most likely method for measuring any potential protein synthesis deficits.

There are several techniques which would be suited to measuring protein synthesis in *Eef1a2* mutant and null mouse neurons. Recently protein synthesis measurements were performed in primary neurons taken from transgenic mice. Most primary neuron studies utilise rat neurons to measure protein synthesis, often transfected with lentiviral vectors containing genes of interest. Recently, however, a growing number of experiments have been published examining the protein synthesis capacity of primary neurons cultured from WT and transgenic mice (222,223). The degree of residual eEF1A1 in neurons would have to be established. Given that there is currently no commercial antibody which can detect the difference between eEF1A1 and eEF1A2 in cells, this might be difficult to achieve at the protein level. However, the down-regulation of eEF1A1 is more likely to occur in

these neurons if taken after p21 than *in vitro* and is more likely to reflect the levels of protein synthesis *in vivo*.

Other techniques involving the study of ribosomes would be an interesting avenue to pursue. Ribosome profiling involves isolating and purifying the short mRNA segments which are protected within ribosomes. Deep-sequencing of these fragments can determine which ribosomes at any point are active, what proteins are being created and by measuring the number of ribosomes translating any given mRNA, a measure of total translation can be obtained (224). On whole brain lysates, ribosome profiling would have the same issue of eEF1A1 expression in glial cells. If centrifugation steps could be performed to isolate neurons, this may be a possible option, but may cause cellular stress which would impede results.

Recently, a technique termed tandem ribosome affinity purification – RNAseq (TRAP-seq) was used in *ex vivo* hippocampal tissue to measure protein synthesis. Experimenters could control for the cell type by dissecting just the hippocampus from mice (225). This method might be appropriate for future experiments, as it would provide a sample enriched with neurons.

An adaptation of the SUnSET technique has recently been reported. The SUnSET-based Ribosome Speed of Elongation (SUnRISE) technique uses puromycin tagging combined with a ribosomal run-off to measure translation elongation rates. Initiation is blocked by the drug harringtone. Doses of puromycin are subsequently administered at specific time points after translation initiation is blocked. This puromycin is incorporated into nascent elongating chains. When all the residual polypeptide chains have completed their elongation, ribosomes are deemed to have 'run-off' their mRNA, and no new mRNA translation can begin. The level of puromycin incorporation in polypeptides can be measured and used as an inverse correlation of elongation rates. Puromycin detection can be measured either through immunoblotting, or flow cytometry. The latter supplies a more specific technique for measuring detection.

Recent advances in measuring protein synthesis mean there are several options for measuring the effect eEF1A2 mutations might have. In this thesis, I have worked to narrow the experimental assays which might detect possible deficits in translation.

6.5 Conclusions

The work presented in this thesis helped expand upon the mechanism behind mutations in eEF1A2. Although no definitive conclusion of gain or loss-of-function mechanism can be determined from these results, my results suggest several hypotheses and have opened avenues for further exploration. It is possible that not all mutations operate through the same mechanism of action, or to the same degree. No correlation between mutations with or without eEF1B interaction disruptions and severity/seizure occurrence can be made yet, but with more cases and information, it will become easier to identify differences. The protein interaction analysis was insightful for determining the mechanism by which protein synthesis will be affected in mutant neurons. A clear gain-of-function element is seen in D252H/D252H mice when comparing their phenotype with age-matched null mice. It is not established whether this gain-of-function element is a mark of protein synthesis disruption occurring at an earlier timepoint, or if the D252H mutation impacts upon another biological process besides.

Moving forward from the findings of this thesis, there are several future experiments which would help establish the role of eEF1A2 in missense mutations. Given the difficulty in discriminating between eEF1A2 and eEF1A1, using CRISPR/Cas9 to introduce epitope tags to isoforms might be useful for establishing the endogenous expression during development and localisation of isoforms. This would require subsequent CRISPR/Cas9 engineering to introduce mutations but would be worth developing. My results also suggest that mutations may operate through different functions. To explore the impact all mutations have on eEF1A2 function, it is essential to generate more *Eef1a2* mouse lines with different eEF1A2 mutations. It would be important to determine if all mutations, like D252H, operate through a loss and dominant negative/gain-of-function.

More work on the mutation mechanisms is required before a treatment strategy could be established. It is key to determine whether mutant eEF1A2 interferes with eEF1A1. If this is the case different treatment strategies might be required at different neurodevelopmental stages. As with many neurodevelopmental disorders,

the solution to treating individuals with eEF1A2 missense mutations might be gene therapy.

The work in this thesis provides avenues for further research in examining the role of eEF1A2 mutations in neurodevelopmental disorders.

Appendices

Appendix A

Appendix A.1 Hierarchical clustering of technical repeats reveals G70S outlier

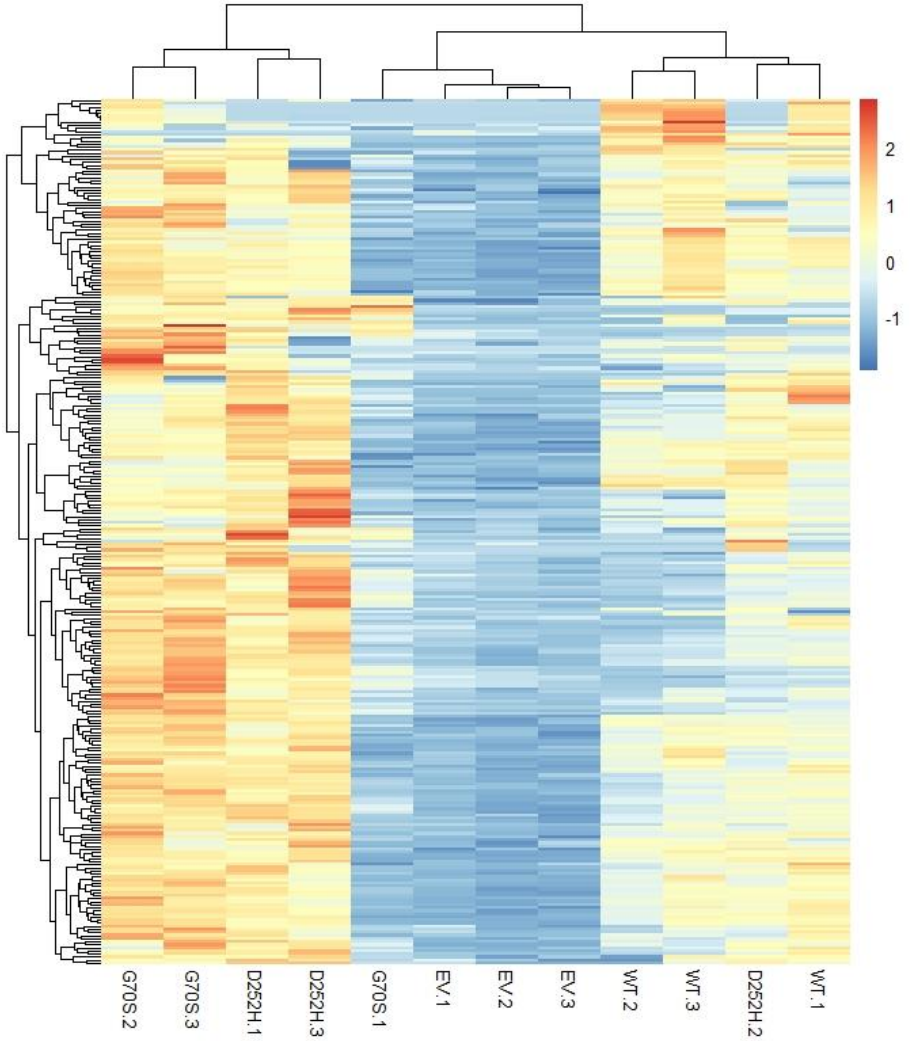

Figure A.1 – ***Heatmap showing hierarchical clustering of technical repeats in affinity-purification mass spectrometry.*** *Heatmap of z-scores for all proteins identified as 'confident interactors' (above empty vector filtering). Hierarchical clustering demonstrates that one G70S mutant (G70S.1) clusters with the empty vector technical repeats. This was used as evidence to identify G70S.1 as an outlier.*

A.2 Transfection of eEF1A2-V5 constructs does not result in nuclear staining

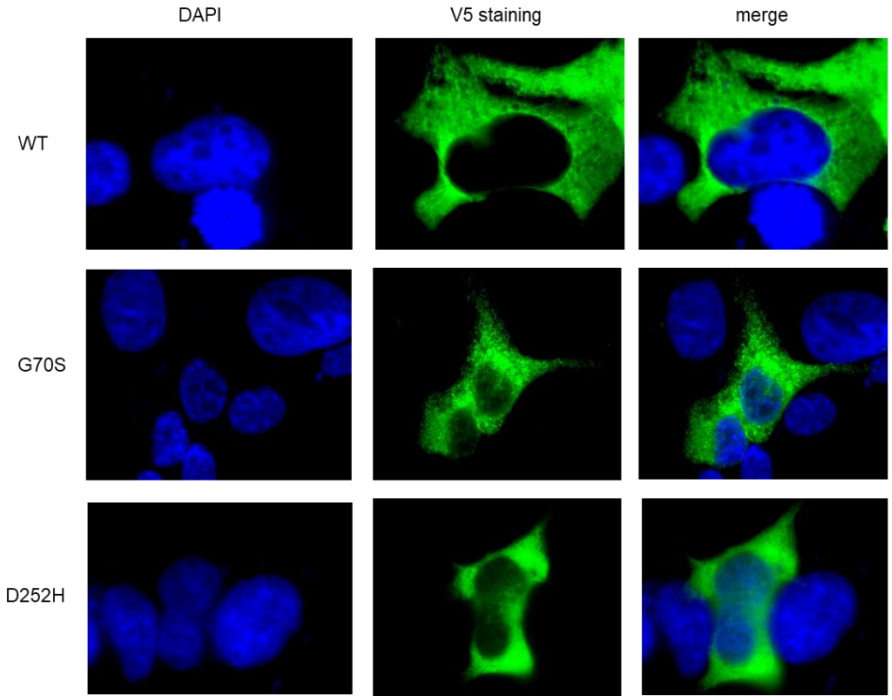

Figure A.2: Staining of HEK293T cells transfected with eEF1A2-V5 constructs*. Staining for V5 shows only cytoplasmic staining (green). This contrasts with the DAPI staining which marks the nucleus (blue).*

A.3 Most-Likely Ratio normalisation strategy of AP-MS data

Most Likely Ratio normalisation analysis as described by Lambert et al (145). Comparing all sample protein intensities against one WT sample (**A**), shows distribution of all samples and how they vary compared to WT. The principal of MLR is that only a minority of proteins will be impacted by mutations whilst most protein intensities will remain equal. The closer the density plot is to zero and the narrower it is, the closer overall to the WT sample this condition is. Using this comparison technique, the most representative sample for both technical replicates and biological repeats can be identified and used for normalisation. Initially within-group normalisation is done, as these samples should be statistically most similar. As one G70S sample had already been identified as an outlier, only one comparison was able to be made and therefore the most representative sample was not able to be determined. In this instance, sample 2 was simply scaled using the apex ratio of sample 1, the distribution of comparison scores pre- and post- this normalisation are displayed in **D** and **G** respectively. For D252H and WT however, 3 samples were included in analysis and therefore were all comparable with each other. Distribution pre-normalisation for each comparison (1 vs 2, 2 vs 3 and 1 vs 3) were plotted and are seen in **B** and **C** respectively. Scores for each comparison were reported in Table A.1. Histogram width and delta from zero for each comparison were calculated. For WT and D252H the most representative sample (highlighted in Table A.1) for each genotype was determined. The apex ratio of this sample was then used to normalise the LFQ intensities of all the samples within the respective genotype. After this, comparison between technical replicates for all genotypes was repeated (D252H, **E**, WT, **F**, and G70S, **G**). In **E** and **F** a better overlap of repeats can now be seen all peaking closer to zero. Comparison of all technical repeat normalised samples to the same WT sample, as before in **A**, now shows better alignment of all technical repeats (**H**). The process above highlighted for technical replicates was then repeated comparing between genotypes. As WT is the genotype both mutants should be normalised to, all G70S and D252H samples were compared to all WT samples (**I** and **J**) to assess which WT sample was the most representative sample for all repeats to be normalised to. Table A.2 shows histogram scores for comparisons. In bold is

the WT sample selected as overall most reflective. All mutant samples and remaining WT samples were then scaled using the apex ratio to normalise between genotypes. All mutant versus WT comparisons were then repeated post-normalisation (**K** and **L**). Much better alignment closer to zero was seen post normalisation as compared to pre-. Finally, all samples were compared to the original WT sample (as in **A**) to check how normalisation steps had impacted overall alignment (**M**). MLR has achieved better alignment of samples overall, normalising protein intensities globally.

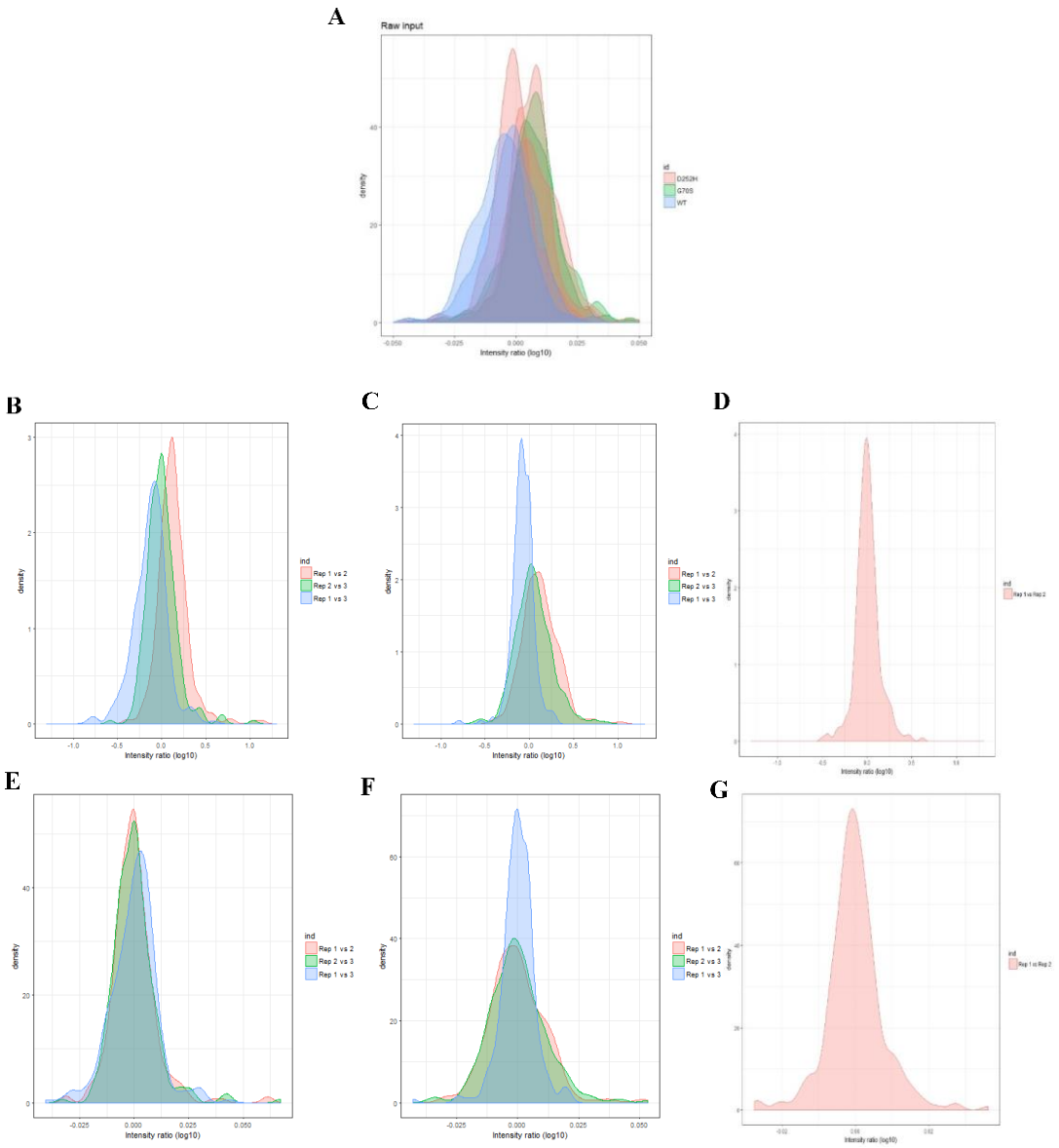

H

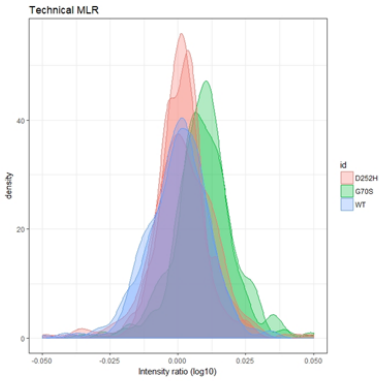
Technical MLR
density
Intensity ratio (log10)
id
D252H
G70S
WT

I

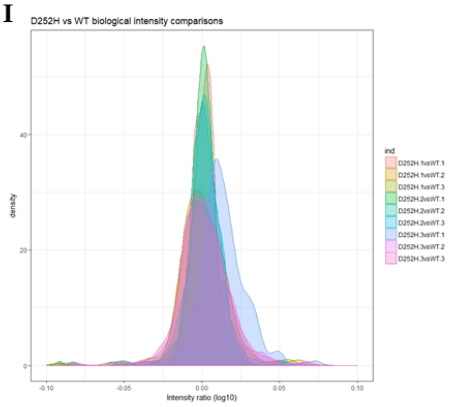
D252H vs WT biological intensity comparisons
density
Intensity ratio (log10)
ind
D252H.1vsWT.1
D252H.1vsWT.2
D252H.1vsWT.3
D252H.2vsWT.1
D252H.2vsWT.2
D252H.2vsWT.3
D252H.3vsWT.1
D252H.3vsWT.2
D252H.3vsWT.3

J

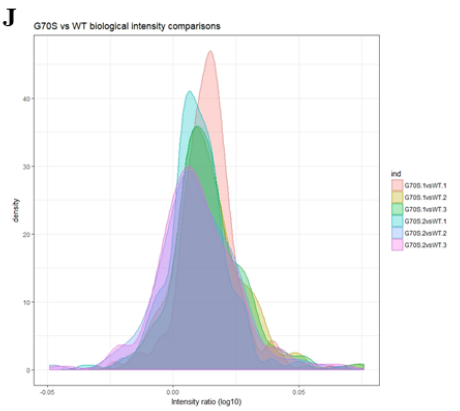
G70S vs WT biological intensity comparisons
density
Intensity ratio (log10)
ind
G70S.1vsWT.1
G70S.1vsWT.2
G70S.1vsWT.3
G70S.2vsWT.1
G70S.2vsWT.2
G70S.2vsWT.3

K

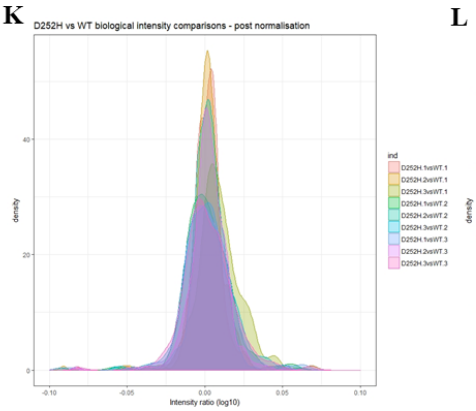
D252H vs WT biological intensity comparisons - post normalisation
density
Intensity ratio (log10)
ind
D252H.1vsWT.1
D252H.2vsWT.1
D252H.3vsWT.1
D252H.1vsWT.2
D252H.2vsWT.2
D252H.3vsWT.2
D252H.1vsWT.3
D252H.2vsWT.3
D252H.3vsWT.3

L

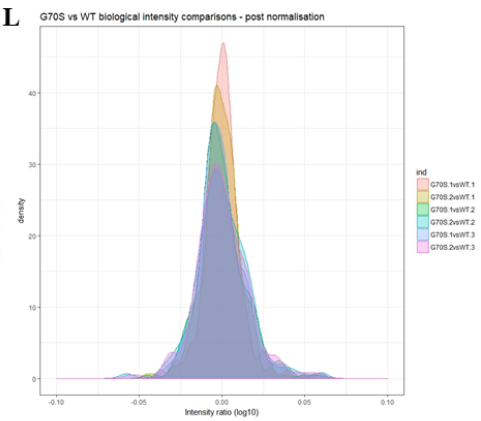
G70S vs WT biological intensity comparisons - post normalisation
density
Intensity ratio (log10)
ind
G70S.1vsWT.1
G70S.2vsWT.1
G70S.1vsWT.2
G70S.2vsWT.2
G70S.1vsWT.3
G70S.2vsWT.3

M

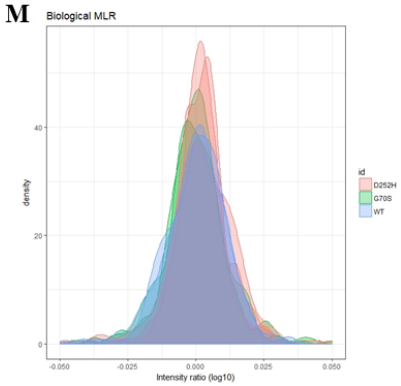
Biological MLR
density
Intensity ratio (log10)
id
D252H
G70S
WT

Figure A.3: Most likely ratio normalisation steps. A *comparison of protein LFQ scores (log-10 of comparative score) for each condition compared to one WT sample. Comparison of each technical repeat against the others in respective genotype pre-normalisation for D252H (**B**), WT (**C**) and G70S (**D**). After determination of the most representative sample and scaling of intensities appropriately, comparison between technical replicates is repeated for D252H (**E**), WT (**F**) and G70S (**G**). After technical normalisation all samples were compared to the same WT sample as in (**A**). Distributions after within-group normalisation are displayed in (**H**). After technical repeat normalisation, biological repeat normalisation was carried out. For each mutant, all repeats were compared to all WT repeats to find the WT sample which best correlates with all mutants. Before normalisation, comparisons were visualised for both D252H (**I**) and G70S (**J**). Scores for each histogram of distributions were calculated and are presented in Table A.2. Once a representative WT sample has been decided and scaling of all other samples conducted, comparison of the distributions are re-visualised for D252H and G70S (**K** and **L**, respectively). **M**, After final normalisation step. Intensities for all conditions are compared to the same WT sample as in (**A** and **H**).*

Table A.1: Histogram scores of technical repeat comparisons for each genotype. *Width of histogram is calculated by measuring the distance between minimum and maximum values. This value along with the delta of the histogram from zero are used to measure and assess the most representative sample. As decided using this method, the sample chosen and its representative scores have been highlighted in bold.*

WT	Rep1 vs Rep2	Rep 2 vs **Rep 3**	Rep 1 vs **Rep 3**
min	-0.0314	-0.03505	-0.04278
max	0.052866	0.053216	0.021538
width	0.084266	**0.088271**	**0.064316**
delta	1.63E-05	**-6.53E-05**	**-8.16E-05**
D252H	**Rep1** vs Rep2	Rep 2 vs Rep 3	**Rep 1** vs Rep 3
min	-0.0317	-0.03305	-0.04044
max	0.062431	0.06712	0.043424
width	**1.548756**	1.62399	**1.405513**
delta	**1.52E-05**	-0.00015	**-0.00016**
G70S	**Rep1** vs Rep2		
min	-0.4992		
max	0.616918		
width	**1.11612**		
delta	**-0.0054**		

Table A.2: Histogram scores of technical repeat comparisons for each mutant compared to WT. *Width of histogram is calculated by measuring distance between minimum and maximum values. This value along with the delta of the histogram from zero are used to measure and assess the most representative sample (the same WT sample for both G70S and D252H). The most reflective WT sample has been highlighted in bold.*

D252H	D252H 1 vs **WT 1**	D252H 2 vs **WT 1**	D252H 3 vs **WT 1**	D252H 1 vs WT 2	D252H 2 vs WT 2	D252H 3 vs WT 2	D252H 1 vs WT 3	D252H 2 vs WT 3	D252H 3 vs WT 3
Min	-0.1191	-0.1597	-0.0351	-0.1330	-0.1736	-0.1466	-0.1300	-0.1706	-0.1436
Max	0.0497	0.0288	0.0699	0.0583	0.0528	0.0615	0.0651	0.0529	0.0694
width	**0.1688**	**0.1885**	**0.1049**	0.1914	0.2265	0.2081	0.1951	0.2235	0.2130
delta	**0.0001**	**0.0001**	**-0.0097**	0.0001	0.0001	0.0002	0.0000	0.0000	0.0002

G70S	G70S.1 vs **WT.1**	G70S.2 vs **WT.1**	G70S. 1vs WT.2	G70S.2 vs WT.2	G70S.1 vs WT.3	G70S.2 vs WT.3
Min	-0.028	-0.036	-0.035	-0.049	-0.028	-0.047
Max	0.059	0.066	0.070	0.071	0.071	0.069
width	**0.087**	**0.102**	0.105	0.120	0.099	0.116
delta	**-0.010**	**-0.010**	-0.010	-0.010	-0.010	-0.010

A.4 Proteins which were most dysregulated in mutant conditions as compared with WT and were identified in both bait and MLR normalisation techniques.

A total list of proteins which show the same differentially expressed trend in mutant compared to WT after normalisation by both bait and MLR techniques. Proteins which had a 0.5 fold change (log_2) in mutant as compared to WT was seen in both normalisation techniques. Figure A.3 demonstrates the correlation of proteins using two normalisation methods. Good correlation is seen between normalisation methods. Proteins with greater than 0.5 fold change in both normalisation techniques were highlighted in red. These proteins are reported in Table A.3 and A.4 for D252H and G70S respectively.

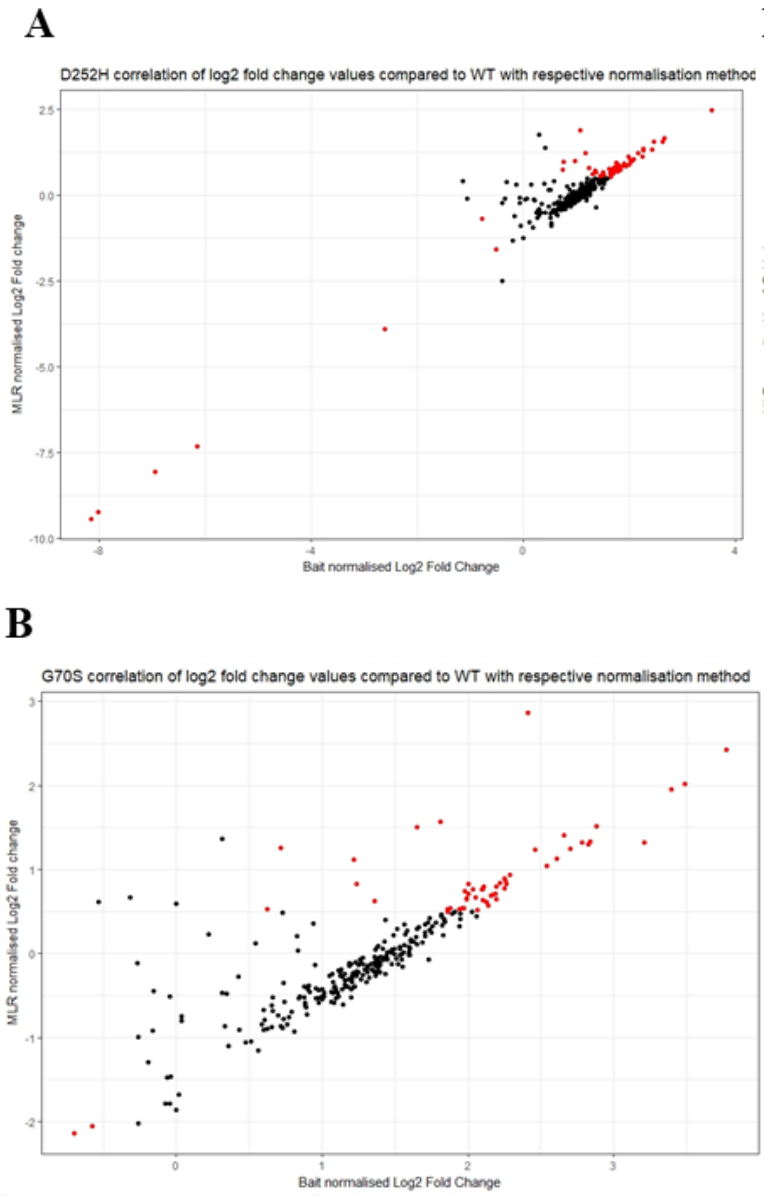

Figure A.4: Correlation of fold change of mutant (A, D252H and B, G70S) log_2 values for each protein compared with WT in dataset as normalised by bait and MLR. *Proteins which had a fold change difference of 0.5 (log_2) in both conditions were coloured red.*

Table A.3: List of proteins with greater than 0.5 log_2 fold change in both normalisation techniques identified with differential expression for D252H mutation as compared to WT.

	Fold Change (Log2)			Fold Change (Log2)			Fold Change (Log2)	
Genes	Bait Normalised	MLR Normalised	Genes	Bait Normalised	MLR Normalised	Genes	Bait Normalised	MLR Normalised
ACAT1	2.053364	0.983462	NOP58	1.98363	1.119742	RPS14	1.932471	0.86676
AKAP17A	1.360616	0.484124	PAICS	1.372918	0.655804	RPS15A	1.45722	0.558429
CPSF1	1.763163	0.926144	PDCD6	-0.51105	-1.5839	RPS2	2.443886	1.320149
DDOST	1.672959	0.613464	PGAM5	1.798381	0.888874	RPS27	1.751548	0.765991
DDX3X; DDX3Y	1.524089	0.50026	PNN	0.426506	1.363454	RPS3	2.638967	1.546385
DDX50	1.407688	0.453551	PPP2R2A; PPP2R2C	1.339535	0.445536	RPS3A	1.944617	0.82938
EEF1B2	-8.14295	-9.43204	PRDX6	2.165308	1.202484	RPS4X	1.809334	0.728728
EEF1D	-8.01752	-9.21745	PYCRL	-0.77824	-0.69642	RPS5	3.553587	2.46505
EEF1G	-6.13795	-7.31046	RANBP1	1.578624	0.463749	RPS7	1.717133	0.639744
EEF2	1.723167	0.703827	RBM28	1.240622	0.785508	RPS8	1.825246	0.843491
EHD1	0.988205	0.98744	RPL13A	1.805868	0.713027	RPS9	1.784788	0.697645
EIF2S1	0.744631	0.719907	RPL14	1.908939	0.868244	RSL1D1	1.635425	0.619999
ENO1	1.785864	0.790423	RPL21	1.84937	0.735727	SAP18	1.742427	0.815406
FARSB	2.461828	1.551497	RPL26	1.656099	0.535884	SLU7	1.528104	0.573113
FHL3	2.268656	1.342084	RPL28	1.84022	0.770248	SRP72	1.676206	0.704083
GMPS	1.462789	0.539015	RPL30	1.185843	1.206601	SRSF6	1.628464	0.767132
HMGA1	1.792662	0.688741	RPL35A	1.911611	0.915504	SSRP1	1.510289	0.658438

HNRNPUL2-BSCL2; HNRNPUL2	2.002699	0.874478	RPL36A-HNRNPH2; RPL36A	1.475431	0.441056	STOML2	1.358155	0.708756
HSP90AA1	1.535131	0.437101	RPL38	1.316425	0.592517	TCEB3	0.767465	0.952573
KIF21A	1.59971	0.482717	RPL4	2.265216	1.287739	TNPO1	2.253471	1.108984
KMT2A	-2.61213	-3.9066	RPL5	2.673188	1.646299	VARS	-6.93822	-8.05306
KPNA2	1.709574	0.788982	RPL7A	2.019287	1.010565			
LBR	1.50039	0.554587	RPL8	2.09498	1.025901			
LGALS1	1.205743	0.47737	RPN1	1.519261	0.471981			
LLPH	1.087212	1.885158	RPS11	1.752172	0.73054			
NEFM	1.789243	0.881793	RPS13	1.805436	0.7643			

Table A.4: List of proteins with greater than 0.5 log_2 fold change in both normalisation techniques identified with differential expression for G70S mutation as compared to WT.

	Fold Change (Log2)			Fold Change (Log2)	
Genes	Bait Normalised	MLR normalised	Genes	Bait Normalised	MLR normalised
ACTA1;ACTC1;ACTG2;ACTA2	1.99247883	0.64555009	RPL23	2.19337157	0.64504546
AKAP17A	1.86180485	0.52989751	RPL26	2.14034553	0.5731495
ARHGAP1	2.0668352	0.512865	RPL28	2.18706194	0.71246792
BOLA2	1.88120464	0.54204594	RPL30	1.81235487	1.56997006
BUD13	1.85944237	0.50126164	RPL34	2.10037337	0.76646773
CPSF1	2.65569826	1.41016897	RPL36A	2.61160825	1.12856125
DLD	0.57516822	2.05287751	RPL38	2.45937738	1.23079693
DYNLT1	1.21559023	1.12083954	RPL4	2.09490544	0.7637137
EIF2S1	1.23623595	0.82857935	RPL5	2.8784672	1.51439644
FARSB	2.11037782	0.80059388	RPL7A	2.22112588	0.83807931
FHL3	2.03232656	0.7590388	RPL8	2.10357423	0.63686272
IDH2	2.24991023	0.7792197	RPLP1	1.96961922	0.5414913
KPNA2	1.99355594	0.65924633	RPS11	2.26000237	0.82296717
LGALS1	1.95713279	0.5394422	RPS13	2.78200056	1.31635887
LLPH	2.41069684	2.86541141	RPS14	2.70358769	1.24888216
LRPPRC	3.20848393	1.32396555	RPS15A	2.25141617	0.8969454
METTL13	2.2873711	0.93688316	RPS2	3.39513485	1.95031421
NEFM	1.97561272	0.73926829	RPS27	2.24886403	0.88963337
NOP58	2.00090926	0.82526735	RPS3	3.48954623	2.0230625
PDCD6	0.70172411	2.14002125	RPS3A	2.82706855	1.29568981

PNN	0.71749446	1.25316493	RPS4X	2.83587969	1.33236003
POLR2C	1.3564562	0.6296095	RPS5	3.77112358	2.42043193
PRPF4	1.64718694	1.50139457	RPS7	2.54359453	1.04451527
RPL11	2.19558739	0.79852408	RPS8	2.05294872	0.67154099
RPL12	2.00037982	0.71097451	RPS9	2.15493897	0.68693705
RPL13A	2.12727898	0.6154282	SLU7	1.93938426	0.52934296
RPL14	2.25950243	0.86963172	TCEB3	0.62529127	0.53309241

Appendix B

B.1 BeAtMuSIC prediction theoretical residues with greatest increase and decrease in binding affinity (174).

Table B.1: Top 25 residue alterations in eEF1A2 which would exert the greatest increase in binding affinity.

Position	Mutation	$\Delta\Delta G_{Bind}$ (kcal/mol)	Solvent accessibility (in partner(s))	Solvent accessibility (in complex)
424	F → D	**5.20**	2.24 %	0 %
424	F → E	**5.14**	2.24 %	0 %
435	V → E	**5.07**	10.03 %	0 %
71	I → P	**4.95**	59.115 %	5.52 %
73	I → G	**4.92**	83.7 %	17.96 %
424	F → K	**4.91**	2.24 %	0 %
71	I → G	**4.84**	59.115 %	5.52 %
254	Y → S	**4.75**	48.35 %	16.68 %
435	V → K	**4.71**	10.03 %	0 %
254	Y → G	**4.65**	48.35 %	16.68 %
435	V → D	**4.58**	10.03 %	0 %
424	F → N	**4.19**	2.24 %	0 %
254	Y → D	**4.18**	48.35 %	16.68 %
86	Y → G	**4.13**	29.35 %	9.71 %
32	G → P	**4.12**	64.695 %	42.57 %
71	I → D	**4.08**	59.115 %	5.52 %
424	F → P	**4.06**	2.24 %	0 %
424	F → Q	**4.05**	2.24 %	0 %
254	Y → P	**3.98**	48.35 %	16.68 %
71	I → S	**3.95**	59.115 %	5.52 %
78	W → P	**3.89**	0.565 %	0.56 %
254	Y → A	**3.82**	48.35 %	16.68 %

254	Y → N	**3.78**	48.35 %	16.68 %
424	F → G	**3.76**	2.24 %	0 %
73	I → D	**3.71**	83.7 %	17.96 %

Table B.2: Top 25 residue alterations in eEF1A2 which would exert the greatest decrease in binding affinity.

Position	Mutation	$\Delta\Delta G_{Bind}$ (kcal/mol)	Solvent accessibility (in partner(s))	Solvent accessibility (in complex)
252	D → W	**-2.75**	40.645 %	2.21 %
252	D → F	**-2.74**	40.645 %	2.21 %
427	R → I	**-2.56**	34.765 %	2.93 %
252	D → Y	**-2.53**	40.645 %	2.21 %
427	R → W	**-2.53**	34.765 %	2.93 %
427	R → F	**-2.51**	34.765 %	2.93 %
427	R → Y	**-2.39**	34.765 %	2.93 %
413	E → Y	**-2.28**	0.27 %	0.27 %
413	E → F	**-2.26**	0.27 %	0.27 %
413	E → I	**-2.25**	0.27 %	0.27 %
413	E → L	**-2.17**	0.27 %	0.27 %
413	E → M	**-2.15**	0.27 %	0.27 %
413	E → W	**-2.11**	0.27 %	0.27 %
427	R → L	**-2.06**	34.765 %	2.93 %
66	E → F	**-2.05**	40.01 %	9.94 %
342	S → F	**-2.05**	0 %	0 %
252	D → M	**-2.04**	40.645 %	2.21 %
436	G → F	**-2.04**	0 %	0 %
413	E → V	**-1.99**	0.27 %	0.27 %
436	G → W	**-1.98**	0 %	0 %
252	D → I	**-1.97**	40.645 %	2.21 %
436	G → Y	**-1.97**	0 %	0 %
342	S → Y	**-1.91**	0 %	0 %
342	S → I	**-1.90**	0 %	0 %
252	D → V	**-1.89**	40.645 %	2.21 %

Appendix C

C.1 Sequence Alignment of alleles from LUHMES clones which had undergone CRISPR/Cas9 to mutate eEF1A2

Clustal OMEGA alignments of sequences identified from sequencing and TOPO cloning of LUHMES genomic DNA. Cells lines are as follows: **A** – 2.5, **B** – 2.7, **C** – 2.8, **D** – 2.13, **E** – 2.16 and **F** – 2.18.

A

```
PCR      TGGTTGAGGAAGGGATCTGGGGGCGTCCGCAGCTTCAGATAAAGGGGAGCCCTCGCCCGGGAGGGGTTTATCCCATCTGGCGGCTTCGCTCGTAGAGCGAGCGACTCCCAGGCCCTTGCG
2.5 A1   TGGTTGAGGAAGGGATCTGGGGGCGTCCGCAGCTTCAGATAAAGGGGAGCCCTCGCCCGGGAGGGGTTTATCCCATCTGGCGGCTTCGCTCGTAGAGCGAGCGACTCCCAGGCCCTTGCG
2.5 A2   TGGTTGAGGAAGGGATCTGGGGGCGTCCGCAGCTTCAGATAAAGGGGAGCCCTCGCCCGGGAGGGGTTTATCCCATCTGGCGGCTTCGCTCGTAGAGCGAGCGACTCCCAGGCCCTTGCG

PCR      CCACCTGCTGGTGGACCTGCGTAGCCGCGCCCATTTCGGAGCAGGTGCGGAGGCCGGCCCTGGGGGGCAGGGTCTGGGTGTGGGGTCCCGACGGAGGGGGCCGGCGTCCCAGGACCCCGA
2.5 A1   CCACCTGCTGGTGGACCTGCATAGCCGCGCCCATTTCGGAGCAGGTGCGGAGGCCGGCCCTGGGGGGCAGGGTCTGGGTGTGGGGTCCCGACGGAGAGCAAGGGGGTCCCAGGACCCCGA
2.5 A2   CCACCTGCTGGTGGACCTGCGTAGCCGCGCCCATTTCGGAGCAGGTGCGGAGGCCGGCCCTGGGGGGCAGGGTCTGGGTGTGGGGTCCCGACGGAGGGGGCCGGCGTCCCAGG-------

PCR      CGGAGAGCAAGGGGGTGCTGGAGCCCATCTCCCGCCTCTCGCGGCCACTCTGCTGTAACAAGCAGCTCGCACCACCAGGGACTCCTGGGTCCCGGGTCCCGCCCTCAGCCGTGACCCTCA
2.5 A1   CGGAGAGCAAGGGGGTGCTGGAGCCCATCTCCCGCCTCTCGCGGCCACTCTGCTGTAACAAGCAGCTCGCACCACCAGGGACTCCTGGGTCCCGGGTCCCGCCCTCAGCCGTGACCCTCA
2.5 A2   ----------------------------------------------------------------------------------------------------------------------------

PCR      CCCGCTCCAGATGGGGAAGGGATCCTTCAAGTATGCCTGGGTGCTGGACAAGCTGAAGGCGGAGCGTGAGCGCGGCATCACCATCGACATCTCCCTCTGGAAGTTCGAGACCACCAAGTA
2.5 A1   CCCGCTCCAGATGGGGAAGGGATCCTTCAAGTATGCCTGGGTGCTGGACAAGCTGAAGGCGGAGCGTGAGCGCGGCATCACCATCGACATCTCCCTCTGGAAGTTCGAGACCACCAA---
2.5 A2   ----------------------------------------------------------------------------------------------------------------------------

PCR      CTACATCACCATCATCGATGCCCCCGGCCACCGCGACTTCATCAAGAACATGATCACGGGTACATCCCAGGTGAGCAGGGCACAGCAGGCGGGGCTGGGGGAGAGGCCGCTGCACCCTTC
2.5 A1   -------------------------GGCCACCGCGACTTCATCAAGAACATGATCACGGGTACATCCCAGGTGAGCAGGGCACAGCAGGCGGGGCTGGGGGAGAGGCCGCTGCACCCTTC
2.5 A2   ------------------TGCCCCCGGCCACCGCGACTTCATCAAGAACATGATCACGGGTACATCCCAGGTGAGCAGGGCACAGCAGGCGGGGCTGGGGGAGAGGCCGCTGCACCCTTC

PCR      AAGGGACACTGGGGGCCCCTGGGGTCACTGGGATGGTAGGGTCTCCTGTGCTTCCTGTGAGGGCAGGGGACCCCTCACCTGGGCCACCCTCACCCAGTCTGGCTCAGAGCCCCCCTAAGG
2.5 A1   AAGGGACACTGGGGGCCCCTGGGGTCACTGGGATGGTAGGGTCTCCTGTGCTTCCTGTGAGGGCAGGGGACCCCTCACCTGGGCCACCCTCACCCAGTCTGGCTCAGAGCCCCCCTAAGG
2.5 A2   AAGGGACACTGGGGGCCCCTGGGGTCACTGGGATGGTAGGGTCTCCTGTGCTTCCTGTGAGGGCAGGGGACCCCTCACCTGGGCCACCCTCACCCAGTCTGGCTCAGAGCCCCCCTAAGG

PCR      ATGAATCCAGTGCTCTGGCATCTGAACCAGTGCCTGTGAAGGCATCCAGCCAGTGTCAGAGTCCCCAGATAGATGGGGGCAGATGGGGACGTGGACACA
2.5 A1   ATGAATCCAGTGCTCTGGCATCTGAACCAGTGCCTGTGAAGGCATCCAGCCAGTGTCAGAGTCCCCAGATAGATGGGGGCAGATGGGGACGTGGACACA
2.5 A2   ATGAATCCAGTGCTCTGGCATCTGAACCAGTGCCTGTGAAGGCATCCAGCCAGTGTCAGAGTCCCCAGATAGATGGGGGCAGATGGGGACGTGGACACA
```

B

```
PCR      TGGTTGAGGAAGGGATCTGGGGGCGTCCGCAGCTTCAGATAAAGGGGAGCCCTCGCCCGGGAGGGGTTTATCCCATCTGGCGGCTTCGCTCGTAGAGCGAGCGACTCCCAGGCCCTTGCG
2.7 A1   TGGTTGAGGAAGGGATCTGGGGGCGTCCGCAGCTTCAGATAAAGGGGAGCCCTCGCCCGGGAGGGGTTTATCCCATCTGGCGGCTTCGCTCGTAGAGCGAGCGACTCCCAGGCCCTTGCG
2.7 A2   TGGTTGAGGAAGGGATCTGGGGGCGTCCGCAGCTTCAGATAAAGGGGAGCCCTCGCCCGGGAGGGGTTTATCCCATCTGGCGGCTTCGCTCGTAGAGCGAGCGACTCCCAGGCCCTTGCG

PCR      CCACCTGCTGGTGGACCTGCGTAGCCGCGCCCATTTCGGAGCAGGTGCGGAGGCCGGCCCTGGGGGGCAGGGTCTGGGTGTGGGGTCCCGACGGAGGGGGCCGGCGTCCCAGGACCCCGA
2.7 A1   CCACCTGCTGGTGGACCTGCGTAGCCGCGCCCATTTCGGAGCAGGTGCGGAGGCCGGCCCTGGGGGGCAGGGTCTGGGTGTGGGGTCCCGACGGAGGGGGCCGGCGTCCCAGGACCCCGA
2.7 A2   CCACCTGCTGGTGGACCTGCATAGCCGCGCCCATTTCGGAGCAGGTGCGGAGGCCGGCCCTGGGGGGCAGGGTCTGGGTGTGGGGTCCCGACGGAGGGGGCCGGCGTCCCAGGACCCCGA

PCR      CGGAGAGCAAGGGGGTGCTGGAGCCCATCTCCCGCCTCTCGCGGCCACTCTGCTGTAACAAGCAGCTCGCACCACCAGGGACTCCTGGGTCCCGGGTCCCGCCCTCAGCCGTGACCCTCA
2.7 A1   CGGAGAGCAAGGGGGTGCTGGAGCCCATCTCCCGCCTCTCGCGGCCACTCTGCTGTAACAAGCAGCTCGCACCACCAGGGACTCCTGGGTCCCGGGTCCCGCCCTCAGCCGTGACCCTCA
2.7 A2   CGGAGAGCAAGGGGGTGCTGGAGCCCATCTCCCGCCTCTCGCGGCCACTCTGCTGTAACAAGCAGCTCGCACCACCAGGGACTCCTGGGTCCCGGGTCCCGCCCTCAGCCGTGACCCTCA

PCR      CCCGCTCCAGATGGGGAAGGGATCCTTCAAGTATGCCTGGGTGCTGGACAAGCTGAAGGCGGAGCGTGAGCGCGGCATCACCATCGACATCTCCCTCTGGAAGTTCGAGACCACCAAGTA
2.7 A1   CCCGCTCCAGATGGGGAAGGGATCCTTCAAGTATGCCTGGGTGCTGGACAAGCTGAAGGCGGAGCGTGAGCGCGGCATCACCATCGACATCTCCCTCTGGAAGTTCGAGACCACCAAGTA
2.7 A2   CCCGCTCCAGATGGGGAAGGGATCCTTCAAGTATGCCTGGGTGCTGGACAAGCTGAAGCGGGAGCGTGAGCGCGGCATCACCATCGACATCTCCCTCTGGAAGTTCGAGACC--------

PCR      CTACATCACCATCATCGATGCCCCCGGCCACCGCGACTTCATCAAGAACATGATCACGGGTACATCCCAGGTGAGCAGGGCACAGCAGGCGGGGCTGGGGGAGAGGCCGCTGCACCCTTC
2.7 A1   CTACATCACCATCATCGATGCCCCCGGCCACCGCGACTTCATCAAGAACATGATCACGGGTACATCCCAGGTGAGCAGGGCACAGCAGGCGGGGCTGGGGGAGAGGCCGCTGCACCCTTC
2.7 A2   ---------------------------GCCACCGCGACTTCATCAAGAACATGATCACGGGTACATCCCAGGTGAGCAGGGCACAGCAGGCGGGGCTGGGGGAGAGGCCGCTGCACCCTTC

PCR      AAGGGACACTGGGGGCCCCTGGGGTCACTGGGATGGTAGGGTCTCCTGTGCTTCCTGTGAGGGCAGGGGACCCCTCACCTGGGCCACCCTCACCCAGTCTGGCTCAGAGCCCCCCTAAGG
2.7 A1   AAGGGACACTGGGGGCCCCTGGGGTCACTGGGATGGTAGGGTCTCCTGTGCTTCCTGTGAGGGCAGGGGACCCCTCACCTGGGCCACCCTCACCCAGTCTGGCTCAGAGCCCCCCTAAGG
2.7 A2   AAGGGACACTGGGGGCCCCTGGGGTCACTGGGATGGTAGGGTCTCCTGTGCTTCCTGTGAGGGCAGGGGACCCCTCACCTGGGCCACCCTCACCCAGTCTGGCTCAGAGCCCCCCTAAGG

PCR      ATGAATCCAGTGCTCTGGCATCTGAACCAGTGCCTGTGAAGGCATCCAGCCAGTGTCAGAGTCCCCAGATAGATGGGGGCAGATGGGGACGTGGACACA
2.7 A1   ATGAATCCAGTGCTCTGGCATCTGAACCAGTGCCTGTGAAGGCATCCAGCCAGTGTCAGAGTCCCCAGATAGATGGGGGCAGATGGGGACGTGGACACA
2.7 A2   ATGAATCCAGTGCTCTGGCATCTGAACCAGTGCCTGTGAAGGCATCCAGCCAGTGTCAGAGTCCCCAGATAGATGGGGGCAGATGGGGACGTGGACACA
```

C

```
2.8 A1      TCGAGACCA-CAAGTACTACATCA--------CATTCGCCCCGGCAACGCGACTTCATCA
2.8 A2      TCGAGACCACCAAGTACTACATCACCATCG------CCCCCGGCCCCCGCGACTTCATCA
PCR         TCGAGACCACCAAGTACTACATCACCATCATCGATGCCCCCGGCCACCGCGACTTCATCA

2.8 A1      AGAACATG-----------------------------------------------------
2.8 A2      AGAACATGA----------------------------------------------------
PCR         AGAACATGATCACGGGTACATCCCAGGTGAGCAGGGCACAGCAGGCGGGGCTGGGGGAGA

2.8_A1      ----------------      59
2.8_A2      ----------------      63
PCR         GGCCGCTGCACCCTTC      136
```

D

```
PCR     TTCCTCATCTCAAAGGGCACGAGGCAAGTTTAGCCTGAACAGCAGTACTCCTGGAAGCACCCTGGGGAGGCCTGAGGGTGGGGAGGCCACCAATGTCTCTTAACGGATTGATTTTCTCCCTTTGGTCCAGA
2.13 A1 TTCCTCATCTCAAAGGGCACGAGGCAAGTTTAGCCTGAACAGCAGTACTCCTGGAAGCACCCTGGGGAGGCCTGAGGGTGGGGAGGCCACCAATGTCTCTTAACGGATTGATTTTCTCCCTTTGGTCCAGA
2.13 A2 TTCCTCATCTCAAAGGGCACGAGGCAAGTTTAGCCTGAACAGCAGTACTCCTGGAAGCACCCTGGGGAGGCCTGAGGGTGGGGAGGCCACCAATGTCTCTTAACGGATTGATTTTCTCCCTTTGGTCCAGA

PCR     TGCCGTGGTTCAAGGGCTGGAAGGTGGAGCGTAAGGAGGGCAACGCAAGCGGCGTGTCCCTGCTGGAGGCCCTGGACACCATCCTGCCCCCCACGCGCCCCACGGACAAGCCCCTGCGCCTGCCGCTGCAG
2.13 A1 TGCCGTGGTTCAAGGGCTGGAAGGTGGAGCGTAAGGAGGGCAACGCAAGCGGCGTGTCCCTGCTGGAGGCCCTGGACACCATCCTGCCTCCCACGCGCCCCACGGACAAGCCCCTGCGCCTGCCGCTGCAG
2.13 A2 TGCCGTGGTTCAAGGGCTGGAAGGTGGAGCGTAAGGAGGGCAACGCAAGCGGCGTGTCCCTGCTGGAGGCCCTGGACACCATCCTGCCCCCCACGCGCCCCACGGACAAGCCCCTGCGCCTGCCGCTGCAG

PCR     GACGTGTACAAGATTGGCGGTGAGCAAGGGCGCTGTGCTGGAGCTCCTGCCTGGCCAGCTCTGCCTGCCCTAGACCAGGGGCCCCTACAAGGCATCTCAAGACTGGGCTGTCTCCAATCTCTCCCCTTACC
2.13 A1 CACGTTTATAAGATCGGAGGTGAGCAAGGGCGCTGTGCTGGAGCTCCTGCCTGGCCAGCTCTGCCTGCCCTAGACCAGGGGCCCCTACAAGGCATCTCAAGACTGGGCTGTCTCCAATCTCTCCCCTTACC
2.13 A2 CACGTTTATAAGATCGGAGGTGAGCAAGGGCGCTGTGCTGGAGCTCCTGCCTGGCCAGCTCTGCCTGCCCTAGACCAGGGGCCCCTACAAGGCATCTCAAGACTGGGCTGTCTCCAATCTCTCCCCTTACC

PCR     ACACACTTTCTGTGGG
2.13 A1 ACACACTTTCTGTGGG
2.13 A2 ACACACTTTCTGTGGG
```

E

```
PCR     TTCCTCATCTCAAAGGGCACGAGGCAAGTTTAGCCTGAACAGCAGTACTCCTGGAAGCACCCTGGGGAGGCCTGAGGGTGGGGAGGCCACCAATGTCTCTTAACGGATTGATTTTCTCCCTTTGGTCCAGA
2.16 A1 TTCCTCATCTCAAAGGGCACGAGGCAAGTTTAGCCTGAACAGCAGTACTCCTGGAAGCACCCTGGGGAGGCCTGAGGGTGGGGAGGCCACCAATGTCTCTTAACGGATTGATTTTCTCCCTTTGGTCCAGA
2.16 A2 TTCCTCATCTCAAAGGGCACGAGGCAAGTTTAGCCTGAACAGCAGTACTCCTGGAAGCACCCTGGGGAGGCCTGAGGGTGGGGAGGCCACCAATGTCTCTTAACGGATTGATTTTCTCCCTTTGGTCCAGA

PCR     TGCCGTGGTTCAAGGGCTGGAAGGTGGAGCGTAAGGAGGGCAACGCAAGCGGCGTGTCCCTGCTGGAGGCCCTGGACACCATCCTGCCCCCCACGCGCCCCACGGACAAGCCCCTGCGCCTGCCGCTGCAG
2.16 A1 TGCCGTGGTTCAAGGGCTGGAAGGTGGAGCGTAAGGAGGGCAACGCAAGCGGCGTGTCCCTGCTGGAGGCCCTGGACACCATCCTGCCTCCCACGCGCCCCACGGACAAGCCCCTGCGCCTGCCGCTGCAG
2.16 A2 TGCCGTGGTTCAAGGGCTGGAAGGTGGAGCGTAAGGAGGGCAACGCAAGCGGCGTGTCCCTGCTGGAGGCCCTGGACACCATCCTGCCCCCCACGCGCCCCACGGACAAGCCCCTGCGCC----------

PCR     GACGTGTACAAGATTGGCGGTGAGCAAGGGCGCTGTGCTGGAGCTCCTGCCTGGCCAGCTCTGCCTGCCCTAGACCAGGGGCCCCTACAAGGCATCTCAAGACTGGGCTGTCTCCAATCTCTCCCCTTACC
2.16 A1 CACGTTTATAAGATCGGAGGTGAGCAAGGGCGCTGTGCTGGAGCTCCTGCCTGGCCAGCTCTGCCTGCCCTAGACCAGGGGCCCCTACAAGGCATCTCAAGACTGGGCTGTCTCCAATCTCTCCCCTTACC
2.16 A2 ----------------------------------------------------------------------------------------------------------------------------------TTACC

PCR     ACACACTTTCTGTGGG
2.16 A1 ACACACTTTCTGTGGG
2.16 A2 ACACACTTTCTGTGGG
```

F

```
PCR     TTCCTCATCTCAAAGGGCACGAGGCAAGTTTAGCCTGAACAGCAGTACTCCTGGAAGCACCCTGGGGAGGCCTGAGGGTGGGGAGGCCACCAATGTCTCTTAACGGATTGATTTTCTCCCTTTGGTCCAGA
2.18 A1 TTCCTCATCTCAAAGGGCACGAGGCAAGTTTAGCCTGAACAGCAGTACTCCTGGAAGCACCCTGGGGAGGCCTGAGGGTGGGGAGGCCACCAATGTCTCTTAACGGATTGATTTTCTCCCTTTGGTCCAGA
2.18 A2 TTCCTCATCTCAAAGGGCACGAGGCAAGTTTAGCCTGAACAGCAGTACTCCTGGAAGCACCCTGGGGAGGCCTGAGGGTGGGGAGGCCACCAATGTCTCTTAACGGATTGATTTTCTCCCTTTGGTCCAGA

PCR     TGCCGTGGTTCAAGGGCTGGAAGGTGGAGCGTAAGGAGGGCAACGCAAGCGGCGTGTCCCTGCTGGAGGCCCTGGACACCATCCTGCCCCCCACGCGCCCCACGGACAAGCCCCTGCGCCTGCCGCTGCAG
2.18 A1 TGCCGTGGTTCAAGGGCTGGAAGGTGGAGCGTAAGGAGGGCAACGCAAGCGGCGTGTCCCTGCTGGAGGCCCTGGACACCATCCTGCCTCCCACGCGCCCCACGGACAAGCCCCTGCGCCTGCCGCTGCAG
2.18 A2 TGCCGTGGTTCAAGGGCTGGAAGGTGGAGCGTAAGGAGGGCAACGCAAGCGGCGTGTCCCTGCTGGAGGCCCTGGACACCATCCTGCCTCCCACGCGCCCCACGGACAAGCCCCTGCGCCTGCCGCTGCAG

PCR     GACGTGTACAAGATTGGCGGTGAGCAAGGGCGCTGTGCTGGAGCTCCTGCCTGGCCAGCTCTGCCTGCCCTAGACCAGGGGCCCCTACAAGGCATCTCAAGACTGGGCTGTCTCCAATCTCTCCCCTTACC
2.18 A1 GACGTGTATAAGATTGGCGGTGAGCAAGGGCGCTGTGCTGGAGCTCCTGCCTGGCCAGCTCTGCCTGCCCTAGACCAGGGGCCCCTACAAGGCATCTCAAGACTGGGCTGTCTCCAATCTCTCCCCTTACC
2.18 A2 GACGTGTATAAGATTGGCGGTGAGCAAGGGCGCTGTGCTGGAGCTCCTGCCTGGCCAGCTCTGCCTGCCCTAGACCAGGGGCCCCTACAAGGCATCTCAAGACTGGGCTGTCTCCAATCTCTCCCCTTACC

PCR     ACACACTTTCTGTGGG
2.18 A1 ACACACTTTCTGTGGG
2.18 A2 ACACACTTTCTGTGGG
```

Figure C.1: Alignments of alleles from LUHMES clones which had been genetically edited using CRISPR/Cas9. ***A*****-*****C*** *shows lines created from gRNAs which targeted exon 3.* ***D*****-*****F*** *shows lines created from gRNAs which targeted exon 5. Green highlighted bases reflect missense mutations and '-' represents a deletion.*

C.2 qPCR standard and melt curves for eEF1A2 mRNA quantification and housekeeping genes.

Figure C.2 standard and melt curves for RPL34, TOP1 and eEF1A2. $R^{2,}$ gradient and y-intercept values have been shown in conjunction with standard curves.

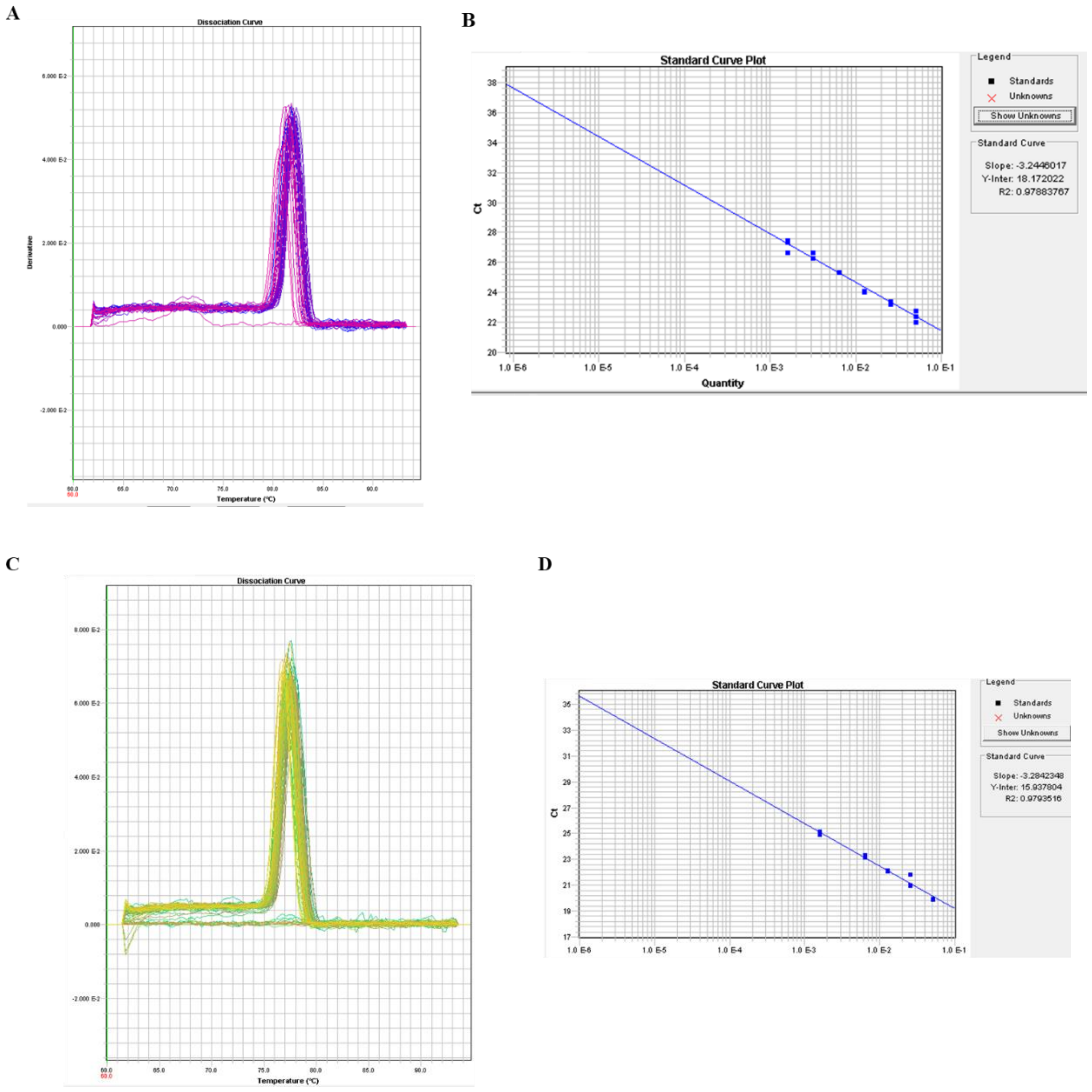

E

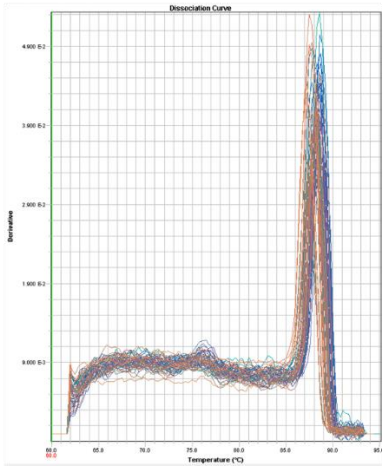

F

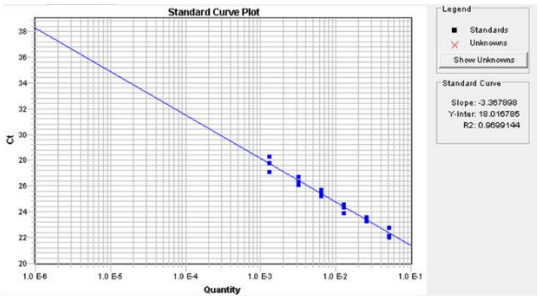

Figure C.2: Melt curve and standard curve plots for qPCR of RPL34 (A & B), TOP1 (C & D) and eEF1A2 mRNA (E & F).

Bibliography

1. Merrick WC. Mechanism and regulation of eukaryotic protein synthesis. Microbiol Rev. 1992 Jun;56(2):291–315.

2. Li D, Wei T, Abbott CM, Harrich D. The unexpected roles of eukaryotic translation elongation factors in RNA virus replication and pathogenesis. Microbiol Mol Biol Rev. 2013 Jun;77(2):253–266.

3. Walldorf U, Hovemann B, Bautz EK. F1 and F2: Two similar genes regulated differently during development of Drosophila melanogaster. Proc Natl Acad Sci U S A. 1985 Sep;82(17):5795–5799.

4. Newbery HJ, Stancheva I, Zimmerman LB, Abbott CM. Evolutionary importance of translation elongation factor eEF1A variant switching: eEF1A1 down-regulation in muscle is conserved in Xenopus but is controlled at a post-transcriptional level. Biochem Biophys Res Commun. 2011 Jul 22;411(1):19–24.

5. Madsen HO, Poulsen K, Dahl O, Clark BF, Hjorth JP. Retropseudogenes constitute the major part of the human elongation factor 1 alpha gene family. Nucleic Acids Res. 1990 Mar 25;18(6):1513–1516.

6. Gao D, Li Z, Murphy T, Sauerbier W. Structure and transcription of the gene for translation elongation factor 1 subunit alpha of zebrafish (Danio rerio). Biochim Biophys Acta. 1997 Jan 3;1350(1):1–5.

7. Lee S, Wolfraim LA, Wang E. Differential expression of S1 and elongation factor-1 alpha during rat development. J Biol Chem. 1993 Nov 15;268(32):24453–24459.

8. Lund A, Knudsen SM, Vissing H, Clark B, Tommerup N. Assignment of human elongation factor 1alpha genes: EEF1A maps to chromosome 6q14 and EEF1A2 to 20q13.3. Genomics. 1996 Sep 1;36(2):359–361.

9. Lee S, Stollar E, Wang E. Localization of S1 and elongation factor-1 alpha mRNA in rat brain and liver by non-radioactive in situ hybridization. J Histochem Cytochem. 1993 Jul;41(7):1093–1098.

10. Knudsen SM, Frydenberg J, Clark BF, Leffers H. Tissue-dependent variation in the expression of elongation factor-1 alpha isoforms: isolation and characterisation of a cDNA encoding a novel variant of human elongation-factor 1 alpha. Eur J Biochem. 1993 Aug 1;215(3):549–554.

11. Svobodová K, Horák P, Stratil A, Bartenschlager H, Van Poucke M, Chalupová P, et al. Porcine EEF1A1 and EEF1A2 genes: genomic structure, polymorphism, mapping and expression. Mol Biol Rep. 2015 Aug;42(8):1257–1264.

12. Pan J, Ruest L-B, Xu S, Wang E. Immuno-characterization of the switch of peptide elongation factors eEF1A-1/EF-1alpha and eEF1A-2/S1 in the central nervous system during mouse development. Brain Res Dev Brain Res. 2004 Mar 22;149(1):1–8.

13. Newbery HJ, Loh DH, O'Donoghue JE, Tomlinson VAL, Chau YY, Boyd JA, et al. Translation elongation factor eEF1A2 is essential for post-weaning survival in mice. J Biol Chem. 2007 Sep 28;282(39):28951–28959.

14. Colantuoni C, Lipska BK, Ye T, Hyde TM, Tao R, Leek JT, et al. Temporal dynamics and genetic control of transcription in the human prefrontal cortex. Nature. 2011 Oct 26;478(7370):519–523.

15. Tebbenkamp ATN, Willsey AJ, State MW, Sestan N. The developmental transcriptome of the human brain: implications for neurodevelopmental disorders. Curr Opin Neurol. 2014 Apr;27(2):149–156.

16. Andersen GR, Pedersen L, Valente L, Chatterjee I, Kinzy TG, Kjeldgaard M, et al. Structural basis for nucleotide exchange and competition with tRNA in the yeast elongation factor complex eEF1A:eEF1Balpha. Mol Cell. 2000 Nov;6(5):1261–1266.

17. Soares DC, Barlow PN, Newbery HJ, Porteous DJ, Abbott CM. Structural models of human eEF1A1 and eEF1A2 reveal two distinct surface clusters of sequence variation and potential differences in phosphorylation. PLoS ONE. 2009 Jul 28;4(7):e6315.

18. Soares DC, Abbott CM. Highly homologous eEF1A1 and eEF1A2 exhibit differential post-translational modification with significant enrichment around localised sites of sequence variation. Biol Direct. 2013 Nov 13;8:29.

19. Kahns S, Lund A, Kristensen P, Knudsen CR, Clark BF, Cavallius J, et al. The elongation factor 1 A-2 isoform from rabbit: cloning of the cDNA and characterization of the protein. Nucleic Acids Res. 1998 Apr 15;26(8):1884–1890.

20. Gross SR, Kinzy TG. Translation elongation factor 1A is essential for regulation of the actin cytoskeleton and cell morphology. Nat Struct Mol Biol. 2005 Sep;12(9):772–778.

21. Novosylna O, Doyle A, Vlasenko D, Murphy M, Negrutskii B, El'skaya A. Comparison of the ability of mammalian eEF1A1 and its oncogenic variant eEF1A2 to interact with actin and calmodulin. Biol Chem. 2017 Jan 1;398(1):113–124.

22. Panasyuk G, Nemazanyy I, Filonenko V, Negrutskii B, El'skaya AV. A2 isoform of mammalian translation factor eEF1A displays increased tyrosine

phosphorylation and ability to interact with different signalling molecules. Int J Biochem Cell Biol. 2008;40(1):63–71.

23. Crepin T, Shalak VF, Yaremchuk AD, Vlasenko DO, McCarthy A, Negrutskii BS, et al. Mammalian translation elongation factor eEF1A2: X-ray structure and new features of GDP/GTP exchange mechanism in higher eukaryotes. Nucleic Acids Res. 2014 Nov 10;42(20):12939–12948.

24. Kurasawa Y, Hanyu K, Watanabe Y, Numata O. F-actin bundling activity of Tetrahymena elongation factor 1 alpha is regulated by Ca2+/calmodulin. J Biochem. 1996 Apr;119(4):791–798.

25. Bunai F, Ando K, Ueno H, Numata O. Tetrahymena eukaryotic translation elongation factor 1A (eEF1A) bundles filamentous actin through dimer formation. J Biochem. 2006 Sep;140(3):393–399.

26. Vlasenko DO, Novosylna OV, Negrutskii BS, El'skaya AV. Truncation of the A,A(∗),A' helices segment impairs the actin bundling activity of mammalian eEF1A1. FEBS Lett. 2015 May 8;589(11):1187–1193.

27. Timchenko AA, Novosylna OV, Prituzhalov EA, Kihara H, El'skaya AV, Negrutskii BS, et al. Different oligomeric properties and stability of highly homologous A1 and proto-oncogenic A2 variants of mammalian translation elongation factor eEF1. Biochemistry. 2013 Aug 13;52(32):5345–5353.

28. Abbott CM, Newbery HJ, Squires CE, Brownstein D, Griffiths LA, Soares DC. eEF1A2 and neuronal degeneration. Biochem Soc Trans. 2009 Dec;37(Pt 6):1293–1297.

29. Mateyak MK, Kinzy TG. eEF1A: thinking outside the ribosome. J Biol Chem. 2010 Jul 9;285(28):21209–21213.

30. Vera M, Pani B, Griffiths LA, Muchardt C, Abbott CM, Singer RH, et al. The translation elongation factor eEF1A1 couples transcription to translation during heat shock response. elife. 2014 Sep 16;3:e03164.

31. Bohnsack MT, Regener K, Schwappach B, Saffrich R, Paraskeva E, Hartmann E, et al. Exp5 exports eEF1A via tRNA from nuclei and synergizes with other transport pathways to confine translation to the cytoplasm. EMBO J. 2002 Nov 15;21(22):6205–6215.

32. Mingot JM, Vega S, Cano A, Portillo F, Nieto MA. eEF1A mediates the nuclear export of SNAG-containing proteins via the Exportin5-aminoacyl-tRNA complex. Cell Rep. 2013 Nov 14;5(3):727–737.

33. Khacho M, Mekhail K, Pilon-Larose K, Pause A, Côté J, Lee S. eEF1A is a novel component of the mammalian nuclear protein export machinery. Mol Biol Cell. 2008 Dec;19(12):5296–5308.

34. Hotokezaka Y, Tobben U, Hotokezaka H, Van Leyen K, Beatrix B, Smith DH, et al. Interaction of the eukaryotic elongation factor 1A with newly synthesized polypeptides. J Biol Chem. 2002 May 24;277(21):18545–18551.

35. Chuang S-M, Chen L, Lambertson D, Anand M, Kinzy TG, Madura K. Proteasome-mediated degradation of cotranslationally damaged proteins involves translation elongation factor 1A. Mol Cell Biol. 2005 Jan;25(1):403–413.

36. Gandin V, Gutierrez GJ, Brill LM, Varsano T, Feng Y, Aza-Blanc P, et al. Degradation of newly synthesized polypeptides by ribosome-associated RACK1/c-Jun N-terminal kinase/eukaryotic elongation factor 1A2 complex. Mol Cell Biol. 2013 Jul;33(13):2510–2526.

37. Meriin AB, Zaarur N, Sherman MY. Association of translation factor eEF1A with defective ribosomal products generates a signal for aggresome formation. J Cell Sci. 2012 Jun 1;125(Pt 11):2665–2674.

38. Gangwani L, Mikrut M, Galcheva-Gargova Z, Davis RJ. Interaction of ZPR1 with translation elongation factor-1alpha in proliferating cells. J Cell Biol. 1998 Dec 14;143(6):1471–1484.

39. Ruest L-B, Marcotte R, Wang E. Peptide elongation factor eEF1A-2/S1 expression in cultured differentiated myotubes and its protective effect against caspase-3-mediated apoptosis. J Biol Chem. 2002 Feb 15;277(7):5418–5425.

40. Li Z, Qi C-F, Shin D-M, Zingone A, Newbery HJ, Kovalchuk AL, et al. Eef1a2 promotes cell growth, inhibits apoptosis and activates JAK/STAT and AKT signaling in mouse plasmacytomas. PLoS ONE. 2010 May 21;5(5):e10755.

41. Chang R, Wang E. Mouse translation elongation factor eEF1A-2 interacts with Prdx-I to protect cells against apoptotic death induced by oxidative stress. J Cell Biochem. 2007 Feb 1;100(2):267–278.

42. McClatchy DB, Knudsen CR, Clark BF, Kahn RA, Hall RA, Levey AI. Novel interaction between the M4 muscarinic acetylcholine receptor and elongation factor 1A2. J Biol Chem. 2002 Aug 9;277(32):29268–29274.

43. Giustetto M, Hegde AN, Si K, Casadio A, Inokuchi K, Pei W, et al. Axonal transport of eukaryotic translation elongation factor 1alpha mRNA couples transcription in the nucleus to long-term facilitation at the synapse. Proc Natl Acad Sci U S A. 2003 Nov 11;100(23):13680–13685.

44. Tsokas P, Grace EA, Chan P, Ma T, Sealfon SC, Iyengar R, et al. Local protein synthesis mediates a rapid increase in dendritic elongation factor 1A

after induction of late long-term potentiation. J Neurosci. 2005 Jun 15;25(24):5833–5843.

45. Inamura N, Nawa H, Takei N. Enhancement of translation elongation in neurons by brain-derived neurotrophic factor: implications for mammalian target of rapamycin signaling. J Neurochem. 2005 Dec;95(5):1438–1445.

46. Huang F, Chotiner JK, Steward O. The mRNA for elongation factor 1alpha is localized in dendrites and translated in response to treatments that induce long-term depression. J Neurosci. 2005 Aug 3;25(31):7199–7209.

47. Antion MD, Hou L, Wong H, Hoeffer CA, Klann E. mGluR-dependent long-term depression is associated with increased phosphorylation of S6 and synthesis of elongation factor 1A but remains expressed in S6K-deficient mice. Mol Cell Biol. 2008 May;28(9):2996–3007.

48. Cambray S, Pedraza N, Rafel M, Garí E, Aldea M, Gallego C. Protein kinase KIS localizes to RNA granules and enhances local translation. Mol Cell Biol. 2009 Feb;29(3):726–735.

49. Kanai Y, Dohmae N, Hirokawa N. Kinesin transports RNA: isolation and characterization of an RNA-transporting granule. Neuron. 2004 Aug 19;43(4):513–525.

50. Baltaci SB, Mogulkoc R, Baltaci AK. Molecular mechanisms of early and late LTP. Neurochem Res. 2019 Feb;44(2):281–296.

51. Huber KM, Kayser MS, Bear MF. Role for rapid dendritic protein synthesis in hippocampal mGluR-dependent long-term depression. Science. 2000 May 19;288(5469):1254–1257.

52. Benito E, Barco A. CREB's control of intrinsic and synaptic plasticity: implications for CREB-dependent memory models. Trends Neurosci. 2010 May;33(5):230–240.

53. Sasikumar AN, Perez WB, Kinzy TG. The many roles of the eukaryotic elongation factor 1 complex. Wiley Interdiscip Rev RNA. 2012 Aug;3(4):543–555.

54. McClatchy DB, Fang G, Levey AI. Elongation factor 1A family regulates the recycling of the M4 muscarinic acetylcholine receptor. Neurochem Res. 2006 Jul 15;31(7):975–988.

55. Bluem R, Schmidt E, Corvey C, Karas M, Schlicksupp A, Kirsch J, et al. Components of the translational machinery are associated with juvenile glycine receptors and are redistributed to the cytoskeleton upon aging and synaptic activity. J Biol Chem. 2007 Dec 28;282(52):37783–37793.

56. Chambers DM, Peters J, Abbott CM. The lethal mutation of the mouse wasted (wst) is a deletion that abolishes expression of a tissue-specific isoform of translation elongation factor 1alpha, encoded by the Eef1a2 gene. Proc Natl Acad Sci U S A. 1998 Apr 14;95(8):4463–4468.

57. Li KW, Klemmer P, Smit AB. Interaction proteomics of synapse protein complexes. Anal Bioanal Chem. 2010 Aug;397(8):3195–3202.

58. Phillips GR, Florens L, Tanaka H, Khaing ZZ, Fidler L, Yates JR, et al. Proteomic comparison of two fractions derived from the transsynaptic scaffold. J Neurosci Res. 2005 Sep 15;81(6):762–775.

59. Grange J, Belly A, Dupas S, Trembleau A, Sadoul R, Goldberg Y. Specific interaction between Sam68 and neuronal mRNAs: implication for the activity-dependent biosynthesis of elongation factor eEF1A. J Neurosci Res. 2009 Jan;87(1):12–25.

60. Cho S-J, Lee H, Dutta S, Seog D-H, Moon IS. Translation elongation factor-1A1 (eEF1A1) localizes to the spine by domain III. BMB Rep. 2012 Apr;45(4):227–232.

61. Hashimoto K, Ishima T. Neurite outgrowth mediated by translation elongation factor eEF1A1: a target for antiplatelet agent cilostazol. PLoS ONE. 2011 Mar 1;6(3):e17431.

62. Khalyfa A, Bourbeau D, Chen E, Petroulakis E, Pan J, Xu S, et al. Characterization of elongation factor-1A (eEF1A-1) and eEF1A-2/S1 protein expression in normal and wasted mice. J Biol Chem. 2001 Jun 22;276(25):22915–22922.

63. Clore AM, Dannenhoffer JM, Larkins BA. EF-1[alpha] Is Associated with a Cytoskeletal Network Surrounding Protein Bodies in Maize Endosperm Cells. Plant Cell. 1996 Nov;8(11):2003–2014.

64. Munshi R, Kandl KA, Carr-Schmid A, Whitacre JL, Adams AE, Kinzy TG. Overexpression of translation elongation factor 1A affects the organization and function of the actin cytoskeleton in yeast. Genetics. 2001 Apr;157(4):1425–1436.

65. Murray JW, Edmonds BT, Liu G, Condeelis J. Bundling of actin filaments by elongation factor 1 alpha inhibits polymerization at filament ends. J Cell Biol. 1996 Dec;135(5):1309–1321.

66. Stapulionis R, Kolli S, Deutscher MP. Efficient mammalian protein synthesis requires an intact F-actin system. J Biol Chem. 1997 Oct 3;272(40):24980–24986.

67. Gross SR, Kinzy TG. Improper organization of the actin cytoskeleton affects protein synthesis at initiation. Mol Cell Biol. 2007 Mar;27(5):1974–1989.

68. Perez WB, Kinzy TG. Translation elongation factor 1A mutants with altered actin bundling activity show reduced aminoacyl-tRNA binding and alter initiation via eIF2α phosphorylation. J Biol Chem. 2014 Jul 25;289(30):20928–20938.

69. Janssen GM, Möller W. Kinetic studies on the role of elongation factors 1 beta and 1 gamma in protein synthesis. J Biol Chem. 1988 Feb 5;263(4):1773–1778.

70. Mansilla F, Friis I, Jadidi M, Nielsen KM, Clark BFC, Knudsen CR. Mapping the human translation elongation factor eEF1H complex using the yeast two-hybrid system. Biochem J. 2002 Aug 1;365(Pt 3):669–676.

71. Cao Y, Portela M, Janikiewicz J, Doig J, Abbott CM. Characterisation of translation elongation factor eEF1B subunit expression in mammalian cells and tissues and co-localisation with eEF1A2. PLoS ONE. 2014 Dec 1;9(12):e114117.

72. Kaitsuka T, Kiyonari H, Shiraishi A, Tomizawa K, Matsushita M. Deletion of Long Isoform of Eukaryotic Elongation Factor 1Bδ Leads to Audiogenic Seizures and Aversive Stimulus-Induced Long-Lasting Activity Suppression in Mice. Front Mol Neurosci. 2018 Oct 2;11:358.

73. Trosiuk TV, Shalak VF, Szczepanowski RH, Negrutskii BS, El'skaya AV. A non-catalytic N-terminal domain negatively influences the nucleotide exchange activity of translation elongation factor 1Bα. FEBS J. 2016 Feb;283(3):484–497.

74. Bec G, Kerjan P, Zha XD, Waller JP. Valyl-tRNA synthetase from rabbit liver. I. Purification as a heterotypic complex in association with elongation factor 1. J Biol Chem. 1989 Dec 15;264(35):21131–21137.

75. Janssen GM, Morales J, Schipper A, Labbé JC, Mulner-Lorillon O, Bellé R, et al. A major substrate of maturation promoting factor identified as elongation factor 1 beta gamma delta in Xenopus laevis. J Biol Chem. 1991 Aug 15;266(23):14885–14888.

76. Matsumoto S, Terui Y, Xi S, Taira H, Ejiri S. Cloning and characterization of the cDNA encoding rice elongation factor 1 beta. FEBS Lett. 1994 Jan 24;338(1):103–106.

77. Sanders J, Raggiaschi R, Morales J, Möller W. The human leucine zipper-containing guanine-nucleotide exchange protein elongation factor-1 delta. Biochim Biophys Acta. 1993 Jul 18;1174(1):87–90.

78. Bec G, Kerjan P, Waller JP. Reconstitution in vitro of the valyl-tRNA synthetase-elongation factor (EF) 1 beta gamma delta complex. Essential roles of the NH2-terminal extension of valyl-tRNA synthetase and of the EF-1 delta subunit in complex formation. J Biol Chem. 1994 Jan 21;269(3):2086–2092.

79. Kaitsuka T, Tomizawa K, Matsushita M. Transformation of eEF1Bδ into heat-shock response transcription factor by alternative splicing. EMBO Rep. 2011 Jul 1;12(7):673–681.

80. Kaitsuka T, Matsushita M. Regulation of translation factor EEF1D gene function by alternative splicing. Int J Mol Sci. 2015 Feb 12;16(2):3970–3979.

81. Andersen GR, Valente L, Pedersen L, Kinzy TG, Nyborg J. Crystal structures of nucleotide exchange intermediates in the eEF1A-eEF1Balpha complex. Nat Struct Biol. 2001 Jun;8(6):531–534.

82. Janssen GM, Maessen GD, Amons R, Möller W. Phosphorylation of elongation factor 1 beta by an endogenous kinase affects its catalytic nucleotide exchange activity. J Biol Chem. 1988 Aug 15;263(23):11063–11066.

83. Kim S, Kellner J, Lee C-H, Coulombe PA. Interaction between the keratin cytoskeleton and eEF1Bgamma affects protein synthesis in epithelial cells. Nat Struct Mol Biol. 2007 Oct;14(10):982–983.

84. Sanders J, Brandsma M, Janssen GM, Dijk J, Möller W. Immunofluorescence studies of human fibroblasts demonstrate the presence of the complex of elongation factor-1 beta gamma delta in the endoplasmic reticulum. J Cell Sci. 1996 May;109 (Pt 5):1113–1117.

85. Minella O, Mulner-Lorillon O, Bec G, Cormier P, Bellé R. Multiple phosphorylation sites and quaternary organization of guanine-nucleotide exchange complex of elongation factor-1 (EF-1betagammadelta/ValRS) control the various functions of EF-1alpha. Biosci Rep. 1998 Jun;18(3):119–127.

86. Lamb HK, van den Hombergh JP, Newton GH, Moore JD, Roberts CF, Hawkins AR. Differential flux through the quinate and shikimate pathways. Implications for the channelling hypothesis. Biochem J. 1992 May 15;284 (Pt 1):181–187.

87. Kapur M, Monaghan CE, Ackerman SL. Regulation of mRNA Translation in Neurons-A Matter of Life and Death. Neuron. 2017 Nov 1;96(3):616–637.

88. Fogli A, Boespflug-Tanguy O. The large spectrum of eIF2B-related diseases. Biochem Soc Trans. 2006 Feb;34(Pt 1):22–29.

89. Ohno M. Roles of eIF2α kinases in the pathogenesis of Alzheimer's disease. Front Mol Neurosci. 2014 Apr 16;7:22.

90. Chang RCC, Wong AKY, Ng H-K, Hugon J. Phosphorylation of eukaryotic initiation factor-2alpha (eIF2alpha) is associated with neuronal degeneration in Alzheimer's disease. Neuroreport. 2002 Dec 20;13(18):2429–2432.

91. Huddleston LB, Visootsak J, Sherman SL. Cognitive aspects of Fragile X syndrome. Wiley Interdiscip Rev Cogn Sci. 2014 Jul;5(4):501–508.

92. Yu S, Pritchard M, Kremer E, Lynch M, Nancarrow J, Baker E, et al. Fragile X genotype characterized by an unstable region of DNA. Science. 1991 May 24;252(5009):1179–1181.

93. Richter JD, Bassell GJ, Klann E. Dysregulation and restoration of translational homeostasis in fragile X syndrome. Nat Rev Neurosci. 2015 Oct;16(10):595–605.

94. Pfeiffer BE, Huber KM. The state of synapses in fragile X syndrome. Neuroscientist. 2009 Oct;15(5):549–567.

95. Sung YJ, Dolzhanskaya N, Nolin SL, Brown T, Currie JR, Denman RB. The fragile X mental retardation protein FMRP binds elongation factor 1A mRNA and negatively regulates its translation in vivo. J Biol Chem. 2003 May 2;278(18):15669–15678.

96. Tsai N-P, Wilkerson JR, Guo W, Maksimova MA, DeMartino GN, Cowan CW, et al. Multiple autism-linked genes mediate synapse elimination via proteasomal degradation of a synaptic scaffold PSD-95. Cell. 2012 Dec 21;151(7):1581–1594.

97. Tang G, Gudsnuk K, Kuo S-H, Cotrina ML, Rosoklija G, Sosunov A, et al. Loss of mTOR-dependent macroautophagy causes autistic-like synaptic pruning deficits. Neuron. 2014 Sep 3;83(5):1131–1143.

98. Patel AB, Loerwald KW, Huber KM, Gibson JR. Postsynaptic FMRP promotes the pruning of cell-to-cell connections among pyramidal neurons in the L5A neocortical network. J Neurosci. 2014 Feb 26;34(9):3413–3418.

99. Chen E, Sharma MR, Shi X, Agrawal RK, Joseph S. Fragile X mental retardation protein regulates translation by binding directly to the ribosome. Mol Cell. 2014 May 8;54(3):407–417.

100. Hekman KE, Yu G-Y, Brown CD, Zhu H, Du X, Gervin K, et al. A conserved eEF2 coding variant in SCA26 leads to loss of translational fidelity and increased susceptibility to proteostatic insult. Hum Mol Genet. 2012 Dec 15;21(26):5472–5483.

101. Beckelman BC, Day S, Zhou X, Donohue M, Gouras GK, Klann E, et al. Dysregulation of Elongation Factor 1A Expression is Correlated with Synaptic Plasticity Impairments in Alzheimer's Disease. J Alzheimers Dis. 2016 Sep 6;54(2):669–678.

102. Najmabadi H, Hu H, Garshasbi M, Zemojtel T, Abedini SS, Chen W, et al. Deep sequencing reveals 50 novel genes for recessive cognitive disorders. Nature. 2011 Sep 21;478(7367):57–63.

103. Reuter MS, Tawamie H, Buchert R, Hosny Gebril O, Froukh T, Thiel C, et al. Diagnostic yield and novel candidate genes by exome sequencing in 152 consanguineous families with neurodevelopmental disorders. JAMA psychiatry. 2017 Mar 1;74(3):293–299.

104. Ugur Iseri SA, Yucesan E, Tuncer FN, Calik M, Kesim Y, Altiokka Uzun G, et al. Biallelic loss of EEF1D function links heat shock response pathway to autosomal recessive intellectual disability. J Hum Genet. 2019 Feb 21;64(5):421–426.

105. Karaca E, Harel T, Pehlivan D, Jhangiani SN, Gambin T, Coban Akdemir Z, et al. Genes that Affect Brain Structure and Function Identified by Rare Variant Analyses of Mendelian Neurologic Disease. Neuron. 2015 Nov 4;88(3):499–513.

106. Meyer-Schuman R, Antonellis A. Emerging mechanisms of aminoacyl-tRNA synthetase mutations in recessive and dominant human disease. Hum Mol Genet. 2017 Oct 1;26(R2):R114–R127.

107. Nakayama T, Wu J, Galvin-Parton P, Weiss J, Andriola MR, Hill RS, et al. Deficient activity of alanyl-tRNA synthetase underlies an autosomal recessive syndrome of progressive microcephaly, hypomyelination, and epileptic encephalopathy. Hum Mutat. 2017 Oct;38(10):1348–1354.

108. Simons C, Griffin LB, Helman G, Golas G, Pizzino A, Bloom M, et al. Loss-of-function alanyl-tRNA synthetase mutations cause an autosomal-recessive early-onset epileptic encephalopathy with persistent myelination defect. Am J Hum Genet. 2015 Apr 2;96(4):675–681.

109. Taft RJ, Vanderver A, Leventer RJ, Damiani SA, Simons C, Grimmond SM, et al. Mutations in DARS cause hypomyelination with brain stem and spinal cord involvement and leg spasticity. Am J Hum Genet. 2013 May 2;92(5):774–780.

110. Puffenberger EG, Jinks RN, Sougnez C, Cibulskis K, Willert RA, Achilly NP, et al. Genetic mapping and exome sequencing identify variants associated with five novel diseases. PLoS ONE. 2012 Jan 17;7(1):e28936.

111. McLaughlin HM, Sakaguchi R, Giblin W, NISC Comparative Sequencing Program, Wilson TE, Biesecker L, et al. A recurrent loss-of-function alanyl-tRNA synthetase (AARS) mutation in patients with Charcot-Marie-Tooth disease type 2N (CMT2N). Hum Mutat. 2012 Jan;33(1):244–253.

112. Wolf NI, Salomons GS, Rodenburg RJ, Pouwels PJW, Schieving JH, Derks TGJ, et al. Mutations in RARS cause hypomyelination. Ann Neurol. 2014 Jul;76(1):134–139.

113. Nowaczyk MJM, Huang L, Tarnopolsky M, Schwartzentruber J, Majewski J, Bulman DE, et al. A novel multisystem disease associated with recessive mutations in the tyrosyl-tRNA synthetase (YARS) gene. Am J Med Genet A. 2017 Jan;173(1):126–134.

114. Kodera H, Osaka H, Iai M, Aida N, Yamashita A, Tsurusaki Y, et al. Mutations in the glutaminyl-tRNA synthetase gene cause early-onset epileptic encephalopathy. J Hum Genet. 2015 Feb;60(2):97–101.

115. Zhang X, Ling J, Barcia G, Jing L, Wu J, Barry BJ, et al. Mutations in QARS, encoding glutaminyl-tRNA synthetase, cause progressive microcephaly, cerebral-cerebellar atrophy, and intractable seizures. Am J Hum Genet. 2014 Apr 3;94(4):547–558.

116. Ishimura R, Nagy G, Dotu I, Zhou H, Yang X-L, Schimmel P, et al. RNA function. Ribosome stalling induced by mutation of a CNS-specific tRNA causes neurodegeneration. Science. 2014 Jul 25;345(6195):455–459.

117. Lo W-S, Gardiner E, Xu Z, Lau C-F, Wang F, Zhou JJ, et al. Human tRNA synthetase catalytic nulls with diverse functions. Science. 2014 Jul 18;345(6194):328–332.

118. Doig J, Griffiths LA, Peberdy D, Dharmasaroja P, Vera M, Davies FJC, et al. In vivo characterization of the role of tissue-specific translation elongation factor 1A2 in protein synthesis reveals insights into muscle atrophy. FEBS J. 2013 Dec;280(24):6528–6540.

119. Newbery HJ, Gillingwater TH, Dharmasaroja P, Peters J, Wharton SB, Thomson D, et al. Progressive loss of motor neuron function in wasted mice: effects of a spontaneous null mutation in the gene for the eEF1 A2 translation factor. J Neuropathol Exp Neurol. 2005 Apr;64(4):295–303.

120. Griffiths LA, Doig J, Churchhouse AMD, Davies FCJ, Squires CE, Newbery HJ, et al. Haploinsufficiency for translation elongation factor eEF1A2 in aged mouse muscle and neurons is compatible with normal function. PLoS ONE. 2012 Jul 25;7(7):e41917.

121. Hope J. Behavioural testing and general phenotyping of mice with mutations in Eef1a2 to investigate autism, intellectual disability and epilepsy. [Doctoral dissertation]. University of Edinburgh; 2018.

122. Cao S, Smith LL, Padilla-Lopez SR, Guida BS, Blume E, Shi J, et al. Homozygous EEF1A2 mutation causes dilated cardiomyopathy, failure to thrive, global developmental delay, epilepsy and early death. Hum Mol Genet. 2017 Sep 15;26(18):3545–3552.

123. Lam WWK, Millichap JJ, Soares DC, Chin R, McLellan A, FitzPatrick DR, et al. Novel de novo EEF1A2 missense mutations causing epilepsy and intellectual disability. Mol Genet Genomic Med. 2016 Jul;4(4):465–474.

124. Epi4K consortium, Epilepsy Phenome/Genome Project. Ultra-rare genetic variation in common epilepsies: a case-control sequencing study. Lancet Neurol. 2017 Feb;16(2):135–143.

125. Landrum MJ, Lee JM, Riley GR, Jang W, Rubinstein WS, Church DM, et al. ClinVar: public archive of relationships among sequence variation and human phenotype. Nucleic Acids Res. 2014 Jan;42(Database issue):D980–5.

126. De Ligt J, Willemsen MH, van Bon BWM, Kleefstra T, Yntema HG, Kroes T, et al. Diagnostic exome sequencing in persons with severe intellectual disability. N Engl J Med. 2012 Nov 15;367(20):1921–1929.

127. Veeramah KR, Johnstone L, Karafet TM, Wolf D, Sprissler R, Salogiannis J, et al. Exome sequencing reveals new causal mutations in children with epileptic encephalopathies. Epilepsia. 2013 Jul;54(7):1270–1281.

128. Lopes F, Barbosa M, Ameur A, Soares G, de Sá J, Dias AI, et al. Identification of novel genetic causes of Rett syndrome-like phenotypes. J Med Genet. 2016 Mar;53(3):190–199.

129. Nakajima J, Okamoto N, Tohyama J, Kato M, Arai H, Funahashi O, et al. De novo EEF1A2 mutations in patients with characteristic facial features, intellectual disability, autistic behaviors and epilepsy. Clin Genet. 2015 Apr;87(4):356–361.

130. Inui T, Kobayashi S, Ashikari Y, Sato R, Endo W, Uematsu M, et al. Two cases of early-onset myoclonic seizures with continuous parietal delta activity caused by EEF1A2 mutations. Brain Dev. 2016 May;38(5):520–524.

131. Lelieveld SH, Reijnders MRF, Pfundt R, Yntema HG, Kamsteeg E-J, de Vries P, et al. Meta-analysis of 2,104 trios provides support for 10 new genes for intellectual disability. Nat Neurosci. 2016 Aug 1;19(9):1194–1196.

132. Iossifov I, O'Roak BJ, Sanders SJ, Ronemus M, Krumm N, Levy D, et al. The contribution of de novo coding mutations to autism spectrum disorder. Nature. 2014 Nov 13;515(7526):216–221.

133. Ostrander BEP, Butterfield RJ, Pedersen BS, Farrell AJ, Layer RM, Ward A, et al. Whole-genome analysis for effective clinical diagnosis and gene discovery in early infantile epileptic encephalopathy. NPJ genomic medicine. 2018 Aug 13;3:22.

134. Mair B, Konopka T, Kerzendorfer C, Sleiman K, Salic S, Serra V, et al. Gain- and Loss-of-Function Mutations in the Breast Cancer Gene GATA3 Result in Differential Drug Sensitivity. PLoS Genet. 2016 Sep 2;12(9):e1006279.

135. Chen B, Altman RB. Opportunities for developing therapies for rare genetic diseases: focus on gain-of-function and allostery. Orphanet J Rare Dis. 2017 Apr 17;12(1):61.

136. Burrone J, O'Byrne M, Murthy VN. Multiple forms of synaptic plasticity triggered by selective suppression of activity in individual neurons. Nature. 2002 Nov 28;420(6914):414–418.

137. Scholz D, Pöltl D, Genewsky A, Weng M, Waldmann T, Schildknecht S, et al. Rapid, complete and large-scale generation of post-mitotic neurons from the human LUHMES cell line. J Neurochem. 2011 Dec;119(5):957–971.

138. Ran FA, Hsu PD, Wright J, Agarwala V, Scott DA, Zhang F. Genome engineering using the CRISPR-Cas9 system. Nat Protoc. 2013 Nov;8(11):2281–2308.

139. Shah RR, Cholewa-Waclaw J, Davies FCJ, Paton KM, Chaligne R, Heard E, et al. Efficient and versatile CRISPR engineering of human neurons in culture to model neurological disorders. [version 1; peer review: 2 approved]. Wellcome Open Research. 2016 Nov 15;1:13.

140. Davies FCJ, Hope JE, McLachlan F, Nunez F, Doig J, Bengani H, et al. Biallelic mutations in the gene encoding eEF1A2 cause seizures and sudden death in F0 mice. Sci Rep. 2017 Apr 5;7:46019.

141. Davies, Joy FC. Role of eEF1A isoforms in neuritogenesis and epilepsy. 2017 Jul 8;

142. Guyenet SJ, Furrer SA, Damian VM, Baughan TD, La Spada AR, Garden GA. A simple composite phenotype scoring system for evaluating mouse models of cerebellar ataxia. J Vis Exp. 2010 May 21;(39).

143. Goodman CA, Hornberger TA. Measuring protein synthesis with SUnSET: a valid alternative to traditional techniques? Exerc Sport Sci Rev. 2013 Apr;41(2):107–115.

144. Vandesompele J, De Preter K, Pattyn F, Poppe B, Van Roy N, De Paepe A, et al. Accurate normalization of real-time quantitative RT-PCR data by geometric averaging of multiple internal control genes. Genome Biol. 2002;

145. Lambert J-P, Ivosev G, Couzens AL, Larsen B, Taipale M, Lin Z-Y, et al. Mapping differential interactomes by affinity purification coupled with data-independent mass spectrometry acquisition. Nat Methods. 2013 Dec;10(12):1239–1245.

146. Braun P. Interactome mapping for analysis of complex phenotypes: insights from benchmarking binary interaction assays. Proteomics. 2012 May;12(10):1499–1518.

147. Vidal M, Cusick ME, Barabási A-L. Interactome networks and human disease. Cell. 2011 Mar 18;144(6):986–998.

148. Fernandez-Castaneda A, Arandjelovic S, Stiles TL, Schlobach RK, Mowen KA, Gonias SL, et al. Identification of the low density lipoprotein (LDL) receptor-related protein-1 interactome in central nervous system myelin suggests a role in the clearance of necrotic cell debris. J Biol Chem. 2013 Feb 15;288(7):4538–4548.

149. Culver BP, Savas JN, Park SK, Choi JH, Zheng S, Zeitlin SO, et al. Proteomic analysis of wild-type and mutant huntingtin-associated proteins in mouse brains identifies unique interactions and involvement in protein synthesis. J Biol Chem. 2012 Jun 22;287(26):21599–21614.

150. Zhong Q, Simonis N, Li Q-R, Charloteaux B, Heuze F, Klitgord N, et al. Edgetic perturbation models of human inherited disorders. Mol Syst Biol. 2009 Nov 3;5:321.

151. Sahni N, Yi S, Taipale M, Fuxman Bass JI, Coulombe-Huntington J, Yang F, et al. Widespread macromolecular interaction perturbations in human genetic disorders. Cell. 2015 Apr 23;161(3):647–660.

152. Dunham WH, Mullin M, Gingras A-C. Affinity-purification coupled to mass spectrometry: basic principles and strategies. Proteomics. 2012 May;12(10):1576–1590.

153. Dong S, Provart NJ. Analyses of protein interaction networks using computational tools. Methods Mol Biol. 2018;1794:97–117.

154. Shalgi R, Hurt JA, Krykbaeva I, Taipale M, Lindquist S, Burge CB. Widespread regulation of translation by elongation pausing in heat shock. Mol Cell. 2013 Feb 7;49(3):439–452.

155. Drissi R, Dubois M-L, Douziech M, Boisvert F-M. Quantitative proteomics reveals dynamic interactions of the minichromosome maintenance complex

(MCM) in the cellular response to etoposide induced DNA damage. Mol Cell Proteomics. 2015 Jul;14(7):2002–2013.

156. Wan C, Borgeson B, Phanse S, Tu F, Drew K, Clark G, et al. Panorama of ancient metazoan macromolecular complexes. Nature. 2015 Sep 17;525(7569):339–344.

157. Huttlin EL, Bruckner RJ, Paulo JA, Cannon JR, Ting L, Baltier K, et al. Architecture of the human interactome defines protein communities and disease networks. Nature. 2017 May 25;545(7655):505–509.

158. Zuo S, Xue Y, Tang S, Yao J, Du R, Yang P, et al. 14-3-3 epsilon dynamically interacts with key components of mitogen-activated protein kinase signal module for selective modulation of the TNF-alpha-induced time course-dependent NF-kappaB activity. J Proteome Res. 2010 Jul 2;9(7):3465–3478.

159. Lee M-H, Choi BY, Cho Y-Y, Lee S-Y, Huang Z, Kundu JK, et al. Tumor suppressor p16(INK4a) inhibits cancer cell growth by downregulating eEF1A2 through a direct interaction. J Cell Sci. 2013 Apr 15;126(Pt 8):1744–1752.

160. Leclercq TM, Moretti PAB, Vadas MA, Pitson SM. Eukaryotic elongation factor 1A interacts with sphingosine kinase and directly enhances its catalytic activity. J Biol Chem. 2008 Apr 11;283(15):9606–9614.

161. Lamberti A, Sanges C, Chambery A, Migliaccio N, Rosso F, Di Maro A, et al. Analysis of interaction partners for eukaryotic translation elongation factor 1A M-domain by functional proteomics. Biochimie. 2011 Oct;93(10):1738–1746.

162. Yang X, Coulombe-Huntington J, Kang S, Sheynkman GM, Hao T, Richardson A, et al. Widespread expansion of protein interaction capabilities by alternative splicing. Cell. 2016 Feb 11;164(4):805–817.

163. Sahni N, Yi S, Zhong Q, Jailkhani N, Charloteaux B, Cusick ME, et al. Edgotype: a fundamental link between genotype and phenotype. Curr Opin Genet Dev. 2013 Dec;23(6):649–657.

164. Smits AH, Vermeulen M. Characterizing Protein-Protein Interactions Using Mass Spectrometry: Challenges and Opportunities. Trends Biotechnol. 2016 Mar 17;34(10):825–834.

165. Carson JH, Cui H, Krueger W, Schlepchenko B, Brumwell C, Barbarese E. RNA trafficking in oligodendrocytes. Results Probl Cell Differ. 2001;34:69–81.

166. Malmqvist T, Anthony K, Gallo J-M. Tau mRNA is present in axonal RNA granules and is associated with elongation factor 1A. Brain Res. 2014 Oct 10;1584:22–27.

167. Lopez-Valenzuela JA, Gibbon BC, Holding DR, Larkins BA. Cytoskeletal proteins are coordinately increased in maize genotypes with high levels of eEF1A. Plant Physiol. 2004 Jul 9;135(3):1784–1797.

168. Kanibolotsky DS, Novosyl'na OV, Abbott CM, Negrutskii BS, El'skaya AV. Multiple molecular dynamics simulation of the isoforms of human translation elongation factor 1A reveals reversible fluctuations between "open" and "closed" conformations and suggests specific for eEF1A1 affinity for Ca2+-calmodulin. BMC Struct Biol. 2008 Jan 25;8:4.

169. Pittman YR, Kandl K, Lewis M, Valente L, Kinzy TG. Coordination of eukaryotic translation elongation factor 1A (eEF1A) function in actin organization and translation elongation by the guanine nucleotide exchange factor eEF1Balpha. J Biol Chem. 2009 Feb 13;284(7):4739–4747.

170. McLachlan F, Sires AM, Abbott CM. The role of translation elongation factor eEF1 subunits in neurodevelopmental disorders. Hum Mutat. 2018 Oct 29;40(2):131–141.

171. Xue LC, Dobbs D, Bonvin AMJJ, Honavar V. Computational prediction of protein interfaces: A review of data driven methods. FEBS Lett. 2015 Nov 30;589(23):3516–3526.

172. Pitre S, Alamgir M, Green JR, Dumontier M, Dehne F, Golshani A. Computational methods for predicting protein-protein interactions. Adv Biochem Eng Biotechnol. 2008;110:247–267.

173. Witvliet DK, Strokach A, Giraldo-Forero AF, Teyra J, Colak R, Kim PM. ELASPIC web-server: proteome-wide structure-based prediction of mutation effects on protein stability and binding affinity. Bioinformatics. 2016 May 15;32(10):1589–1591.

174. Dehouck Y, Kwasigroch JM, Rooman M, Gilis D. BeAtMuSiC: Prediction of changes in protein-protein binding affinity on mutations. Nucleic Acids Res. 2013 Jul;41(Web Server issue):W333–9.

175. Li M, Simonetti FL, Goncearenco A, Panchenko AR. MutaBind estimates and interprets the effects of sequence variants on protein-protein interactions. Nucleic Acids Res. 2016 Jul 8;44(W1):W494–501.

176. Kumabe T, Sohma Y, Yamamoto T. Human cDNAs encoding elongation factor 1 gamma and the ribosomal protein L19. Nucleic Acids Res. 1992 May 25;20(10):2598.

177. Sun S, Yang F, Tan G, Costanzo M, Oughtred R, Hirschman J, et al. An extended set of yeast-based functional assays accurately identifies human disease mutations. Genome Res. 2016 Mar 14;26(5):670–680.

178. Dixit A, Torkamani A, Schork NJ, Verkhivker G. Computational modeling of structurally conserved cancer mutations in the RET and MET kinases: the impact on protein structure, dynamics, and stability. Biophys J. 2009 Feb;96(3):858–874.

179. Wolf U. Identical mutations and phenotypic variation. Hum Genet. 1997 Sep;100(3-4):305–321.

180. Woodbury-Smith M, Nicolson R, Zarrei M, Yuen RKC, Walker S, Howe J, et al. Variable phenotype expression in a family segregating microdeletions of the NRXN1 and MBD5 autism spectrum disorder susceptibility genes. NPJ genomic medicine. 2017 May 3;2.

181. Taddei I, Morishima M, Huynh T, Lindsay EA. Genetic factors are major determinants of phenotypic variability in a mouse model of the DiGeorge/del22q11 syndromes. Proc Natl Acad Sci U S A. 2001 Sep 25;98(20):11428–11431.

182. Nadeau JH. Modifier genes in mice and humans. Nat Rev Genet. 2001 Mar;2(3):165–174.

183. Dorfman R. Modifier gene studies to identify new therapeutic targets in cystic fibrosis. Curr Pharm Des. 2012;18(5):674–682.

184. Vu V, Verster AJ, Schertzberg M, Chuluunbaatar T, Spensley M, Pajkic D, et al. Natural variation in gene expression modulates the severity of mutant phenotypes. Cell. 2015 Jul 16;162(2):391–402.

185. Naz M, Kodamullil AT, Hofmann-Apitius M. Reasoning over genetic variance information in cause-and-effect models of neurodegenerative diseases. Brief Bioinformatics. 2016;17(3):505–516.

186. Peaston AE, Whitelaw E. Epigenetics and phenotypic variation in mammals. Mamm Genome. 2006 May;17(5):365–374.

187. Lelieveld SH, Wiel L, Venselaar H, Pfundt R, Vriend G, Veltman JA, et al. Spatial Clustering of de Novo Missense Mutations Identifies Candidate Neurodevelopmental Disorder-Associated Genes. Am J Hum Genet. 2017 Sep 7;101(3):478–484.

188. Niday Z, Tzingounis AV. Potassium channel gain of function in epilepsy: an unresolved paradox. Neuroscientist. 2018 Mar 15;24(4):368–380.

189. Siekierska A, Isrie M, Liu Y, Scheldeman C, Vanthillo N, Lagae L, et al. Gain-of-function FHF1 mutation causes early-onset epileptic encephalopathy with cerebellar atrophy. Neurology. 2016 Jun 7;86(23):2162–2170.

190. Milligan CJ, Li M, Gazina EV, Heron SE, Nair U, Trager C, et al. KCNT1 gain of function in 2 epilepsy phenotypes is reversed by quinidine. Ann Neurol. 2014 Apr 14;75(4):581–590.

191. Proietti Onori M, Koopal B, Everman DB, Worthington JD, Jones JR, Ploeg MA, et al. The intellectual disability-associated CAMK2G p.Arg292Pro mutation acts as a pathogenic gain-of-function. Hum Mutat. 2018 Dec;39(12):2008–2024.

192. Guzmán YF, Ramsey K, Stolz JR, Craig DW, Huentelman MJ, Narayanan V, et al. A gain-of-function mutation in the GRIK2 gene causes neurodevelopmental deficits. Neurology Genetics. 2017 Feb;3(1):e129.

193. López-Erauskin J, Tadokoro T, Baughn MW, Myers B, McAlonis-Downes M, Chillon-Marinas C, et al. ALS/FTD-Linked Mutation in FUS Suppresses Intra-axonal Protein Synthesis and Drives Disease Without Nuclear Loss-of-Function of FUS. Neuron. 2018 Nov 21;100(4):816–830.e7.

194. Kabashi E, Lin L, Tradewell ML, Dion PA, Bercier V, Bourgouin P, et al. Gain and loss of function of ALS-related mutations of TARDBP (TDP-43) cause motor deficits in vivo. Hum Mol Genet. 2010 Feb 15;19(4):671–683.

195. Sartor F, Anderson J, McCaig C, Miedzybrodzka Z, Müller B. Mutation of genes controlling mRNA metabolism and protein synthesis predisposes to neurodevelopmental disorders. Biochem Soc Trans. 2015 Dec;43(6):1259–1265.

196. Schmidt EK, Clavarino G, Ceppi M, Pierre P. SUnSET, a nonradioactive method to monitor protein synthesis. Nat Methods. 2009 Apr;6(4):275–277.

197. Tom Dieck S, Kochen L, Hanus C, Heumüller M, Bartnik I, Nassim-Assir B, et al. Direct visualization of newly synthesized target proteins in situ. Nat Methods. 2015 May;12(5):411–414.

198. Onder TT, Daley GQ. New lessons learned from disease modeling with induced pluripotent stem cells. Curr Opin Genet Dev. 2012 Oct;22(5):500–508.

199. Liu-Yesucevitz L, Bassell GJ, Gitler AD, Hart AC, Klann E, Richter JD, et al. Local RNA translation at the synapse and in disease. J Neurosci. 2011 Nov 9;31(45):16086–16093.

200. Bear MF, Dölen G, Osterweil E, Nagarajan N. Fragile X: translation in action. Neuropsychopharmacology. 2008 Jan;33(1):84–87.

201. Hanson JE, Madison DV. Presynaptic FMR1 genotype influences the degree of synaptic connectivity in a mosaic mouse model of fragile X syndrome. J Neurosci. 2007 Apr 11;27(15):4014–4018.

202. Kim E, Jung H. Local protein synthesis in neuronal axons: why and how we study. BMB Rep. 2015 Mar;48(3):139–146.

203. Ravi V, Jain A, Ahamed F, Fathma N, Desingu PA, Sundaresan NR. Systematic evaluation of the adaptability of the non-radioactive SUnSET assay to measure cardiac protein synthesis. Sci Rep. 2018 Mar 15;8(1):4587.

204. Jacquemont S, Pacini L, Jønch AE, Cencelli G, Rozenberg I, He Y, et al. Protein synthesis levels are increased in a subset of individuals with fragile X syndrome. Hum Mol Genet. 2018 Jun 15;27(12):2039–2051.

205. Marciano R, Leprivier G, Rotblat B. Puromycin labeling does not allow protein synthesis to be measured in energy-starved cells. Cell Death Dis. 2018 Jan 18;9(2):39.

206. Osterweil EK, Krueger DD, Reinhold K, Bear MF. Hypersensitivity to mGluR5 and ERK1/2 leads to excessive protein synthesis in the hippocampus of a mouse model of fragile X syndrome. J Neurosci. 2010 Nov 17;30(46):15616–15627.

207. Borgo C, Franchin C, Salizzato V, Cesaro L, Arrigoni G, Matricardi L, et al. Protein kinase CK2 potentiates translation efficiency by phosphorylating eIF3j at Ser127. Biochim Biophys Acta. 2015 Jul;1853(7):1693–1701.

208. Narla A, Ebert BL. Ribosomopathies: human disorders of ribosome dysfunction. Blood. 2010 Apr 22;115(16):3196–3205.

209. Slomnicki LP, Pietrzak M, Vashishta A, Jones J, Lynch N, Elliot S, et al. Requirement of neuronal ribosome synthesis for growth and maintenance of the dendritic tree. J Biol Chem. 2016 Mar 11;291(11):5721–5739.

210. Harigaya Y, Parker R. Fragile X mental retardation protein and the ribosome. Mol Cell. 2014 May 8;54(3):330–332.

211. Auerbach BD, Osterweil EK, Bear MF. Mutations causing syndromic autism define an axis of synaptic pathophysiology. Nature. 2011 Nov 23;480(7375):63–68.

212. Ravanidis S, Kattan F-G, Doxakis E. Unraveling the Pathways to Neuronal Homeostasis and Disease: Mechanistic Insights into the Role of RNA-Binding Proteins and Associated Factors. Int J Mol Sci. 2018 Aug 3;19(8).

213. Anderson P, Kedersha N. Stress granules: the Tao of RNA triage. Trends Biochem Sci. 2008 Mar;33(3):141–150.

214. Goulet I, Boisvenue S, Mokas S, Mazroui R, Côté J. TDRD3, a novel Tudor domain-containing protein, localizes to cytoplasmic stress granules. Hum Mol Genet. 2008 Oct 1;17(19):3055–3074.

215. Turnbull DH, Mori S. MRI in mouse developmental biology. NMR Biomed. 2007 May;20(3):265–274.

216. Santini E, Huynh TN, MacAskill AF, Carter AG, Pierre P, Ruggero D, et al. Exaggerated translation causes synaptic and behavioural aberrations associated with autism. Nature. 2013 Jan 17;493(7432):411–415.

217. Sanges C, Scheuermann C, Zahedi RP, Sickmann A, Lamberti A, Migliaccio N, et al. Raf kinases mediate the phosphorylation of eukaryotic translation elongation factor 1A and regulate its stability in eukaryotic cells. Cell Death Dis. 2012 Mar 1;3:e276.

218. Migliaccio N, Ruggiero I, Martucci NM, Sanges C, Arbucci S, Tatè R, et al. New insights on the interaction between the isoforms 1 and 2 of human translation elongation factor 1A. Biochimie. 2015 Nov;118:1–7.

219. Behrmann E, Loerke J, Budkevich TV, Yamamoto K, Schmidt A, Penczek PA, et al. Structural snapshots of actively translating human ribosomes. Cell. 2015 May 7;161(4):845–857.

220. Young FI, Telezhkin V, Youde SJ, Langley MS, Stack M, Kemp PJ, et al. Clonal heterogeneity in the neuronal and glial differentiation of dental pulp stem/progenitor cells. Stem Cells Int. 2016 May 26;2016:1290561.

221. Van de Leemput J, Boles NC, Kiehl TR, Corneo B, Lederman P, Menon V, et al. CORTECON: a temporal transcriptome analysis of in vitro human cerebral cortex development from human embryonic stem cells. Neuron. 2014 Jul 2;83(1):51–68.

222. Genheden M, Kenney JW, Johnston HE, Manousopoulou A, Garbis SD, Proud CG. BDNF stimulation of protein synthesis in cortical neurons requires the MAP kinase-interacting kinase MNK1. J Neurosci. 2015 Jan 21;35(3):972–984.

223. Zhu S, Henninger K, McGrath BC, Cavener DR. PERK Regulates Working Memory and Protein Synthesis-Dependent Memory Flexibility. PLoS ONE. 2016 Sep 14;11(9):e0162766.

224. McGlincy NJ, Ingolia NT. Transcriptome-wide measurement of translation by ribosome profiling. Methods. 2017 Aug 15;126:112–129.

225. Thomson SR, Seo SS, Barnes SA, Louros SR, Muscas M, Dando O, et al. Cell-Type-Specific Translation Profiling Reveals a Novel Strategy for Treating Fragile X Syndrome. Neuron. 2017 Aug 2;95(3):550–563.e5.